Title
Developing Zircon as a Probe of Planetary Impact History

Author
Wielicki, Matthew M.

Publication Date
2014

Peer reviewed|Thesis/dissertation

UNIVERSITY OF CALIFORNIA

Los Angeles

Developing Zircon as a Probe of Planetary Impact History

A dissertation in partial satisfaction of the

requirements for the Doctor of Philosophy

in Geochemistry

by

Matthew Wielicki

2014

ABSTRACT OF THE DISSERTATION

Developing Zircon as a Probe of Planetary Impact History

by

Matthew Wielicki

Doctor of Philosophy in Geochemistry

University of California, Los Angeles, 2014

Professor Mark Harrison, Chair

The identification of Meteor Crater in Arizona as an extraterrestrial impact by Eugene Shoemaker provided the first evidence of this geologic phenomenon and opened the door to a new field of research that has eventually lead to the identification of over ~150 terrestrial impact structures. Subsequently impacts have been evoked in the formation of the moon, delivery of volatiles and bio-precursors to early Earth, creation of habitats for the earliest life and, in more recent times, major mass extinction events. However, understanding the impact flux to the Earth-Moon system has been complicated by the constant weathering and erosion at Earth's surface and the complex nature of impactite samples such that only a hand full of terrestrial craters have been accurately and precisely dated. Currently $^{40}Ar/^{39}Ar$ step-heating analysis of impactite samples is commonly used to infer impact ages but can be problematic due to the presence of relic clasts, incomplete ^{40}Ar outgassing or excess ^{40}Ar, and recoil and shock effects. The work presented here attempts to develop zircon geochronology to probe planetary impact

histories as an alternative to current methods and provides another tool by which to constrain the bolide flux to the Earth-Moon system.

Zircon has become the premier geo-chronometer in earth science and geochemical investigation of Hadean zircon from Western Australia has challenged the long-standing, popular conception that the near-surface Hadean Earth was an uninhabitable and hellish world; Zircons may preserve environmental information regarding their formation and thus provide a rare window into conditions on early Earth. Isotopic and petrologic analyses of these ancient grains have been interpreted to suggest that early Earth was more habitable than previously envisioned, with water oceans, continental crust, and possibly even plate tectonics. The Hadean is also suspected to be a time of major planetary bombardment however identifying impact signatures within the Hadean population remains difficult and this study hopes to develop criteria to recognize impact zircon and possibly provide constraints on the early impactor flux.

Five large terrestrial craters, Vredefort and Morokweng, South Africa, Sudbury and Manicouagan, Canada, and Popigai, Russia, are the focus of this study as smaller craters do not have the energy to produce thick melt sheets, which persist over time-scales sufficient for crystallization of zircon, permitting geochemical and geochronological analysis. Geochemical analysis of these impact-produced zircons yields similar chemical signatures to endogenic igneous zircon from crustal melts and highlights the need for well-developed criteria for discriminating impact and endogenic grains for impact geochronology. One such criterion is modeling of impact zircon crystallization temperature spectra for simulated impact events on targets of varying composition. Provided some assumptions the zircon crystallization spectra can be estimated from well established Zr systematics in crustal melts. Results for impacts into

an Archean terrestrial surface (used as a proxy for the Hadean as little to no rock record exists >4.0 Ga) yields a crystallization spectra significantly higher than that reported for the Hadean zircon population and appears to rule out impacts as a dominant source for these ancient grains.

When no dateable impact melt sheet exists, either due to the lack of energy of the impact itself or from subsequent erosion at Earth's surface, loss of radiogenic lead, Pb*, has been suggested as an alternative method to date the event. Pb*-loss was investigated from target rocks from Vredefort and Morokweng and suggests that Pb* diffusion, even in zircon isolated from shocked and brecciated target rocks, is remarkably slow. This may explain the seeming lack of 'reset' zircon in terrestrial impactites. Little is known about Pb* diffusion pathways associated with shock microstructures introduced during impact cratering and future diffusion studies may provide better constraints on this problem.

Although little disturbance was identified in Pb* of target zircon, other low temperature geochronometers, zircon (U-Th)/He dating in this case, have been shown to be completely 'reset' and accurately date impacts. Zircon (U-Th)/He ages isolated from the target rock below ~850 m of well-dated impact melt at Morokweng yield ages consistent with the impact melt sheet and provide an alternative tool to dating events where such melts no longer exists. This geochronometer was also applied to impactites from Popigai, Russia and results in an age that is significantly younger than that reported in the literature and coincident with the Eocene-Oligocene boundary mass extinction event however the lack of any impact signatures at this boundary is puzzling.

Constraining the impact flux to the Earth-Moon system not only allows for a better understanding into early Earth evolution and the formation of a habitable planet but also provides

constraints on the modern impactor flux, important criteria for estimating the likelihood of future impact events. Zircon geochronology offers an exciting new tool by which to date impact events and has the potential to assist understanding of complex impactite samples from terrestrial craters and future sample return missions.

The dissertation of Matthew M. Wielicki is approved

David A. Kring

Brad Hansen

Axel K. Schmitt

Kevin D. McKeegan

T. Mark Harrison, Committee Chair

University of California, Los Angeles

2014

This thesis is dedicated to my family, Anna, Tomasz, and Tommie, and my beautiful wife, Michelle, for their love and support and most of all patience during the completion of my graduate career. Thank you and I love you all.

Table of contents

Abstract ii
Committee Page vi
Dedication vii
Table of Contents viii
Acknowledgments xiv
Vita xvi
1. Introduction 1
1.1 Introduction to terrestrial impacts 1
1.2 Zircon geochronology 3
1.2.1 Introduction to zircon 3
1.2.2 Zircon and early Earth 3
1.2.3 Zircon impact geochronology 4
1.3 Impact cratering, morphology and melt production 5
1.3.1 Impact cratering processes 5
1.3.2 Impact geomorphology 7
1.3.3 Impact melt production 8
1.4 Impact flux through time 8
1.4.1 Impacts on early Earth 8
1.4.2 Constraining the impact flux with 'late veneer' 10
1.5 Zircon as a recorder of impact events 11
1.5.1 Neoformed zircon in impact melt sheets 11
1.5.2 Partially and completely 'reset' zircon 12
1.6 Conclusion 12
1.6 Figures and Tables 13
1.6.1 Figure 1.1 14
1.6.2 Figure 1.2 14
1.6.3 Figure 1.3 15
1.6.4 Figure 1.4 16
1.6.5 Figure 1.5 17

1.6.6 Figure 1.6 18
1.6.7 Table 1.1 19
2. Terrestrial impact zircon 19
2.1 Introduction 19
2.2 Terrestrial impacts sampled 21
2.2.1 Vredefort impact structure, South Africa 21
2.2.2 Morokweng impact structure, South Africa 23
2.2.3 Sudbury impact structure, Canada 23
2.2.4 Manicouagan impact structure, Canada 25
2.2.5 Popigai impact structure, Russia 25
2.3 Methods 26
2.3.2 Imaging of zircon 27
2.3.3 Ion microprobe (U-Pb, Trace elements) 27
2.3.3 Ion microprobe (Oxygen isotopes) 28
2.4 Results 28
2.4.1 SEM imaging and textural analysis 28
2.4.2 U-Pb Geochronology 29
2.4.3 Ti-in-zircon thermometry 31
2.4.4 Oxygen isotopes 34
2.4.5 Trace elements 34
2.5 Discussion 35
2.5.1 U-Pb geochronology 35
2.5.2 Ti-in-zircon thermometry 36
2.5.3 Trace elements 37
2.6 Conclusion 37
2.7 Figures 39
2.7.1 Fig. 2.1 39
2.7.2 Fig. 2.2 40
2.7.3 Fig. 2.3 41
2.7.4 Fig. 2.4 42

2.7.5 Fig. 2.5 43
2.7.6 Fig. 2.6 44
2.7.7 Fig. 2.7 46
2.7.8 Fig. 2.8 47
2.7.9 Fig. 2.9 48
2.7.10 Fig. 2.10 50
2.7.11 Fig. 2.11 50
3. Modeling zircon crystallization in simulated impact melts 51
3.1 Introduction 51
3.2 Zircon saturation and 'M' 52
3.3 Ti-in-zircon crystallization temperature vs. bulk saturation temperature 53
3.3.1 Vredefort impact structure, South Africa 53
3.3.2 Morokweng impact structure, South Africa 53
3.3.2 Sudbury impact structure, Canada 53
3.3.3 Manicouagan impact structure, Canada 54
3.4 Zircon saturation model for simulated LHB event 54
3.5 Results 57
3.5.1 Zircon saturation vs. Impact zircon $\boldsymbol{Tzirxtln}$ 57
3.5.2 Impacts modeled on modern terrestrial target 58
3.5.3 Impacts modeled on ancient terrestrial target 58
3.5.4 Impacts modeled on lunar target 59
3.5.5 Impacts modeled on Martian target 60
3.6 Discussion 60
3.7 Conclusion 62
3.8 Figures 63
3.8.1 Figure 3.1 63
3.8.2 Figure 3.2 64
3.8.3 Figure 3.3 67
3.8.4 Figure 3.4 68
3.8.5 Figure 3.5 69

3.8.6 Figure 3.6 69
3.8.7 Figure 3.7 70
4. Investigating Pb*-loss in impact zircon 71
4.1 Introduction to Pb*-diffusion in zircon 71
4.2 Reports of 'reset' zircon in terrestrial l impactites 71
4.2.1 Vredefort impact structure, South Africa 72
4.2.2 Cretaceous ejecta 72
4.2.3 Modeled Pb* diffusion in impact zircon 72
4.3 Samples 73
4.3.1 Vredefort granophyre and pseudotachylite breccia 73
4.3.2 Morokweng basement zircon 74
4.3.3 Popigai suevite and shocked gneiss 76
4.3.4 Sudbury breccia and Onapping formation 76
4.4 Methods 76
4.4.1 Multi-spot analysis 77
4.4.2 U-Pb depth profile 77
4.5 Results 78
4.5.1 Vredefort impactites 78
4.5.2 Morokweng basement 79
4.5.3 Popigai impactites 80
4.5.4 Sudbury impactites 80
4.6 Discussion 80
4.7 Conclusion 82
4.8 Figures 83
4.8.1 Figure 4.1 83
4.8.2 Figure 4.2 85
4.8.3 Figure 4.3 86
4.8.4 Figure 4.4 86
4.8.5 Figure 4.5 87
4.8.6 Figure 4.6 88

4.8.7 Figure 4.7 89
4.8.8 Figure 4.8 90
4.8.9 Figure 4.9 92
4.8.9 Figure 4.9 92
5. Zircon (U-Th)/He ages of terrestrial craters 93
5.1 Introduction 93
5.2 Background 94
5.3 Samples 95
5.3.1 Morokweng impact structure, South Africa 95
5.3.2 Vredefort impact structure, South Africa 96
5.3.3 Popigai impact structure, Russia 97
5.4 (U-Th)/He dating method 97
5.5 Results 98
5.5.1 Morokweng impact structure, South Africa 98
5.5.2Vredefort impact structure, South Africa 99
5.5.3Popigai impact structure, Russia 99
5.6 Discussion 100
5.6.1 Evaluating zircon (U-Th)/He dating of terrestrial impacts 100
5.6.2 Implications of new Popigai age 101
5.7 Conclusion 105
5.8 Tables and Figures 106
5.8.1 Figure 5.1 107
5.8.2 Figure 5.2 108
5.8.3 Figure 5.3 108
5.8.4 Figure 5.4 110
5.8.5 Figure 5.5 110
6. Conclusions and Future work 111
6.1 Geochemical signatures of impact produced zircon 111
6.2 Modeling zircon formation in simulated impacts 111
6.3 Pb*-loss in zircon from shocked impactites 112

6.4 (U-Th)/He dating of zircon from terrestrial impactites 113
6.5 Future work..... 114
6.5.1 Pb* diffusion within naturally and experimentally shocked zircon to assess the effects of different shock microstructures..... 114
6.5.2 Zircon geochronology of unconstrained terrestrial craters to better asses cratering rate and correlation with mass extinctions and global change. 114
6.5.3 Further modeling of zircon crystallization in response to impact melting as site selection criteria for future sample return missions. 115
6.6 Summary..... 115
7. Appendices..... 116
7.1 Appendix 1 116
7.2 Appendix 2 124
7.3 Appendix 3 129
7.4 Appendix 4 134
7.5 Appendix 5 145
8.6 Appendix 6 162
7.7 Appendix 7 170
8. References..... 173

Acknowledgments

Numerous people have helped me during my graduate career. First and foremost is my advisor Mark Harrison who has mentored me throughout my time at UCLA not only in geochemistry, but also in life at an academic institution. His knowledge of geochemistry and in particular zircon geochronology has been invaluable to my dissertation. Mark allowed me to develop my own project, not what we originally discussed when I arrived at UCLA, while also pushing me into other fields such as experimental petrology. I will always be grateful for the hours we spent carefully reviewing my papers and proposals, as painful as it may have been at the beginning for both of us, which has greatly improved my scientific writing ability. He exposed me to grant writing and the nuance of external funding which I hope to apply in funding my future research career. Mark was not only a mentor in the class room and lab but also in the field. We had the wonderful opportunities to travel to Western Australia and sample the Jack Hills as well as spend time in Tibet working on the evolution of the Tibetan Plateau.

The UCLA SIMS group has also been a source of constant support during my research at UCLA. The ion microprobe is a difficult instrument to master and there was not a day that went by that I did not rely on the expertise of Kevin McKeegan, Axel Schmitt and/or Rita Economos during my data collection. From simple questions about tuning the instrument to reducing the data afterwards, they were always available during my research. Also deserving of thanks are my office mates and colleagues, particularly Beth Ann Bell and Patrick Boehnke, for putting up with me and some of my crazy ideas for the last six years. We always supported each other, from reading drafts to attending talks at conferences, and I hope that our relationships evolve from graduate colleagues to research colleagues and co-investigators in the future. I would also like to thank Brad Hansen, astronomy at UCLA, for agreeing, with very short notice, to being the

outside department member for my committee and reviewing my dissertation from an astronomical view point.

Outside of UCLA I have also received guidance and support from multiple people. David Kring, from the Lunar and Planetary Institute, has provided an expertise in impact research that was not present at UCLA. He has greatly increased my knowledge of the impact cratering processes and the history of impact research. Along with Gordon Osinski, from Western Ontario University, David has provided me the opportunity to spend weeks of field research at Sudbury and Meteor Craters. This field work has been very important in my understanding of complex impact structures and impactite samples. I would also like to thank the people who provided impactite samples for this work including: Marco Andreoli, Roger Gibson, Uwe Reimold, Don Davis, Sandra Kamo, Doreen Ames, John Spray, Victor Masaitis, and Boris Burakov. Without their generous support this work would not have been possible. Also I would like to acknowledge Danny Stockli, from UT-Austin, has allowed me the opportunity to develop zircon (U-Th)/He chronology for dating impact structures within his lab and has been a source of advice and support over the last couple of years.

Finally I would like to acknowledge the wonderful staff at UCLA that has always provided me with wonderful advice and support. From travel grants, reimbursements, and payroll to filing this dissertation the staff of the Department of Earth, Planetary, and Space Sciences were wonderful to deal with and have my up most appreciation.

Vita

EDUCATION

UC Los Angeles - Los Angeles, CA — Graduation: 06/2013
M.S. Geochemistry — Overall GPA: 3.80

UC San Diego - San Diego, CA — Graduation: 06/2001
B.S. Biochemistry and Cellular Biology — Overall GPA: 3.00

PUBLICATIONS

Wielicki, M.M., Stockli, D., Harrison, T.M., 2014. Popigai impact and association with Eocene-Oligocene boundary mass extinction. Proceedings of the National Academy of Sciences, submitted.

Wielicki, M.M., Harrison T.M., 2014. Zircon formation in lunar impact melts: Complications for deciphering planetary impact histories. GSA Special Paper. Large Meteorite Impacts and Planetary Evolution V. submitted.

Wielicki, M.M., Harrison, T.M., Stockli, D., 2014. Dating terrestrial impact structures: U-Pb depth profiles and (U-Th)/He ages of zircon. Geophysical Research Letters 41, 4168-4175.

Wielicki, M.M., Harrison, T.M., Schmitt, A.K., 2012. Geochemical signatures and magmatic stability of terrestrial impact produced zircon. Earth and Planetary Science Letters 321-322, 20-31.

INVITED PRESENTATIONS

Wielicki, M.M., Stockli, D., Harrison, T.M., 2014, Zircon (U-Th)/He dating of terrestrial impact structures. 2nd ELSI International Symposium, Tokyo, Japan.

Wielicki, M. M., Harrison, T. M., 2013. Impacts and Life: New Methods for Identifying Ancient Terrestrial Cratering Events. GSC-GSA Joint Meeting, Chengdu, China.

ABSTRACTS AND PRESENTATIONS

Wielicki, M. M., Harrison, T. M., 2013. Sieve textures in impact zircon from Vredefort, South Africa: Implications to impact geochronology. 23rd V.M. Goldschmidt Conference, abstract #6031.

Wielicki, M. M., Harrison, T. M., 2012. Experimental Calibration of a Microscale White Mica Barometer. American Geophysical Union, abstract #V51B-2788.

Prescher, C.,Allupeddinti, D., Bell, E. A., Bello, L., Černok, A., Ghosh, N., Tucker, J. M., Wielicki, M. M., Zahnle, K., 2012. Origin and Mixing Timescale of Earth's Late Veneer. American Geophysical Union, abstract #V51B-2775.

Wielicki, M.M., Harrison, T.M., Boehnke, P., Abramov, O., 2012. Zircon as a Probe of Planetary Impact History. 22nd V.M. Goldschmidt Conference, abstract #3334.

Wielicki, M.M., Harrison, T.M., Schmitt, A.K., 2012. Geochemical Signatures and Magmatic Stability of Impact Produced Zircon. Earth and Planetary Science Letters 321-322, 20-31.

Wielicki, M.M., Harrison, T.M., 2011. Ti-in-Zircon Thermometry and Trace Element Geochemistry of Impact Produced Zircons: Implications for Hadean Zircons. 42nd Lunar and Planetary Science Conference: abstract #2346.

Wielicki, M.M., Harrison, T.M., 2011. Habitability of the Hadean Earth: Implications from terrestrial impact produced zircon. UHNIA/Nordic Astrobiology Winter School. University of Hawaii.

Wielicki, M.M., Harrison, T.M., 2010. The Late Heavy Bombardment and the Habitability of the Hadean Earth. Astrobiology Graduate Conference 2010. Tallberg, Sweden.

Bell, E.A., Wielicki, M.M., Abbott, S.S., Mojzsis, S.J., Harrison, T.M., 2009. Do the Jack Hills zircons record evidence of the Late Heavy Bombardment? American Geophysical Union: abstract #V13C-2041.

Wielicki, M.M., Lu, X., Bell, E.A., Schmitt, A.K., Harrison, T.M., 2008. Are there impact-formed zircons in the Hadean record? American Geophysical Union: abstract #V12B-01.

RELATED WORK AND TEACHING EXPERIENCE

GameDesk Inc.

Geosciences consultant (2012 - present)

- Provide geosciences consultation for the development of GeoMoto, a K-12 science education game platform supported by the NSF.

UC, Los Angeles – Los Angeles, CA

Graduate Teaching Assistant (Aug. 2008 – Present)

- Develop and manage lab activities with lecture instructors for undergraduate courses offered within the ESS department.

- Currently TA'ed for: ESS 3 (Astrobiology), ESS 8 (Earthquakes), ESS 116 (Paleontology), ESS 16 (Major Events in the History of Life), ESS 101 (Earths Energy and Environment).

State Center Community College District – Willow International Center – Clovis, CA

Adjunct Professor (Jan. 2007 – Aug. 2008)

- Instructor of Geology 9 'Intro to Earth Science' and Geography 9 'Intro to Physical Geography' courses at local community college.
- Develop lecture information and lab activities to meet CA state requirements for geology and geography at the community college level.
- Create a fun and challenging learning environment for non-science majors through demanding exercises and individual attention

HONORS AND ACTIVITIES

- The Nininger Meteorite Award Honorable Mention - ASU and Center for Meteoritic Studies (2011)
- TA Award (2010, 2011) – UC, Los Angeles
- Vice-president of events (2008-2010) – UC, Los Angeles - Earth and Space Science Student Organization
- Eugene M. Shoemaker Impact Cratering Award (2009) – Geological Society of America

PROFESSIONAL AFFILIATIONS

- American Geophysical Union member (2008-present)
- Meteoritical Society member (2010-present)
- Geochemical Society member (2010-present)

1. Introduction

1.1 Introduction to terrestrial impacts

Since the discovery of meteorites near Meteor Crater in northern Arizona by Albert Foote, and further expeditions by Daniel Barringer in the early 1900's, hypothesis of a meteoritic origin existed. Although meteorite falls had been known for centuries, the recognition of coesite and stishovite, both high-pressure polymorphs of quartz and evidence of high shock pressure, by Eugene Shoemaker in 1960 as impact minerals and their presence at Meteor Crater was the first evidence that asteroids and comets can produce craters at the Earth's surface and thus opened up a new field of scientific research. The intensity of bombardment on Earth has implications for the chemical and thermal evolution, and the habitability of the planet. Although implicated in later mass extinction events (Hildebrand et al., 1991), impactors on early Earth may have played a vital role in the emergence of a habitable planet: 1) a giant impact is believed to have formed the Moon (Canup and Asphaug, 2001); 2) impacts are thought to have significantly affected the early atmosphere through erosion and/or blow-off (Ahrens, 1993); 3) spikes in bolide flux, like that hypothesized at ~3.9 Ga known as the Late Heavy Bombardement (LHB; Turner et al., 1973), are believed to produce thermophilic niches (Abramov and Mojzsis, 2009), thought to be at the root of the tree of life (Pace, 1997); 4) numerous biotic precursor molecules found in carbonaceous chondrites (Cronin and Pizzarello, 1983) suggests that such vital molecules may also have been delivered via impacts; 5) finally, impacts may have re-introduced volatiles such as H_2O, thought to have been driven off during planetary accretion, necessary for the emergence of life (Alexander et al., 2012).

Although impacts may have been vital in the emergence of a habitable Earth, their role subsequently has been primarily as life frustrators (Table 1.1; Kring, 2003). They are believed to have lead to the extinction of the dinosaurs in the Cretaceous-Paleogene (K-Pg) extinction event at ~65 Ma, thought to have been caused by the Chicxulub impact in Yucatan, Mexico (Hildebrand et al., 1991), as well as the lesser known Jurassic-Cretaceous (J-K) extinction at ~145 Ma, thought to be caused by the Morokweng impact event, South Africa (Hart et al., 1997). Although many extinction events have not been correlated with an impact, particularly the largest mass extinction event at ~250 Ma, known as the Permian-Triassic extinction (Erwin, 2000), this is possibly due to the lack of tools to accurately identify and date ancient impact structure on Earth.

The work presented here attempts to develop techniques by which impact events can be accurately dated from complex impactite samples, tools that can be applied to investigating possible terrestrial impact craters to further assess the role of impacts on the global climate and biosphere. Alternatively, future sample return missions have been planned by multiple space agencies and will certainly sample impactites, as impact processes are the most common surficial processes on air-less bodies; Thus developing the tools that allow scientists to decipher the complex histories of these samples is essential if we are to fully exploit these technologically difficult missions. The focus of this study is on developing zircon as a probe of planetary impact history with the goal to further constrain the early impact history of the Earth-Moon system and to better understand the modern day bolide flux.

1.2 Zircon geochronology

1.2.1 Introduction to zircon

Zircon ($ZrSiO_4$) occurs as a common accessory mineral in a variety of rock types and geologic environments, including terrestrial impactites. It is widely used for geochemical and isotopic studies because of its capacity to retain trace elements, including actinides, lanthanides and radiogenic daughter products under high pressure and temperature, and intense geologic conditions. The preferential incorporation of U and Th into zircon coupled with its highly refractory nature, often surviving multiple geologic cycles, has made zircon a premier terrestrial geochronometer (Figure 1.1; Finch and Hanchar, 2003).

1.2.2 Zircon and early Earth

Hadean zircon crystals may preserve environmental information regarding their formation, thus provide a rare window into conditions on early Earth, where little to no rock record exists and when it is believed to be punctuated by intense bombardment. The long-standing, popular conception that the near-surface Hadean Earth was an uninhabitable, hellish world (Kaula, 1979; Wetherill, 1980; Solomon, 1980) has been challenged by the discovery (Froude et al., 1983; Compston and Pigeon, 1986) and geochemical characterization (see review in Harrison, 2009) of >4 Ga zircon grains from Mt. Narryer and Jack Hills, Western Australia. Isotopic and petrologic analyses of these ancient grains have been interpreted to suggest that early Earth was more habitable than previously envisioned, with water oceans, continental crust, and possibly even plate tectonics (Figure 1.2; Harrison, 2009; Hopkins et al., 2010).

1.2.3 Zircon impact geochronology

The early Earth is also believed to be dominated by intense bombardment. As little to no rock record exists from the Hadean, terrestrial evidence for early impacts has primarily been identified in these ancient zircons (Figure 1.3). Trail et al., (2007) documented epitaxial over-growth rims coincident with the hypothesized LHB impactor flux. Furthermore Abbott et al., (2012) identified similar aged rims with elevated Ti-in-zircon crystallization temperatures (Watson and Harrison, 2005a), consistent with those modeled for large impacts on an ancient crustal surface (Wielicki et al., 2012b). Finally, investigations of grains at the Hadean-Eoarchean transition yields a population of grains that appear to have undergone transgressive recrystallization (Hoskins and Black, 2000), possibly related to the LHB. With the lack of rock record from this time period, zircons may provide our only record impactor flux on the early Earth.

Because the early bombardment history of Earth has been all but erased, the lunar surface is widely seen as retaining the best impact record in the solar system (Fassett and Minton, 2013) and its study is given the highest priority for future lunar scientific exploration (Paulikas et al., 2007). Recent studies have focused on U-Pb geochronology in lunar zircon as a new tool with which to identify ancient large scale impact events from Apollo samples and lunar meteorites (Figure 1.3; Gnos et al., 2004; Pidgeon et al., 2007; Pidgeon et al., 2010; Norman and Nemchin, 2014), however little is known about zircon crystallization or the behavior of radiogenic elements in response to impact events, information that is crucial if we are to use these grains as accurate recorders of past impact events. Zr-saturation in simulated impact events on the lunar surface is explored in this study to distinguish between impact produced gains, which can be

used to date the event, and endogenic zircon likely inherited from the target with little information regarding the timing of the impact.

Many well-preserved terrestrial impact sites have now been dated using U-Pb geochronology of impact produced zircon (e.g., Krogh and Kamo, 1993; Kamo et al., 1996; Hart et al., 1997; Moser et al., 2011; Wielicki et al., 2012). Although low energy impacts do not produce thick melt sheets, those that result in widespread shock melting of the crust (Grieve et al. 2006) should persist over time-scales sufficient for crystallization of zircon, provided target rock composition and Zr-content are conducive to zircon formation, with dimensions of >10 μm permitting geochemical and geochronological analysis. Such information could provide a baseline for understanding the geochemical signatures of impact produced zircon and permit comparison with the other zircon populations, such as the Hadean zircon record (see review in Harrison, 2009), to assess whether the zircons formed in impact environments. Although zircon has been used with much success in large differentiated impact melt sheets (Krogh et al., 1984), in many terrestrial craters such melt sheets do not exist, either due to erosion or lack of impact energy in melting the target, thus, other lower temperature zircon chronometers, particularly (U-Th)/He, are also explored to accurately date these impactites.

1.3 Impact cratering, morphology and melt production

1.3.1 Impact cratering processes

The impact cratering processes can be sud-divided into three stages: contact and compression (either with the atmosphere or surface), excavation, and collapse. Although these stages are not discreet they are all dominated by different physical processes (Melosh, 1989). As few documented account of witnessed impact events exist, much of what we know about impact

cratering processes comes from the mechanics of nuclear explosions (French, 1966), hydrocode simulations of impact scenarios (Collins, 2002) and/or experiments conducted on large scale multi-stage gas guns (Schultz and Gault, 1985). Although each method has its short-comings the combination of these has provided a large wealth of knowledge about the processes occurring within large impact events and provides a basis for understanding how the rocks and minerals will respond to these dramatic effects.

As a high velocity projectile enters the atmosphere it transfers some of its kinetic energy to the atmosphere and heats and compresses the gas in front of the projectile. The deceleration and stresses encountered at this stage can lead to the thermal destruction of the projectile as witnessed in the Tunguska (Chyba et al., 1993) and Chelyabinsk (Brown et al., 2013) fireballs in 1908 and 2013, respectively, as well as the creation of a blast wave (Ivanov, 1991). Although these are high energy events capable of dramatic effects, they do not appear to leave a traceable signal, such as a crater or impact melt, thus, are very difficult to identify in the geologic record.

Larger or more coherent objects will pass through the atmosphere and strike the surface of the target at velocities comparable to that of the escape velocity of the target body (i.e. Earth escape velocity = 11.2 km/s; average estimated impact velocity = 17 km/s). At the point of contact two compression shock waves are generated and propagate into the impactor as well as the target (Figure 1.4A). This causes pressures in excess of hundreds of gigapascals and temperatures that exceed 10,000 K (Collins et al., 2012). Following this compression, rarefaction (release) waves propagate inward dropping the pressure, along a near-adiabatic path, and the temperature however in many cases temperatures remain high enough to leave the material molten or vaporized. Much of the kinetic energy is transferred into the thermal and

internal energy of the target material, while residual kinetic energy is used in displacing and ejecting material to form the transient crater (Melosh, 1989). The excavation stage is a result of the imparted residual velocity which works to excavate material in a hemispherical path, resulting in a deep bowl at the surface many times larger than the impactor (Figure 1.4B&C). This unstable surface geomorphology quickly begins to collapse in a gravity-driven modification of the crater walls to form the final simple or complex crater (Figure 1.4D; Dence, 1964).

1.3.2 Impact geomorphology

Simple craters, formed by low-energy, small impactors, are circular, bowl-shaped depressions with raised rims and approximately parabolic interior profiles (Figure 1.5; Melosh, 1989). One example of a simple crater is that of Meteor Crater, Arizona, a 1.2 km in diameter bowl-shaped crater, where Eugene Shoemaker's identification of highly shocked minerals confirmed the presence of the first extraterrestrial impact crater on Earth (Shoemaker, 1963). Simple craters are widely distributed within the solar system and dominate surface features of small asteroids (Melosh and Ivanov, 1999).

Complex craters form when material collapses with such energy as to produce substantial uplift of the crater floor and underlying strata, resulting in much lower depth/diameter ratios (Figure 1.5; Melosh, 1989). This rising material may melt through decompression melting however this appears not to be the major source of melt production as much more heat is imparted from the shock wave. The maximum stratigraphic uplift is equivalent to approximately one-tenth of the final crater diameter (Melosh and Ivanov, 1999).

1.3.3 Impact melt production

Another aspect of impact cratering is the melting and vaporization of the target rocks, which is governed by the thermodynamics of shock compression and release (Pierazzo et al., 1997; Wünnemann et al., 2008). As experimental studies do not reach the velocity of impactors, hydrocode simulations have been used to model impact melt production. The melt and vapor produced is related to the energy of the impact event as well as the target composition and has major implications to the climatic and environmental consequences of an impact event (Pierazzo et al., 1997). Pierazzo et al. (1997) showed in their models that the melt volume scales approximately with the kinetic energy of the impactor ($\mu = 2/3$, energy scaling). However, Pierazzo and Melosh (2000) showed that in oblique impacts impact melt volume does not scale with impact energy. Bjorkman and Holsapple (1987) showed that at impact velocities greater than 50 km/s, melt volume scales in the same way as crater volume. The produced melt can either be ejected from the crater or remain within the crater to form an impact melt sheet. The production of an impact melt sheet also allows for the growth of dateable accessory minerals such as zircon, allowing for accurate determination of impact age. Production of melt can also provide the long lived thermal perturbations necessary to 'reset' accessory minerals, such as zircon, and accurately date the impact event.

1.4 Impact flux through time

1.4.1 Impacts on early Earth

The impact history of the early solar system remains controversial. Investigation of lunar samples returned during the Apollo missions, led to the 'Late Heavy Bombardment' (LHB) concept (Turner et al., 1973) which hypothesized a sharp increase in bolide flux at ~3.85 Ga.

Evidence for this cataclysm was first derived from whole-rock U-Pb and Rb-Sr ages (Tera et al., 1974; Turner et al., 1973) and has also relied on interpretations of ^{40}Ar-^{39}Ar lunar sample data (Apollo and lunar meteorites; Dalrymple and Ryder, 1993; Cohen et al., 2000) which can be challenging due to the presence of relic clasts, incomplete Ar outgassing, diffusive modification during shock and heating, and exposure to solar wind and cosmic rays (Harrison and Lovera, 2013).

Although the LHB concept remains popular, multiple other hypotheses of early bombardment history are gaining recognition, such as the multiple cataclysm (Tera et al., 1974) or 'saw-tooth pattern' hypotheses (Morbidelli et al., 2012). Recent zircon studies have suggested large scale impact events as early as 4.2 Ga (Norman and Nemchin, 2014), and a significantly older age for the Imbrium impact, typically the center of the LHB spike, of ~3.92 Ga (Liu et al., 2012). Zircons in both studies have been attributed to forming within an impact melt, thus recording the impact event, however no criteria have been established in determining an impact-formed zircon from an endogenic grain. Until such criteria exist it remains possible that these grains are merely dating lunar magmatism not associated with impacts.

Subsequent to this period of intense bombardment the impactor flux appears to have been relatively stable for the past ~3.6 Ga, with size-frequency distributions (SFD) very similar to that of the Main-Belt asteroids (Neukum et al., 2001). Although the impact flux appears relatively in steady state as compared to the early flux, smaller spikes have been reported in the literature and may greatly affect the flux at any one time period (Tera et al., 1974; Bottke et al., 2012). One major hurdle in understanding the long-term flux of impacts on Earth is identifying, usually heavily eroded, impact structures and accurately dating them. Due to planetary resurfacing and

the inherent difficulties in dating complex, impact-derived samples, fewer than 10% of all known craters can be regarded as accurately and precisely dated (Jourdan et al., 2012). We note that currently two-thirds of all impacts will strike the ocean basins, with evidence of a crater remaining until that portion of oceanic crust is subducted, on the order of a few hundred million years.

Establishing a better record of impacts through time provides a better understanding into the frequency of these events and may offer better constraints on global climate change and extinction events possibly associated with such impacts. It is not a matter of if but merely a matter of when another large impact event will occur on Earth and work done in understanding the environmental effects of impacts will be crucial in society's response to such an event.

1.4.2 Constraining the impact flux with 'late veneer'

The highly siderophile elements (HSE) should be highly depleted in Earth's silicate mantle because they partition into the metal that formed the core (Mann et al., 2012). However, the present HSE contents of Earth's mantle are ~3 orders of magnitude higher than that predicted by experimental work (Holzheid et al., 2000). This apparent over abundance of HSE and their roughly chondritic proportions within the mantle has commonly been explained by the addition of chondritic meteoritic material in a "late veneer", following core formation (Meisel et al., 1996).

If the late veneer is a direct result of impactor material delivered to Earth it may be possible to use the abundance of material added to infer the impact flux through time (Figure 1.6). The only present constraint on early impactor flux is the lunar cratering record which

remains controversial but appears to be dominated by early spikes, such as the LHB, in impactor flux followed by a relatively steady-state flux since ca. 3.6 Ga (Zahnle et al., 2007).

To further explore the flux of impactors on early Earth, we estimate the mass of PGE added during the LHB by scaling the lunar record for the increased gravitational cross-section of Earth (20-30x larger gravitational cross-section). Our results indicate that merely 0.2-0.3% of the mass necessary for the late veneer was added by the five largest LHB basins and only 1.8-2.7% when South Pole Aiken (SPA) is included as an LHB event, which appears not to be the case as the surface of SPA has been suggest to be much older (Head et al., 1993). We note that the lunar mantle has been shown to be significantly depleted in PGE (20x; Walker et al., 2004) possibly the result of the largest impactors, carrying significant amounts of PGE, simply missing the Moon and striking Earth. If we scale the mass added during the LHB for this apparent lunar depletion, our calculations still indicate that only ~4-6% of the mass needed for the 'late veneer' was delivered during the LHB (~35-55% if SPA included), suggesting the likelihood of other LHB-type events prior to ~4.0 Ga and arguing against the single cataclysm hypothesis, possibly for multiple episodes of increased impactor flux as proposed by Morbidelli et al., (2012).

1.5 Zircon as a recorder of impact events

Zircons can record impact events in a number of ways, such as growing within an impact melt sheet or can being completely or partially 'reset' by shock and thermal effects associated with an impacts, all of which can provide a good constraint on the age of the event.

1.5.1 Neoformed zircon in impact melt sheets

Thus far the most accurate impact ages come from large impact melt sheets that cool sufficiently slow as to grow recoverable zircons. Such grains have been used to date multiple

terrestrial craters where impact melt sheets exist (Davis, 2008; Wielicki et al., 2012b). Although these grains provide the best age determination the presence of large impact melt sheets requires large impact event, thus such grains tend to be rare in smaller impact with less melt production.

1.5.2 Partially and completely 'reset' zircon

When no neoformed zircons exist or if the presumed impact melt sheet has been eroded, zircons from the target may have had their isotopic systems affected by shock and heating during the impact. Shock microstructures have been proposed to allow for the rapid diffusion of Pb*, radiogenic lead, essentially 'resetting' the U-Pb clock of the zircon and dating the impact event (Moser et al., 2011; Abramov et al., 2013). Shock-damaged zircons, thought to be 'reset', within ejecta associated with the K-Pg boundary have also been reported (Krogh and Kamo, 1993). Although it has been proposed to occur regularly for Sudbury sized craters the relatively few 'reset' zircons identified in terrestrial impactites suggest that Pb* diffusion, even in shocked zircons, may be remarkably slow.

However, other geochronometers, with lower closure temperatures, may allow for this rapid 'resetting' as their daughter products are less retentive in zircon. One such chronometer is (U-Th)/He, characterized by a He closure temperature of ~180 °C (Wolfe and Stockli, 2010), and is further discussed in chapter 5.

1.6 Conclusion

The goal of this study is to develop the use of zircon as a probe of impact history for terrestrial samples, which can eventually also be applied to extraterrestrial samples. These techniques can help refine the terrestrial impact record and may provide better correlations between global climate change and impact events to assess their role in recent mass extinctions.

Zircon impact signatures can also be compared to other zircon populations, such as the Hadean Jack Hills population to evaluate the presence of impact related zircons and provide some insights into the early impact history of the Earth-Moon system. Finally as human space exploration grows and sample return missions become more feasible, techniques that allow for investigation of complex impactite samples will be of vital importance as impact cratering is the most common surficial process on many planetary bodies.

1.6 Figures and Tables

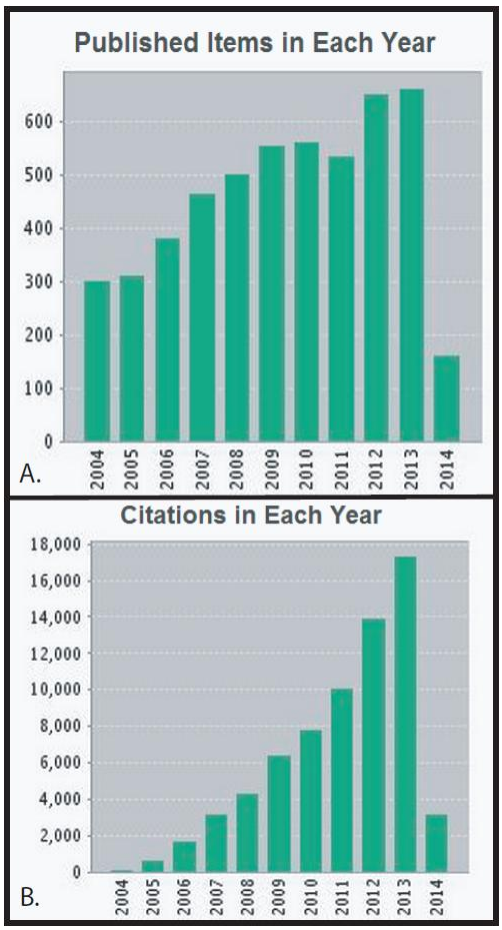

1.6.1 Figure 1.1

Web of science search for published items with zircon in the title (A) as well as number of citations of papers with zircon in the title (B) for the last decade ("Web of Science," 2014). Rise of zircon as the premier terrestrial geochronometer is reflected by the steady increase in published zircon work and the continued citation rate of this work by the earth science community.

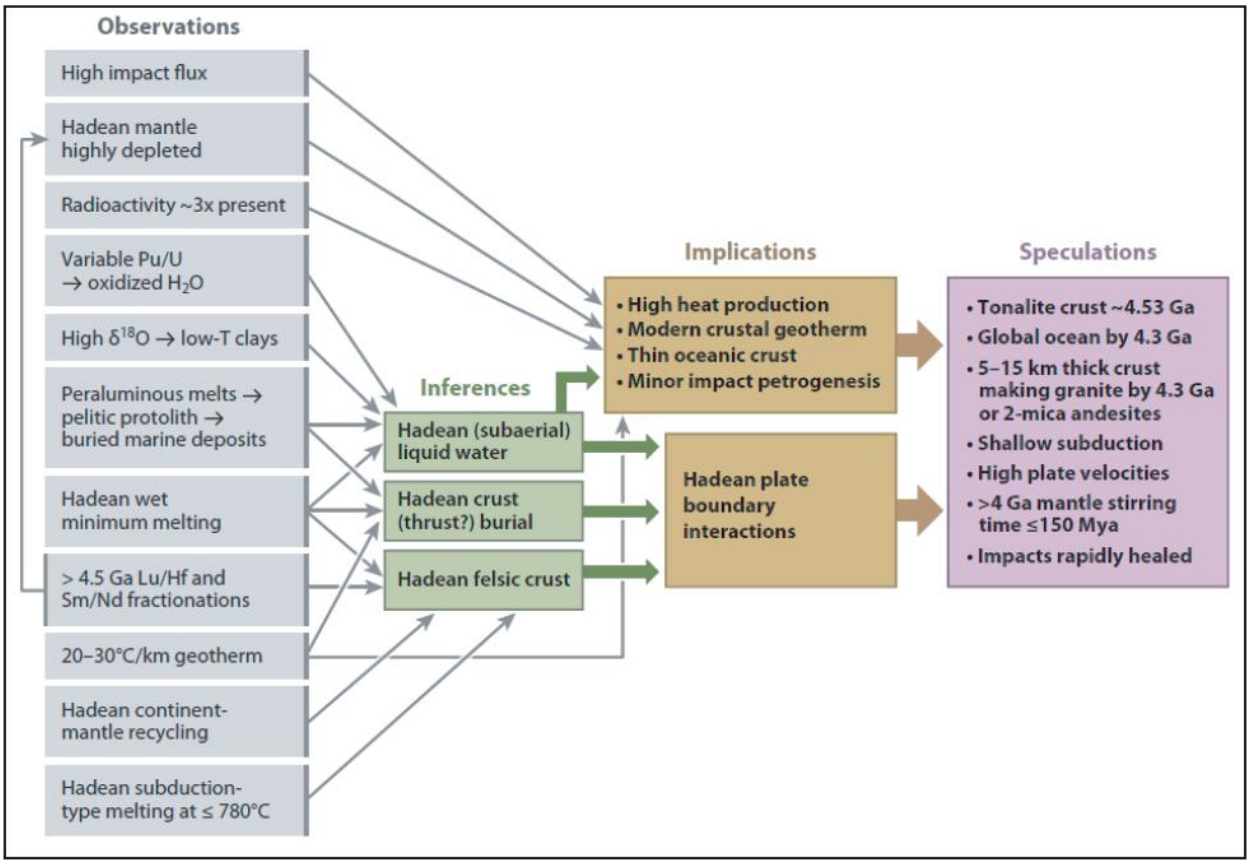

1.6.2 Figure 1.2

Flow chart showing observations (*gray*) derived from analytical and sample characterization studies of Hadean Jack Hills zircons. These data lead to the following three inferences: a Hadean hydrosphere, continental crust, and underthrusting. Together these suggest

the existence of Hadean plate boundary interactions. Speculations based on this possibility are shown in the purple box (Harrison, 2009).

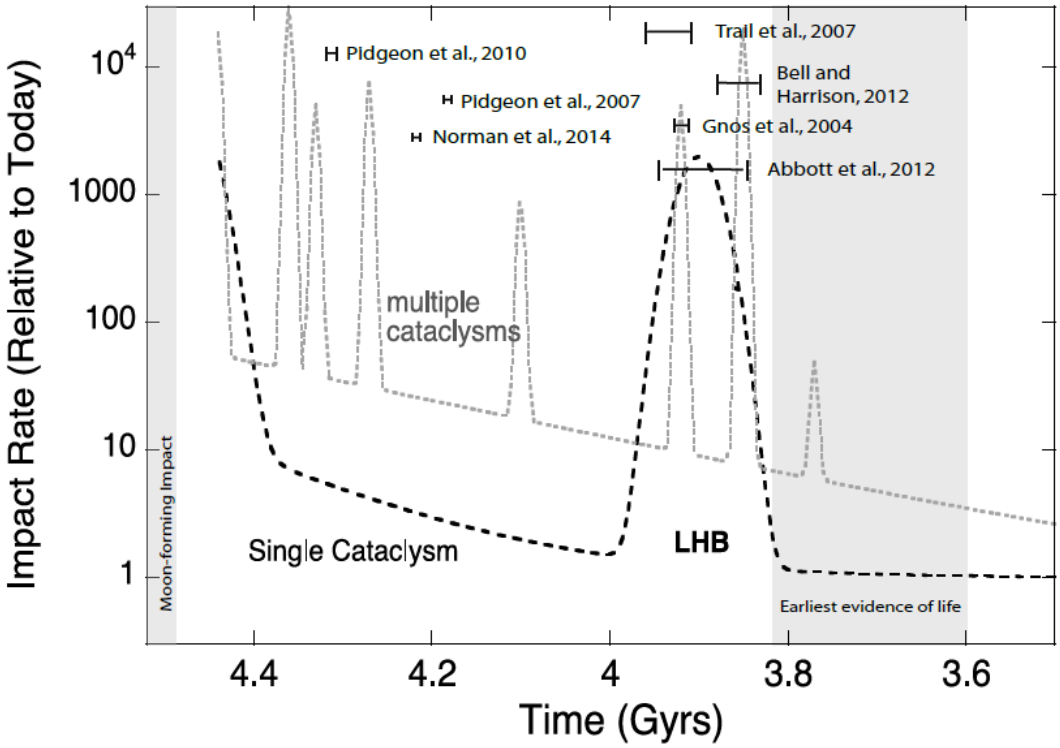

1.6.3 Figure 1.3

Concepts of the late lunar bombardment. The "single cataclysm" is a schematic but quantitatively representative of a late cataclysm (Ryder, 2002). "Multiple cataclysms" scatters several cataclysms over the Hadean (Tera et al., 1974; Morbidelli et al., 2012). Also shown are recent studies suggesting early impact events from terrestrial zircon (Trail et al., 2007a; Abbott et al., 2012; Bell and Harrison, 2013) as well as lunar grains (Gnos et al., 2004b; Pidgeon et al., 2007; Pidgeon et al., 2010; Norman and Nemchin, 2014) showing the recent rise of zircon as a probe of planetary impact history. Adopted from Zahnle et al., (2007).

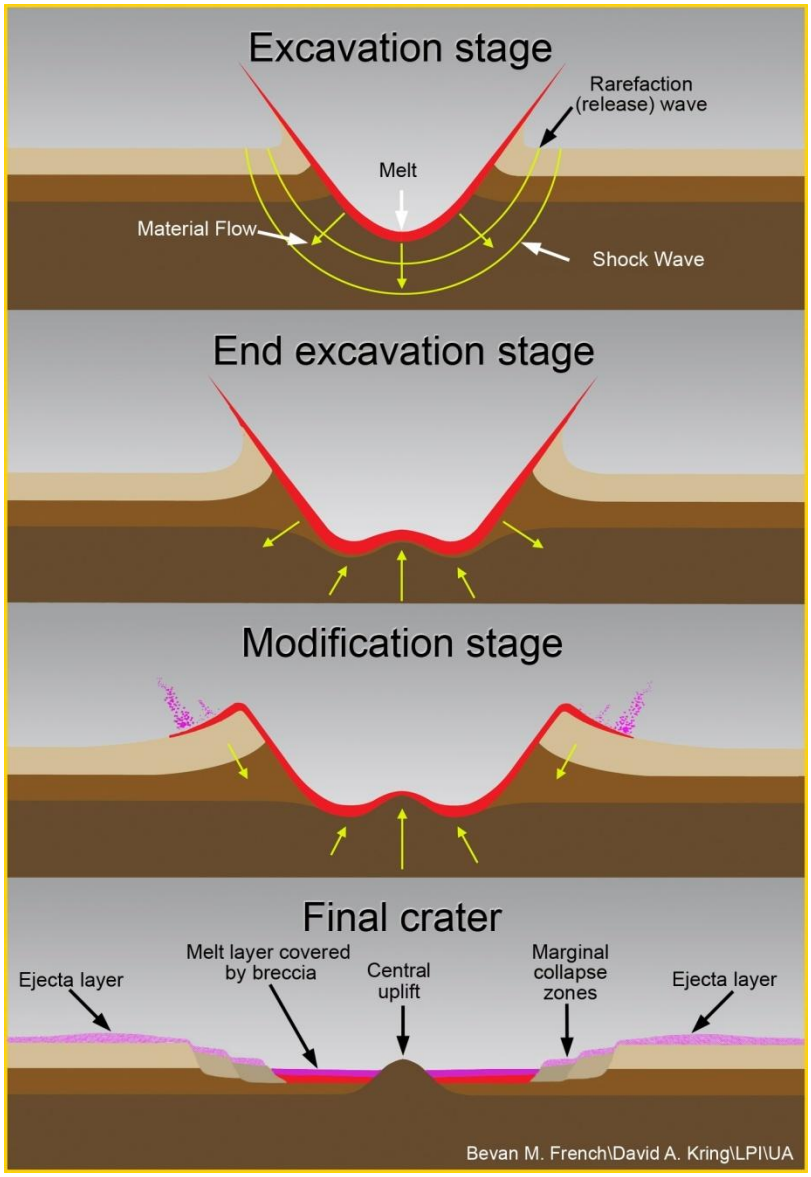

1.6.4 Figure 1.4

Schematic diagram showing the stages of impact cratering in the formation of a complex crater. Excavation stage (A) consists of the contact of the meteorite with the surface and the propagation of shock waves and rarefaction waves through the impactor and target. End of excavation stage (B) and the beginning of modification (B&C) through inward slumping of

crater walls and rebound of crater floor. Final structure (D) of a complex crater. Image credit : Greive (1990).

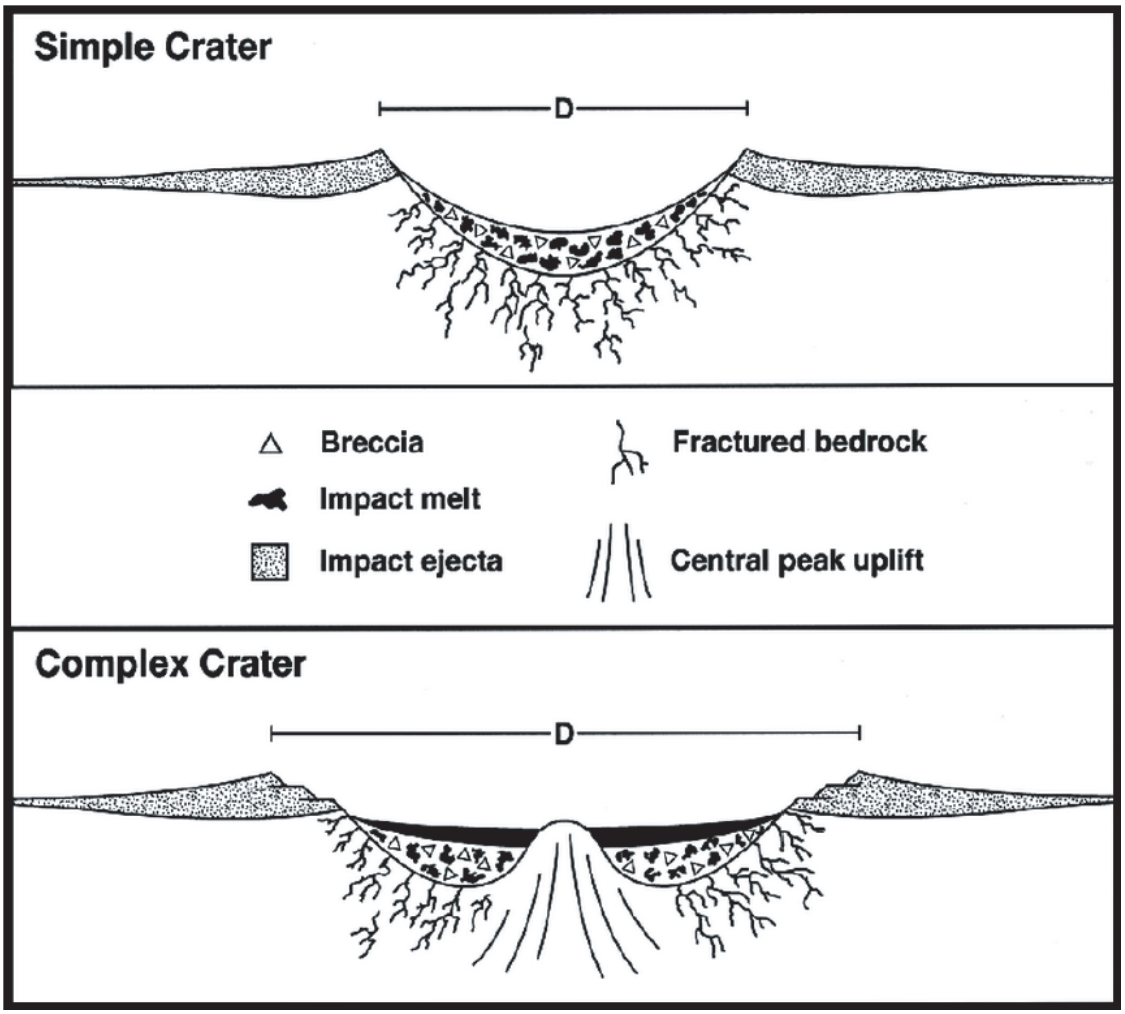

1.6.5 Figure 1.5

Schematic diagram of simple craters which are circular, bowl-shaped depressions with raised rims and approximately parabolic interior profiles and complex craters, which form when material collapses with such energy as to produce substantial uplift of the crater floor and underlying strata, resulting in much lower depth/diameter ratios. Image adopted from Kiefer, (2003).

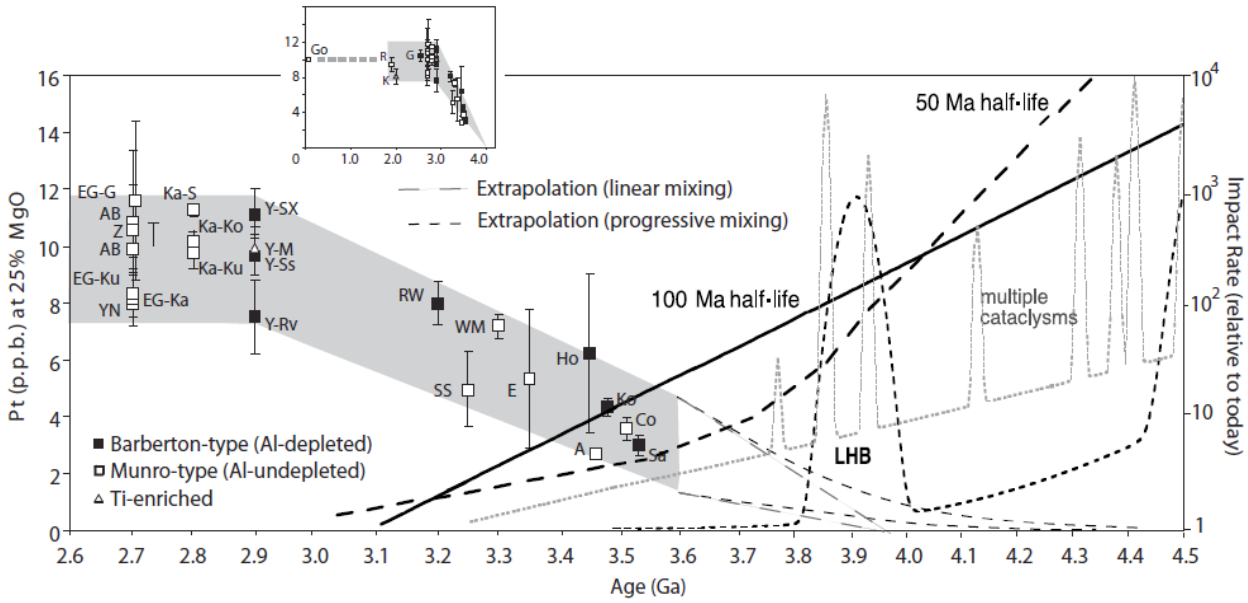

1.6.6 Figure 1.6

Pt versus age of komatiites along with concepts of bombardment history to show late in growth of presumably meteoritic PGE components. Data are normalized to 25% MgO. Data include those from Maier et al., (2009) and Barnes and Fiorentini (2008). EG, Eastern Goldfields superterrane (EG-G, Gindalbie terrane; EG-Ka, Kalgoorlie terrane; EG-Ku, Kurnalpi terrane). YN, Yilgarn North (Plutonic Marymia belt). Ka, Karelian terrane (Ka-Ko, Kostamuksha belt; Ka-Ku, Kuhmo belt; Ka-S, Sumozero-Kenozero belt). Y, Youanmi terrane (Y-M, Murchison domain; Y-Ss, Sandstone belt; Y-Rv, Ravensthorpe belt). RW, Ruth Well formation. SS, Sulphur Springs formation. WM, Weltevreden-Mendon formation. E, Euro basalt unit. A, Apex basalt unit. Ho, Hooggenoeg formation. Ko, Komati formation. Co, Coonterunah subgroup. Sa, Sandspruit formation. The inset shows additional data for Proterozoic komatiites (Go, Gorgona island; R, Raglan belt; K, Karasjok belt; G, Gawler craton). Error bars represent one standard error of the mean for each belt, except for suites with fewer

than five samples, in which error bars represent standard deviation. Figure adopted from Zahnle et al. (2007) and Maier et al. (2009).

Table 1 | The 'Big Five' mass extinction events

Event	Proposed causes
The Ordovician event ended, 443 Myr ago; within 3.3 to 1.9 Myr 57% of genera were lost, an estimated 86% of species.	Onset of alternating glacial and interglacial episodes; repeated marine transgressions and regressions. Uplift and weathering of the Appalachians affecting atmospheric and ocean chemistry. Sequestration of CO_2.
The Devonian event ended, 359 Myr ago; within 29 to 2 Myr 35% of genera were lost, an estimated 75% of species.	Global cooling (followed by global warming), possibly tied to the diversification of land plants, with associated weathering, paedogenesis, and the drawdown of global CO_2. Evidence for widespread deep-water anoxia and the spread of anoxic waters by transgressions. Timing and importance of bolide impacts still debated.
The Permian event ended, 251 Myr ago; within 2.8 Myr to 160 Kyr 56% of genera were lost, an estimated 96% of species.	Siberian volcanism. Global warming. Spread of deep marine anoxic waters. Elevated H_2S and CO_2 concentrations in both marine and terrestrial realms. Ocean acidification. Evidence for a bolide impact still debated.
The Triassic event ended, 200 Myr ago; within 8.3 Myr to 600 Kyr 47% of genera were lost, an estimated 80% of species.	Activity in the Central Atlantic Magmatic Province (CAMP) thought to have elevated atmospheric CO_2 levels, which increased global temperatures and led to a calcification crisis in the world oceans.
The Cretaceous event ended, 65 Myr ago; within 2.5 Myr to less than a year 40% of genera were lost, an estimated 76% of species.	A bolide impact in the Yucatán is thought to have led to a global cataclysm and caused rapid cooling. Preceding the impact, biota may have been declining owing to a variety of causes: Deccan volcanism contemporaneous with global warming; tectonic uplift altering biogeography and accelerating erosion, potentially contributing to ocean eutrophication and anoxic episodes. CO_2 spike just before extinction, drop during extinction.

Myr, million years. Kyr, thousand years.

1.6.7 Table 1.1

Table of the 'big five' mass extinction events and their proposed causes (adopted from Barnosky et al., 2011). Of the 'big five' only one, the Cretaceous event, has significant evidence to suggest bolide impact played a major role. Multiple minor extinction events have also been tied to impacts and are discussed further in the text.

2. Terrestrial impact zircon

2.1 Introduction

If zircon is to be as an accurate recorder of impact events we first need criteria with which to identify grains that grew within impact melt sheets, as opposed to endogenic or inherited zircons. In order to better understand the geochemical signatures of zircons grown within impact melts I have analyzed zircons from five large terrestrial impact craters: Vredefort

and Morokweng, South Africa; Sudbury and Manicouagan, Canada; and Popigai, Russia. As these are some of the largest known terrestrial craters the volume of melt production is sufficient as to grow neoformed zircons in the impact melt (Pierazzo et al., 1997). The search for ancient terrestrial impacts has largely focused on shock features in minerals or impact melt spherules (e.g., Glass and Simonson, 2012; Erickson et al., 2013). We are, however, unaware of any report of such shock features in zircon from Hadean or Archean detritus, possibly due to destruction of such grains in repeated rock cycles and thus focus our work on zircons grown within impact melts as these presumably have a better chance of survival until present day.

Although low energy impacts do not produce thick melt sheets, those that result in widespread shock melting of the crust (Grieve et al., 2006) should persist over time-scales sufficient for crystallization of zircon, provided target rock composition and Zr-content are conducive to zircon formation, with dimensions of >10 μm (Harrison and Watson, 1983; Watson, 1996) permitting geochemical and geochronological analysis. Many well-preserved terrestrial impact sites have now been dated using U-Pb geochronology of impact produced zircon (e.g., Krogh et al., 1984; Kamo et al., 1996; Moser, 1997; Hart et al., 1997; Wielicki et al., 2012), but using zircon to constrain the thermal (Watson and Harrison, 2005b; Ferry and Watson, 2007; Gibson et al., 1997) or compositional (Maas and Mcculloch, 1991; Grimes et al., 2007) evolution of impact melt sheet magmas is in its infancy.

In this chapter, I present U-Pb zircon geochronology, Ti-in-zircon thermometry, and trace-element geochemistry from multiple terrestrial impactites to develop criteria for deciphering impact formed zircon from endogenic zircon. These data reveal a limited range of formation conditions that strongly contrast with that documented for Hadean detrital zircon.

Such information could provide a baseline for understanding conditions on early Earth and permit comparison with the Hadean zircon record (see review in Harrison, 2009) to assess the hypothesis that Hadean detrital zircon formed in impact environments.

2.2 Terrestrial impacts sampled

2.2.1 Vredefort impact structure, South Africa

The Vredefort impact structure in South Africa is the largest known terrestrial impact site ("Earth Impact Database," 2014) and represents the deeply eroded remnant of an originally ~300 km wide crater (Reimold and Gibson, 1996). Although the main melt sheet has been eroded due to post-impact uplift, underlying pseudotachylite breccia and granophyre veins remain. U-Pb dating (isotope dilution thermal ionization mass spectrometry ID-TIMS) of zircon isolated from a 45cm pseudotachylite breccia vein at ~140 m depth within a borehole near the center of the remnant crater yield an impact age of 2023±4 Ma (Kamo et al., 1996). Similar analysis of zircon extracted from a syn- to post-impact norite dike also yield an age of 2019±2 Ma (Moser, 1997; Moser et al., 2011). The target rocks of the Vredefort impact were the 2.7-3.6 Ga Kaapvaal craton granite-greenstone terrane (Schmitz et al., 2004) and sediments and volcanics of the Witwatersrand basin.

I obtained zircon and whole rock samples of Vredefort impactite from three different sources: (1) pseudotachylite breccia collected near the quarry at Leeukop (provided by Mark Harrison), just west of Parys was used for mineral separation (VD_PB) as well as in-situ thin section analysis (VD_1A and VD_1B; Fig. 2.1); (2) granophyre (VD_G; Fig. 2.1) from the Kommandonek Nature Preserve (provided by Roger Gibson, University of Witwatersrand); and

(3) zircon from the INL borehole (VD_INL; Fig. 2.1) collected just south of the geographical center of the Vredefort Dome (provided by Sandra Kamo, University of Toronto).

Pseudotachylite breccia sample VD_PB consists of 1-3 cm clasts of Archean granite to granodioritic gneiss target material within a fine grained crystalline matrix (Reimold and Gibson, 2006). The separated zircon crystals (~35 grains isolated) range in length from 20 to 100 μm and exhibit igneous textures (i.e., elongate faceted faces, high axial ratio, pyramidal terminations; Corfu et al., 2003) and show no planar deformation features. Thin sections (VD_PB_1A and VD_PB_1B) were also imaged via SEM to identify zircon (~8 grains) within the melt fraction in-situ and avoid inherited grains associated with target rock clasts.

Granophyre sample VD_G consists of fine-grained crystalline quartz, plagioclase and alkali feldspar with long laths of hypersthene and small grains of magnetite (Reimold and Gibson, 2006). Zircon grains (~20 grains isolated) average ~100 μm and are fractured. Crystals lack igneous oscillatory zonation and are generally intimately intergrown with an Mg-rich pyroxene phase identified by energy dispersive X-ray analysis.

The INL borehole (VD_INL) sample was taken at 139.10 m depth, a few cm below the top contact of a ~45 cm wide intersection of pseudotachylitic breccia (Kamo et al., 1996). We obtained a zircon mineral separate of two optically distinct populations of zircon crystals (13 grains total): larger, dark, subrounded grains which appear to have younger overgrowths on old shocked grains and smaller, clear, multi-faceted grains that appear to represent new impact produced zircon.

2.2.2 Morokweng impact structure, South Africa

Morokweng impact structure, South Africa is a ~70 to 130-km-sized crater (Andreoli et al., 2008; "Earth Impact Database," 2014). Zircon and biotite from the ~450 m thick quartz norite poprtion of the impact melt sheet yield a concordant age of 145±0.8 Ma (U-Pb TIMS zircon age, 40Ar/39Ar biotite age; Hart et al., 1997), which is coincident with the minor mass extinction event at the Jurassic-Cretaceous boundary (Koeberl et al., 1997). Basement target rocks for the Morokweng impact structure are primarily Archean granitoids (~2.9-3.0 Ga; Poujol et al., 2002) and meta-volcanics (ca. 2.7 Ga Ventersdorp Lava; Koeberl and Reimold, 2003).

Drill core splits and crushed samples (provided by Marco Andreoli) were obtained from the M3 borehole drilled into the center of the aeromagnetic anomaly (Fig. 1; Hart et al., 2002). This drill hole intersects ~870 m of impact melt sheet consisting of differentiated granophyric to noritic rocks which overlay brecciated and shocked basement gneisses. Core splits from 155, 400, and 1069 m as well as crushed samples associated with the drilling processes from 156.5-157.98, 341.79-343.29, and 399.20 m were provided for this study. Zircon grains were separated from both the 156.5-157.98 and the 399.20 m crushed samples as well as the 1069 m target rock core split (MK_157; MK_399; MK_1069). Separated zircon crystals from both crushed samples (~35 grains from each of the 156.5-157.98 and 399.20 m) range in length from 20-80 μm while those separated from the 1069 m target rock core split tend to be larger, ranging from 50-120 μm, with both populations exhibiting igneous textures (Corfu et al., 2003).

2.2.3 Sudbury impact structure, Canada

The Sudbury Igneous Complex (SIC; ~250 km; Earth Impact Database, 2011) is a 2.5-3.0 km thick, elliptical igneous body with four major subunits from surface to base: granophyre,

quartz gabbro, norite, contact sublayer (Therriault et al., 2002). These units of the SIC is exposed predominatley in the northern and southern ranges of the crater. Zircon U-Pb results from the norite member yield an impact age of 1849.5±0.2 Ma (TIMS; Davis, 2008). Target rocks are a mix of Archean granite-greenstone terrains (~2.7 Ga; Krogh et al., 1996) with a small component of supracrustal Huronian rocks (Grieve, 1991).

Zircon mineral separates (provided by Don Davis) were obtained from both the mafic (SUD_ M) and felsic norite (SUD_ F) members (Fig. 2.3) along a transect of the southern exposed limb of the melt sheet (Lightfoot and Zotov, 2005). The mafic and felsic norites are sheets at the bottom of the 2.5 – 3.0 km thick SIC, directly above brecciated target rocks (Therriault et al., 2002) and consist of hypersthene and augite (~2:1), plagioclase, quartz, biotite, and Fe-Ti oxides (Darling et al., 2009). Separated zircon grains range from ~20 to >100 μm in length and show igneous textures, with those from the felsic norite being more euhedral. Some grains isolated from the mafic norite contain dark domains in SEM imaging that are characterized by high alkali and Fe contents and may reflect post-crystallization alteration (Abramov, 2004) and were avoided during analysis.

Samples analyzed from Sudbury were also collected during the 2012 Short Course and Field School under the auspices of NASA Lunar Science Institute and hosted by the Canadian Lunar Research Network. Samples of pseudotachylite breccia were collected approximately 2 km west of Windy Lake and 2-3 km from the edge of the Sudbury Igneous Complex (N42^{0}36.457', W81^{0}32.006') as well as samples of Onaping formation, which is presumed to suevite impact fallback and caps the SIC, collected within the crater (N46^{0}35.962', W81^{0}22.968'). Pseudotachylite breccia consists of subrounded target rock fragments set in a

dark, fine-grained to aphanitic matrix and show remarkable similarity to the rocks of the Vredefort Dome (Rousell et al., 2003). Grains isolated from the Sudbury pseudotachylite breccia show no direct evidence for shock features however large amounts of melt present in the rock suggest elevated temperatures and possible Pb-loss.

2.2.4 Manicouagan impact structure, Canada

The Manicouagan structure is a ~100 km impact crater in Quebec, Canada ("Earth Impact Database," 2014). Post-impact uplift (Spray and Thompson, 2008) resulted in exposure of a ~55-km-long island surrounded by an annular, ~5-km-wide lake. Zircon isolated from the upper portions of the melt sheet near the center of the uplift yield an age of 214±1 Ma (TIMS; Hodych and Dunning, 1992). The target rocks for the Manicouagan impact consist predominately of the Grenville province of the Canadian Shield ranging in age from 1.0-1.7 Ga (Cox et al., 1998).

Hand samples of Manicouagan from the main impact melt (MC_MM) near the base of the melt sheet on the west side of Memory Bay (provided by John Spray) are homogenous, medium-grained quartz monzodiorite showing only minor variations in major elements (O'Connell-Cooper and Spray, 2011; Fig. 1). Zircon crystals isolated (~40 grains) from the main melt sheet (to avoid inherited and altered grains possibly associated with cross cutting dykes) are 40-120 μm in length with prismatic elongations and pyramidal terminations indicative of an igneous origin (Corfu et al., 2003).

2.2.5 Popigai impact structure, Russia

The Popigai impact structure, Siberia, Russia, has an estimated crater diameter of ~100 km ("Earth Impact Database," 2014) and late-Eocene in age. Although an $^{40}Ar/^{39}Ar$ study of Popigai melt breccias yielded total degassing ages ranging from 33.6 to 38.3 Ma, the authors

interpreted ages within 60% of gas released from only one of twelve analyses to date the Popigai impact event at 35.7±0.2 Ma (2σ; Bottomley et al., 1997), however no zircon grains have been reported with this age.

Zircon were separated from a total of three hand samples: two hand samples of luecocratic to mesocratic gneiss (PG_7407w and PG_7407k; provided by Victor Masaitis of the A.P. Karpinsky Russian Geological Research Institute) documented to have reached shock stages from II-IV (Stoffler et al., 1991), and collected in the SW sector of the crater (approximate coordinates 71°30' N, 110°30' E) and a suevite sample collected along the Rassokha River in the northern sector of the crater (provided by Doreen Ames from Geological Survey of Canada). Zircon separated from three hand samples of shocked gneiss and suevite were subrounded, ovoid to multifaceted grains and range in size from 50-100 μm with no CL activity. Samples from Popigai are shocked target rocks with little to no impact melt and we predict no neoformed zircon to be present however believe these samples to be good candidates for Pb-loss and zircon (U-Th)/He dating.

2.3 Methods

Analysis of zircon was accomplished both in thin section and as separated grains. For all hand samples thin-sections were obtained and to assess zircon crystal size and abundance. Mineral separates were obtained from bulk rocks samples by standard heavy liquid separation procedures. Separated zircon crystals were handpicked and mounted in 1" diameter epoxy mounts together with AS3 zircon standard (Paces and Miller, 1993).

2.3.2 Imaging of zircon

Imaging was mainly accomplished using a LEO 1430 VP scanning electron microscope (SEM) at UCLA. A combination of BSE imaging and EDAX were used to verify the presence of zircon and any internal shock features (Wittmann et al., 2006). Cathodoluminescence (CL) imaging was used to elucidate internal structures and zoning and the presence of possible impact rims (Trail et al., 2007a), for subsequent depth profiles (see chapter 4).

2.3.3 Ion microprobe (U-Pb, Trace elements)

Ion microprobe analyses were conducted with a CAMECA ims1270 at UCLA using an ~8-12 nA mass-filtered $^{16}O^-$ beam focused to spots between ~20 to 35 μm. I initially screened zircon grains for U-Pb dating to discriminate between inherited zircon (i.e., those older than the accepted impact age) and those formed within the impact melt. Zircon crystals with U-Pb ages similar to those of previously published impact dates (i.e., impact produced zircon) were then re-analyzed for trace elements (all rare earth elements REE, Ti, and Hf) within the same area as the U-Pb analysis, ensuring that the data acquired are from the same crystal domain. The trace element protocol also included mass/charge stations at ^{26}Mg, ^{55}Mn, and ^{57}Fe permitting monitoring of beam overlap onto inclusions in zircon that could overwhelm the low abundances of some critical trace elements in zircon (e.g., Ti). Conditions for trace element analyses were broadly similar to those of U-Pb dating, with a ~10-15 nA mass-filtered $^{16}O^-$ beam focused to a ~25-35 μm spot. Analysis yielding high Ti and Fe were re-imaged by SEM to make sure no visible cracks were within the spot. When cracks were identified grains were re-analyzed on fresh clean surfaces to avoid contamination of Ti associated with crystal defects (Harrison and Schmitt, 2007). NIST 610 glass was used as a primary REE standard (Pearce et al., 1997), checked against 91500 zircon (Wiedenbeck et al.). We used SL13 (6.32±0.3 ppm Ti) and AS3

(21.6±1.6 ppm Ti) as titanium standards (Aikman, 2007). For reconnaissance analysis, we also used a rapid analysis protocol for $^{48}Ti^{+}$ and SiO^{+} (excluding other trace elements) by multi-collection with dual electron multipliers which yield equivalent results. The U-Th-Pb, Ti, and REE data are individually tabulated in appendices 8.1-8.3.

2.3.4 Ion microprobe (Oxygen isotopes)

Analyses of oxygen isotopes in selected grains were also made using the CAMECA *ims*1270 ion microprobe at UCLA. A ~1.5 nA Cs+ beam was focused to a ~20 μm spot and 10 keV secondary ions were admitted to the mass spectrometer after passing through a 30 eV energy slit, broadly similar to Trail et al., (2007). The AS3 zircon standard ($\delta^{18}O_{SMOW}$ = 5.34‰; Trail et al., 2007) was used for correction of raw $^{18}O/^{16}O$ ratios. Zircons were presputtered for 1 min with a total integration time per analysis of 5 min. Errors based on counting statistics are 0.1%or less in almost all cases.

2.4 Results

2.4.1 SEM imaging and textural analysis

The majority of grains appear to be magmatic with euhedral to subhedral faces, high aspect ratio and little evidence of shock. Grains from Vredefort, Sudbury and Manicouagan showed little to no CL activity while those from Morokweng show nice CL oscillatory zoning. Some grains from Sudbury were found to exhibit alteration signatures in BSE associated with high Fe and Na possibly due to post-impact alteration. Zircon isolated from Popigai are rounded to ovoid, with little evidence of igneous textures, expected from the metamorphic sample petrology.

2.4.2 U-Pb Geochronology

Separated zircon crystals are first analyzed for U-Pb to discriminate between grains grown within the impact melt and those that have been inherited into the impact melt from the target. Thos grains with ages coincident with that of the impact are assumed to have grown within the impact melt sheet and are the focus of this chapter. Inherited grains provide a unique opportunity to constrain Pb-loss within impact (see chapter 4) events and allow for testing of lower-temperature chronometers such as (U-Th)/He (see chapter 5).

2.4.2.1 Vredefort Impact Structure, South Africa

Separated zircon crystals from the pseudotachylite breccia sample (VD_PB) yield $^{207}Pb/^{206}Pb$ ages of ~2.9-3.0 Ga (n=31), with several grains (n=6) showing varying amounts of Pb-loss, presumably representing the Archean target rocks and not neo-crystalline zircon from the impact itself (Fig. 2.1). Eight zircon grains were analyzed in-situ (VD_1A and VD_1B; Fig. 2) within the fine-grained melt matrix associated with the pseudotachylite breccia, to avoid grains from target rock clasts and focus on zircon within the impact melt matrix. However, all grains also yield $^{207}Pb/^{206}Pb$ ages of ~2.8-3.0 Ga, indicative of target rock ages. This result is consistent with the presumably short cooling duration of such thin (cm to m) veins of pseudotachylite breccia, which are insufficient for resorption of inherited zircon and hence never reach zircon saturation. Similarly zircon crystals isolated from the granophyre hand sample (VD_G) yield $^{207}Pb/^{206}Pb$ ages ranging from ~2.6-3.1 Ga (n=17; Fig. 2) with less evidence for significant Pb-loss, however still representative of the target material and not impact produced zircon. Although no grains analyzed from the Vredefort samples provide equivalent ages to those published for the impact, two zircon grains isolated from the borehole INL yield concordant $^{207}Pb/^{206}Pb$ ages (1978±17 Ma, 2σ, MSWD = 0.3, n = 2), about 2% lower than TIMS

U-Pb zircon ages of 2020±3 Ma and 2019±2 (Kamo et al., 1996; Moser, 1997). We provisionally ascribe this difference to minor Pb loss. Only these two grains were selected for further analysis within this study.

2.4.2.2 Morokweng impact structure, South Africa

Zircon grains separated from both the 156.5-157.98 m and the 399.20 m crushed samples yield concordant U-Pb ages of 149±4 Ma (2σ, MSWD = 2.9, n = 56; Fig. 2.2) slightly older than previously reported ages of 145±0.8 Ma and 144±4 Ma ($^{207}Pb/^{206}Pb$ ID-TIMS zircon age and $^{40}Ar/^{39}Ar$ biotite age respectively; Hart et al., 1997). U-Pb analysis from zircon separated from the 1069 m target rock core split yield concordant ages ranging from ~2.8-3.3 Ga, similar to but slightly older than those estimated for the target rocks (~2.7-3.0 Ga; Poujol et al., 2002; Koeberl and Reimold, 2003), with half of these grains showing evidence for Pb-loss possibly associated with impact shock. Although these older, isotopically disturbed grains are not the focus of this portion of the study they are further discussed in the Pb*-loss and (U-Th)/He dating chapters. As the focus of this section is on neoformed zircon, only grains extracted from the 156.5-157.98 m and the 399.20 m depth intervals were selected for further analysis.

2.4.2.3 Sudbury impact structure, Canada

Ion microprobe analysis of zircon separates from the felsic and mafic norite members of the SIC yield concordant U-Pb ages of 1848±6 Ma (2σ, MSWD = 1.7, n = 10; Fig. 2), in close agreement with the published $^{207}Pb/^{206}Pb$ age of 1849.5±0.2 Ma (Davis, 2008). Only one grain shows evidence for Pb-loss whereby post-analysis SEM imaging revealed likely post-crystalline alteration associated with high alkali and Fe contents for this crystal. There is no evidence, within the melt sheet, of zircon associated with the Archean granitic gneisses which comprise the

target lithologies, and the uniform age distribution suggests that the impact energy associated with the Sudbury event was sufficient to fully resorb all inherited zircon. Consequently, we selected all grains for further analysis.

2.4.2.4 Manicouagan impact structure, Canada

U-Pb analysis of zircon crystals separated from the main melt sheet of the Manicouagan impact yield concordant U-Pb ages of 214±2 Ma (2σ, MSWD = 1.7, n = 32; Fig. 2) in close agreement with previous studies (214±1 Ma, $^{207}Pb/^{206}Pb$ TIMS zircon age; Hodych and Dunning, 1992). Zircon crystals show no evidence of Pb loss and inherited grains were absent, suggesting similar conditions to that of Sudbury where the impact melt had sufficient time and heat to fully dissolve all relic zircon. All the grains isolated were selected for further analysis.

2.4.2.5 Popigai impact structure, Russia

Zircon separated from both the suevite and the shocked gneiss and from the Popigai impact mostly yield Proterozoic concordant U-Pb ages (~1.8-2.0 Ga) with one grain yielding an Archean age of ~2.5 Ga (Fig. 2). The majority of zircon ages (~80 %) are concordant, with a minor population (~20 %) of discordant ages. None of the ~120 crystals analyzed correspond to the 35.7±0.2 Ma age associated with the impact event (Bottomley et al., 1997). Although no neoformed grains were discovered in the Popigai impactites, inherited grains allow a unique opportunity to gain further understanding into Pb-loss in impact events and allow for testing of other low-temperature chronometers as discussed in chapter 5.

2.4.3 Ti-in-zircon thermometry

Experimental results as well as analyses of natural samples have shown that the concentration of titanium, [Ti], within a zircon is a direct function of crystallization temperature

(Watson and Harrison, 1983; Harrison and Watson, 1983; Watson and Harrison, 2005b). Although calculation of accurate magmatic zircon crystallization temperatures (T_{zir}^{xtln}) require knowledge of a_{TiO2} and a_{SiO2} activities (Ferry and Watson, 2007), we instead ultimately wish to compare calculated temperatures to detrital Hadean zircon, a population for which these parameters are in most cases unknown (Watson and Harrison, 2005b). Although the activity of Ti and Si, a_{TiO2} and a_{SiO2}, are largely subunity for the samples at hand, equal sub-unity values are directly compensatory and magmatic activities of either being ≤0.5 are relatively rare (Ferry and Watson, 2007) and would result in 50-80°C increases in calculated temperatures. Where bulk rock compositions are known, T_{zir}^{xtln} can be compared to zircon saturation model temperatures (T_{zir}^{sat}; Harrison and Watson, 1983; Watson and Harrison, 1983; Boehnke et al., 2013).

2.4.3.1 Vredefort impact structure, South Africa

Of over 60 grains analyzed from three separate samples of Vredefort, only two grains isolated from the INL drill core provided ages suitable (i.e. within 10% of the published impact age) for further analysis. Titanium concentrations in these two grains are 11±0.7 and 20±1.1 ppm which corresponds to T_{zir}^{xtln} of 750±15 and 810±15°C, respectively (Watson and Harrison, 2005b). All other grains from Vredefort samples yield age's significantly older than the impact date and are presumed to be associated with target rock zircon, thus do not fit the criteria for an impact produced zircon.

2.4.3.2 Morokweng impact structure, South Africa

Average Ti concentrations of zircon crystals separated from 157 and 399 m within borehole M3 are 25±19 and 15±9 ppm respectively (n=31 for 157 m sample; n=19 for 399 m sample). This corresponds to a T_{zir}^{xtln} of ~830°C for the 157 m sample and ~780°C for the 399 m

sample and an overall average of 797±70°C (Fig. 3b). Relatively little variation in T_{zir}^{xtln} is observed from the 399 m sample, although significant variations exist within the 155 m sample with T_{zir}^{xtln} ranging from 720-990°C. High sensitivity ion imaging (Harrison and Schmitt, 2007) may be helpful in ruling out contamination as a cause of the high apparent temperatures (although no cracks are apparent in SEM images).

2.4.3.3 Sudbury impact structure, Canada

Zircon separated from the felsic (n=12) and mafic norite (n=13) members of the SIC yield overlapping average Ti concentrations of 10±4 and 12±7 ppm, corresponding to T_{zir}^{xtln} of ~740 and ~760°C, respectively (Fig. 3a). There is relatively little within sample variation with >75% of the data plotting within 700-780°C. This temperature is lower than that given in an earlier study of Sudbury (~800°C for zircon grains isolated from the norite member and analyzed LA-ICPMS; Darling et al., 2009). This relatively small difference could potentially be due to Ti hosted in cracks (Harrison and Schmitt, 2007) which are more likely to be encountered in the larger analysis volume required by laser ablation than when using SIMS as opposed to ion sputtering.

2.4.3.4 Manicouagan impact structure, Canada

Zircon separated from the main melt sheet of Manicouagan yield an average Ti concentration of ~12±6 ppm, corresponding to a T_{zir}^{xtln} of 747 ±35°C (n=32; Fig. 3c). Crystals analyzed in replicate using single- and multi-collection techniques yield similar values, with the exception of four crystals where single-collection Ti data are higher relative to the same grains analyzed in multi-collection (possibly due to beam overlap onto cracks). Averages for each

method agree well (Ti average concentration = 11.4 ppm in multi-collection; Ti average concentration = 12.2 ppm in single-collection).

2.4.4 Oxygen isotopes

Impacts have long been suspected of maintaining long-lived hydrothermal systems (Osinski et al., 2005; Abramov, 2004; Abramov and Kring, 2005). To investigate the consequences of hydrothermal activity we have analyzed the impact zircons for oxygen isotopes to see if any effects are observed from exchange with meteoritic water. The majority of zircon $\delta^{18}O$ results yield essentially mantle values (5.3±0.3‰, 2σ; Valley et al., 1998) suggesting those zircon did not exchange with meteoric water in a hydrothermal system. However, one interesting result is the presence of 7 zircon crystals with anomalously low $\delta^{18}O$ (1.4±0.7‰) from the 155 m drill core split from the M3 borehole at Morokweng impact structure. These anamolously low $\delta^{18}O$ zircons are not present in the 399 m drill core split and hint at the possibility of a hydrothermal system within the upper few hundred meters of the Morokweng impact melt.

2.4.5 Trace elements

Results from REE analysis of all impactite-produced zircon are, as expected, similar to terrestrial igneous zircon from a broad range of ages (Quaternary to Hadean; Peck et al., 2001; Grimes et al., 2007; Fig. 2.8). They are characterized by a relatively steep slope from LREE to HREE, and display positive Ce- and negative Eu-anomalies. The positive Ce-anomaly is commonly interpreted as evidence for oxidized magmas in which partitioning of Ce^{4+} dominates over Ce^{3+} (Hoskin and Schaltegger, 2003). The negative Eu-anomaly almost certainly reflects plagioclase fractionation of the parent magma as Eu easily substitutes for Ca within plagioclase

(Hoskin and Schaltegger, 2003), and plagioclase is ubiquitously present in large impact target rocks. Differences in REE contents of differing impact sites likely reflect local concentration variations.

The trace element compositions of impact-produced zircon from Sudbury, Morokweng and Manicouagan (Fig. 2.8) fall generally within the fields (in U vs. Yb, U/Yb vs. Hf or Y space) defined by zircon crystallized from continental crust as do detrital Hadean zircon from the Jack Hills region (Grimes et al., 2007). Trace elements may also be useful in discriminating between neoformed and reset zircon (Abramov et al., 2013). For example, if elements that diffuse slower than Pb (e.g., Ti and REE; Cherniak et al., 1997; Cherniak and Watson, 2003) are distinctly different between melt sheet zircon and those from the target rock, it would appear likely that the zircon crystals are neoformed. REE patterns in zircon analyzed from the Morokweng M3 drill core target rock material (1069 m) show a clear distinction (primarily in the lack of a HREE enrichment) from those isolated from the melt sheet, reflecting the different geochemical conditions during crystallization of impact produced zircon and target rock zircon. While they are consistent within target populations, we emphasize that REE signatures of zircon cannot be used to clearly identify zircon provenance.

2.5 Discussion

2.5.1 U-Pb geochronology

Results from U-Pb analysis of impacts with large melt sheets (Sudbury and Manicouagan, Canada, and Morokweng, South Africa) all have ages consistent with the accepted impact age. Igneous textures and, in the case of Morokweng, differing REE patterns from target zircon suggest these grains are neoformed zircon crystallizing at Zr-saturation of the impact melt

and not 'reset' zircon, complete loss of Pb*. We assume that any inherited zircons from target clasts, that were most likely mixed into the impact melt, were completely resorbed prior to saturation of the melt in Zr as no older cores have been identified. Where large melt sheets were no longer present (Vredefort and Morokweng basement, South Africa and Popigai, Russia) inherited zircons dominated the grains extracted. This can reflect only small amounts of partial melting in the target rock, thus never providing an opportunity to grow neoformed zircon. The grains from these samples are further interrogated (see chapter 4) for Pb*-loss associated with the high shock and heating associated with impacts as well as investigated for (U-Th)/He age (see chapter 5).

2.5.2 Ti-in-zircon thermometry

Crystallization temperatures of 111 zircon crystals separated from Sudbury, Vredefort, Morokweng, and Manicouagan impacts indicate an average crystallization temperature of 773±87°C. This crystallization temperature spectrum is remarkably consistent with the average zircon saturation temperature (T_{zir}^{sat}) of ca. 780°C calculated by Watson and Harrison (2005) from a large (~19,000) database of whole rock samples across Australasia. Estimates of bulk continental crust composition yield similar T_{zir}^{sat} values (ca. 780°C, Gao et al., 1998; Rudnick and Gao, 2003). Since it is broadly assumed that impact melts largely reflect shock melting of large portions of the lithosphere (Melosh, 1989), we note that calculated saturation temperatures for compositions of modern middle crust yield T_{zir}^{sat} of ca. 740°C (Rudnick and Fountain, 1995; Rudnick and Gao, 2003). Although the observed apparent crystallization temperatures (T_{zir}^{xtln}) for impact produced zircon are consistent with T_{zir}^{sat} for present crustal compositions, they appear to be distinctly higher than that for detrital Hadean zircon population (i.e., ~680°C; Watson and Harrison, 2005). Based on the Ti-in-zircon thermometry results, we conclude that zircon derived

from impactites do not represent a dominant source for the Hadean grains thus far documented from Western Australia.

2.5.3 Trace elements

Impact-produced zircon is indistinguishable from that of igneous or Hadean grains in REE, however plots of U vs. Yb and U/Yb vs. Hf or Y suggest that some inference can be made about target rock composition (continental vs. oceanic crust). Trace element geochemistry can be used to distinguish between grains that have had their ages reset to that of the impact and those that crystallized from the impact melt, assuming that magmatic conditions within the melt sheet are different than those of the target rocks.

2.6 Conclusion

Impacts investigated in this study contain either predominately neoformed (Sudbury, Morokweng, Manicouagan) or inherited zircon (Popigai, Vredefort). Inherited grains yield ages consistent with local target rocks and their survivability reflects either low target rock [Zr] (i.e., never allowing zircon saturation), rapidly cooling melt sheets (i.e., a kinetic barrier to dissolution), or low energy impacts that never completely melted the middle crust. We note that although Vredefort is currently the largest known terrestrial impact site, erosion and resurgence of the central dome have removed much of the presumably large melt sheet that once existed (Therriault et al., 1997) explaining the rarity of impact produced zircon in the samples studied.

U-Pb geochronology of zircon from the Sudbury and Manicouagan impact melts agree well with published ages, however those for Vredefort and Morokweng do not (no impact produced zircon was observed within the Popigai samples). An impact age of ~1980 Ma for Vredefort is younger than the previously published age of ~2020 Ma, probably reflecting minor

Pb loss. Morokweng U-Pb zircon ages (~149 Ma) are slightly older, but within error, of the previously published TIMS U-Pb age of ~145 Ma. No relic zircon grains were discovered associated with the target rocks within the Morokweng melt sheet.

Impact-produced zircon is indistinguishable from that of igneous or Hadean grains in REE, however plots of U vs. Yb and U/Yb vs. Hf or Y suggest that some inference can be made to the target rock composition (continental vs. oceanic crust). Trace element geochemistry can be used to distinguish between grains that have had their ages reset to that of the impact and those that crystallized from the impact melt, assuming that magmatic conditions within the melt sheet are different than those of the target rocks.

Crystallization temperatures (T_{zir}^{xtln}) of 111 zircon crystals separated from Sudbury, Vredefort, Morokweng, and Manicouagan impacts indicate an average crystallization temperature of 773±87°C, significantly higher than that reported for the Hadean Jack Hills (~680±40°C; Watson and Harrison, 2005; Harrison and Schmitt, 2007). Based on the Ti-in-zircon thermometry results, we conclude that zircon derived from impactites do not represent a dominant source for the Hadean grains thus far documented from Western Australia.

2.7 Figures

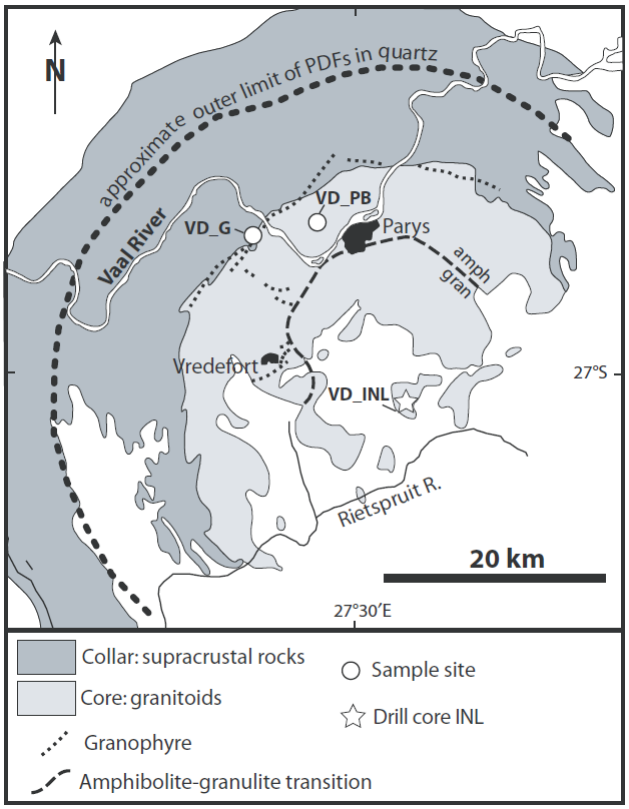

2.7.1 Fig. 2.1

Simplified geologic map of the Vredefort impact structure (simplified after Gibson and Reimold, 2005) with sample localities for pseudotachylite breccia and granophyre samples (circles) as well as drill core INL (star; Kamo et al., 1996). Also shown is the shocked quartz limit as approximated by Therriault et al., (1997). PDF—planar deformation features.

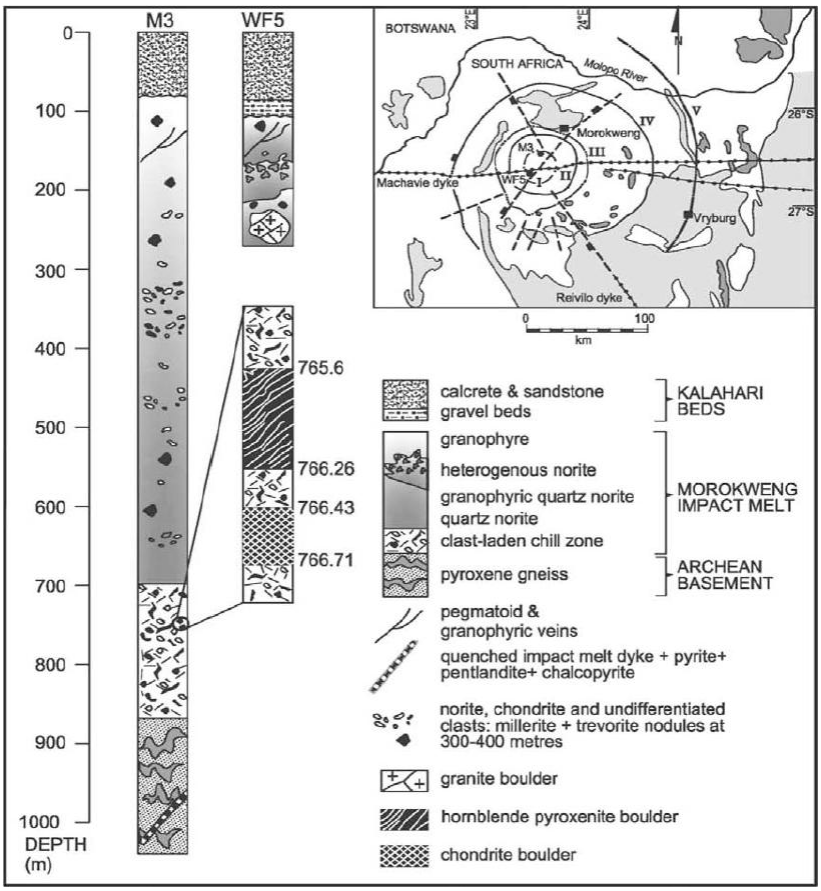

2.7.2 Fig. 2.2

Log summary of borehole M3 that includes the Morokweng meteorite and the short neighboring borehole WF5 from the Morokweng impact structure, South Africa. Inset: simplified sketch map of the crater showing the location of boreholes M3 and WF5. Ring I, limit of melt and meteorite clasts; ring II, limit of allochthonous breccia and melt; ring III, limit of (para) autochthonous breccia; ring IV, ring of water boreholes and faulting; arc V, (sub)outcrops of highly magnetic BIFs (after Hart et al., 2002; Jourdan et al., 2010). Zircons extracted from the 157, 399 and 1069 m splits.

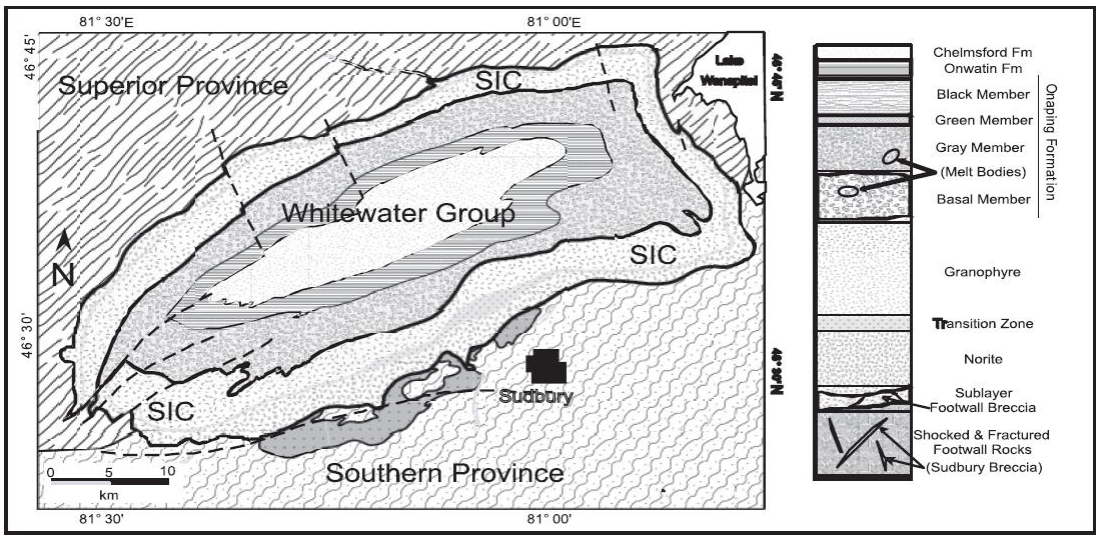

2.7.3 Fig. 2.3

Map of Sudbury impact structure, Canada and cross-section of the Sudbury Igneous Complex (after Zieg and Marsh, 2005). Zircons were provided from the basal norite member which has been subsequently divided into an upper felsic and lower mafic region (Sud_F and Sud_M, respectively). Samples of Sudbury breccia and Onaping formation were also collected and analyzed for Pb-loss in chapter 4.

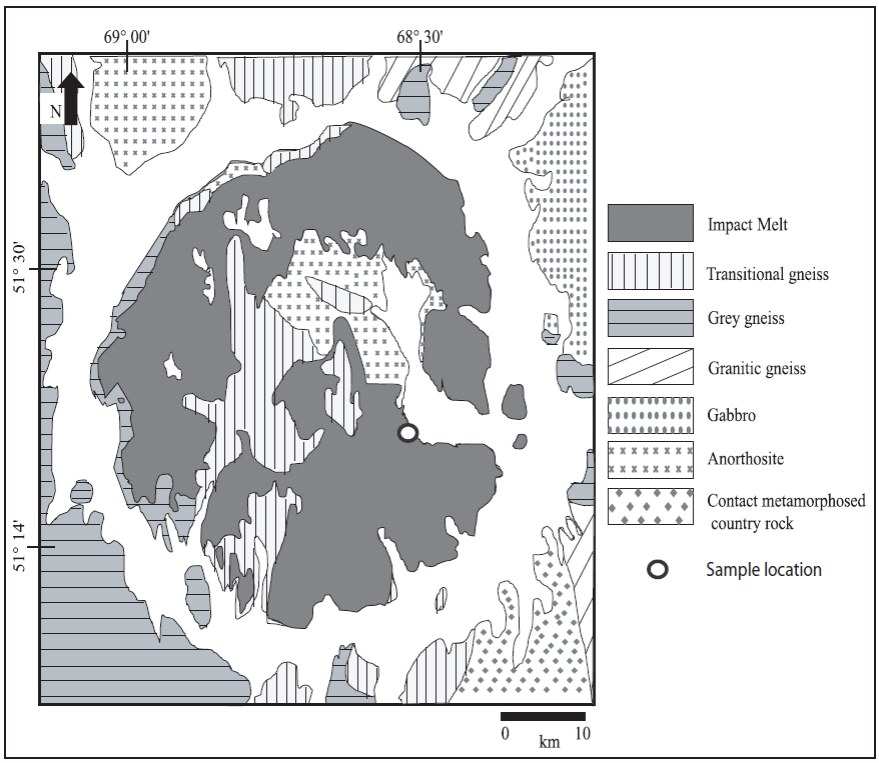

2.7.4 Fig. 2.4

Map of the Manicouagan impact structure, Canada. Hand samples of Manicouagan from the main impact melt sheet (MC_MM) were collected near the base of the melt sheet on the west side of Memory Bay (after O'Connell-Cooper and Spray, 2011).

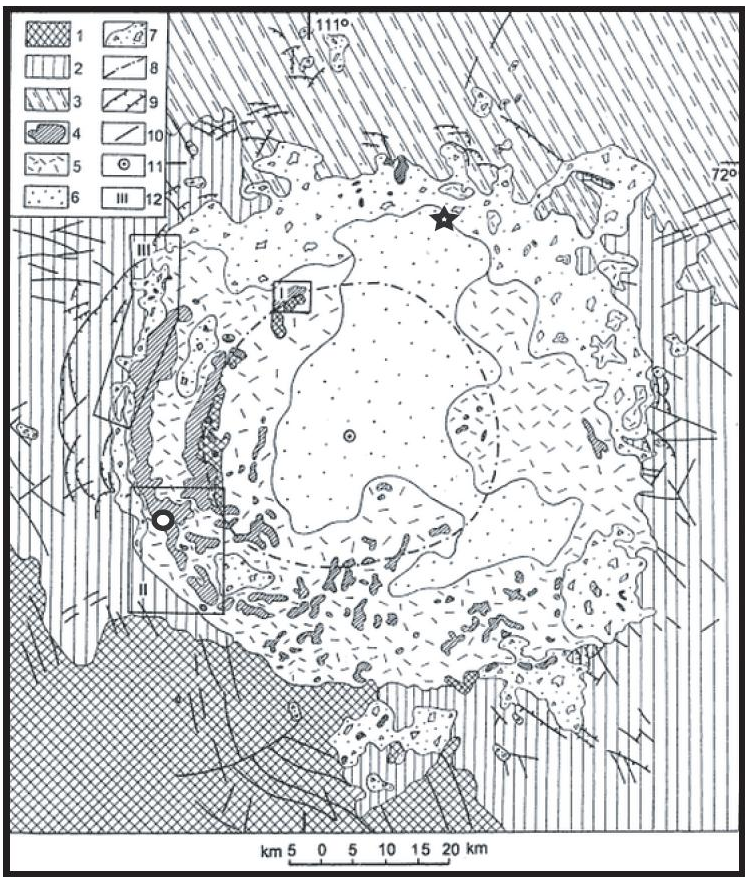

2.7.5 Fig. 2.5

Simplified geologic map of Popigai impact structure. Rock descriptions: 1) Archean crystalline rocks; 2) Upper Proterozoic and lower Paleozoic sedimentary rocks; 3) upper Paleozoic and Mesozoic sedimentary and igneous rocks; 4) tagamites; 5) suevites; 6-7) allogenic lithic breccia; 8) axis of annular uplift; 9) thrust faults; 10) faults; 11) geometric center of the crater (after Masaitis et al., 1999). Zircons extracted from two hand samples of suevite collected in the SW portion of the crater (circle) and shocked gneiss collected near the Rassokha river in the northern section of the crater (star).

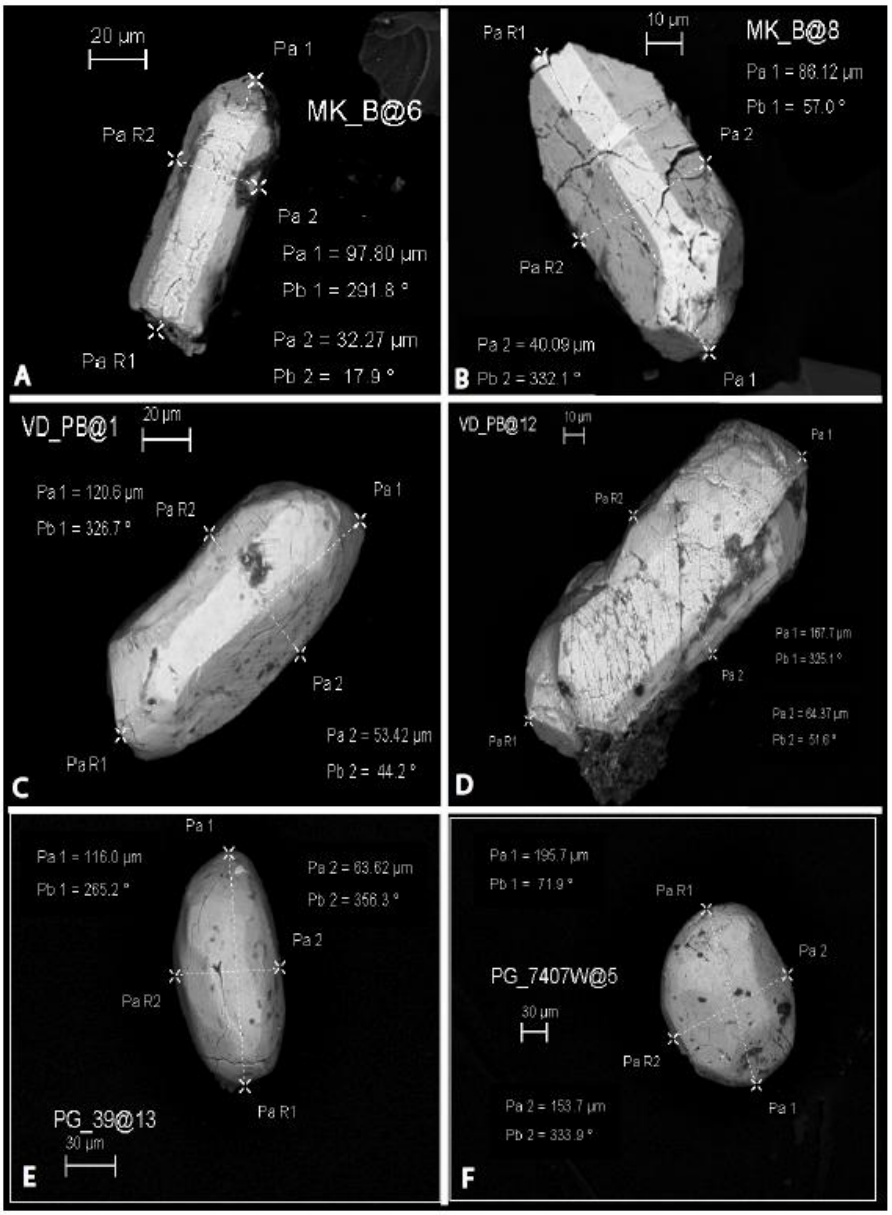

2.7.6 Fig. 2.6

Compilation of SEM backscatter images showing some of the crystal morphologies found within zircon extracted from terrestrial impactites. We note that although some shock features have been identified on the surface of some zircons (see chapter 5), none of these features appear to penetrate into the core of the zircons.

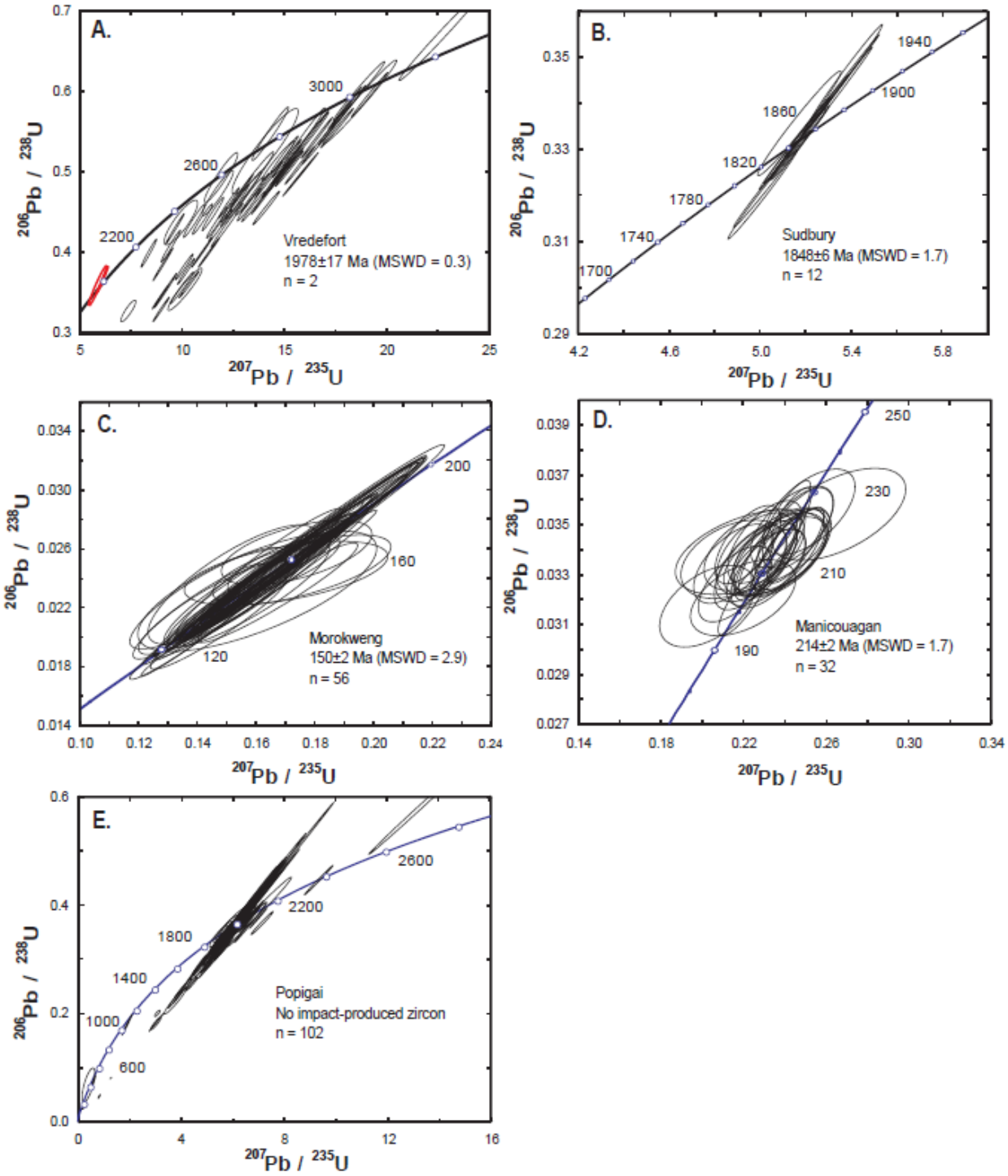
A.
Vredefort
1978±17 Ma (MSWD = 0.3)
n = 2
3000
2600
2200
B.
Sudbury
1848±6 Ma (MSWD = 1.7)
n = 12
1940
1900
1860
1820
1780
1740
1700
C.
Morokweng
150±2 Ma (MSWD = 2.9)
n = 56
200
160
120
D.
Manicouagan
214±2 Ma (MSWD = 1.7)
n = 32
250
230
210
190
E.
Popigai
No impact-produced zircon
n = 102
2600
2200
1800
1400
1000
600
$^{206}Pb / ^{238}U$
$^{207}Pb / ^{235}U$

2.7.7 Fig. 2.7

Concordia diagrams of zircon extracted from preserved terrestrial impactites calibrated against AS3 zircon standard (Paces and Miller, 1993). (A) Nearly all grains extracted from Vredefort are inherited from the target with exception of two grains from the INL borehole (denoted in red) which yield ages similar to the published impact age (~2020 MA; $^{207}Pb/^{206}Pb$ TIMS zircon age; Kamo et al. 1996; Moser 1997). (B) Zircon from the mafic norite of the Sudbury Igneous Complex yield ages in agreement with the published impact age (1849.5±0.2 Ma; $^{207}Pb/^{206}Pb$ TE-TIMS zircon age; Davis 2008) with no signs of inheritance from the target rock. (C) Grains from the Morokweng borehole M3 yield ages similar to, however slightly older than, the published impact age (145±0.8 Ma; $^{207}Pb/^{206}Pb$ ID-TIMS zircon age, $^{40}Ar/^{39}Ar$ biotite age; Hart et al 1997) with no sign of inheritance. (D) Zircon from the Manicouagan impact yield ages identical to those from previous studies (214±1 Ma; $^{207}Pb/^{206}Pb$ TIMS zircon age; Hodych and Dunning 1992) and show no inheritance also. (E) No impact produced zircon has been extracted from the Popigai samples provided for this study with all grains reflecting target rock ages (see chapter 5 for Popigai U-Pb results).

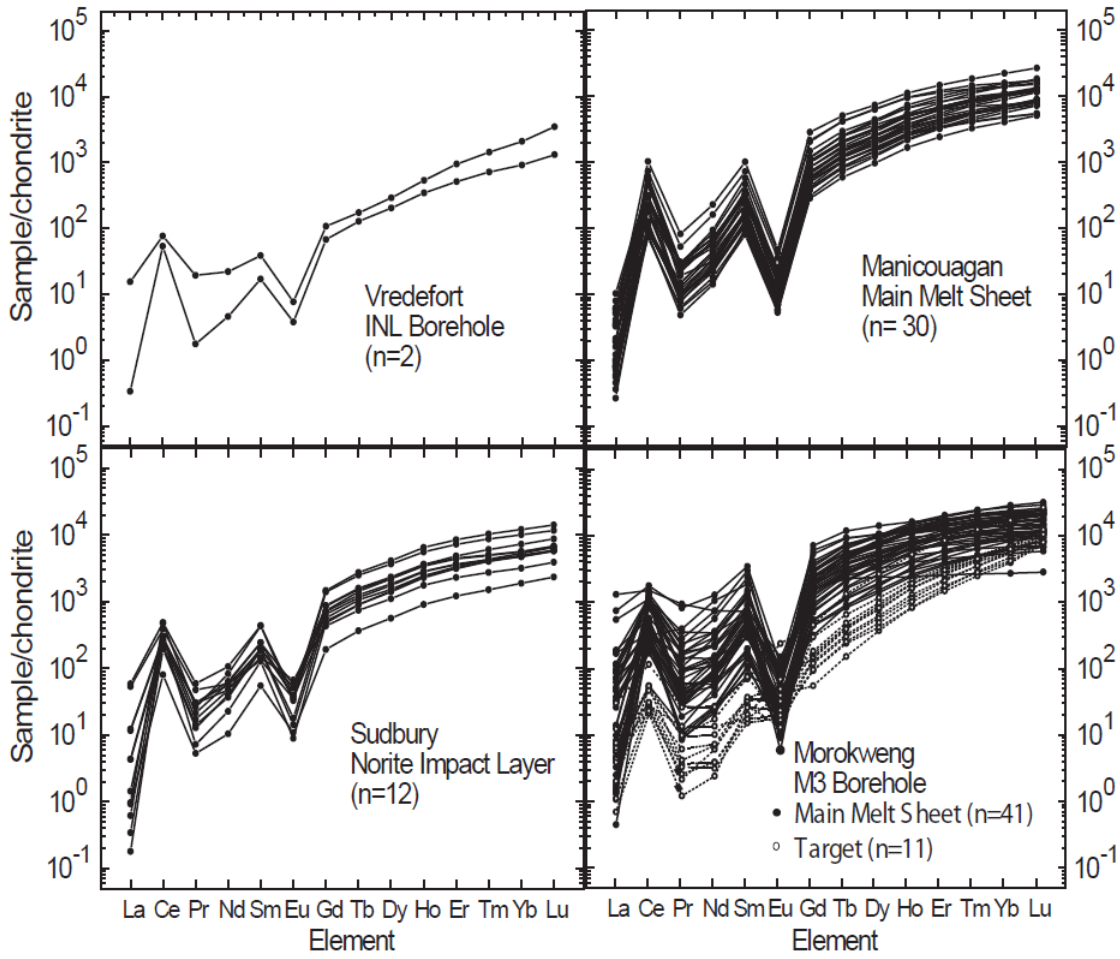

2.7.8 Fig. 2.8

Chondrite-normalized rare earth element abundances in impact produced zircon from ion microprobe measurements. REE patterns are indistinguishable from igneous zircon of all ages (Quaternary to Hadean; Hoskin and Schaltegger 2003; Peck et al. 2001; Grimes et al. 2007), characterized by a relatively steep slope from LREE to HREE and displaying a positive Ce-anomaly and a negative Eu-anomaly.

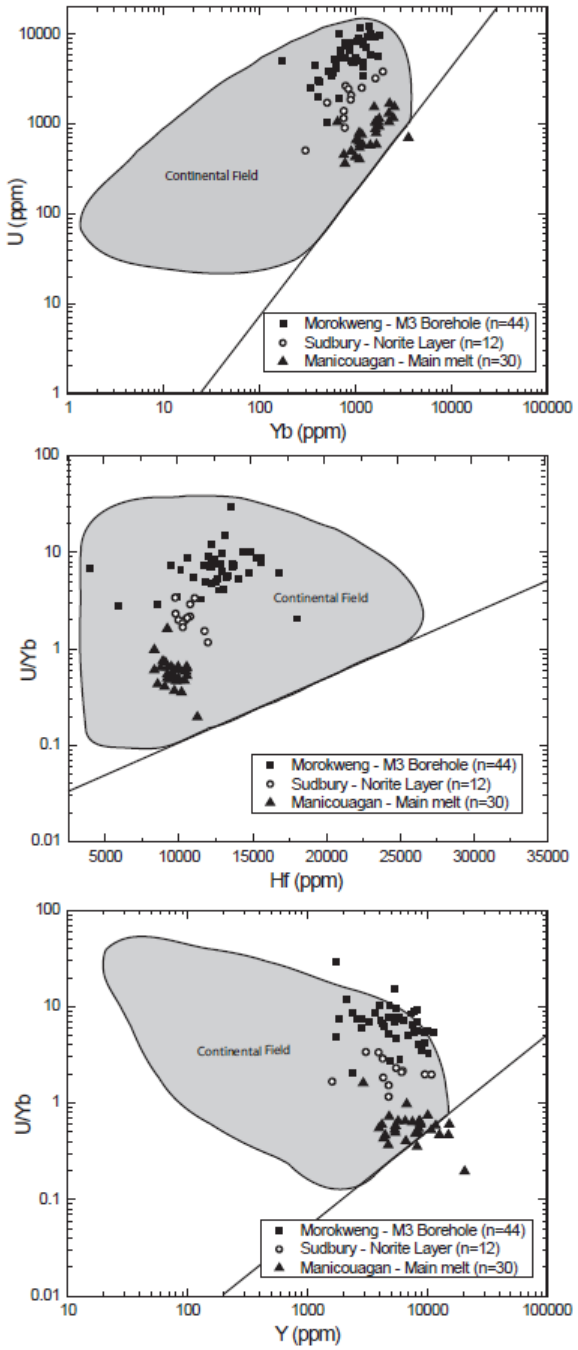

2.7.9 Fig. 2.9

Trace element plots of impact produced zircon from Morokweng, Sudbury and Manicouagan to discriminate between continental and oceanic target rock compositions. All grains are corrected for uranium decay. Continental field from Grimes et al. (2007) with lower

boundary denoted by a solid line on each diagram, indicating the upper most limit of unambiguously oceanic zircon. End points for lines: U vs. Yb (25, 1), (20000, 10000); U/Yb vs. Hf (5000, 0.05), (35000, 5); U/Yb vs. Y (200, 0.01), (100000, 5). Nearly all impact produced zircon suggest continental target lithologies however Manicouagan plots nearly in the oceanic field possibly due to a slightly more mafic target

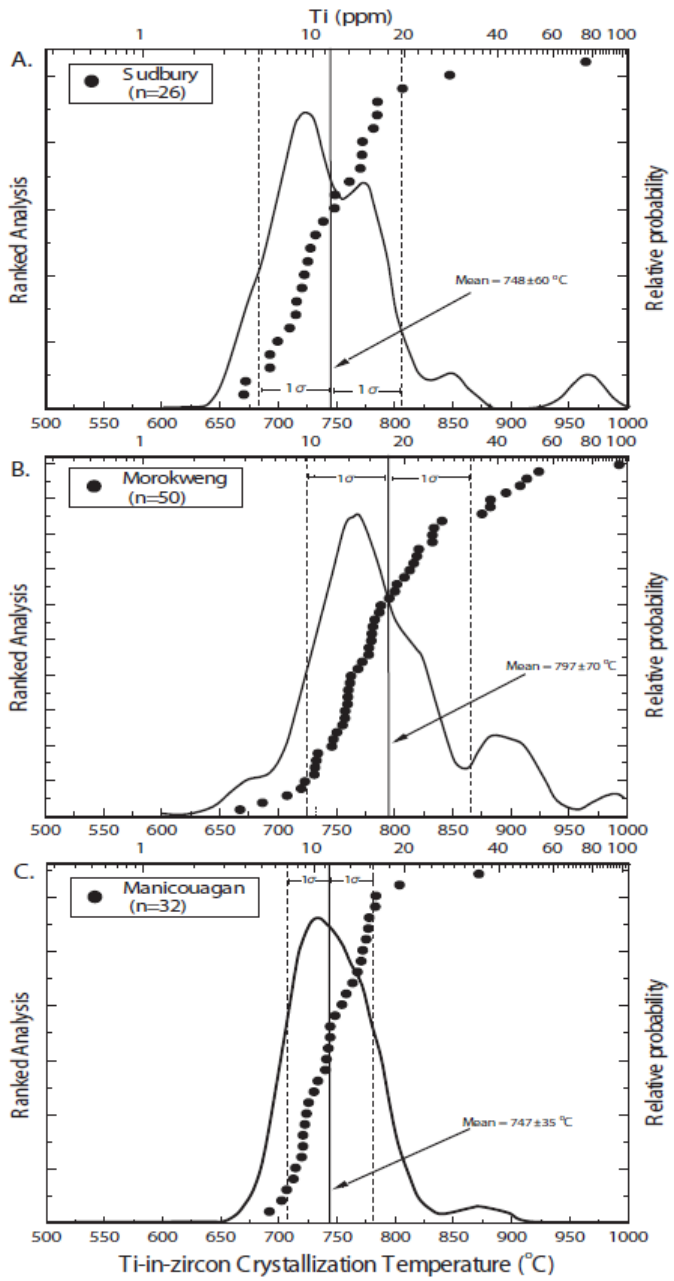

2.7.10 Fig. 2.10

Titanium concentrations and Ti-in-zircon crystallization temperature, assuming a_{TiO2}=1 (Watson and Harrison 2005), of impact produced zircon. (A) Sudbury impact produced zircon T_{zir}^{xtln} = 748±60°C; (B) Morokweng impact produced zircon T_{zir}^{xtln} = 797±70°C; (C) Manicouagan impact produced zircon T_{zir}^{xtln} = 747±35°C.

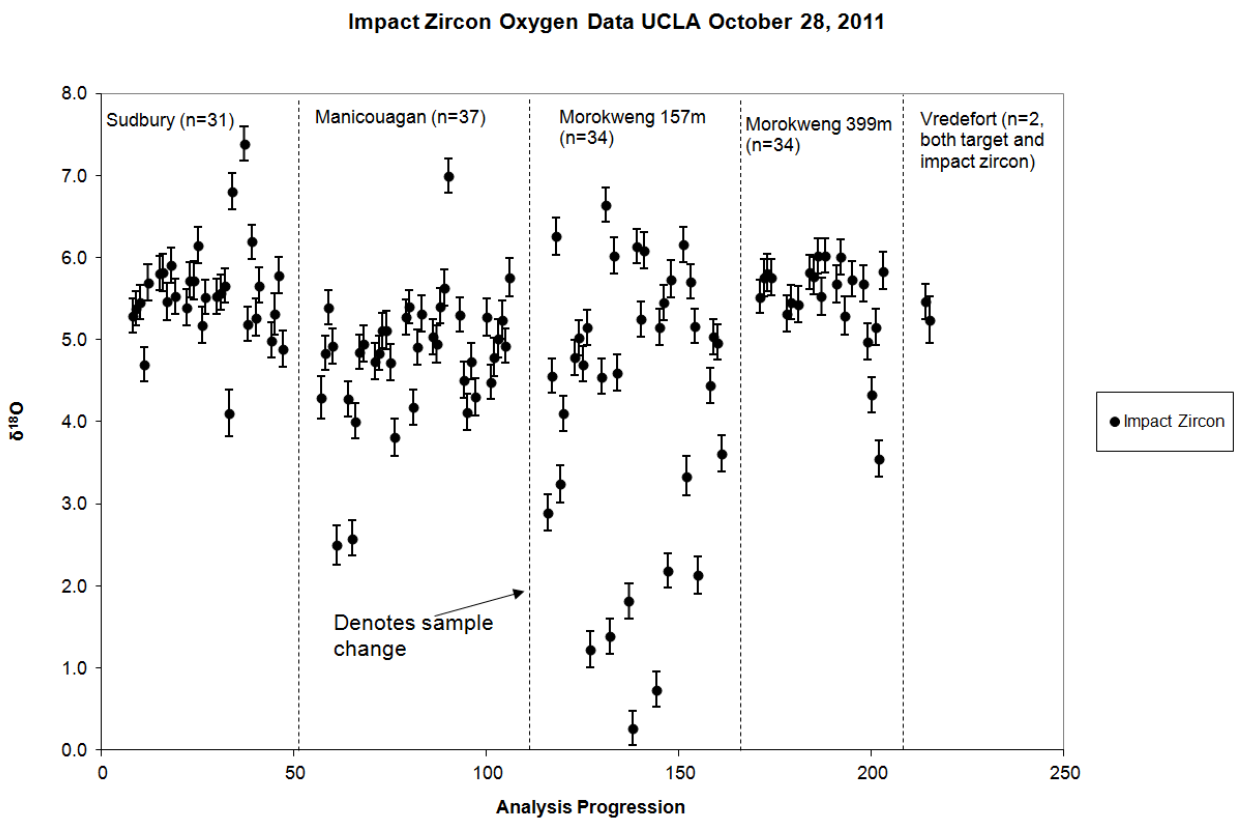

2.7.11 Fig. 2.11

$\delta^{18}O$ results for all zircons extracted from terrestrial impactites showing a majority of mantle values (5.3±0.3‰, 2σ; Valley et al., 1998), with some anomalously low $\delta^{18}O$ zircons from the upper portion of the Morokweng impact melt sheet possibly suggesting exchange with meteoric water in an impact-induced hydrothermal system.

3. Modeling zircon crystallization in simulated impact melts

3.1 Introduction

Previous geochemical data such as Ti-in-zircon temperatures can be used along with zircon saturation experiments to develop models that allow for predictions to be made of the zircon crystallization spectra and abundance of neoformed impact zircon in simulated impact melts. Provided some assumptions about target composition and impactor size, these predictions can then be compared to data from zircon populations, such as the Hadean or lunar zircon populations, to assess their possible formation within an impact event. This type of model provides a basis to identify which grains should be used to accurately date impact events and which grains should be avoided due to probable inheritance from the target.

For example, the recent identification of poikilitic zircon, which appear as branching, interstitial networks of zircon enclosing other phases (Fig. 3.1 A&B), within the melt matrix from lunar meteorite SaU 169 and Apollo 12 samples (Gnos et al., 2004; Liu et al., 2012; Grange et al., 2013a) have been interpreted as primary growth during equilibrium crystallization of the impact melt. Zircon U-Pb ages for these grains has been suggested as a means with which to date their growth from impact melts (and thus the impact event age). Results of such analyses have been offered as constraints on the age of the Imbrium basin and as such would introduce an important new means with which to probe planetary impact histories (Liu et al., 2012; Grange et al., 2013). Although such textures have been observed in plagioclase (Nelson and Montana, 1992), they appear very rare in terrestrial environments (Scoates and Chamberlain, 1995). The model developed below can help assess the likelihood of such grains growing within an impact melt and their use in identifying planetary impact histories.

3.2 Zircon saturation and 'M'

Zircon solubility in crustal melts is a simple function of zirconium content [Zr], temperature, and rock chemistry (i.e., 'M' = (2Ca+Na+K)/(Al·Si); (Watson and Harrison, 1983; Harrison and Watson, 1983). Thus knowledge of 'M', [Zr], *T'* (i.e., ambient temperature plus the ΔT associated with impacts), and the relationship between 'M' and melting conditions permits any random association of analyzed rock and possible *T'* to be evaluated for the potential to produce impact zircon. Similarly, dissolution and growth of zircon in an impact melt is a function of the solubility of Zr, which itself is a function of composition (i.e. cation ratio 'M' = (Na+K+2Ca) / (Al*Si)) within the impact melt generated as well as the diffusivity of Zr within such a melt; and the temperature and rate of cooling (Harrison and Watson, 1983; Watson and Harrison, 1983; Watson, 2011).

To obtain a relationship between 'M' and melting conditions, we first note that the GEOROC database of analyzed Archean rocks (restricted to SiO_2 values between 35 and 85% to preclude sampling of non-silicates and quartzites) plots in a coherent fashion with a negative slope on a 'M' vs. SiO_2 diagram (Fig. 3.2). We take this as evidence that this parameter appropriately characterizes petrogenic variation in this broad suite of rocks. Also shown in Fig. 3.2 is the regression of 'M' vs. SiO_2 of the felsic, intermediate and mafic rocks utilized in the classic melting studies of Wyllie, (1977) which essentially reproduce the Archean database trend. Using either the 5 kbar solidus temperatures (T_{sol}) or 5% H_2O (i.e., the average water content of Archean GEOROC samples is ~3%) liquidus temperatures (T_{liq}) from Wyllie (1977) permits us to translate M into a melting or crystallization temperature (note that the calculations are not sensitive to assumed *P*).

3.3 Ti-in-zircon crystallization temperature vs. bulk saturation temperature

3.3.1 Vredefort impact structure, South Africa

Ti concentrations results for two grains, with U-Pb ages close but slightly younger than the accepted impact age (see chapter 2.4.2.1), are 11±0.7 and 20±1.1 ppm which corresponds to T_{zir}^{xtln} of 750±15 and 810±15°C, respectively (Watson and Harrison, 2005a). All other grains dated from Vredefort samples are presumed to be associated with target rock zircon and do not fit the criteria for an impact produced zircon. Although these results agree well with the bulk zircon saturation temperature of 772°C calculated from Reimold, (1991) for the pseudotachylite breccia, more impact formed zircon grains are needed to verify this result. This result (T_{zir}^{xtln}~T_{zir}^{sat}) is also consistent with the lack of differentiation expected within such small veins of melt.

3.3.2 Morokweng impact structure, South Africa

Average Ti concentrations of zircon crystals separated from 157 and 399 m within borehole M3 are 25±19 and 15±9 ppm respectively (n=31 for 157 m sample; n=19 for 399 m sample). This corresponds to a T_{zir}^{xtln} of ~830°C for the 157 m sample and ~780°C for the 399 m sample and an overall average of 797±70°C. Morokweng is a differentiated impact melt sheet (Hart et al., 2002), thus, the zircon saturation of ~730°C (Andreoli et al., 1999) underestimates the onset of zircon crystallization by ~50-100°C (Harrison et al., 2007; Fig. 3.3).

3.3.2 Sudbury impact structure, Canada

Zircon separated from the felsic (n=12) and mafic norite (n=13) members of the SIC yield overlapping average Ti concentrations of 10±4 and 12±7 ppm, corresponding to T_{zir}^{xtln} of ~740 and ~760°C, respectively. T_{zir}^{xtln} agrees well with the calculated T_{zir}^{sat} of ~650°C for bulk

norite compositions (Lightfoot and Zotov, 2005) in that such temperatures are typically ~50-100°C (Fig. 3.3) lower than that expected for the onset of zircon crystallization in a fractionating magma (Harrison et al., 2007), due to the much lower 'M' present in the melt during zircon crystallization as opposed to that calculated from the bulk rock composition.

3.3.3 Manicouagan impact structure, Canada

Zircon separated from the main melt sheet of Manicouagan yield an average Ti concentration of ~12±6 ppm, corresponding to a T_{zir}^{xtln} of 747 ±35°C (n=32). The Ti-in-zircon temperatures agrees well with zircon saturation temperatures calculated from averaged bulk rock analyses (Floran et al., 1978) which predict T_{zir}^{sat} ~752°C (Fig. 3.3). This agreement is consistent with Manicouagan being an undifferentiated impact melt. Whereas recent studies suggest possible pockets of differentiation throughout the melt (O'Connell-Cooper and Spray, 2011), we did not observe this in the sampled zircon population.

3.4 Zircon saturation model for simulated LHB event

The LHB is generally interpreted as a relatively brief spike in impact flux (Gomes et al., 2005), although it remains possible that it instead reflects the terminal phase of a protracted cataclysm ("Lunar 'Cataclysm': A Misconception ?," 1975). In either interpretation, the terrestrial impact flux at the time is expected to be broadly similar. Thus given an estimate of that flux, we should be able to estimate the resulting T_{zir}^{xtln} spectrum and approximate the fraction of Zr in the continental crust that was processed through impact melting. We can then use these calculations to estimate the fraction of detrital zircon from a post-LHB terrane that would bear the thermal signature of an impact origin and to compare with the other zircon population distribution as a partial test of whether they could reflect an impact origin.

To calculate the expected abundance of impact produced zircon within a detrital LHB-era zircon population, that of the Jack Hills, we have used results of the thermal model of Abramov and Mojzsis (2009). They constructed a numerical framework to assess the amount of crustal heating resulting from an LHB impact history. Although their goal was to assess variations in the scale of the subsurface micro-biosphere due to the LHB, we can use their data to estimate crustal temperature changes that would lead to melting and re-precipitation of zircon on multiple targets such as, modern terrestrial surface, ancient terrestrial surface, lunar surface and Martian surface.

Using the LHB impact flux inferred from the lunar cratering record and asteroid belt size distribution, Abramov and Mojzsis (2009) found that less than 10% of the lithosphere would have experienced temperature increases (ΔT) of ≥500°C. Although for the case of the Jack Hills zircon, an elevated ancient geotherm could permit a significant fraction of the crust to achieve anatexis. Assuming a surface temperature of 0°C and an Archean geothermal structure, no data exists for the thermal structure of the Hadean so this is used as a best proxy, that reaches 800°C at 40 km (Condie, 1984). We coupled the thermal anomaly data of Abramov and Mojzsis (2009) with those samples from the Archean GEOROC database containing sufficient data to calculate zircon saturation temperatures to create a stochastic model of zircon formation temperatures during the LHB. In our model we ignored the limited potential of oceanic crust to preserve impact formed zircon, implicitly assume that the Archean GEOROC database is representative of continental crust between 4.0-3.8 Ga, and limit the upper temperature in the ΔT distribution to 1200°C. The latter assumption is justified on the basis that this exceeds all predicted solidus temperatures (T_{sol}) in the database and only 1% of the lithosphere is predicted to have reached ≥1200°C (Abramov and Mojzsis, 2009).

To obtain impact-associated temperatures, we randomly coupled an ambient temperature (between 0° and 800°C) with a ΔT value scaled to the distribution given in Fig. 3 of Abramov and Mojzsis (2009) (e.g., a ΔT of 50°C was encountered 40 times more often than 1000°C and there is no depth dependence). We then arrayed the 10059 samples in the database and randomly linked each synthetic impact temperature with an analyzed rock. Thus each rock is associated with an 'M' and [Zr], a calculated solidus (T_{sol}) and liquidus (T_{liq}) temperature (i.e., via the 'M' vs. T relationships), and a value of T'. Note that 'M' will be much lower than the bulk rock value for low melt fractions. This will be particularly pronounced for mafic compositions thus requiring parameterization of 'M' with melt fraction (described below based on synthetic experiments using MELTS; Fig. 3.4; Ghiorso and Sack, 1995). The following logical statements were then applied to each of the collective data sets in the sequence (Fig 3.5):

1) Did the rock melt due to impact (i.e., is $T'>T_{sol}$)? If not, the event does not produce magmatic zircon. If true, T' is recorded and the calculation continues.

2) Is $T_{zir}^{sat}<T_{sol}$? If true, the whole rock composition will not saturate zircon and the calculation terminates unless $T' > T_{\mathrm{liq}}$, in which case we assume the melt differentiates and thus produces zircon with $T_{zir}^{xtln} = T_{zir}^{sat}$ + 50°C if > T_{sol} (i.e., we account for the high-temperature onset of zircon saturation in crystallizing intermediate to mafic melts by adding the conservative lower limit of the observed 50-100°C difference between T_{zir}^{xtln} and T_{zir}^{sat} (see Harrison et al., 2007). If $T_{zir}^{sat}>T_{sol}$ and $T_{sol} \leq T' \leq T_{zir}^{sat} T$, then T' is taken to be T_{zir}^{xtln} .

3) In cases where $T_{\mathrm{sol}} <T'<T_{\mathrm{liq}}$, we scaled M according to the relationships M$'$= 0.4·M if $T_{\mathrm{sol}} <T'<(T_{\mathrm{liq}}–T_{\mathrm{sol}})\cdot 0.5+T_{\mathrm{sol}}$, or M$'$=0.8·M if $T_{\mathrm{sol}} <T'>(T_{\mathrm{liq}} – T_{\mathrm{sol}})\cdot 0.5+T_{\mathrm{sol}}$ (these relationships

approximate the compositional response of the Wyllie (1977) rock analyses to melting using the MELTS algorithm).

Only a small percentage within each run batch resulted in conditions permitting zircon formation. Thus in order to attain a robust result, we executed the algorithm 1000 times for each model run.

3.5 Results

3.5.1 Zircon saturation vs. Impact zircon T_{zir}^{xtln}

The crystallization temperature spectrum of impact produced zircon from four terrestrial impacts (average T_{zir}^{xtln}= 773±87°C) is remarkably consistent with the average zircon saturation temperature (T_{zir}^{sat}) of ca. 780°C calculated by Watson and Harrison (2005) from a large (~19,000) database of whole rock samples across Australasia. Estimates of bulk continental crust composition yield similar T_{zir}^{sat}values (ca. 780°C, Rudnick and Gao, 2003; ca. 760°C, Gao et al., 1998). Since impact melts largely reflect shock melting of the crust (Melosh, 1989), we note that calculated saturation temperatures for the composition of modern middle crust yield T_{zir}^{sat} of ca. 740°C (Rudnick and Fountain, 1995, Rudnick and Gao, 2003). Although the observed apparent crystallization temperatures (T_{zir}^{xtln}) for impact produced zircon are consistent with T_{zir}^{sat} for present crustal compositions, they appear to be distinctly higher than that for detrital Hadean zircon population (i.e., ~680°C; Watson and Harrison, 2005). On the assumption that the Hadean crust was compositionally closer to Archean than modern crust, we determined T_{zir}^{sat} for Archean rocks in the GEOROC database with sufficient compositional data to permit calculation (n=10059). The resulting T_{zir}^{sat} distribution is bimodal with peaks at ca. 600°C and 775°C with an average value of 690°C (Fig. 3.6).

Although this average T_{zir}^{sat} is close to the Hadean value, several interpretive complexities warrant discussion when comparing T_{zir}^{xtln} and T_{zir}^{sat} spectra. We first note that T_{zir}^{xtln} are sensitive to the activities of silica and rutile during zircon crystallization (i.e., an apparent sub-minimum melting temperatures could reflect either sub-unity activities or sub-solidus growth). Second, the expected T_{zir}^{xtln} for zircon crystallizing from fractionating magmas are expected to be 50-100°C higher than that predicted from zircon saturation calculations (Harrison et al., 2007). These complications notwithstanding, the correspondence between average crustal T_{zir}^{sat} and the impact melt formed zircon reported here suggests that the small population of preserved terrestrial impact melts may be representative of a global average.

3.5.2 Impacts modeled on modern terrestrial target

As a test of robustness, we also ran the model using the same large database from which Watson and Harrison (2005) reported an average T_{zir}^{sat} of 780°C and obtained an average T_{zir}^{xtln} of 810°C. Despite model simplifications, the consistency and relative order of results from the two databases (i.e., $T_{zir}^{xtln} > T_{zir}^{sat}$) suggests that the model is at the least internally consistent and likely predicts accurate temperature spectra. Thus we infer that the zircon crystallization temperature spectra of our necessarily limited empirical results is broadly representative of that produced globally in crustal impact melts.

3.5.3 Impacts modeled on ancient terrestrial target

The average T_{zir}^{xtln} resulting from our model on an ancient simulated target is ~783°C – essentially identical to our observed value for craters formed within the last 2 Ga. The modeled T_{zir}^{xtln} spectrum is shown in Fig. 3.7. A surprising result to us was that the average 'M' value of the zircon forming events is only 1.1 with no value exceeding 'M'=2 (i.e., felsic sources

dominate). This indicates that, although mafic samples (which dominate the database) can contain substantial [Zr], their high melting temperatures and solidi restrict their ability to contribute significantly to impact produced zircon in the crust. Also of note is that the average T_{zir}^{xtln} of 780°C is significantly higher than the average T_{zir}^{sat} of 690°C for the Hadean population. The impact-melt formed zircon temperature distribution partially overlaps the Gaussian-form Hadean temperature distribution but the overall misfit does not support an impact origin for the Hadean zircon grains.

3.5.4 Impacts modeled on lunar target

For simulating the target composition for the Moon we have used both Apollo mission samples as well as lunar meteorites reported by JSC curators. This allows us to have an increased target sample size and may be more representative of the Moon as a whole than that sampled by the Apollo missions alone. To assign a target rock temperature we have adopted the lunar geotherm of Dyal et al., (1973) and used the ΔT associated with the LHB from Abramov and Mojzsis, (2009). We note that this thermal anomaly was calculated for Earth however since the impact flux scales with planetary size the thermal anomaly of such an event should be similar. Modeled crystallization temperature spectra for zircon growth in lunar impact melts indicate that zircon crystallizes in only ~2% of the simulations, reflecting the high abundance of [Zr] necessary to nucleate zircon in predominantly mafic lunar compositions (Boehnke et al., 2013). Interestingly, model temperatures are typically ~100-200°C higher than those for the ancient terrestrial case, presumably reflecting the anhydrous lunar melts, although significantly lower than Ti-in-zircon crystallization temperatures reported for lunar grains (Taylor et al., 2009; Fig. 3.7).

3.5.5 Impacts modeled on Martian target

For the case of Mars, target rock compositions were adopted from Martian meteorites reported by JSC curators, however future Mars missions could provide a better surface composition. The martian-therm is adopted from Squyres and Kasting, (1994) and preliminary results suggest that only a few rock types allow for zircon crystallization with temperatures concentrated around 925° C (Fig. 3.7) and could explain the apparent scarcity of Martian zircon found to date.

3.6 Discussion

As expected, impact produced zircon T_{zir}^{xtln} values are consistent with that calculated from bulk rock [Zr] saturation for the undifferentiated impact melt (Manicouagan). Zircon T_{zir}^{xtln} values for Sudbury and Morokweng – both differentiated bodies – are 50-100°C higher than T_{zir}^{sat}, consistent with previous observations. A Monte Carlo model relating impact thermal anomalies associated with the LHB with Archean rock chemistry supports our T_{zir}^{xtln} estimate – despite its limited size – as being globally representative. The significant temperature contrast between modeled impact formed zircon on Archean crust and that observed for Hadean zircon grains effectively rules out an impact source as a significant contribution to the Hadean population.

An implication of this model is that the relative absence of mafic targets contributing to the zircon temperature distribution could lead to incorrect inferences regarding the nature of the crust drawn from the chemistry and inclusion assemblages in detrital zircon. For example, Harrison (2009) emphasized that the low T_{zir}^{xtln} distribution and felsic inclusion assemblage (i.e., quartz + muscovite) that characterizes the vast majority of the detrital Hadean zircon population

is indicative of their origin at near water saturated granitoids. Given our model result, caution should be exercised when drawing inferences regarding whole-rock mineralogy from inclusion assemblages. Indeed, Darling et al. (2009) found rare muscovite inclusions in impact produced Sudbury zircon crystals. Nonetheless, the high T_{zir}^{xtln} found by both us and Darling et al. (2009) are distinctively higher than the detrital Hadean zircon population to effectively rule out an impact source as a significant contributor to their origin. For impacts to generate such low temperatures the crustal rocks in the Hadean would have to be much more felsic than the Archean rocks of the GEOROC database, used as a proxy for the Hadean surface composition.

Modeled crystallization temperatures appear to argue against most lunar zircons for which U-Pb age and Ti temperature have been determined as forming in response to impact melting (Wielicki et al., 2012b; Grange et al., 2013). One possible complication of Ti crystallization temperatures for lunar zircons is the different behavior of elements in melts of variable redox states, presumably much more reduced (Sato et al., 1973) in lunar as compared to terrestrial melts. However, partitioning coefficients of Ti between zircon and melt were found to be independent of fO_2 (Burnham and Berry, 2012) suggesting little presence of Ti^{3+} in even the most reduced melts and similar behavior in lunar and terrestrial melts. Ti-in-zircon crystallization temperatures of lunar poikilitic grains might provide another discrimination criterion to identify whether or not grains are melt neoformed or inherited. However for lunar zircons incorporated within predominantly mafic lunar melts (SaU 'M' = 3.32; Liu et al., 2012), a high degree of resorption is likely given the propensity of high 'M' magmas to dissolve zircon (Boehnke et al., 2013), potentially accounting for the poikilitic texture. For the composition of SaU 169, growth of zircon would require twenty times higher [Zr] (Boehnke et al., 2013) than

that reported by Lui et al. (2012), essentially ruling out the possibility of this grain growing in equilibrium with the impact melt.

Martian model results, although limited due to the small sample size of Martian meteorites to assess crustal composition, suggest that very few simulated impacts would crystallize zircon with temperatures of ~925° C and may explain the seeming lack of zircon within SNC meteorites.

3.7 Conclusion

Zircon geochronology has the potential to record thermal events associated with impacts, however care must be taken when discriminating between impact-formed zircon and inherited grains from the target, providing no information about the timing of the impact itself. Understanding the mechanism of zircon saturation in crustal melts and coupling this with thermal signatures associated with impacts allows for models to be developed, as described above, that may be used as a discrimination criterion for which to determine whether a grain or populations of grtains is formed within an impact melt or inherited from the target. This discrimination is essential if zircon is to be used as an accurate probe of planetary impact history.

3.8 Figures

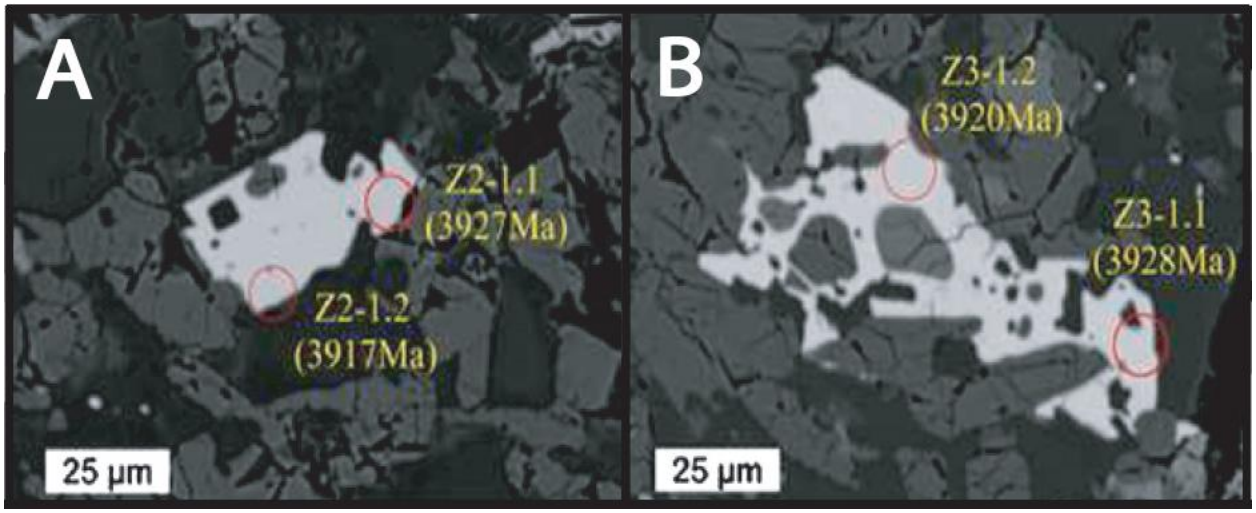

3.8.1 Figure 3.1

A) Rectangular grain with rounded, embayed and straight crystal-face boundaries with adjacent grains. B) Interpreted poikilitic zircon penetrating surrounding pyroxene and plagioclase, and enclosing small silicate mineral grains. Ages noted in parentheses are ^{204}Pb corrected ^{207}Pb/^{206}Pb ages. From Liu et al., (2012).

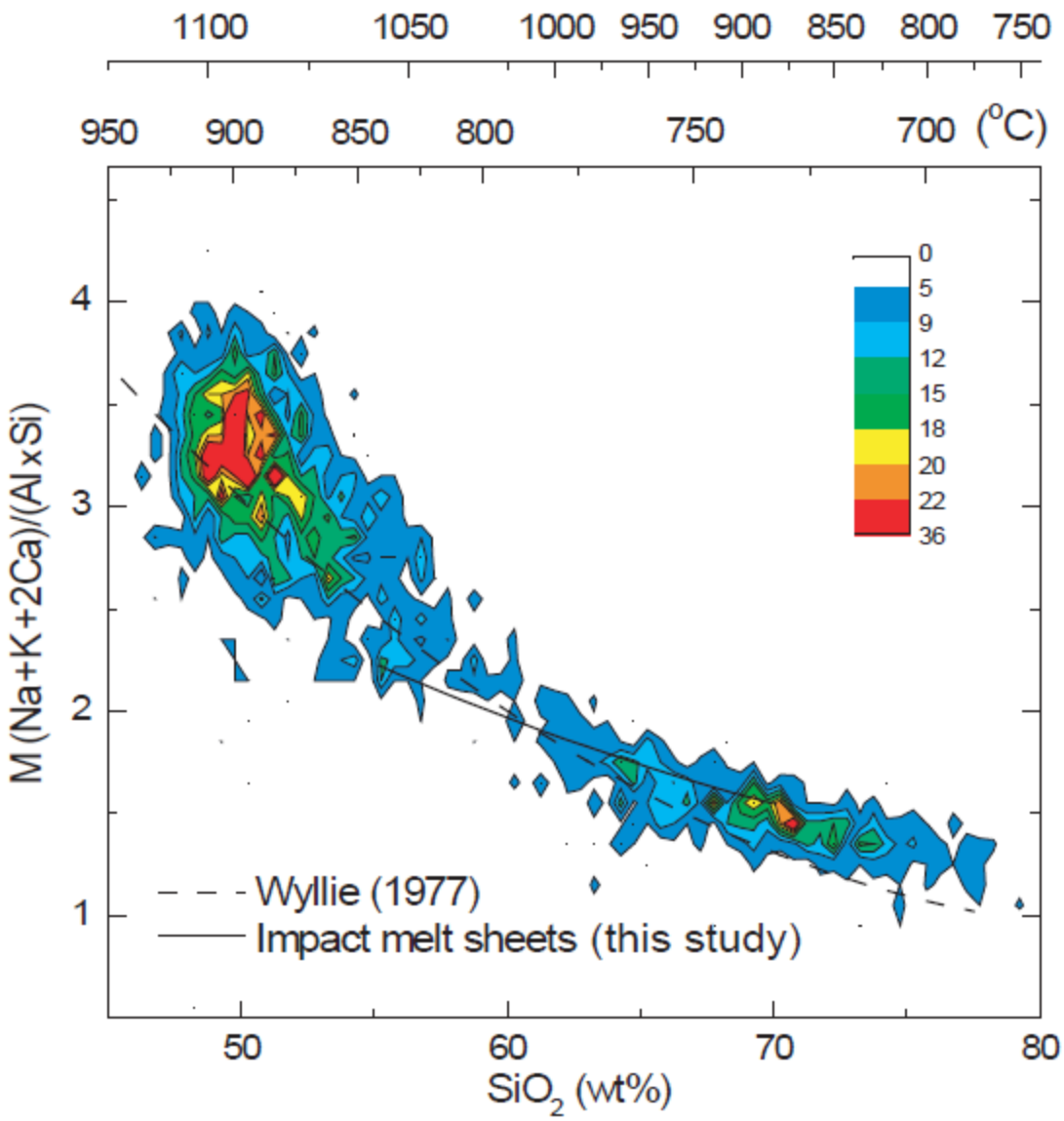

3.8.2 Figure 3.2

GEOROC Archean database (n=10058) plotted as M vs SiO_2. Top axes are experimental results from Wyllie (1977) at 5 kbar, whereby the upper and lower axes represent liquidus temperatures at 5 wt% H_2O and water-undersaturated solidus temperatures, respectively. Wyllie (1977) dashed line is a fit of M vs. SiO_2 for melting experiments using felsic, intermediate and mafic compositions. This fit coincides with the regression of M vs. SiO_2 for bulk composition

of impactites from this study, which underscores the validity of using experimental melting relations to model impactite formation.

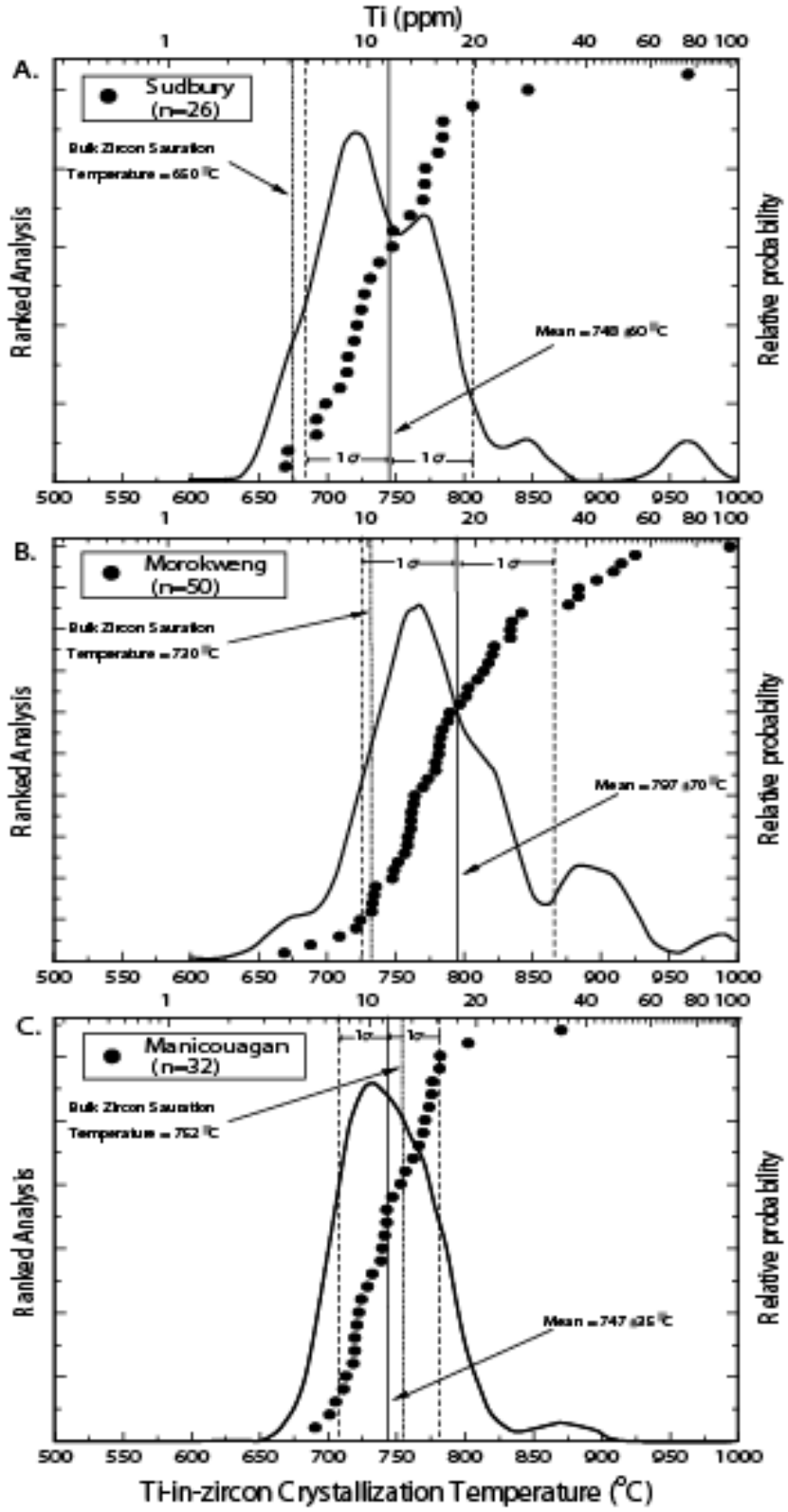
Ti (ppm)
A.
Sudbury
(n=26)
Bulk Zircon Saturation
Temperature = 650 °C
Mean = 748 ±60 °C
1σ
1σ
Ranked Analysis
Relative probability
B.
Morokweng
(n=50)
Bulk Zircon Saturation
Temperature = 720 °C
Mean = 797 ±70 °C
C.
Manicouagan
(n=32)
Bulk Zircon Saturation
Temperature = 752 °C
Mean = 747 ±35 °C
Ti-in-zircon Crystallization Temperature (°C)

3.8.3 Figure 3.3

Titanium concentrations and Ti-in-zircon crystallization temperature, assuming a_{TiO2}=1 (Watson and Harrison 2005), of impact produced zircon. Saturation temperature underestimates crystallization temperature for differentiated impact melts (i.e. Sudbury and Morokweng; Watson and Harrison, 2005) (A) Sudbury impact produced zircon T_{zir}^{xtln} = 748±60°C, bulk norite T_{zir}^{sat} = 650ºC (calculated from Lightfoot and Zoltov, 2005). (B) Morokweng impact produced zircon T_{zir}^{xtln} = 797±70°C, bulk melt sheet T_{zir}^{sat}= 730ºC (calculated from Andreoli et al., 1999). (C) Manicouagan impact produced zircon T_{zir}^{xtln} = 747±35°C, bulk melt sheet T_{zir}^{sat}= 752ºC (calculated from Floran et al., 1978).

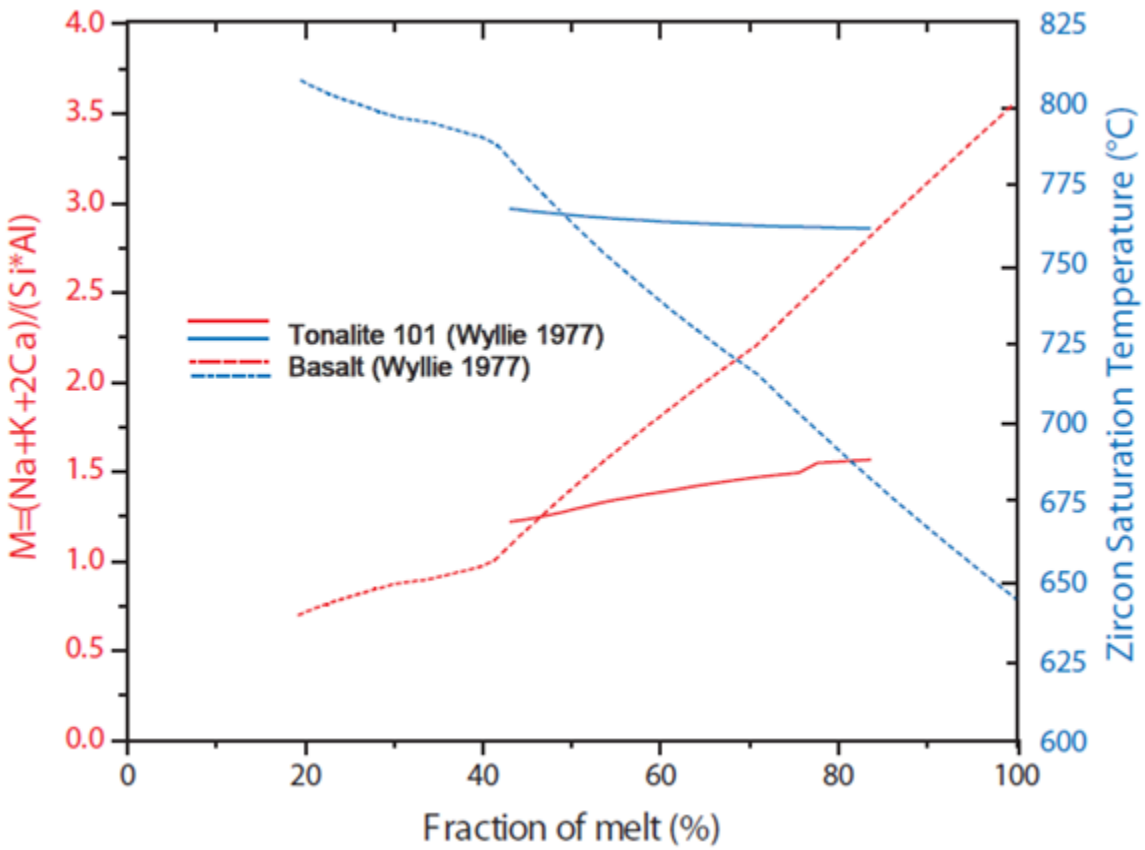

3.8.4 Figure 3.4

Plot of M and zircon saturation temperature (assuming a constant [Zr]) vs. fraction of melt to show the large variations in M of partial melts. Note that this effect is much greater for mafic rocks.

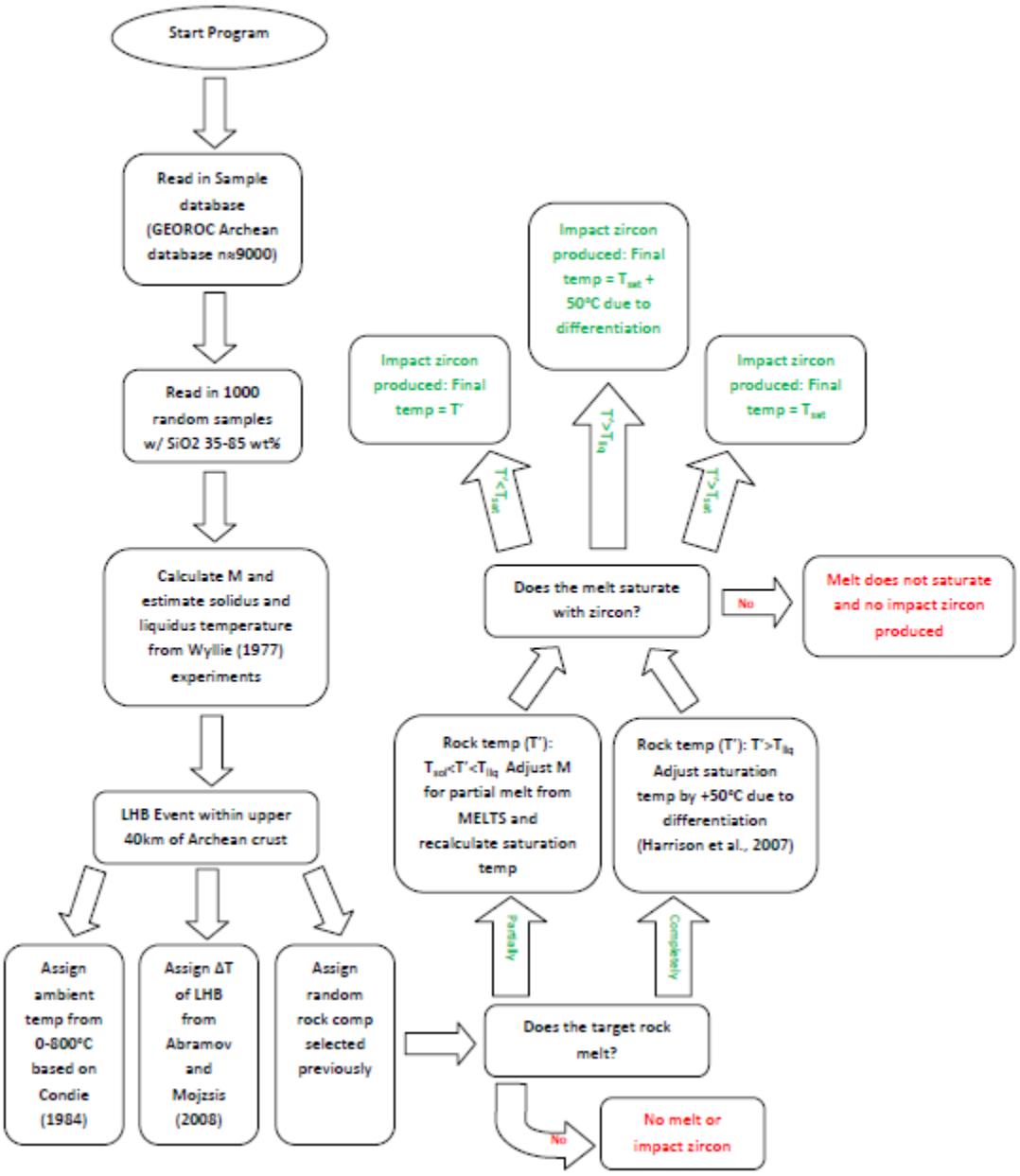

3.8.5 Figure 3.5

Flow cart of logic statements for zircon saturation model within simulated impact scenarios described in the text..

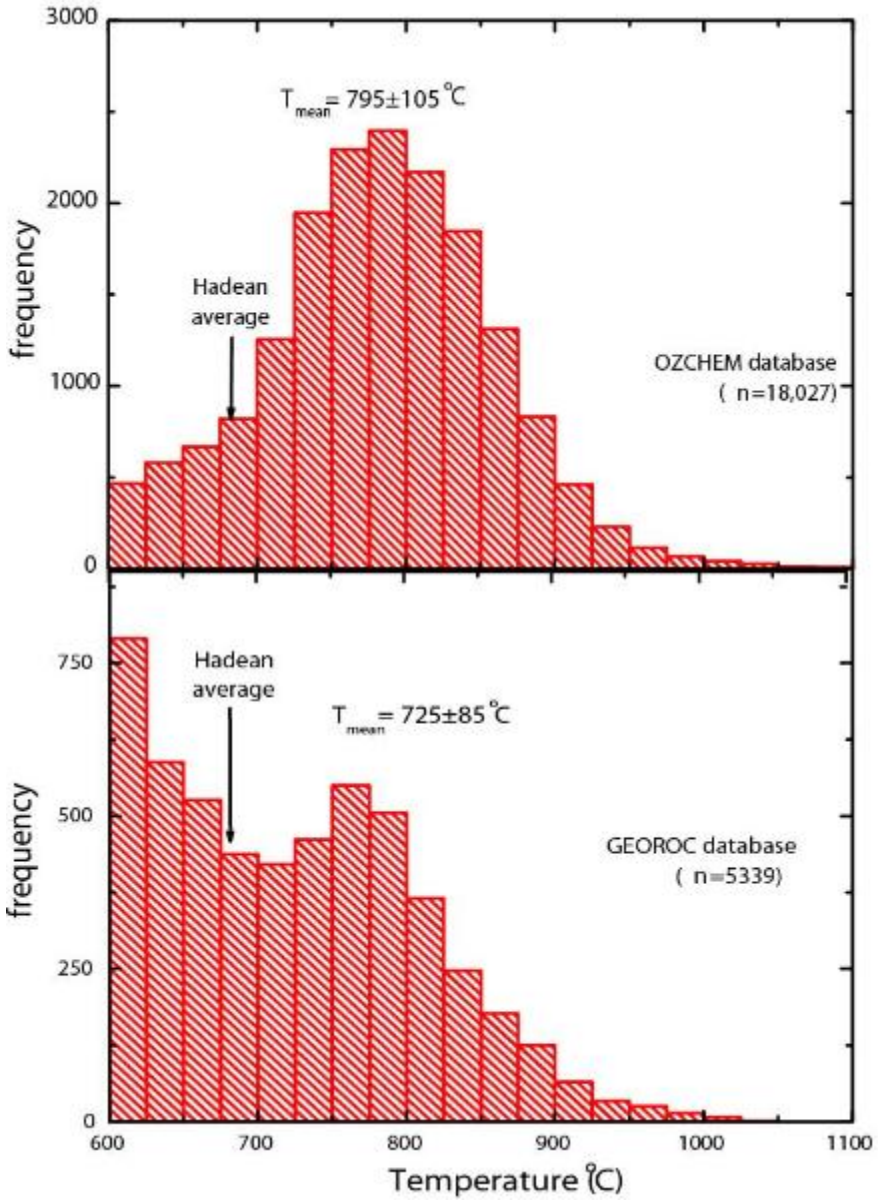

3.8.6 Figure 3.6

Calculated whole rock zircon saturation temperatures for OZCHEM and GEOROC databases described in the text.

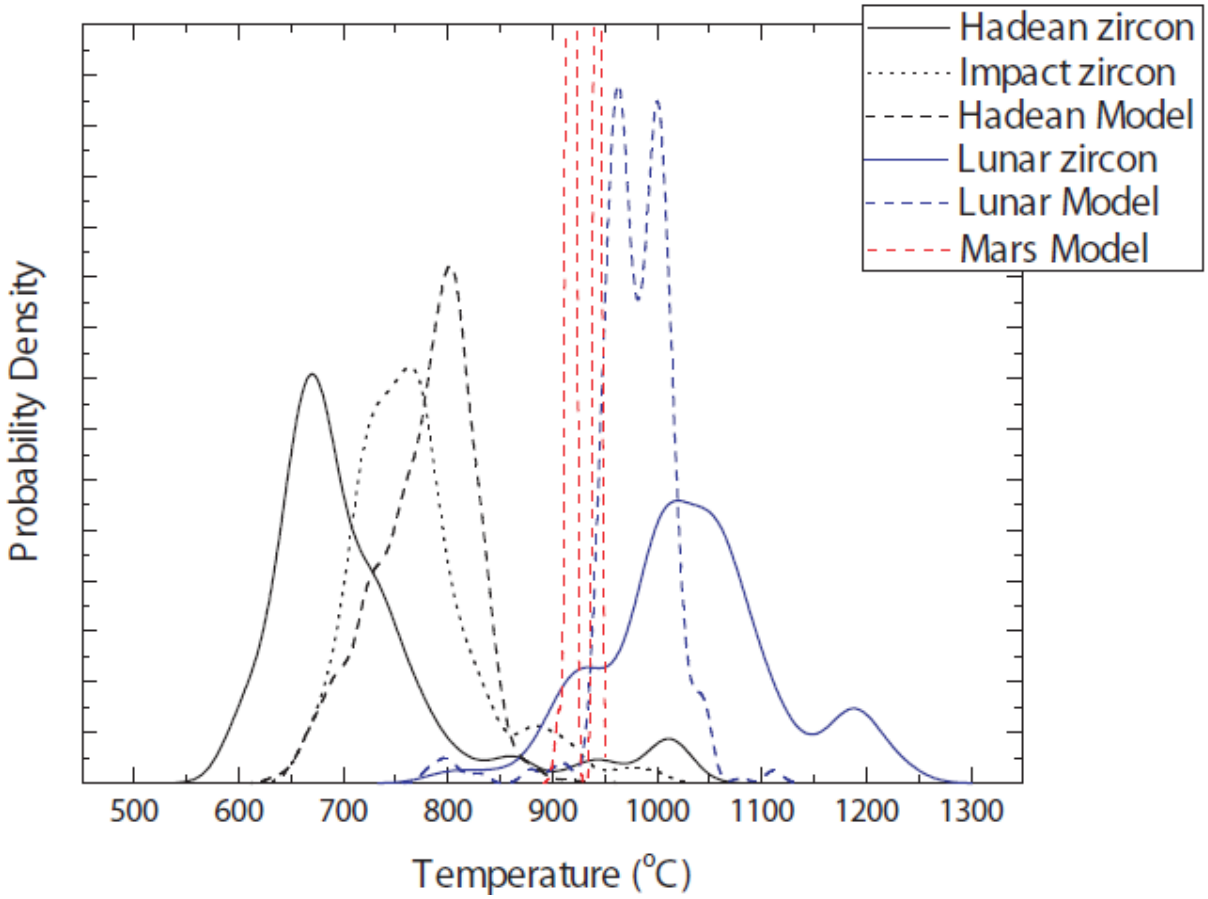

3.8.7 Figure 3.7

Probability density plot of Ti-in-zircon crystallization temperature for terrestrial Hadean zircon (Harrison et al., 2008), terrestrial impact produced zircon (Wielicki et al., 2012; Darling et al., 2009), and Lunar zircon (Taylor et al., 2009; Taylor personal communication) . Also plotted are the modeled crystallization temperatures for an Archean crust (based on Archean samples from the GEOROC database), lunar surface (based on lunar meteorites) and a Martian surface (based on Martian meteorites).

4. Investigating Pb*-loss in impact zircon

4.1 Introduction to Pb*-diffusion in zircon

Many efforts have been made to quantify and characterize diffusion in zircon, primarily for Pb, as this is vital to the use of zircon as an accurate geochronometer. Experimental data on various cations and anions shows the remarkably slow diffusion of certain elements such as REE and Pb at standard crustal temperatures. This extremely slow diffusion and the relative insolubility of zircon in crustal melts often results in the existence of several generations of geochemical information in a single zircon grain (Cherniak and Watson, 2003) and contributes to the rise of zircon as the premier geochronometer in Earth Science.

Understanding the effects of Pb-loss within zircon subjected to thermal and shock environments associated with large impacts is investigated. Many impacts either do not produce large melt sheets or have been eroded away such that no neoformed zircons remain to date the impact. Although neoformed grains are the most accurate and robust for dating, zircons that have lost Pb* as a result of the impact event may also be utilized to accurately date impacts.

4.2 Reports of 'reset' zircon in terrestrial impactites

Although rare in the literature on terrestrial impactites, there have been a few reports of 'reset', complete loss of Pb*, zircons as well as modeling to predict the occurrence of such grains. The presence of partially or completely 'reset' zircon would allow for determination of the age of the thermal event associated with the Pb*-loss and presumably the age of the impact event. However this requires substantial Pb*-loss to provide good estimates of lower intercept age, presumably the impact age.

4.2.1 Vredefort impact structure, South Africa

Currently the Vredefort impact structure, South Africa is the most commonly reported crater with partially and/or completely 'reset' zircon (Fig. 4.1). Two studies have reported the presence of 'reset' zircon (Kamo et al., 1996; Moser et al., 2011) associated with the Vredefort impact structure. Although both studies suggest that these grains may have been shocked and heated such that all of the Pb* was rejected from the grain, the authors acknowledge the possibility of recrystallization as opposed to loss of Pb* (Moser et al., 2011). The grains are primarily found in what is known as the 'hot shock' zone where the heat and pressure from the impact cause the majority of the grains to be partially or completely 'reset' (Moser et al., 2011).

4.2.2 Cretaceous ejecta

'Reset' zircons have also been identified in ejecta (Krogh et al., 1993) associated with the K-Pg impact, linked to the Chicxulub impact structure (Hildebrand et al., 1991). Dating ejecta layers permits dating of impact events when no known crater exists (as is the case of older impacts into ocean basins), and provides yet another tool with which to determine the age of an impact event. Ejecta blankets tend to be clast rich and cool on relatively short timescales, as compared with impact melt sheets (Abramov et al., 2013), however if Pb* diffusion in shocked grains is rapid the heating within an ejecta blanket may be sufficient to 'reset' zircon. The grains identified in distal ejecta associated with Chicxulub may also have been 'reset' while transported in the vapor plume rather than in the ejecta blanket.

4.2.3 Modeled Pb* diffusion in impact zircon

Abramov et al. (2013) modeled a Sudbury sized crater (diameter: ~180 km) with the diffusion behavior of both shocked (Cherniak et al., 1991) and unshocked zircon (Cherniak and

Watson, 2000). We note that for impact shock damaged zircon, the lack of diffusion studies required the use of radiation damaged grains as shocked analogs when modeling impact induced Pb*-loss. The model predicts a large number of 'reset' zircon within the center of a Sudbury sized crater. The Abramov et al. (2013) modeled crater is substantially larger than Morokweng (diameter: ~90-130 km) and Popigai (~100 km), thus the fraction of predicted 'reset' grains for these two craters would be lower; conversely the opposite should be the case at the larger Vredefort impact (diameter: ~300 km). While a few 'reset' zircons have been reported from Vredefort (Kamo et al., 1996; Moser et al., 2011), the majority of grains analyzed have been inherited (Kamo et al., 1996; Moser et al., 2011; Wielicki et al., 2012b) from the target rock with varying degrees of Pb*-loss. Analysis presented here permits tests of the model predictions on the occurrence of 'reset' zircon and the mobility of Pb* within shocked grains.

4.3 Samples

4.3.1 Vredefort granophyre and pseudotachylite breccia

The Vredefort impact structure in South Africa is the largest known terrestrial impact site (Earth Impact Database, 2013) and represents the deeply eroded remnant of a ~2.0 Ga, (Krogh et al., 1996b) ~300 km wide crater (Reimold and Gibson, 1996). Although the melt sheet has been eroded due to post-impact uplift, pseudotachylite breccia and granophyre veins remain. Thin-sections of pseudotachylite breccia (VD_PB; Fig. 4.3A) collected near the quarry at Leeukop, just west of Parys and separated zircons and thin-sections from the granophyre (VD_G) sampled near the Kommandonek Nature Preserve (provided by Roger Gibson, University of Witwatersrand and W. Uwe Reimold, Humboldt-University Berlin; Gibson and Reimold, 2005) were used for analysis (for sample locations see chapter 2.2.1). Pseudotachylite breccia sample

VD_PB consists of 1-3 cm clasts of Archean granite to granodioritic gneiss target material within a fine grained crystalline matrix (Reimold and Gibson, 2006). Granophyre sample (VD_G) consists of fine-grained crystalline quartz, plagioclase and alkali feldspar with long laths of hypersthene and small grains of magnetite (Reimold and Gibson, 2006). Zircon grains (~20 grains isolated) average ~100 μm and tend to be fractured. Crystals lack igneous oscillatory zoning in CL and are intimately intergrown with a Mg-rich pyroxene phase identified by energy dispersive X-ray analysis (Fig. 4.3 and inset of Fig.4.6).

Zircon grains from the granophyre were imaged via BSE as unpolished single loose grains (Figure 4.3B), in polished thin-section (Figure 4.3C & D), in polished 1" epoxy mounts (Figure 4.3E & F) and compared to images from polished thin-sections of lunar meteorite SaU 169 (Figure 4.3G & H; Nemchin et al., 2008; Liu et al., 2012).

4.3.2 Morokweng basement zircon

Morokweng impact structure, South Africa, is a ~100 km-diameter impact crater (Andreoli et al., 2008; Earth Impact Database, 2014) and provides a unique opportunity to investigate the use of zircon as a probe of planetary impact history as the age of the impact melt sheet has been well-established at ~145 Ma (Hart et al., 1997; Wielicki et al., 2012b), and multiple drill cores exist that penetrate the melt sheet into the brecciated and shocked target below (Hart et al., 1997). Thus, chronometers used to date zircons from the target rocks, directly below the melt sheet can be compared with the known age of the impact event to asses which systems record the age of the impact. Samples from the M3 borehole (provided by Marco Andreoli), drilled ~12 km NW of the reputed center of the aeromagnetic anomaly ($26^0$30' S, $23^0$30' E; Koeberl and Reimold, 2003; Jourdan et al., 2010), which intersects ~870 m of impact

melt consisting of differentiated granophyric to noritic rocks overlaying brecciated and shocked basement gneisses (Hart et al., 2002) were utilized for this study. Zircons were previously separated from samples at depths of 155 m and 400 m from the main impact melt sheet and are euhedral to subhedral with no evidence for shock (see chapter 2.4.2.2; Wielicki et al., 2012). Zircon separated from the 1069 m core split (MKB), within the shocked pyroxene gneissic basement (Hart et al., 2002) directly below an impact melt dyke and approximately 200 m below the main impact melt sheet ranged from 50-120 μm in size and exhibit igneous textures and oscillatory zoning, with no evidence of shock features analogous to those reported by Erickson et al., (2013) for Vredefort zircon. We note that although no micro-scale shock features have been identified within the zircons analyzed, the grains do appear fractured (inset of Fig. 4.7 and Fig. 4.9) relative to those of the main melt sheet. The sample location, in the center of the magnetic anomaly and 200 m below the impact melt sheet, would be expected to reach >100 Gpa and >10000 K (Collins et al., 2012) during the contact and compression stage of impact and thus are presumably highly shocked, even if some of these features have been annealed by relatively low temperatures post-impact (Nasdala et al., 2004). The sample location is also consistent with the hot-shock zone (Moser et al., 2011), where it is estimated that all grains, damaged or un-damaged, will be 'reset' in U-Pb (Abramov et al., 2013). Shock features such as multiple PDF's in quartz and pebbles of the underlying basement have been identified previously (Hart et al., 1997) in drill cores adjacent to the M3 core, and also suggests a highly shocked target. As the majority of the sample was used to extract the relatively few zircons used, shock features have not been investigated within this sample; however we presume it to be equally shocked.

4.3.3 Popigai suevite and shocked gneiss

The Popigai impact structure, Siberia, Russia, has an estimated crater diameter of ~100 km ("Earth Impact Database," 2014) and late-Eocene in age. Due to post-impact uplift and erosion, no melt sheet remains today within Popigai and efforts to date the impact event have relied on tagamites, impact melt rocks with some target rock clasts (10-20%; Bottomley et al., 1997), or dating of Eocene ejecta and microkrystites from Italy and ocean drill cores (Glass et al., 2004; Whitehead et al., 2000). The presence of impact melt and the shocked nature of the samples warranted investigation into Pb*-loss and the presence of 'reset' zircon.

4.3.4 Sudbury breccia and Onapping formation

Samples of pseudotachylite breccia were collected approximately 2 km west of Windy Lake and 2-3 km from the edge of the Sudbury Igneous Complex (N42°36.457', W81°32.006') as well as samples of Onaping formation, which is presumed to be suevite impact fallback and caps the SIC (Grieve et al., 2010), collected within the crater (N46°35.962', W81°22.968'). Sudbury pseudotachylite breccia and Onaping formation zircons (see chapter 2.2.3) show no direct evidence for shock features however varying amounts of impact melt suggest elevated temperatures and warrant investigation of Pb*-loss.

4.4 Methods

For all hand samples, thin-sections were obtained and examined via electron imaging using a LEO 1430 VP scanning electron microscope (SEM) to assess zircon crystal size and abundance. Mineral separates were obtained from bulk rock samples by standard heavy liquid separation procedures. Separated zircon crystals were handpicked and mounted in 1 in. diameter epoxy mounts together with AS3 zircon standard (Paces and Miller, 1993). Ion

microprobe analyses were conducted with a CAMECA ims1270 at UCLA in three collection modes: 1) single spot mode (see chapter 2.3.3); 2) multi-spot analysis; and 3) depth profiles. Multi-spot analysis allows for a broad investigation of an entire grain to identify portions possibly 'reset' by the impact, which may occur within grains associated with crystal lattice defects (Moser et al., 2009). Depth profile allow for very high resolution investigation of the outer several microns of the zircon surface to see if any 'reset' rims exist.

4.4.1 Multi-spot analysis

Multi- spot analysis mode was done using an ~8–12 nA mass-filtered $^{16}O^{-}$ beam focused to spots between ~20 and 35 μm (see chapter 2.3). Spots were placed such that each spot did not overlap with the other and grains that allowed at least three spots were focused on for statistical reasons.

4.4.2 U-Pb depth profile

U-Pb depth profile mode was done using a ~12–20 nA mass-filtered $^{16}O^{-}$ beam de-focused to spots between ~40 and 60 μm with a small aperture setting to ensure transmission of ions originating from the crater bottom only. Analytical procedures for depth profiling zircons were broadly similar to those outlined in Abbott et al., (2012). Each depth profile analysis session began with depth profiling a 91500 zircon, followed by an AS3 to calibrate the elemental abundances and the U/Pb sensitivity in each unknown grain. Data reduction for zircons was performed using in-house software package ZIPS v3.04.

Although it was found that the Pb-Pb age and Th/U ratio remain constant with depth for a concordant and isotopically homogeneous grain during a zircon depth profile, Trail et al. (2007) noted a predictable inter-element discrimination that occurs due to varying ion counts of Pb and

U as a function of depth. This secular change influences the apparent U/Pb concordance calculation (i.e. [^{206}Pb/^{238}U age]/[^{207}Pb/^{235}U age]*100, expressed as % concordance). To monitor and correct for this effect, we also depth profile AS3 for an equal amount of time.

4.5 Results

4.5.1 Vredefort impactites

U-Pb depth profiles were carried out on multiple zircon grains separated from the pseudotachylite and granophyre units from the Vredefort impact structure. Pseudotachylite samples from Vredefort have been shown to contain both inherited and neoformed zircon and thus showed the most promise for cores with epitaxial overgrowths (Kamo et al., 1996; Moser, 1997; Wielicki et al., 2012b), as the melt is presumed to be saturated in [Zr] prior to resorption of all of the inherited grains. Depth profiles of a single zircon from the INL drill core (Kamo et al., 1996) did reveal multiple apparent rims (plateaus in the depth profile) including an outer rim of 2224±54 Ma and an inner rim of 2542±48 Ma overgrown on a 2710±28 ma core (Fig. 4.4). Although these ages do not correspond with the Vredefort impact they do show the potential of inherited zircons to grow epitaxial overgrowths that can be spatially resolved from the core age. No other Vredefort zircon grains showed any evidence for overgrowth rims suggesting this phenomenon may not be common in impactites.

Multi-spot analysis results, from 7 spots on one grain, yield different Pb-loss domains that suggest a heating event presumably associated with emplacement of Anna's Rust Sheet, a suite of mineralogically and chemically related intrusions in the core and collar of the Vredefort Dome at ~1.1 Ga – a common thermal overprint reported in previous studies (Reimold et al., 2000; Fig. 4.5). Although not uniform, Pb-loss did appear to be highest near the grain edges,

contrary to that previously observed by Moser et al., (2009). No other zircons yield results consistent with thermal events associated with the impact or other known thermal events in the region.

Zircons isolated from the granophyre unit (VD_G) of the Vredefort impact show an intimate relationship with Mg-rich pyroxene (i.e. possibly poikilitic texture; identified via energy-dispersive X-ray spectroscopy) similar to that discovered in lunar meteorite SaU 169 (Liu et al., 2012). Although not ideal analogous to lunar grains the presence of such a texture within the largest terrestrial impact crater deserved further investigation. Twelve of twenty isolated grains were analyzed as the other eight were so inter-grown that no continuous surface was available to place the ion beam without possibility of common Pb contamination. One grain was rejected due to high common Pb presumably contributed from contaminated areas or from the inter-grown pyroxene. Results indicate that all the grains were inherited from the Archean target, as noted in previous reports (Fig. 4.6), with a crystallization age of 3077±74 Ma, similar to that of VD_PB, and a lower intercept of 1984±150 Ma (MSWD = 2.6). No grains appear to have grown or been 'reset' within the impact melt. Interestingly, grains from a small hand sample and thus in close proximity showed dramatically varying amounts of Pb-loss (0-80%; Fig. 4.6) which may suggest vastly different shock pressures on the mineral grain scale.

4.5.2 Morokweng basement

Zircons from the Morokweng main impact melt sheet previously analyzed yield U-Pb ages consistent with crystallization from a single large impact melt sheet and show no evidence for inheritance of zircons from the target rock (see chapter 2.4.2.2; Fig. 4.7 & 4.8). U-Pb depth profile analysis from zircon separated from the brecciated basement ~850 m below the impact

melt (Jourdan et al., 2010) yield concordant ages ranging from ~2.8-3.3 Ga, similar to but slightly older than those estimated for the target rocks (~2.7-3.0 Ga; Koeberl and Reimold, 2003). CL images of two grains showed CL-active outer rims (inset in Fig. 4.9) similar to those observed in Hadean zircons and possibly associated with the Late Heavy Bombardment (Trail et al., 2007a), however depth profiles of these grains did not yield any evidence for the presence of overgrowth or 'reset' rims (Fig. 4.9).

4.5.3 Popigai impactites

Zircons from multiple suevites previously shown to have Proterozoic core ages (see chapter 2.4.2.5), presumably inherited from the target rock, were investigated for rims associated with the ~35 Ma crater (Bottomley et al., 1997). No evidence for rims associated with the impact was identified possibly due to the small amount of impact melt within these samples. However, multiple grains yield outer rim ages coincident with the nearby Siberian Flats (Kamo et al., 2003).

4.5.4 Sudbury impactites

Multi-spot analysis of zircon from the Sudbury breccia yield ages ranging from ~3.3 Ga to ~250 Ma, with no evidence of a thermal event associated with the impact. Multiple concordant grains aged to ~250 Ma suggest a substantial heating event at this time which may have overprinted any thermal evidence of the impact, presuming the signal existed originally. We have found no related literature to this ~250 Ma heating event.

4.6 Discussion

Previous research has shown that zircons from terrestrial impactites can be aggregates of multiple grains that may not be distributed as inherited cores and impact induced rims. Thus,

domains indicative of the impact can sometimes be found within grain cores (Moser et al., 2009). To investigate this phenomenon we used a multi-spot approach to acquire ages of many different parts of polished zircons from multiple impactites. Our results showed no evidence for internal domains of 'reset' zircon within the samples investigated.

Our results indicate that zircon grains beneath ~870 m of impact melt at Morokweng, South Africa show relatively little disturbance within the U-Pb system, presumably due to the slow diffusion of Pb (Cherniak and Watson, 2003) in zircon from shocked impactites. This appears to contradict recent studies (Moser et al., 2011; Abramov et al., 2013), which predict many 'reset' grains within the brecciated basement below the impact melt. This result suggests that Pb*-diffusion in zircon, separated from brecciated and shocked impactites, is remarkably slow. We note that Abramov et al., (2013) modeled a Sudbury sized crater (diameter: ~180 km) for their Pb*-diffusion study, which is substantially larger than Morokweng (diameter: ~90-130 km), thus the fraction of predicted 'reset' grains for Morokweng would be lower; conversely the opposite should be the case at the larger Vredefort impact (diameter: ~300 km). Slow diffusion of Pb* in impact zircon may explain the relatively few 'reset' zircons reported from Vredefort, South Africa (Kamo et al., 1996; Moser, 1997; Moser et al., 2011; Wielicki et al., 2012b) and the seeming lack of 'reset' grains from other large craters such as Sudbury, Canada (Krogh et al., 1996b) and Morokweng, South Africa. Although a few 'reset' zircons have been reported from Vredefort (Kamo et al., 1996; Moser et al., 2011), the majority of grains analyzed have been inherited (Kamo et al., 1996; Moser et al., 2011; Wielicki et al., 2012b) from the target rock with varying degrees of Pb*-loss. Recrystallization of these grains may also be responsible for apparent impact ages, as noted by Moser et al., (2011) for at least a few of the grains reported, making 'reset' zircon appear very rare in terrestrial impactites. This apparent over prediction of

'reset' zircon, particularly for damaged zircon, may be attributed to the lack of diffusion studies on shocked zircon and the use of radiation damaged grains as shocked analogs when modeling impact induced Pb*-loss. However it appears that the unshocked model (Abramov et al., 2013) also over predicts the abundance of 'reset' zircon, possibly due to rapid annealing of zircon shock damage (Nasdala et al., 2004) in target grains near the impact melt. Future work on Pb*-diffusion and annealing times in naturally shocked zircon could be used to refine models and better predict the occurrence of 'reset' zircon in impacts.

The lack of any identifiable epitaxial overgrowths in depth profiles of Morokweng zircon, and the seemingly few reports in terrestrial impactites, suggests that the formation of such rims requires specific conditions that may not be present in the majority of recent impact events, possibly suggesting an alternative mechanism for the formation of rims on Jack Hills zircons (Trail et al., 2007a; Abbott et al., 2012). However, we note that this may be due to the dramatic decrease in basin forming events, believed to be occurring regularly during the LHB, and may indicate that only the largest of impacts provide the conditions necessary to grow such epitaxial over-growth rims.

4.7 Conclusion

Although some reports exist about reset zircon within samples primarily from the 'hot shock' area from Vredefort (Moser et al., 2011), the scarcity of such grains demonstrates the remarkably slow diffusion of Pb* from zircon that presumably reached extremely high temperatures and pressures associated with the impact (Collins et al., 2012). This may be associated with the rapid passing of the compression shock wave (few to tens of msec) and the possibility for rapid annealing of shock damage due to the remaining heat. When Pb*-loss does occur, the amount of loss is directly related to the error of the lower intercept and in many cases,

such as the example for Vredefort Granophyre discussed above, the lack of substantial Pb* loss results in >100 Ma errors associated with the impact event, thus not allowing for accurate dates to be established. Diffusion experiments on shocked zircon are necessary to fully understand the effects of shock microstructures on Pb*-loss.

4.8 Figures

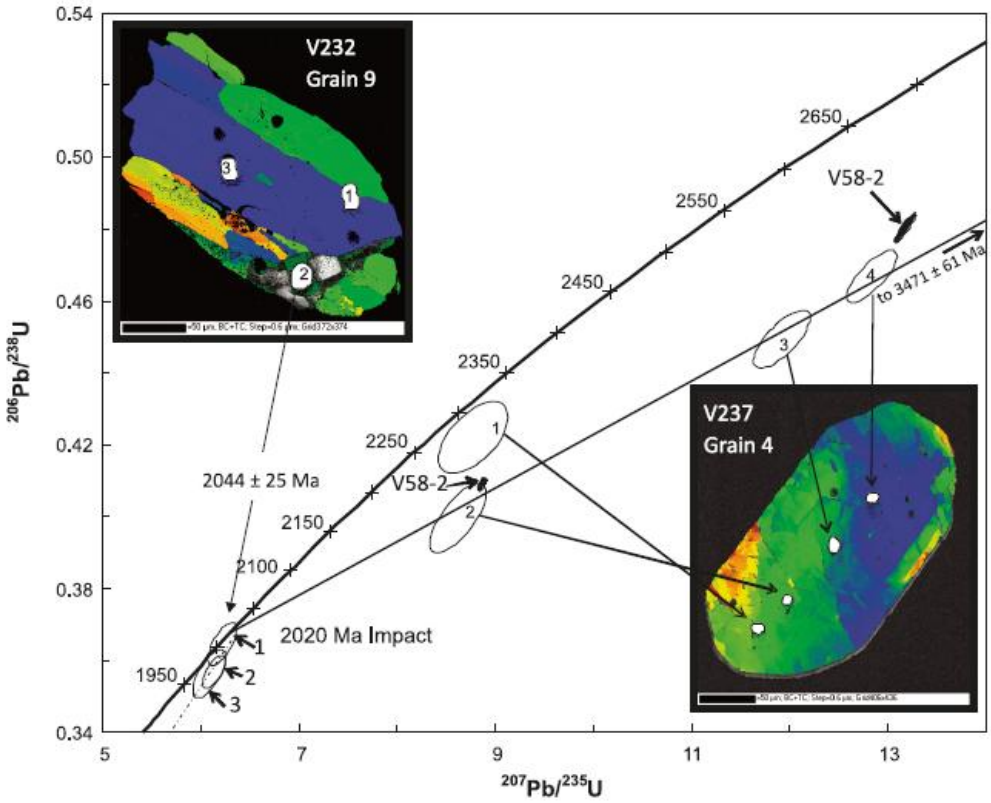

4.8.1 Figure 4.1

Concordia plot showing SHRIMP-RG spot analyses from two zircon grains (V237 G4 and V232 G9) from the Vredefort impact structure. Also shown is ID-TIMS analysis of single grains from sample (V58-2; Moser, 1997), collected approximately ~1 km away. Inset images are EBSD relative misorientation maps, with misorientations between domains color coded (warmer color is greater degree of misorientation). Degree of discordance in the V237 G4

appears to be highest in the zone of greatest impact deformation (spots 1 and 2). For V232 G9, all domains give an impact age, suggesting total Pb-loss from the xenocryst during impact heating, shock, and crystal-plastic deformation. From Moser et al., (2011).

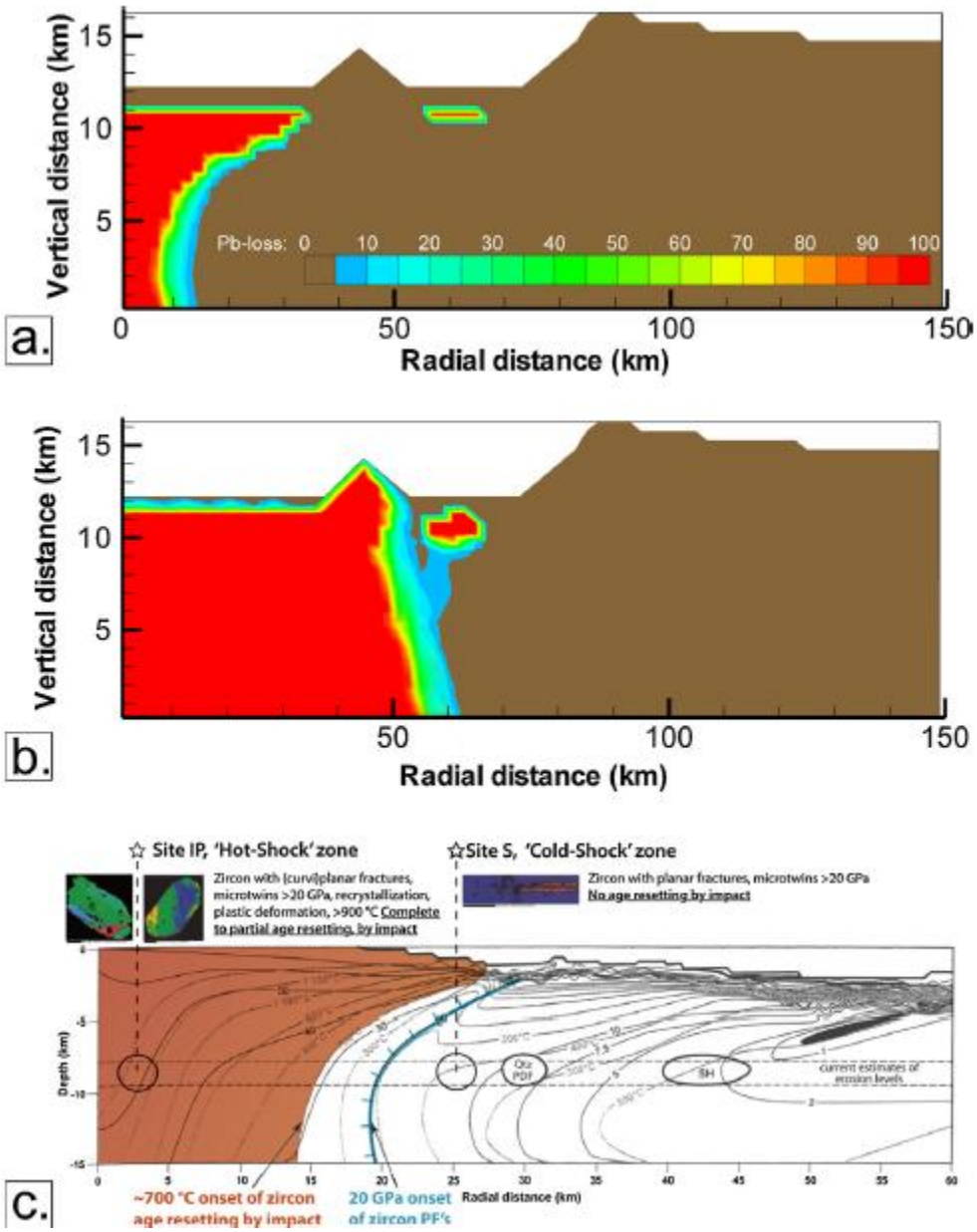

4.8.2 Figure 4.2

Percentage of Pb*-loss in 100 µm zircon grains within a 180 km terrestrial impact. A. Normal zircon grains; B. Radiation damaged zircon grain; C. Comparison with estimate of age-resetting within the Vredefort impact structure constrained by field observations of Moser et al., (2011). From Abramov et al., (2013).

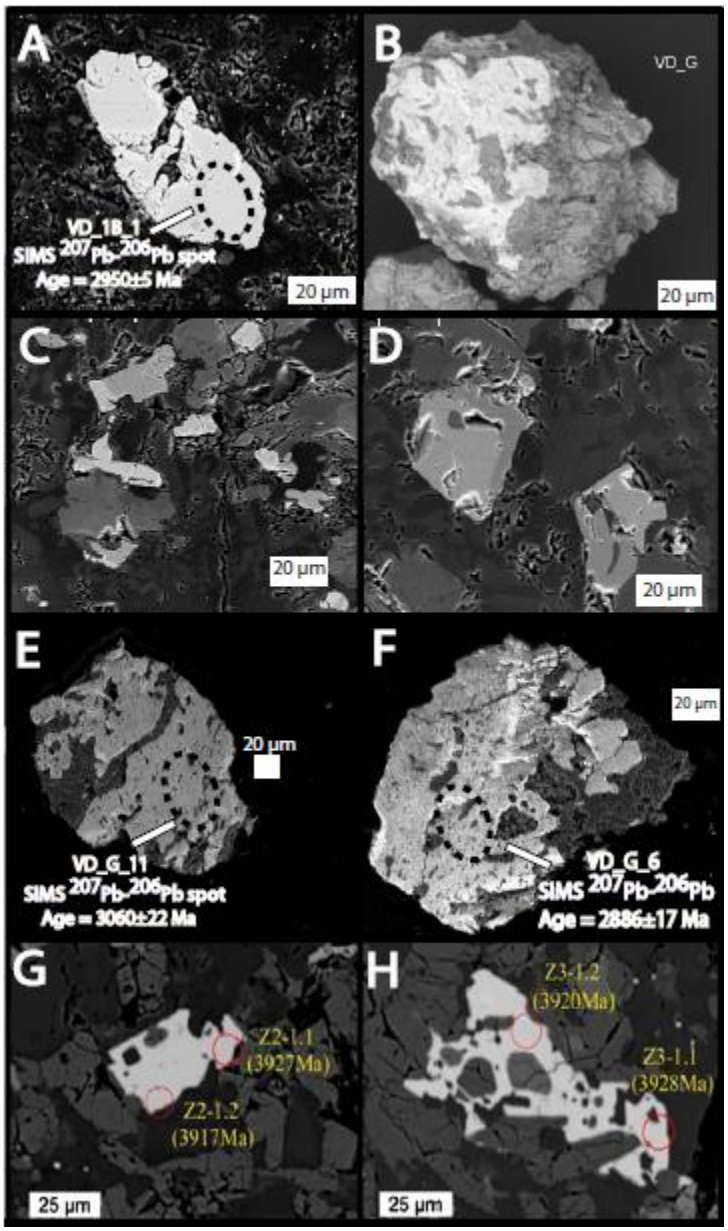

4.8.3 Figure 4.3

BSE images of in-situ VD_PB zircon (image A) and VD_G zircon (images B-F) compared to images of lunar meteorite SaU 169 (images G & H; Liu et al., 2012), highlighting similar textures. See text for further description.

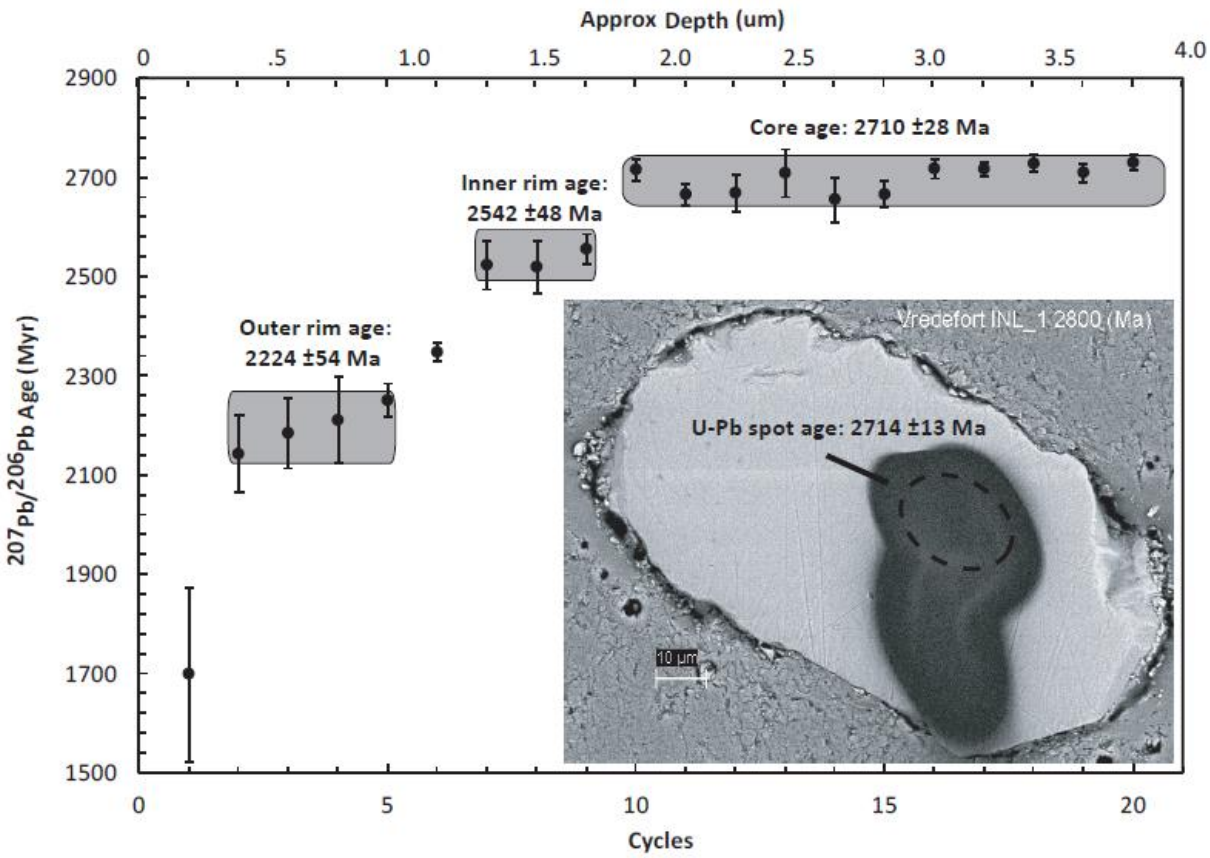

4.8.4 Figure 4.4

$^{207}Pb/^{206}Pb$ age depth profile for Vredefort zircon from INL drill core (Kamo et al., 1996). Although two rims appear to be present on the ~2700 Ma core, no rims with ages consistent with the accepted impact age have been identified. The oldest rim of ~2550 Ma may reflect some previous metamorphic event with the younger rim possibly attributed to partial Pb*-loss during the Vredefort impact event.

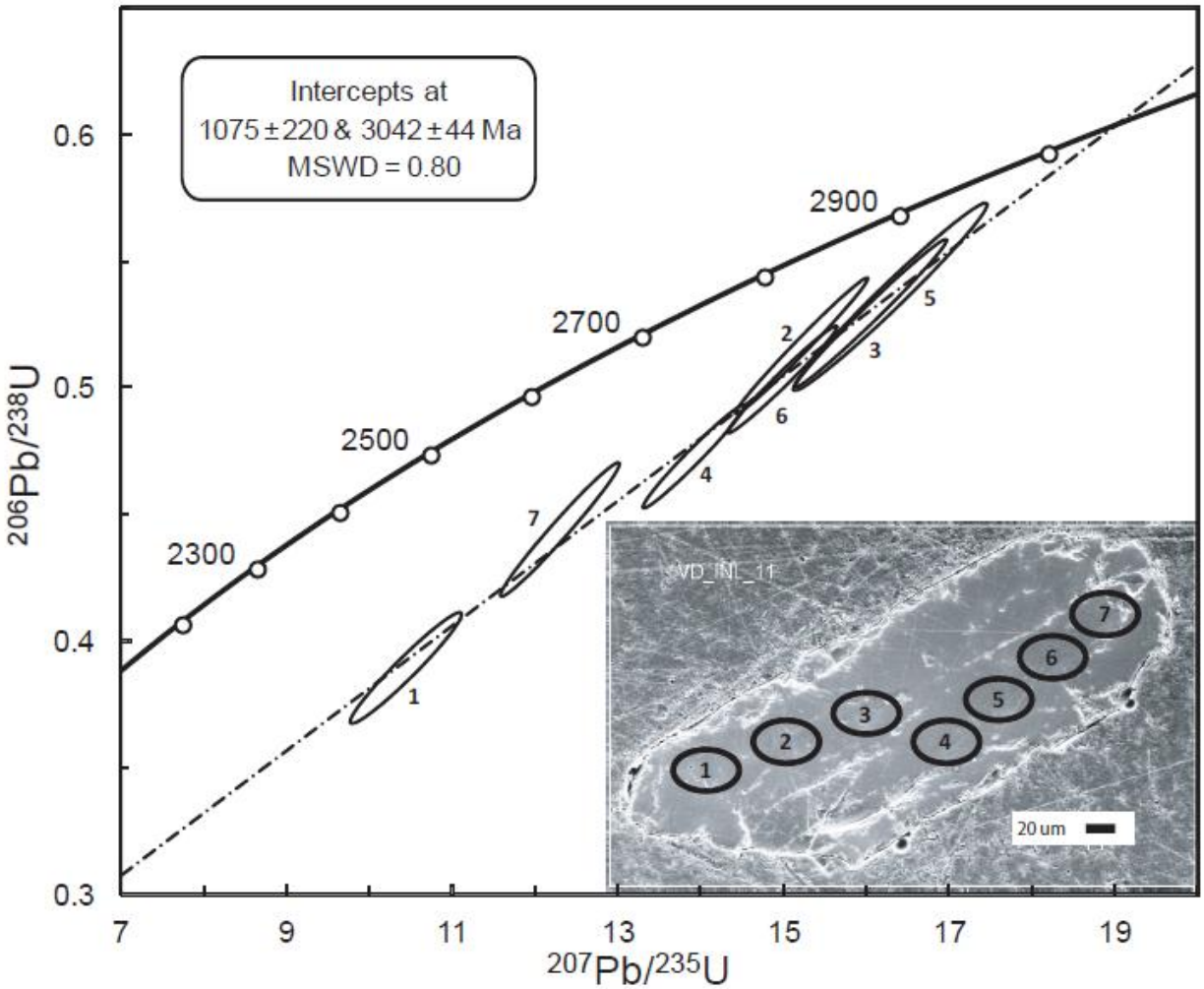

4.8.5 Figure 4.5

Concordia diagram showing 7 SIMS analysis spots from a single zircon isolated from INL drill core split (Kamo et al., 1996). Upper intercept or interpreted crystallization age of ~3000 Ma is consistent with other grains extracted from Vredefort samples, however the lower intercept of ~1100 Ma appears to be thermal overprint of Anna's Rust Sheet, a suite of mineralogically and chemically related intrusions in the core and collar of the Vredefort Dome at ~1.1 Ga – a common thermal overprint reported in previous studies (Reimold et al., 2000).

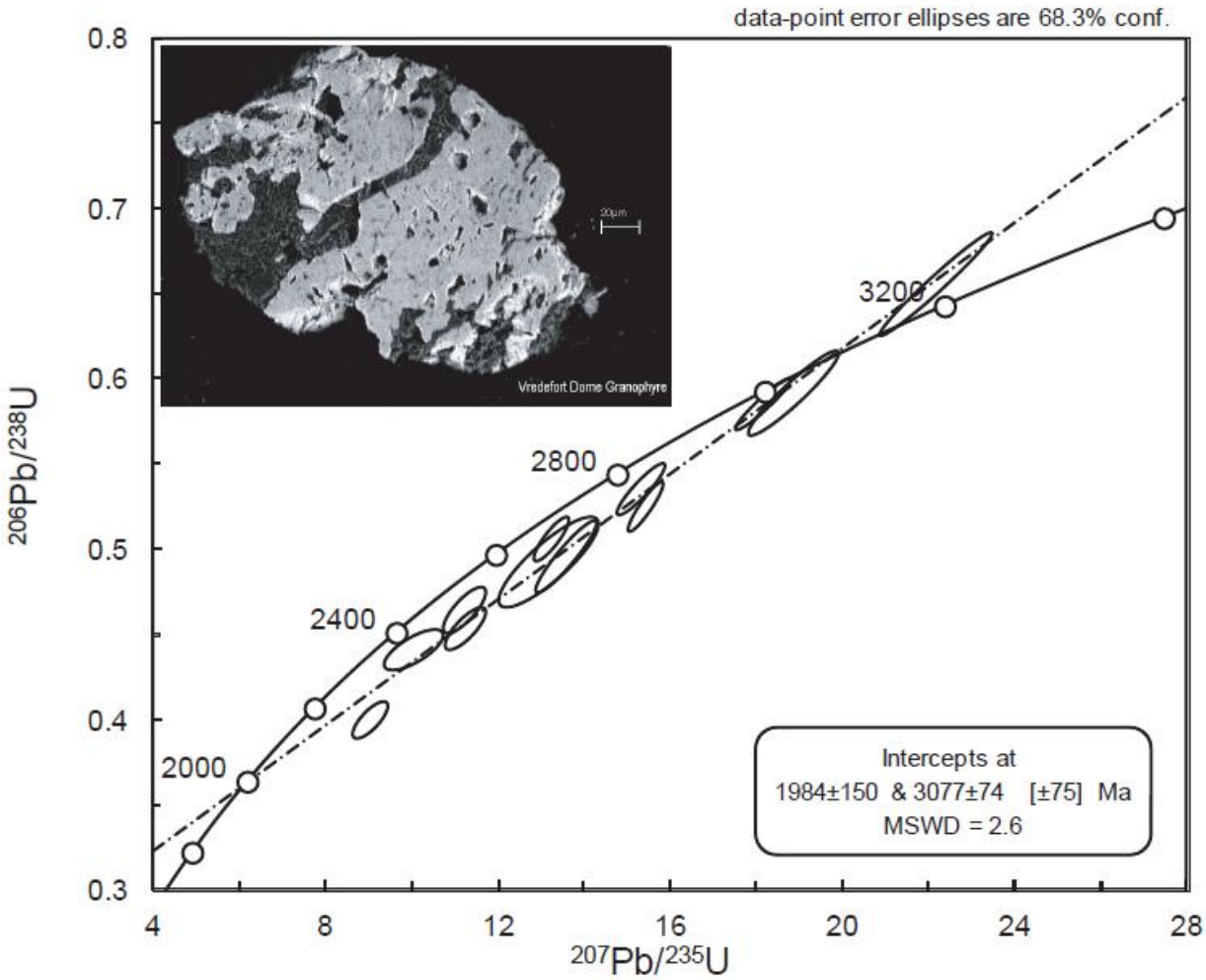

4.8.6 Figure 4.6

Grains isolated from the granophyre unit (VD_G) which exhibit similar textures to lunar grains that have been suggested to be poikolitic, also show inheritance from the Archean target, with varying amounts of Pb-loss and a lower intercept presumably associated with the impact.

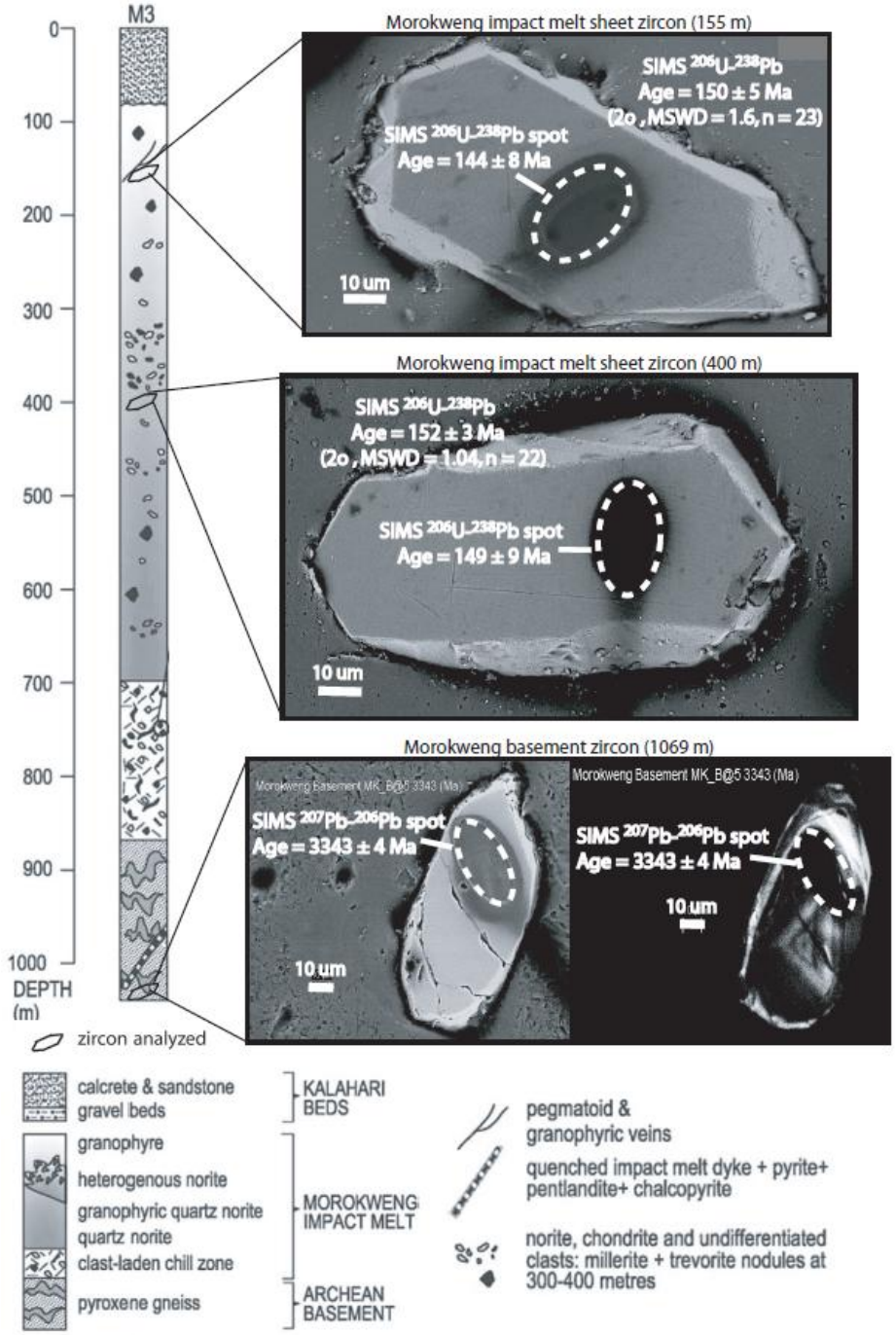

4.8.7 Figure 4.7

Log record of borehole M3, which includes the Morokweng meteorite, drilled into the center of the aeromagnetic anomaly at the impact structure, showing locations where zircons were extracted and analyzed. Inset are BSE images of grains from individual portions of the

melt with their SIMS spot ages showing little disturbance of the target in U-Pb, Archean Pb-Pb ages, but complete resetting in (U-Th)/He age. Modified after (Hart et al., 2002).

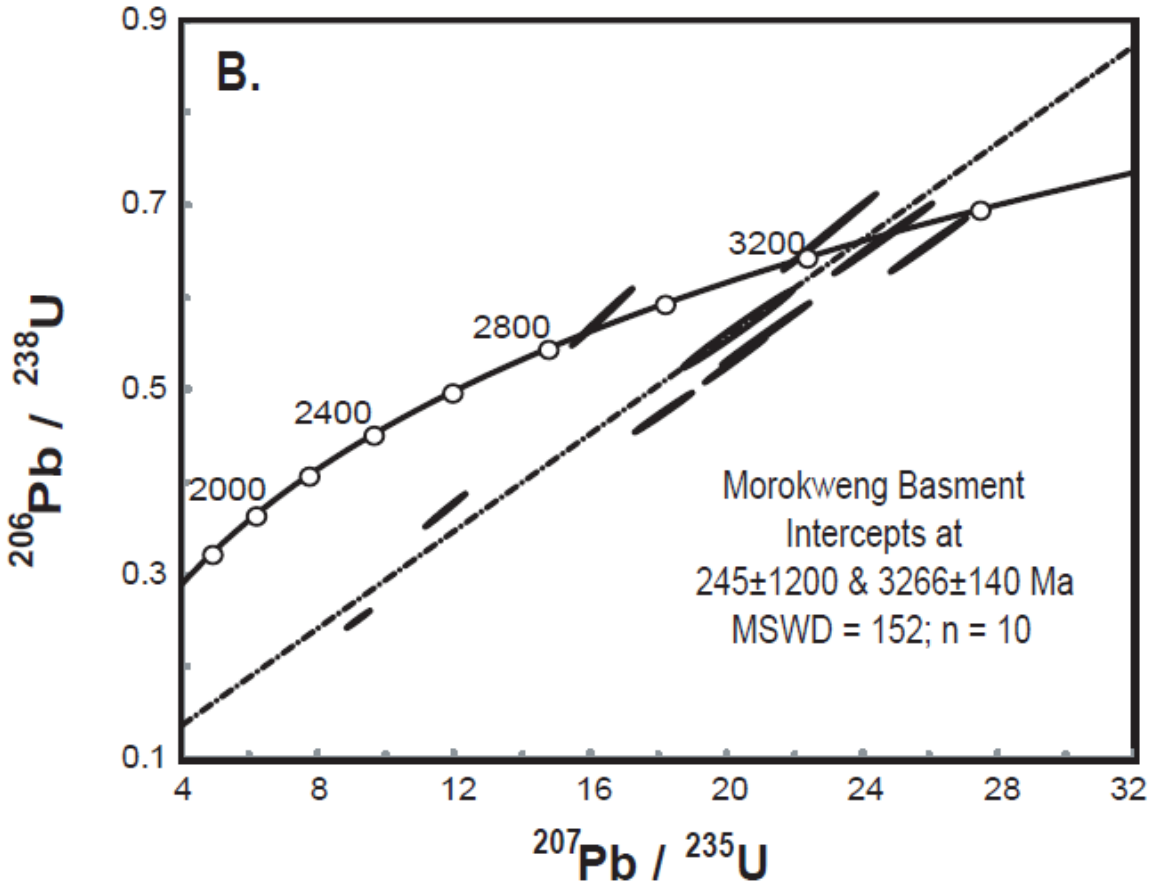

4.8.8 Figure 4.8

Concordia plot for zircons extracted from the shocked basement gneiss, from the 1069 m core split. Basement zircons show inherited Archean ages with some Pb*-loss, however errors on lower intercept are much too large to assign an accurate impact age. No evidence for grains 'reset' in U-Pb has been identified suggesting slow Pb* diffusion even in the 'hot shock' zone (Moser et al., 2011; Abramov et al., 2013).

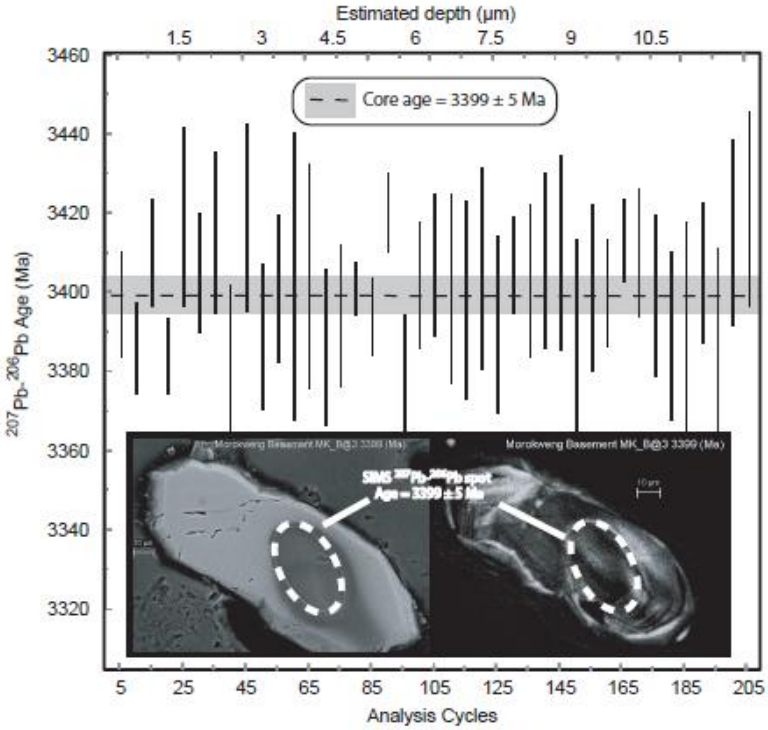
Estimated depth (µm)
1.5
3
4.5
6
7.5
9
10.5
Core age = 3399 ± 5 Ma
^{207}Pb-^{206}Pb Age (Ma)
3460
3440
3420
3400
3380
3360
3340
3320
Morokoweng Basement MK_B@3 3399 (Ma)
SIMS ^{207}Pb-^{206}Pb spot
Age = 3399 ± 5 Ma
5
25
45
65
85
105
125
145
165
185
205
Analysis Cycles

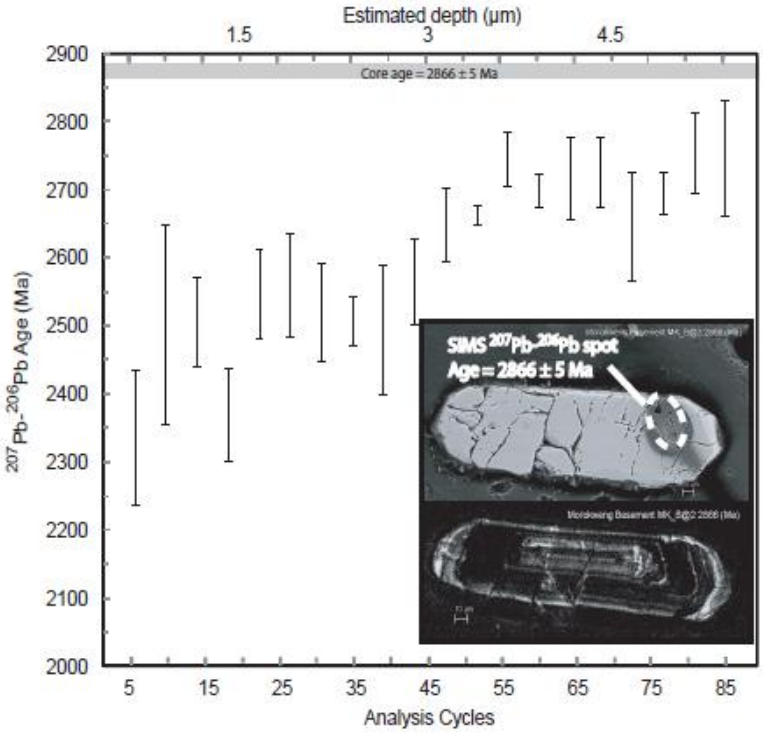
Estimated depth (µm)
1.5
3
4.5
Core age = 2866 ± 5 Ma
^{207}Pb-^{206}Pb Age (Ma)
2900
2800
2700
2600
2500
2400
2300
2200
2100
2000
SIMS ^{207}Pb-^{206}Pb spot
Age = 2866 ± 5 Ma
5
15
25
35
45
55
65
75
85
Analysis Cycles

4.8.9 Figure 4.9

Depth profiles of Morokweng basement zircon to identify presence of epitaxial overgrowth rims coincident with the impact. No evidence of rims with Morokweng impact ages were observed on Archean target zircon cores. Insets are BSE and CL images of depth profiled grains showing oscillatory zoning and CL-active rims.

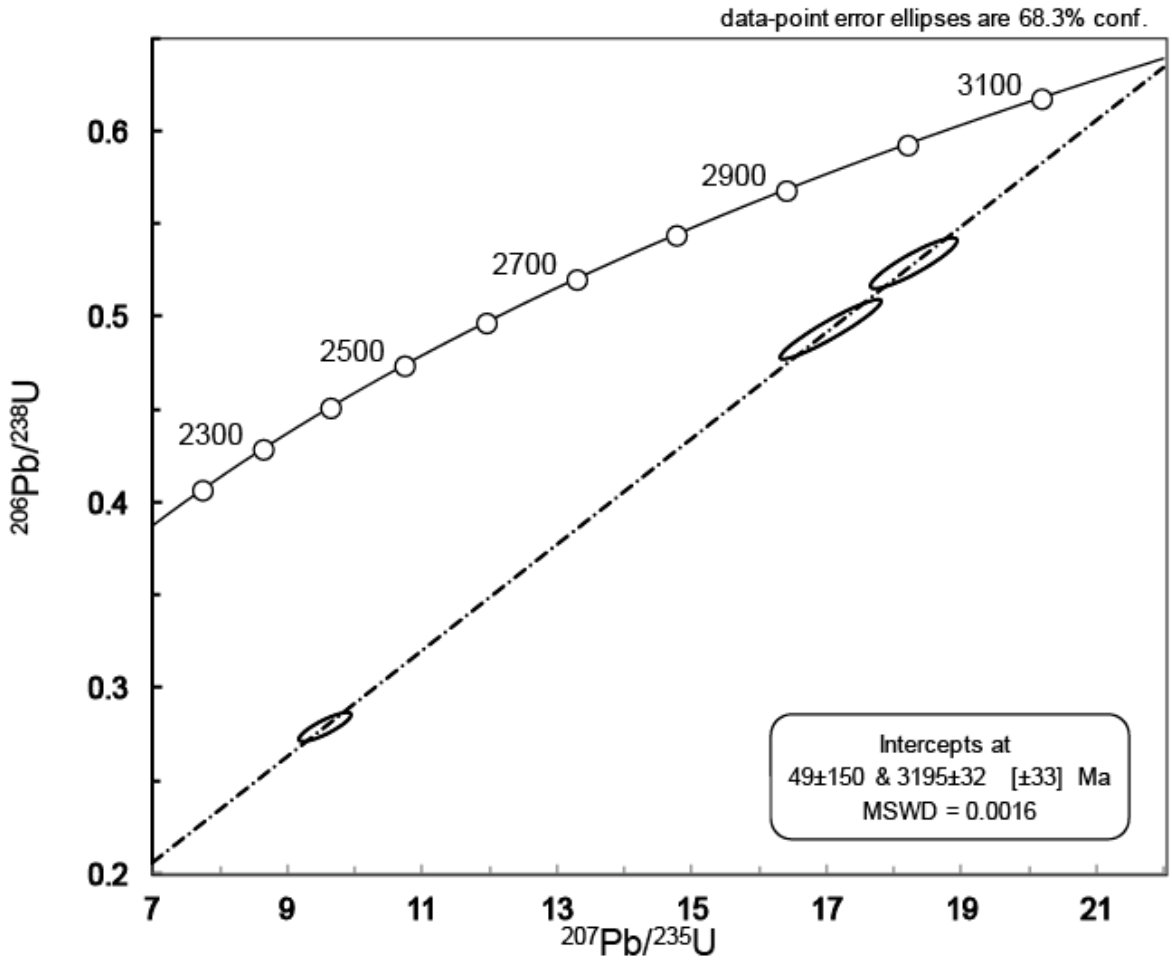

4.8.9 Figure 4.9

Concordia diagram of three SIMS spots from one zircon from Sudbury pseudotachylite breccia showing no evidence for Pb*-loss associated with the ~1850 Ma impact event however

providing evidence for a much more recent event consistent with other grains extracted from these samples.

5. Zircon (U-Th)/He ages of terrestrial craters

5.1 Introduction

The presence of well-defined melt sheets provides opportunities to date, as described in chapter 2, neoformed zircons using the U-Pb method. Provided the scale of the melt sheet is less than several-km's, the time of zircon growth is so brief as to be tantamount to directly dating the impact event. However relatively few impact structures on Earth have large melt sheets associated with them, the vast majority form without significant melt production or are sufficiently old to have their melt sheets eroded. When no datable impact melt sheet exists, ^{40}Ar-^{39}Ar step-heating analysis of various impactites is commonly used to infer impact ages. However, this can be challenging due to the presence of relic clasts, incomplete ^{40}Ar outgassing or excess ^{40}Ar, and recoil and shock effects (e.g. Harrison and Lovera, 2013).

Although some disturbance was observed within the U-Pb system from zircons extracted from Morokweng (shocked basement), Vredefort, and Popigai, the limited Pb*-loss did not provide well-constrained lower intercepts, thus these zircons are not good recorders of the impact events. These grains do, however, allow for the evaluation of other low temperature chronometers, such as zircons (U-Th)/He dating, from the same samples as previously analyzed for U-Pb. Zircon (U-Th)/He dating may provide another tool for age determinations of impact events, long after erosion of the impact melt sheet, and perhaps even when little to no melt remains in the shocked target rocks.

5.2 Background

Zircon (U-Th)/He thermochronometer has a closure temperature of 170–190° C for typical plutonic cooling rates and crystal sizes and is not significantly affected by radiation damage except in relatively rare cases of high radiation dosage with long-term low-temperature histories (Reiners et al., 2004). Recent studies have utilized (U-Th)/He dating of zircon to date impacts: 1) Young et al., (2013) used this method to establish an age of 22.5±2.0 Ma for basement clasts of crater fill breccia from the Haughton impact structure; 2) van Soest et al., (2011) used this method to date neoformed zircons from the Manicouagan melt sheet with ages (214±1.0 Ma) matching U-Pb ages of zircon reported from the main melt sheet (214±1.0 Ma, Hodych and Dunning, 1992; 214±2.0 Ma, Wielicki et al., 2012). Although the age for the Haughton impact structure agrees well with previous Ar-Ar (Jessberger, 1988) and fission track ages (Omar et al., 2014), the lack of a dateable melt sheet does not allow for accurate constraints on the age of the impact event and it remains possible that all techniques are dating a post-impact thermal event. The majority of identified impact structures on Earth do not have dateable melt sheets, either due to post-impact uplift and erosion or the lack of impactor energy to sufficiently melt the target rocks, thus most impact structures ages have been established from the remaining target rocks. The low closure temperature of zircon for He* makes the (U-Th)/He method a good candidate to date impact target rocks, even when little to no impact melt remains, as shock and heating associated with the contact and compression stage should be sufficient to reset the grains (Collins et al., 2012).

This chapter reports on (U-Th)/He ages for zircons separated from brecciated and shocked impactites from the Morokweng and Vredefort impact structures, South Africa as well

as from Popigai, Russia to evaluate the validity of zircon (U-Th)/He dates as accurate recorders of impact events, particularly for target rocks with little impact melt.

5.3 Samples

5.3.1 Morokweng impact structure, South Africa

Morokweng impact structure, South Africa, provides a unique opportunity to investigate the use of zircon as a probe of planetary impact history as the age of the impact melt sheet has been well-established at ~145 Ma (Hart et al., 1997; Wielicki et al., 2012b), and multiple drill cores exist that penetrate the melt sheet into the brecciated and shocked target (Hart et al., 1997). Thus, chronometers used to date zircons from the target rocks, directly below the melt sheet can be compared with the known age of the impact event to asses which systems record the age of the impact. Samples from the M3 borehole (provided by Marco Andreoli), drilled ~12 km NW of the reputed center of the aeromagnetic anomaly (26°30' S, 23°30' E; Koeberl and Reimold, 2003; Jourdan et al., 2010), which intersects ~870 m of impact melt consisting of differentiated granophyric to noritic rocks overlaying brecciated and shocked basement gneisses (Hart et al., 2002) were utilized for this study. Zircons were previously separated from samples at depths of 155 m and 400 m from the main impact melt sheet and appear igneous with no evidence for shock (Wielicki et al., 2012b). Zircon separated from the 1069 m core split (MKB), within the shocked pyroxene gneissic basement (Hart et al., 2002) directly below an impact melt dyke and approximately 200 m below the main impact melt sheet. Separated zircon crystals ranged from 50-120 μm in size and exhibit igneous textures and oscillatory zoning (Fig. 5.1), with no evidence of shock features analogous to those reported by Erickson et al., (2013) for Vredefort zircon. We note that although no micro-scale shock features have been identified within the

zircons analyzed, the grains do appear fractured (inset of Fig. 5.4) relative to those of the main melt sheet. The sample location, in the center of the magnetic anomaly and 200 m below the impact melt sheet, would be expected to reach >100 Gpa and >10000 K (Collins et al., 2012) during the contact and compression stage of impact and thus are presumably highly shocked, even if some of these features have been annealed by relatively low temperatures post-impact (Nasdala et al., 2004). The sample location is also consistent with the hot-shock zone (Moser et al., 2011), where it is estimated that all grains, damaged or un-damaged, will be 'reset' in U-Pb (Abramov et al., 2013). Shock features such as multiple PDF's in quartz and pebbles of the underlying basement have been identified previously (Hart et al., 1997) in drill cores adjacent to the M3 core, and also suggests a highly shocked target; however a majority of the sample was used to extract the relatively few zircons used and thus shock features have not been investigated within this sample, we presume it to be equally shocked.

5.3.2 Vredefort impact structure, South Africa

The Vredefort impact structure in South Africa is the oldest (~2.0 Ga; Kamo et al., 1996; Moser, 1997; Moser et al., 2011; Wielicki et al., 2012) and largest known terrestrial impact (Earth Impact Database, 2014) and represents the deeply eroded remnant of an originally ~300 km wide crater (Reimold and Gibson, 1996). Zircon was separated from whole the pseudotachylite breccia collected near the quarry at Leeukop, just west of Parys (VDPB). This sample is, presumably, in the hot-shock zone (Moser et al., 2011) where the majority of grains are modeled to be 'reset' (Abramov et al., 2013). Pseudotachylite breccia consists of 1-3 cm clasts of Archean granite to granodioritic gneiss target material within a fine grained crystalline matrix (Reimold and Gibson, 1996). The separated zircon crystals (VDPB) range in length from 55 to 170 μm (Fig. 5.1) and exhibit igneous textures (i.e., elongate faceted faces, high axial

ratio, pyramidal terminations) with some shock features (Erickson et al., 2013) present on the outer surface of a few grains (Fig.5.1), although no internal planar deformation features have been previously identified from the same samples (Wielicki et al., 2012b).

5.3.3 Popigai impact structure, Russia

The Popigai impact, Siberia, Russia, has an estimated crater diameter of ~100 km ("Earth Impact Database," 2014). Zircon was separated from two hand samples of luecocratic to mesocratic shocked gneiss (PG_7407w and PG_7407k, respectively; Masaitis, 1994), provided by Victor Masaitis of the A.P. Karpinsky Russian Geological Research Institute (shock stages from II-IV; Stoffler et al., 1991), collected in the SW sector of the crater (approximate coordinates 71°30' N, 110°30' E). Zircon was also separated from a suevite sample collected along the Rassokha River in the northern sector of the crater, provided by Doreen Ames from Geological Survey of Canada. All grains were subrounded, ovoid to multifaceted ranging in size from 50 to >200 μm (Fig. 5.1).

5.4 (U-Th)/He dating method

Grains were picked from the remaining unmounted fractions of samples that had previously undergone SIMS U-Pb dating. However the analyses were not performed on zircons that had been previously dated, as to avoid large α-ejection corrections associated with substantially thinned (i.e. polished) grains. Zircons were handpicked and selected based on minimum dimensions of 55 μm across a/b axes, between 80 and >200 μm along the c axis, and on the lack of visible fractures and minimal inclusions. All analyses were carried out on single grains. Selected zircons were wrapped in Pt foil, heated for 10 min at ~1300 °C, and reheated until >99% of the He* was extracted. All ages were calculated by using standard α-ejection

corrections using morphometric analyses (Reiners, 2005). After laser heating, zircons were unwrapped from Pt foil and dissolved using HF-HNO_3 and HCl pressure vessel digestion procedures. U and Th concentrations were determined by isotope dilution ICP-MS analysis. Uncertainties (2σ) of single-grain ages reflect the reproducibility of replicate analyses of FCT zircon laboratory standard (Wolfe and Stockli, 2010; 28.4±2.3 Ma; n=438) and are ~8% (2σ) for zircon He* ages.

5.5 Results

5.5.1 Morokweng impact structure, South Africa

Zircons separated from the shocked basement appear subhedral, ovoid to multifaceted grains with some CL oscillatory zoning and CL-active rims (inset of Fig. 5.4). Some grains appear fractured, however no evidence for internal planar deformation features (Wielicki et al., 2012b) or other shock effects (Wittmann et al., 2006) have been identified. SIMS spot analysis on the cores of these grains yield Archean Pb-Pb ages ranging from ~2.9 to 3.4 Ga with varying Pb*-loss (see chapter 2&4). (U-Th)/He zircon age results for 8 of 10 Morokweng basement zircons date the impact to 143±9 Ma (2σ, MSWD = 3.2; Fig. 5.3) in good agreement with U-Pb ages of the main impact melt sheet. Two grains yield anomalously old ages of 266 and 543 Ma and thus were rejected. These old ages could possibly be due to partial loss of the grain during unpacking following He* extraction and incomplete zircon recovery before dissolution, from zonation within discrete age domains, or from incomplete He* degassing; However no determination of this error can be made at this time. We note that the MSWD is slightly greater than the 95% confidence interval for 7 degrees of freedom (Mahon, 1996) suggesting an unaccounted error term. Excess scatter from unaccounted analytical error is propagated by

multiplying the weighted average age uncertainty by the square root of the MSWD and provides for an age estimate of 143±16 Ma for Morokweng, which we infer as the heating event associated with the impact.

5.5.2Vredefort impact structure, South Africa

Separated zircons range in length from 55 to 175 μm and exhibit igneous textures (i.e., elongate faceted faces, high axial ratio, pyramidal terminations; Corfu et al., 2003) and show no planar deformation features. Some shock features were observed on the outer surface of a few grains analogous to those reported by Erickson et al., (2013), however these features do not appear to pass beyond the outer few microns of the surface. (U-Th)/He ages for 12 grains separated from the pseudotachylite breccia from Vredefort, South Africa yielded ages ranging from ~117 to 567 Ma, significantly younger than the estimated age for the impact event of ~2.0 Ga (Kamo et al., 1996; Moser, 1997; Wielicki et al., 2012b). These young ages may have been affected by sampling issues discussed above; however this suggest that the grains are even younger than identified.

5.5.3Popigai impact structure, Russia

We interpret the results of 13 of the 14 Popigai zircons analyzed for (U-Th)/He age as dating the impact to 33.9±1.3 Ma (2σ; MSWD=2.4, n=13; Fig. 5.3). One zircon yielded an anomalously old age of 67.0 Ma, possibly due to partial loss of the grain during unpacking following He extraction and/or incomplete zircon recovery before dissolution, and thus was rejected. We note that the MSWD is slightly greater than the 95% confidence interval for 12 degrees of freedom (Mahon, 1996) suggesting an unaccounted error term. We examined several different statistical approaches, which result in small changes to the age estimate (from 33.9 to

34.1 Ma) but may provide a more accurate error assignment. If we are underestimating the ability to replicate standards, then a larger error of, say, 6% (1σ) may be warranted and result in an average age of 33.9±1.1 Ma (2σ; MSWD=1.06). Another approach to deal with the missing error is via a random effects model, which accounts for undersized uncertainties in individual analyses (R Core Team, 2013; Schwarzer, 2013). This yields a Popigai impact age of 34.17±1.17 Ma (2 SE). Finally, a Popigai impact age estimate from the mean of 10,000 bootstrap replicates (Efron, 1979) of the collected zircon (U-Th)/He data yields an age 34.1±1.2 Ma (2 SE). While these techniques are more statistically rigorous than the MSWD approach, they do not significantly change the age of Popigai. However this analysis does highlight the fact that the uncertainty of individual (U-Th)/He analyses may be routinely underestimated, likely attributable to parent nuclide (U, Th) zonation that is not accounted for in the α-ejection.

5.6 Discussion

5.6.1 Evaluating zircon (U-Th)/He dating of terrestrial impacts

Although relatively little disturbance is observed in the U-Pb system (see chapter 4), zircons from the Morokweng basement appear completely 'reset', loss of radiogenic helium (He*), in (U-Th)/He, presumably due to the rapid diffusion of He* in zircon (Watson and Cherniak, 2013; Young et al., 2013; Fig. 5.4). Although some grains appear fractured no shock features have been identified in MKB zircons suggesting that these suspected diffusion pathways, vital for Pb*-loss (Moser et al., 2011; Abramov et al., 2013), may not be necessary for He* diffusion. As evidenced by the Vredefort analysis the use of such ages can be complicated by endogenic post-impact thermal events which could overprint the impact (U-Th)/He signal, presuming that there was one, and yield an age that is younger than the impact event; thus, the

use of such data requires a good understanding of post-impact regional thermal events. As Vredefort is significantly older than Morokweng it is not surprising that these grains have experienced more post-impact thermal events and thus no longer record the timing of the Vredefort impact. We suggest thermal 'resetting' post-impact via emplacement of intrusive bodies, known within the Vredefort region (Reimold et al., 2000) for these anomalously young ages. The relatively young age of Morokweng and few regional thermal perturbations of the Kaapvaal craton near the impact structure over the last ~145 Ma (Reimold et al., 1999) permit these grains to maintain their He-record of the impact event.

5.6.2 Implications of new Popigai age

While the (U-Th)/He age of 33.9±1.3 Ma is consistent with the broad range of $^{40}Ar/^{39}Ar$ ages previously reported (Bottomley et al., 1997), it is significantly younger than the essentially arbitrarily chosen age of 35.7±0.2 Ma (2σ) for sample P21a which was inferred to date the impact. The range of ages of Bottomley et al. (1997) overlaps with our new age from the eight samples analyzed however all but one sample was disregarded and the age is based on only four heating steps and less than ~15% of the total data.This new age, with a robust estimate of variance, appears to exclude Popigai as a possible source of the ~35 Ma ejecta deposits (Glass, 2002), but overlaps within error with the Eocene-Oligocene boundary mass extinction (33.7±0.5 Ma; Prothero, 1994; Figure 3).

The transition from the Eocene to the Oligocene marks a dramatic change in global climate (Zachos et al., 2001), from the warmest temperatures over the previous 65 Ma, to the icehouse conditions at the Eocene-Oligocene Boundary (33.7±0.5 Ma; Prothero, 1994). This time period is one of the greatest marine invertebrate extinctions of the Cenozoic (Raup and

Sepkoski, 1986). Evidence for this transition includes: 1) a rapid decline in minimum sea surface temperature (Figure 3A) together with selective extinction of warm-water taxa (Liu et al., 2009; Ivany et al., 2000; Hansen, 1987); 2) a 4-6°C decrease in mean annual air temperature in northern Europe (Hren et al., 2013), also supported by $\delta^{18}O$ of fossil teeth in North America (Zanazzi et al., 2007); and 3) an isotope-capable global climate/ice model prediction of rapid Antarctic ice sheet growth followed by episodic northern-hemisphere glaciation (Deconto et al., 2008). However the mechanism driving these global changes remains uncertain.

Interestingly, the late Eocene was also a time of numerous asteroid and/or cometary (Farley et al., 2005) impacts, with four craters appearing to date from this period (i.e., Chesapeake Bay and Toms Canyon, eastern USA; Mistastin, Canada; Popigai, Russia; "Earth Impact Database," 2014). Since these craters do not have readily datable melt sheets, available age estimates come from potentially ambiguous interpretations of $^{40}Ar/^{39}Ar$ plateau ages of breccias (Bottomley et al., 1997; Mak et al., 1976) or fission track dating of tektites (Glass, 2002) assumed to be associated with the impact and put all four craters at ~35-36 Ma. Our new age for Popigai (33.9±1.3 Ma) suggests that the previous lag of ~2 Ma between impact events and global change at 33.7±0.5 Ma (Prothero, 1994) may no longer exist, at least for the largest of the four late Eocene impactors.

Late Eocene impact ejecta has been identified in deposits in Italy (Clymer et al., 1996) and multiple ocean cores (Glass and Zwart, 1973; Swinski and Glass, 1979) and is comprised of shocked quartz as well as glassy (microtektites) and semicrystalline spheres, droplets, and fragments (microkrystites; Whitehead et al., 2000) which have been dated to ~35 Ma (Glass, 2002). It remains controversial as to the number impact related layers that exist from ocean drill

cores (Glass and Burns, 1987; D'Hondt et al., 1987; Hazel, 2014), however it is clear that at least two large impacts occurred approximately 1-2 Ma prior to global changes associated with the Eocene-Oligocene boundary. Geochemical evidence linking Italian ejecta and ODP core microkrystites to Popigai have been reported (Whitehead et al., 2000; Glass et al., 2004) and rely on the similarity of major element chemistry and Sr-Nd isotope data in microkrystites and Popigai impact melt rocks (tagamites). Although other reports suggest that the microkrystite layers have higher FeO, MgO and CaO and lower Al_2O_3 than Popigai impactites (Glass and Koeberl, 1999), they have, nonetheless, been assigned a provenance from Popigai (Whitehead et al., 2000). We note that Popigai tagamites are remarkably similar to average continental crust (Rudnick and Gao, 2003) and the similarity with microkrystites, particularly the melanocratic layer as two other layers did not correlate as well with Popigai (Whitehead et al., 2000), appears to merely restrict the tektites to an impact on continental crust and not uniquely Popigai. Major elements do suggest that some of the other late Eocene impacts are not the source of microkrystites however the lack of impact melt rock analysis from the Chesapeake impact means that this crater cannot be ruled out as a possible source (Whitehead et al., 2000). The variability of Sr-Nd values of Popigai target rocks and the lack of good correlation between Popigai melt rocks and microkrystites (see Fig. 5 in Kettrup et al., 2003) also does not uniquely identify Popigai as the source crater. Italian ejecta and shocked quartz has also been associated with a quartz-rich target rock (Langenhorst and Clymer, 1996), such as existed at Popigai prior to impact, but surely not exclusive to Popigai. There appears to be no inverse correlation between the concentration of microkrystites and the distance from Popigai (Glass and Koeberl, 1999), another argument against Popigai as the source crater for these ejecta layers. The ~1-2 Ma difference in time between these seemingly clustered impact events and global climate change

(Vonhof et al., 2000) appears too great a lag to infer causation by impact. Although many stratigraphic benefits exist with ocean drill cores and much can be learned from tektite layers within such cores, assigning provenance to these ejecta layers is difficult and rarely provides a unique solution. Thus we elected to return to the impact rocks within Popigai to place better constraints on the timing of impact and its possible association with the observed global change and mass extinction at the Eocene-Oligocene boundary.

Rapid global temperature declines have been modelled due to large gas fluxes, primarily CO_2 and SO_2, following large impacts if the SO_2 flux dominates over the warming effects of the CO_2. For example, models of the Chicxulub impact predict a net 292 W/m^2 decrease in solar radiation received, causing an 'impact winter' and possibly contributing to the K-Pg mass extinction (Pope et al., 1994; Fig. 5.5A). Estimated SO_2 fluxes for the Popigai impact are only surpassed by those inferred for the Chicxulub event (Kring, 2003) and thus global thermal effects are predicted to be broadly similar (Pope et al., 1994). Recent results also suggest large production of acid rain from such sulfur flux's (Ohno et al., 2014), consistent with observations of preferential extinctions in warm water taxa (Hansen, 1987) due to ocean acidification. Our new age for the Popigai impact (Fig. 5.5B) is consistent with its occurrence immediately prior to the observed global cooling trend. Although the new age for Popigai is consistent with the E-O boundary, an impact of ~90 km seems unlikely to leave no trace in ocean drill cores. Alternatively, if the microkrystites and microtektites that have been observed ~1-2 Ma below the E-O boundary are in fact from Popigai then the ages of this boundary may need to be re-examined as these results would suggest that the E-O boundary is ~1 Ma younger than current estimates (Hansen, 1987).

5.7 Conclusion

Many terrestrial craters do not have melt sheets preserved (e.g. Vredefort, South Africa and Popigai, Russia); either due to post-impact uplift and erosion or to the lack of energy of the impact event in producing large volumes of melt. Thus, impact ages are commonly estimated from $^{40}Ar/^{39}Ar$ method of the basement impactites. Our results from Morokweng target rocks with little impact melt, highlight the ability of (U-Th)/He zircon ages in identifying accurate impact dates, particularly when no dateable melt sheet is present. However, thermal overprints may alter the ages and thus a regional thermal history is needed to accurately understand the age.

Zircon (U-Th)/He dating suggests that Popigai is 1.5 to 2 Ma younger than previous estimates and concurrent with rapid global climate change at the Eocene-Oligocene boundary however significantly younger than the ~35.5 Ma global ejecta layer (Glass, 2002), which may be due to other late Eocene impacts. If our new age is correct it suggests that the dramatic cooling trends observed at the Eocene-Oligocene boundary are coincident with the impact event, providing the first evidence of possible impact induced mass extinctions in the Cenozoic. Although no definitive link can be established between the Popigai impact and the climate change at the end of the Eocene, both the timing and effects are consistent with predicted impact scenarios (Pope et al., 1994; Kring, 2003). Alternatively, it seems unlikely that such a large impact would not produce a global ejecta layer and thus may possibly suggest that the E-O boundary global change is ~1-2 Ma younger than current estimates (Hansen, 1987).

The relatively low retention of He* by zircon may also be exploited to also date ejecta blankets, which may cool sufficiently rapid to not diffuse Pb but in many cases have elevated temperatures that allow for He* diffusion. This may provide another tool with which to identify

impact events when no crater has yet been identified but ejecta exists, or possibly to date large ejecta blankets from lunar sample return missions.

5.8 Tables and Figures

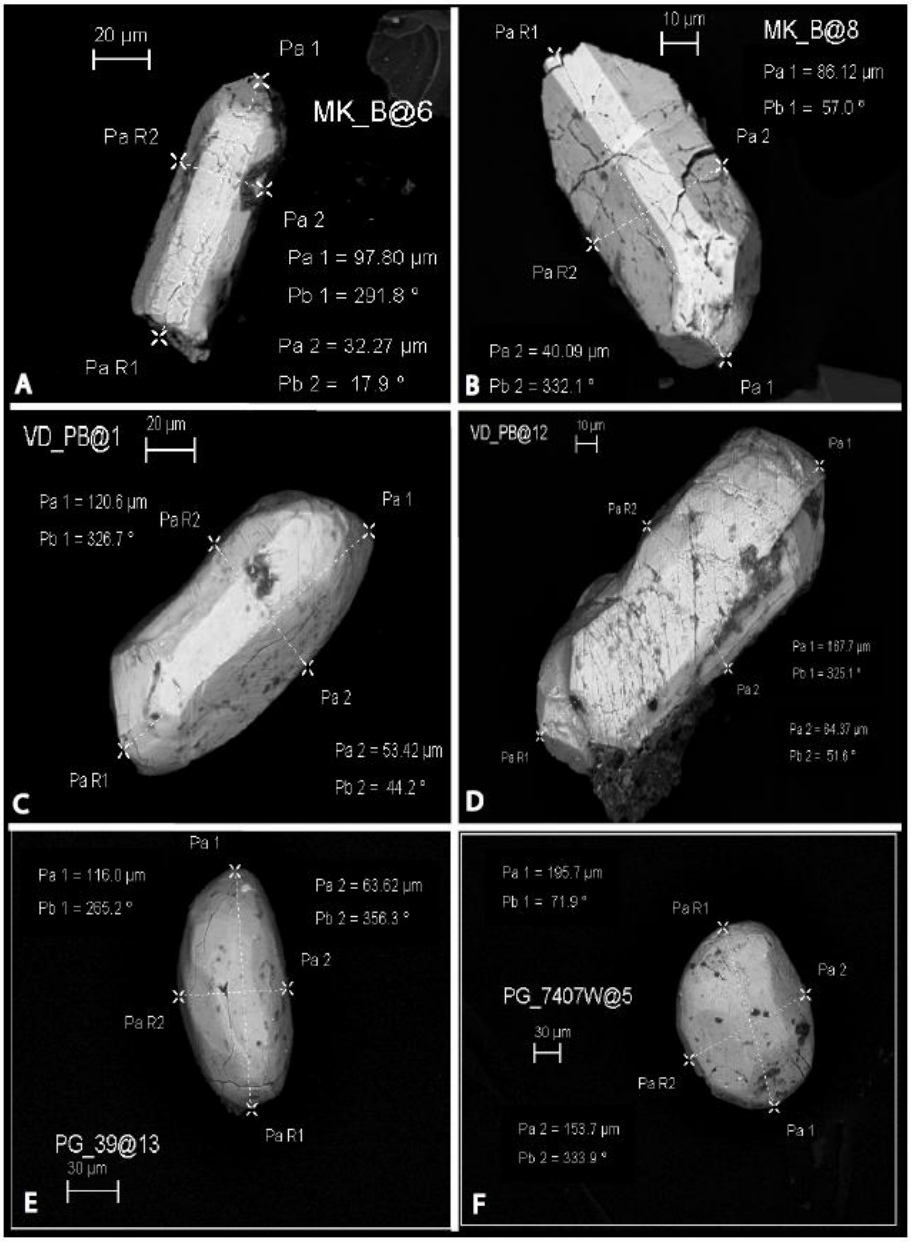

5.8.1 Figure 5.1

Back scattered electron images via LEO 1430 VP scanning electron microscope with measurements used for standard α-ejection corrections and morphometric analyses (Reiners, 2005). Grains appear euhedral to subhedral for both Morokweng (A&B) and Vredefort (C&D) with some exterior fractures (D) but no evidence for impact shock features within zircon cores (Wittmann et al., 2006), and subrounded to ovoid for Popigai (E&F) with no evidence of shock.

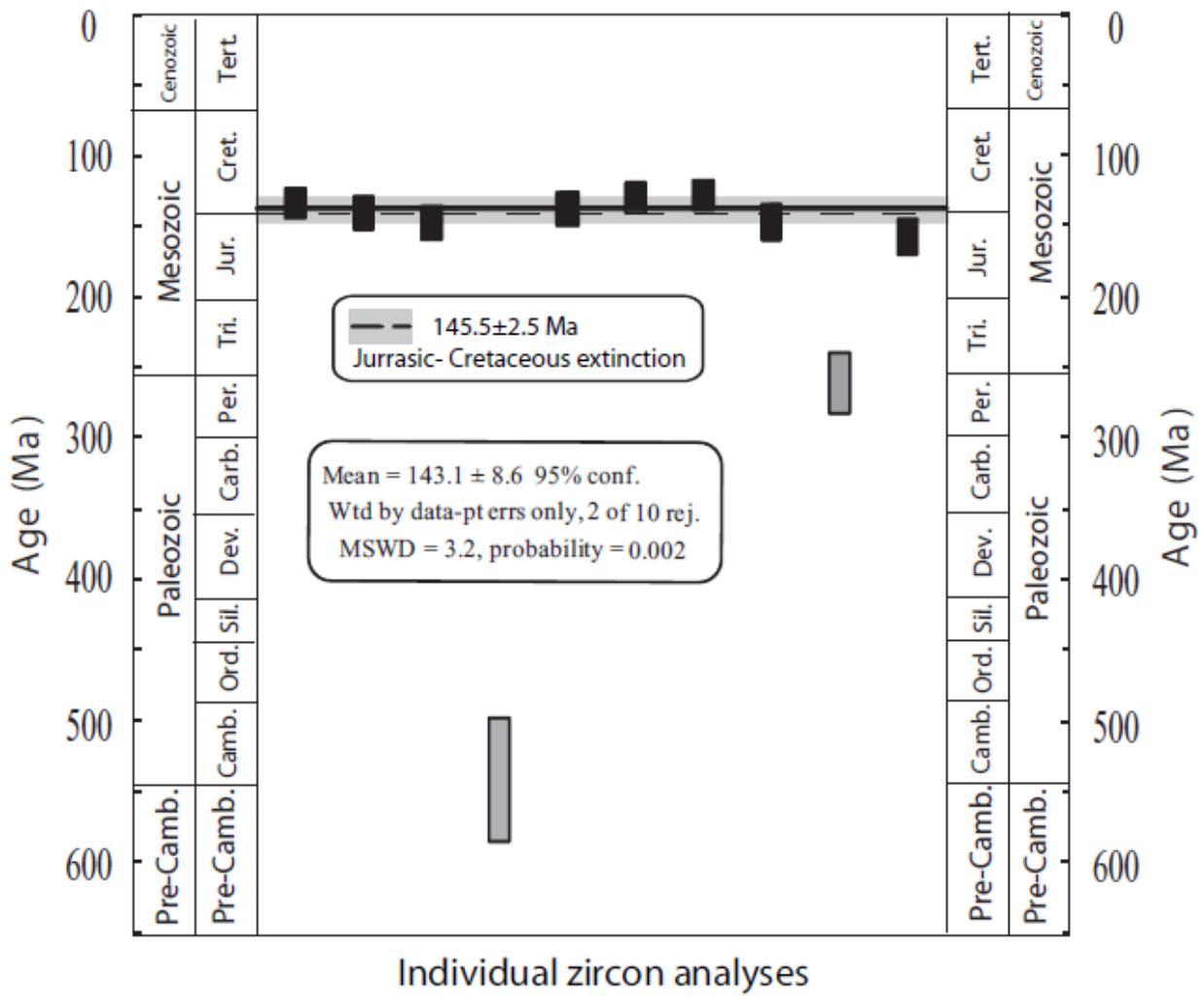

5.8.2 Figure 5.2

Individual zircon (U-Th)/He ages from Morokweng basement (MKB) yield an age of 143±9 Ma (2σ; MSWD=2.9), in good agreement with the impact age (~145 Ma). Uncertainties (2σ) of single-grain ages reflect the reproducibility of replicate analyses of FCT zircon laboratory standard (28.4±2.3 Ma; n=438; Wolfe and Stockli, 2010) and are ~8% (2σ) for zircon He ages.

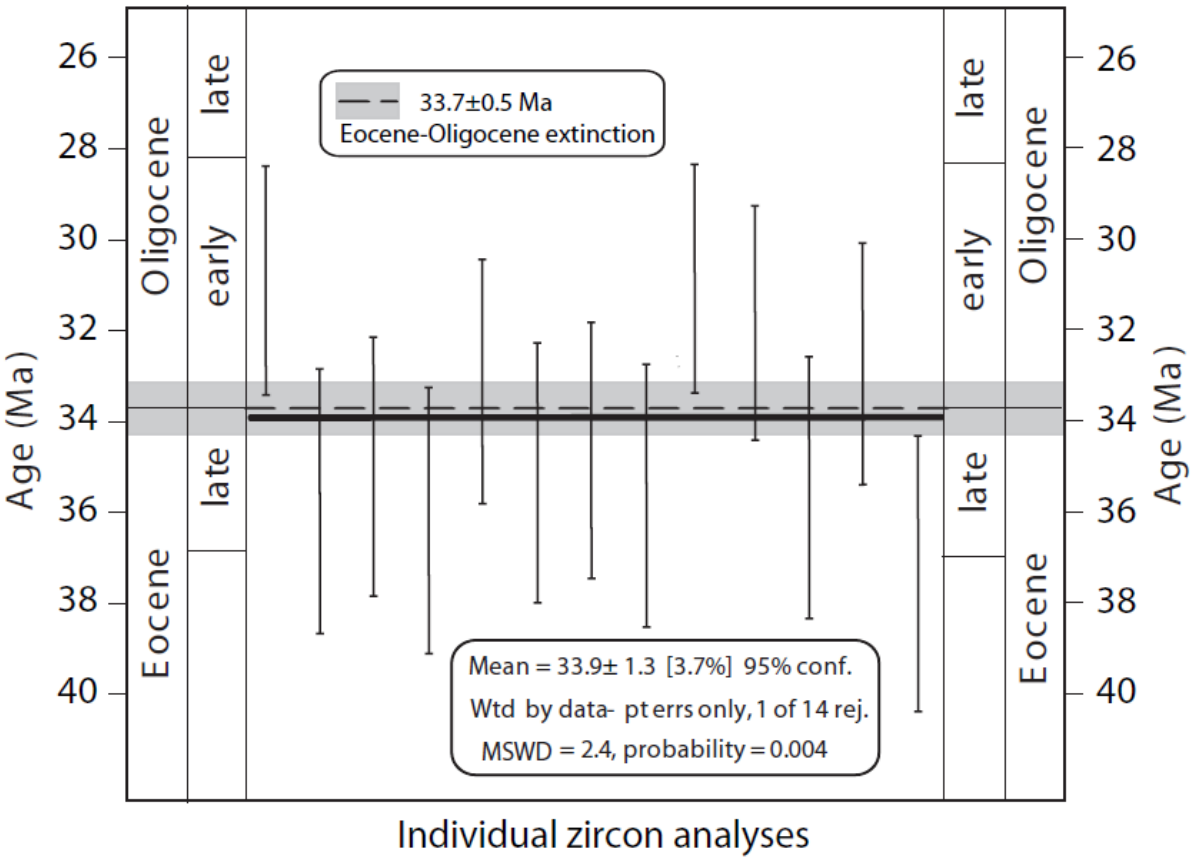

5.8.3 Figure 5.3

Individual zircon (U-Th)/He ages from Popigai impactites yielding an impact age of 33.9±1.3 Ma, significantly younger than previous estimates (Bottomley et al., 1997). Uncertainties (2σ) of single-grain ages reflect the reproducibility of replicate analyses of FCT

zircon laboratory standard (28.4±2.3 Ma; n=438; Wolfe and Stockli, 2010) and are ~8% (2σ) for zircon He ages.

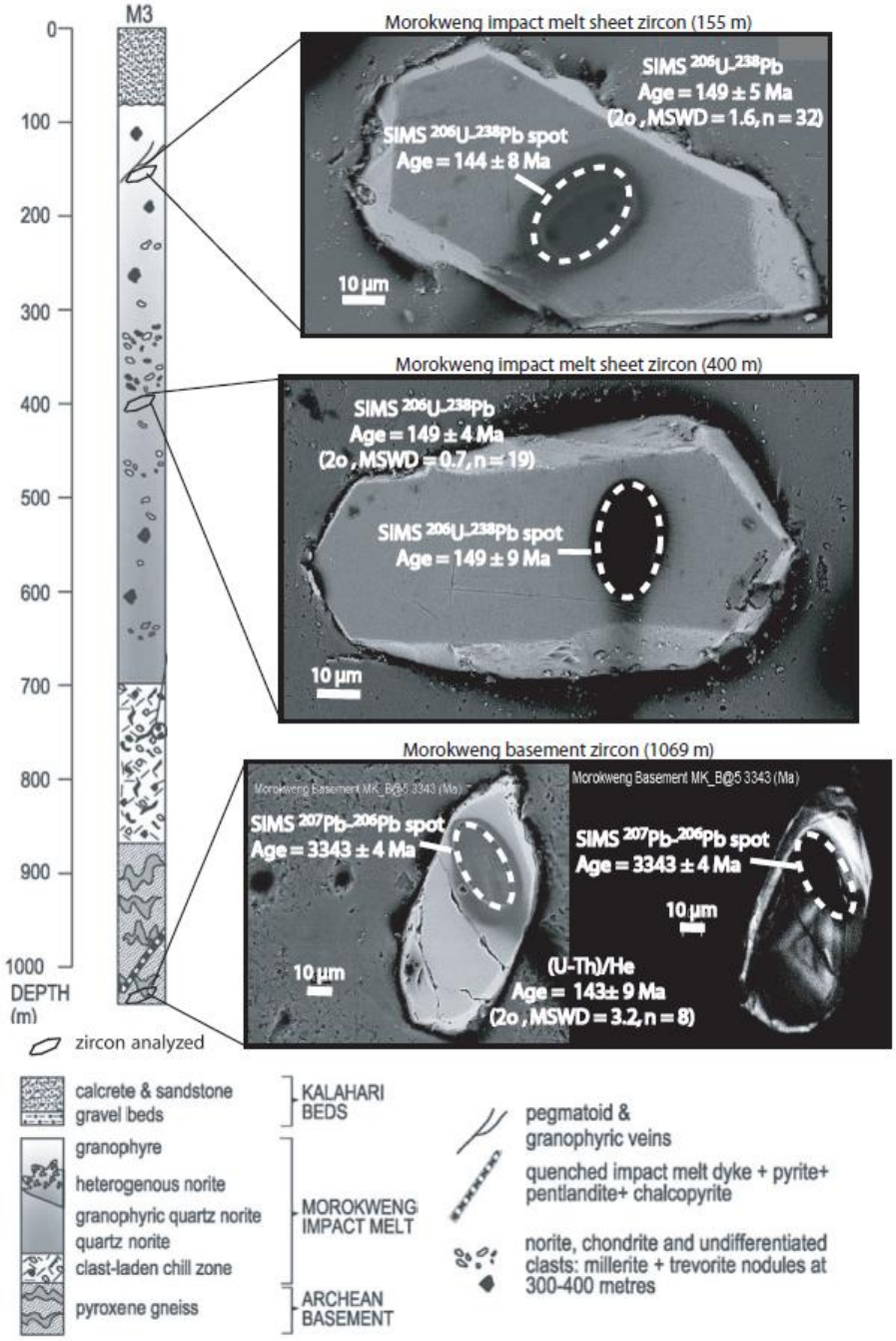

5.8.4 Figure 5.4

Log record of borehole M3, which includes the Morokweng meteorite, drilled into the center of the aeromagnetic anomaly at the impact structure, showing locations where zircons were extracted and analyzed. Inset are BSE images of grains from individual portions of the melt with their SIMS spot ages showing little disturbance of the target in U-Pb, Archean Pb-Pb ages, but complete resetting in (U-Th)/He age. Modified after Hart et al., (2002).

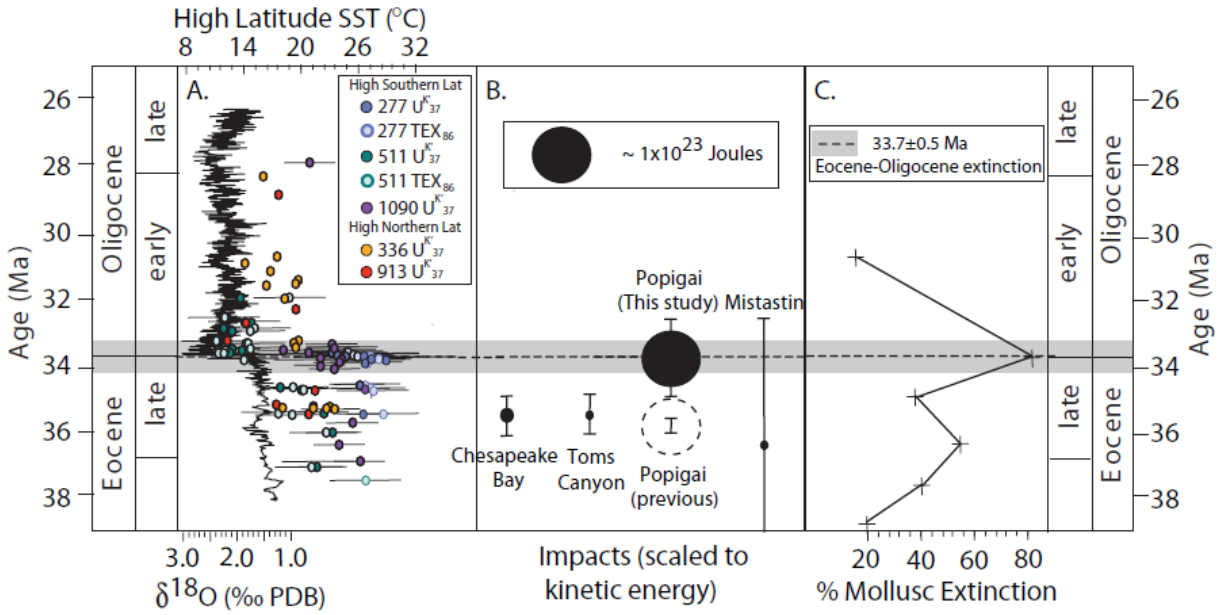

5.8.5 Figure 5.5

Diagram of the Eocene-Oligocene boundary, showing dramatic global climate change and extinction event coincident with the new age of the Popigai impact. (A) High latitude sea surface temperature (SST) reconstructions from multiple ocean drilling sites. Black line represents a composite benthic $\delta^{18}O$ record (Zachos et al., 2001). (B) Current age estimates (including our new age for Popigai) of late Eocene impacts scaled to their individual pre-

atmospheric kinetic energy: bolide diameter = 1/10 final crater diameter, velocity = 17 km/s and density = 2500 kg/m. (C) Percent extinction of molluscs (Hansen, 1987).

6. Conclusions and Future work

6.1 Geochemical signatures of impact produced zircon

If zircon is to be used as an accurate recorder of past impact events, it is essential to understand the geochemical signatures associated with grains that crystallize within impact generated melts. The data developed for this thesis is the largest set of geochemically characterized zircons generated from such impacts on the terrestrial surface and forms the foundation for understanding the formation of impact produced zircon. Although no distinct signature has been identified to conclusively determine a zircon as crystallizing from an impact melt, the data developed here can be used in combination with other data (Zr saturation modeling, shock identifiers, field work, etc.) to confidently determine if a zircon is in fact crystallized from a impact melt. This would allow for accurate determination of the impact age and could possibly be transformative in the understanding of bolide flux through time to the Earth-Moon system. Results suggest that impact melts of sufficient size have the potential to fully resorb inherited grains and crystallize new grains that accurately date the impact. However, lower energy impacts seem to only partially resorb inherited zircon without reaching [Zr] saturation and crystallizing zircon. Only the Vredefort impact thus far possessed both neoformed zircon and inherited zircon.

6.2 Modeling zircon formation in simulated impacts

Understanding the mechanism by which zircon crystallizes within crustal melts coupled with melt evolution models and thermal models associated with impacts allows for the

development of simple but informative models of the crystallization behavior of zircon within impact melts. This model can be used as another tool by which to discriminate between impact produced zircon, grains that will allow for age determination of the impact event, and endogenic zircon not associated with the impact, presumably inherited from the target. Such a model can also be very useful for samples where little geologic context exists, such as samples returned from other planetary bodies and meteorites, to determine if the grains identified crystallized within the sample or were inherited. Modeled results appear to rule out an impact source for the Hadean Jack Hills population, a time period of suspected heavy bombardment. Results for the lunar surface also seemingly rule out all reported lunar grains from forming from impact melts including those found in lunar meteorite SaU169. Preliminary model results for impacts on the Martian surface suggest very little possibility of zircon formation within impact melts and may explain the apparent lack of zircons reported from SNC meteorites.

6.3 Pb*-loss in zircon from shocked impactites

Many terrestrial impacts either do not have the energy to generate melts of sufficient size as to crystallize zircon or, in the case of older craters, the impact melt sheet has long been eroded with only the brecciated basement remaining. Thus no neoformed zircons are available to accurately provide an age for the event. In such cases partially or completely 'reset' zircon, Pb*-loss, has been suggested as an alternative to date the impact. Recent model results suggest that such grains should be abundant for large impact events however the relatively few 'reset' grains suggests that Pb* mobility in shocked zircon may not be as common as thought. Results investigating Pb*-loss within zircons from shocked terrestrial impactites failed to produce any 'reset' zircon and partial Pb*-loss within such grains was never sufficient as to have accurate estimates of lower intercepts in concordia plots. Pb diffusion has been known to be remarkably

slow within unshocked zircon and the results presented here suggest that shock microstructures do not act as efficient pathways for Pb diffusion.

6.4 (U-Th)/He dating of zircon from terrestrial impactites

Although Pb* mobility appears to be remarkably slow even in zircon from shocked impactites the low retentivity of He* allows for zircons to be rapidly 'reset', complete He*-loss, within the impact stages described in chapter 2. The (U-Th)/He geochronometer provides an alternative to accurately date an impact event, particularly when no dateable melt sheet exists. Results for Morokweng clearly show the large retention difference between Pb and He within a zircon as grains isolated from below ~850 m of impact melt within the brecciated and shocked target show little disturbance in Pb, however appear completely 'reset, in He with (U-Th)/He ages agreeing well with U-Pb ages from the main melt sheet. Although this is a promising result, the low retention of He can also be effected by regional thermal events post-dating the impact which can cause post-impact He*-loss and yield inaccurate ages. This is evidenced by the results from Vredefort which all post-date the impact event by many 100's of Ma, most likely due to ~2 Ga of regional thermal events documented in the area. (U-Th)/He results for Popigai suggest that the impact is ~1 ma younger than previous estimates and coincident with the Eocene-Oligocene mass extinction. However evidence linking global ejecta that appears ~1-2 Ma below the E-O boundary with Popigai in ODP cores and the lack of impact components associated with the E-O boundary does not lend confidence to this interpretation. Alternatively if the global ejecta found ~1-2 Ma below the E-O boundary is indeed from Popigai and the new age is correct this would suggest that the E-O boundary is ~1 Ma younger than current estimates. (U-Th)/He can provide accurate impact ages and provides another tool by which to accurately date impact events, particularly when no dateable melt sheet exists.

6.5 Future work

6.5.1 Pb* diffusion within naturally and experimentally shocked zircon to assess the effects of different shock microstructures

Understanding how impact affects Pb*-diffusion within zircon is essential if we are to use zircon as a probe of planetary impact history. This would involve diffusion studies on naturally shocked zircon, such as those found in the Vaal river near the Vredefort structure which display through going planar deformation features, as well as experimentally shocked zircon, to better constrain the pressure necessary to provide the pathways for rapid Pb diffusion. Current models have relied on radiation damaged zircon as a proxy for shocked grains and this may be the basis for the apparent over-prediction of 'reset' zircon in terrestrial impacts. Diffusion studies of zircon will allow for better models to further understand the effects of Pb mobility as a result of impact shock and heating.

6.5.2 Zircon geochronology of unconstrained terrestrial craters to better asses cratering rate and correlation with mass extinctions and global change.

As zircon is further developed to accurately date impact events, it can be used to constrain currently unconstrained terrestrial impacts, such as the Santa Fe impact structure which currently has an age range of many 100's of Ma. As only a small fraction of terrestrial structures are currently accurately and precisely dated, such constraints will provide a better understanding of the terrestrial impact flux through time and allow for better predictions of impactor flux in the future.

6.5.3 Further modeling of zircon crystallization in response to impact melting as site selection criteria for future sample return missions.

Models developed to predict the abundance of zircon crystallizing from impacts on geochemically distinct targets may be used to as site selection criteria for sample return missions. The main science goal identified in a NRC report in 2007 for future exploration of the moon highlighted the impact history as the primary science goal and thus knowing where zircon may have been formed in response to impact events will be important for selecting where samples will be returned from. Understanding zircon formation in terrestrial impact melts has direct implications on planetary science and future sample return missions and may be transformative for our understanding of planetary impact histories.

6.6 Summary

Zircon occurs as a common accessory mineral in terrestrial impactites. The preferential incorporation of U and Th into zircon coupled with its highly refractory nature, often surviving multiple geologic cycles, has made zircon the premier terrestrial geochronometer. Zircon has the potential to be a probe of planetary impact history and may provide the only tool by which to identify the earliest of impact flux. The work presented here provides an in depth analysis of the potential for zircon to accurately date impact events. Future work will be able to further constrain the effects of impact shock and heating on zircon, and its radiogenic daughter products, to provide better constraints on the impact flux through time. Impacts are essential in planetary formation and may have provided the key to a habitable planet, while also causing major mass extinctions events and thus our knowledge of the timing of such events throughout history provides for a better understanding of the evolution of our planet.

7. Appendices

7.1 Appendix 1

Table 7.1.1 - SIMS U-Pb data table for all zircon extracted from terrestrial craters.

Sample: Vredefort	$^{207}Pb/^{235}U$ Value	1 s.e.	$^{206}Pb/^{238}U$ Value	1 s.e.	Correlation of Concordia Ellipses	$^{206}Pb/^{238}U$ Age (Ma)	1 s.e. (Ma)	$^{207}Pb/^{235}U$ Age (Ma)	1 s.e. (Ma)	$^{207}Pb/^{206}Pb$ Age (Ma)	1 s.e. (Ma)
VD_1A_1	15.7500	0.7077	0.4974	0.0221	0.9988	2600	95	2860	43	3050	4
VD_1A_2	12.1900	0.6299	0.4338	0.0222	0.9942	2320	100	2620	49	2860	9
VD_1A_3	9.2090	0.4496	0.3528	0.0173	0.9955	1950	83	2360	45	2740	8
VD_1A_4	12.8600	0.8148	0.4668	0.0280	0.9900	2470	123	2670	60	2820	15
VD_1A_5	16.0400	0.9469	0.5368	0.0308	0.9937	2770	129	2880	56	2960	11
VD_1B_1	15.8000	1.0770	0.5314	0.0361	0.9992	2750	152	2870	65	2950	4
VD_1B_3	11.7200	0.4160	0.4373	0.0161	0.9848	2340	72	2580	33	2780	11
VD_1B_4	10.0100	0.4831	0.3557	0.0166	0.9869	1960	79	2440	45	2860	13
VD_INL_1	10.1800	0.3490	0.3759	0.0132	0.9885	2060	62	2450	32	2800	9
VD_INL_2	10.9700	0.3932	0.4408	0.0153	0.9756	2350	69	2520	33	2660	13
VD_INL_3	6.1370	0.2225	0.3656	0.0131	0.9920	2010	62	2000	32	1980	8
VD_INL_4	11.4600	0.4318	0.4477	0.0169	0.9834	2390	75	2560	35	2710	11
VD_INL_5	12.3200	0.4144	0.4615	0.0156	0.9913	2450	69	2630	32	2770	7
VD_INL_6	8.3820	0.3031	0.3991	0.0143	0.9837	2170	66	2270	33	2370	11
VD_INL_8	9.6580	0.3605	0.4286	0.0156	0.9935	2300	70	2400	34	2490	7
VD_INL_9	12.6700	0.4669	0.4626	0.0172	0.9874	2450	76	2660	35	2820	10
VD_INL_10	9.0720	0.3969	0.3849	0.0169	0.9959	2100	79	2350	40	2570	7
VD_INL_11	10.6400	0.4266	0.4390	0.0169	0.9760	2350	76	2490	37	2610	15
VD_INL_12	9.4610	0.3784	0.4084	0.0162	0.9854	2210	74	2380	37	2540	11
VD_INL_15	12.8800	0.4780	0.4757	0.0173	0.9972	2510	76	2670	35	2800	5
VD_INL_16	5.8840	0.3628	0.3590	0.0201	0.9613	1980	95	1960	54	1940	31
VD_PB_1	13.5700	0.5760	0.4745	0.0198	0.9942	2503	86	2720	40	2886	7
VD_PB_2	13.5000	0.4653	0.4571	0.0156	0.9899	2427	69	2715	33	2938	8
VD_PB_3	14.2400	0.5466	0.4907	0.0187	0.9963	2574	81	2766	36	2909	5
VD_PB_4	15.2500	0.5571	0.5037	0.0182	0.9947	2630	78	2831	35	2977	6
VD_PB_5	15.1200	0.5750	0.5165	0.0195	0.9954	2684	83	2823	36	2923	6

VD_PB_7	15.1000	0.5886	0.5085	0.0196	0.9963	2650	84	2821	37	2946	5
VD_PB_8	11.0000	0.4184	0.3997	0.0152	0.9970	2167	70	2523	35	2823	5
VD_PB_9	16.6700	0.6441	0.5347	0.0205	0.9955	2761	86	2916	37	3025	6
VD_PB_10	17.4900	0.6619	0.5594	0.0210	0.9960	2864	87	2962	36	3029	5
VD_PB_11	19.1700	0.7333	0.5958	0.0228	0.9966	3013	92	3051	37	3075	5
VD_PB_12	10.1500	0.6780	0.3538	0.0214	0.9451	1953	102	2449	62	2890	36
VD_PB_15	8.9420	0.3272	0.3444	0.0125	0.9944	1908	60	2332	33	2728	6
VD_PB_16	13.3100	0.5556	0.4697	0.0191	0.9709	2482	84	2702	39	2871	16
VD_PB_17	18.1600	0.6752	0.5817	0.0216	0.9958	2956	88	2998	36	3027	5
VD_PB_18	13.2700	0.4794	0.4591	0.0164	0.9833	2436	73	2699	34	2903	11
VD_PB_19	8.9890	0.3359	0.3292	0.0123	0.9927	1834	59	2337	34	2810	7
VD_PB_20	14.1100	0.5293	0.4550	0.0171	0.9922	2417	76	2757	36	3016	8
VD_PB_21	17.5800	0.6458	0.5541	0.0202	0.9968	2842	84	2967	35	3053	5
VD_PB_22	15.2600	0.5393	0.5076	0.0180	0.9954	2646	77	2831	34	2966	5
VD_PB_23	14.5400	0.5301	0.4887	0.0177	0.9949	2565	77	2786	35	2949	6
VD_PB_24	10.1200	0.3594	0.3817	0.0134	0.9869	2084	63	2446	33	2762	9
VD_PB_25	15.7400	0.5966	0.5077	0.0192	0.9961	2647	82	2861	36	3016	5
VD_PB_26	11.3100	0.4151	0.3996	0.0146	0.9968	2167	67	2549	34	2868	5
VD_PB_27	14.6000	0.5361	0.4910	0.0179	0.9932	2575	77	2789	35	2949	7
VD_PB_28	17.9600	0.6719	0.5793	0.0218	0.9985	2946	89	2988	36	3016	3
VD_PB_29	13.9700	0.4899	0.4668	0.0163	0.9970	2469	72	2748	33	2959	4
VD_PB_30	11.8900	0.4594	0.4340	0.0165	0.9850	2324	74	2596	36	2815	11
VD_PB_31	14.9800	0.5627	0.5209	0.0195	0.9923	2703	83	2814	36	2895	8
VD_PB_32	14.9000	0.5431	0.4979	0.0181	0.9955	2605	78	2809	35	2959	6
VD_PB_33	10.3600	0.4017	0.3605	0.0137	0.9933	1984	65	2467	36	2893	7
VD_PB_35	16.5900	0.6320	0.5424	0.0206	0.9971	2794	86	2911	36	2994	5
VD_G_1	13.1900	1.0520	0.4812	0.0362	0.9867	2694	75	2532	158	2817	22
VD_G_2	14.0600	1.3230	0.5256	0.0435	0.9321	2754	89	2723	184	2777	56
VD_G_3	11.9100	0.6746	0.4931	0.0250	0.9439	2597	53	2584	108	2607	31
VD_G_5	11.7600	0.6246	0.4740	0.0229	0.9441	2586	50	2501	100	2652	29
VD_G_6	7.3860	0.3061	0.3269	0.0109	0.8812	2159	37	1823	53	2496	33
VD_G_7	15.9700	0.8252	0.5435	0.0294	0.9908	2875	49	2798	123	2930	12
VD_G_8	14.7000	0.6422	0.5140	0.0201	0.9750	2796	42	2674	85	2886	17
VD_G_9	9.9480	0.6674	0.4372	0.0226	0.8646	2430	62	2338	101	2508	58
VD_G_10	22.6800	1.7070	0.6698	0.0459	0.9932	3213	73	3305	177	3156	17
VD_G_11	18.7000	1.4750	0.5867	0.0430	0.9860	3026	76	2976	175	3060	22
VD_G_12	18.6500	1.0270	0.6002	0.0302	0.9893	3024	53	3031	122	3019	15

VD_G_13	14.3200	0.7285	0.5473	0.0274	0.9789	2771	48	2814	114	2740	17
Sample: Sudbury	**$^{207}Pb/^{235}U$ Value**	**1 s.e.**	**$^{206}Pb/^{238}U$ Value**	**1 s.e.**	**Correlation of Concordia Ellipses**	**$^{206}Pb/^{238}U$ Age (Ma)**	**1 s.e. (Ma)**	**$^{207}Pb/^{235}U$ Age (Ma)**	**1 s.e. (Ma)**	**$^{207}Pb/^{206}Pb$ Age (Ma)**	**1 s.e. (Ma)**
Sud_F_2	5.1610	0.0947	0.3319	0.0061	0.9973	1848	30	1846	16	1845	2
Sud_F_3	5.1550	0.1050	0.3313	0.0067	0.9965	1845	32	1845	17	1846	3
Sud_F_8	4.6560	0.0909	0.2992	0.0058	0.9986	1687	29	1759	16	1846	2
Sud_F_12	5.3040	0.1250	0.3401	0.0080	0.9981	1887	39	1869	20	1850	3
Sud_F_16	5.2490	0.0938	0.3372	0.0059	0.9980	1873	29	1861	15	1847	2
Sud_F_26	5.3550	0.1130	0.3441	0.0071	0.9991	1906	34	1878	18	1846	2
Sud_M_5	5.1730	0.1210	0.3357	0.0075	0.9816	1866	36	1848	20	1829	8
Sud_M_7	5.0520	0.1120	0.3236	0.0070	0.9955	1807	34	1828	19	1852	4
Sud_M_9	5.1710	0.0875	0.3314	0.0054	0.9947	1845	26	1848	14	1851	3
Sud_M_18	5.3810	0.1040	0.3467	0.0069	0.9926	1919	33	1882	17	1842	4
Sud_M_19	5.1690	0.0798	0.3311	0.0051	0.9907	1844	25	1848	13	1852	4
Sud_M_22	5.0120	0.1010	0.3202	0.0064	0.9929	1791	31	1821	17	1856	4
Sample: Morokweng	**$^{207}Pb/^{235}U$ Value**	**1 s.e.**	**$^{206}Pb/^{238}U$ Value**	**1 s.e.**	**Correlation of Concordia Ellipses**	**$^{206}Pb/^{238}U$ Age (Ma)**	**1 s.e. (Ma)**	**$^{207}Pb/^{235}U$ Age (Ma)**	**1 s.e. (Ma)**	**$^{207}Pb/^{206}Pb$ Age (Ma)**	**1 s.e. (Ma)**
MK_157m_1	0.0214	0.0012	0.1460	0.0082	0.9840	136	8	138	7	164	23
MK_157m_2	0.0232	0.0015	0.1570	0.0105	0.9860	148	10	148	9	141	27
MK_157m_3	0.0240	0.0017	0.1630	0.0118	0.9890	153	11	154	10	166	25
MK_157m_4	0.0236	0.0016	0.1620	0.0107	0.9950	151	10	152	9	182	16
MK_157m_5	0.0221	0.0013	0.1490	0.0094	0.9790	141	8	141	8	133	31
MK_157m_6	0.0239	0.0017	0.1630	0.0117	0.9840	152	11	153	10	172	29
MK_157m_7	0.0201	0.0012	0.1380	0.0086	0.9700	128	8	131	8	179	35
MK_157m_8	0.0203	0.0012	0.1410	0.0083	0.9860	130	8	134	7	205	23
MK_157m_9	0.0239	0.0018	0.1590	0.0120	0.9880	152	11	150	11	113	27
MK_157m_10	0.0240	0.0019	0.1680	0.0135	0.9910	153	12	158	12	229	25
MK_157m_11	0.0268	0.0020	0.1800	0.0136	0.9970	170	13	168	12	142	13
MK_157m_12	0.0268	0.0022	0.1810	0.0149	0.9940	171	14	169	13	145	22
MK_157m_13	0.0262	0.0020	0.1780	0.0138	0.9970	167	13	166	12	157	14
MK_157m_14	0.0268	0.0021	0.1810	0.0142	0.9980	171	13	169	12	151	12
MK_157m_15	0.0264	0.0022	0.1780	0.0152	0.9920	168	14	166	13	143	25
MK_157m_16	0.0231	0.0014	0.1570	0.0096	0.9700	147	9	148	8	162	35
MK_157m_17	0.0307	0.0030	0.2070	0.0203	0.9950	195	19	191	17	142	24

MK_157m_18	0.0236	0.0014	0.1600	0.0097	0.9960	150	9	150	8	151	12
MK_157m_19	0.0269	0.0022	0.1800	0.0155	0.9960	171	14	168	13	130	18
MK_157m_20	0.0264	0.0024	0.1780	0.0160	0.9900	168	15	166	14	139	31
MK_157m_21	0.0265	0.0024	0.1800	0.0156	0.9930	169	15	168	13	164	25
MK_157m_22	0.0250	0.0020	0.1690	0.0132	0.9950	159	12	158	11	148	19
MK_157m_23	0.0250	0.0019	0.1690	0.0124	0.9940	159	12	159	11	158	19
MK_157m_24	0.0273	0.0024	0.1840	0.0164	0.9880	174	15	172	14	143	33
MK_157m_25	0.0253	0.0020	0.1740	0.0136	0.9980	161	13	163	12	180	12
MK_157m_26	0.0223	0.0013	0.1500	0.0089	0.9940	142	8	142	8	149	16
MK_157m_27	0.0237	0.0015	0.1620	0.0106	0.9940	151	10	152	9	169	17
MK_157m_28	0.0208	0.0011	0.1400	0.0077	0.9830	133	7	133	7	144	24
MK_157m_29	0.0226	0.0014	0.1530	0.0095	0.9880	144	9	144	8	148	23
MK_157m_30	0.0255	0.0017	0.1720	0.0117	0.9930	162	11	161	10	149	20
MK_157m_31	0.0264	0.0019	0.1790	0.0131	0.9920	168	12	167	11	158	22
MK_157m_32	0.0244	0.0018	0.1670	0.0128	0.9810	155	11	157	11	177	35
MK_157m_33	0.0235	0.0015	0.1580	0.0099	0.9950	150	9	149	9	140	14
MK_157m_34	0.0245	0.0016	0.1660	0.0114	0.9850	156	10	156	10	150	28
MK_399m_1	0.1694	0.0078	0.0250	0.0008	0.7637	159	5	159	7	161	70
MK_399m_3	0.1612	0.0116	0.0244	0.0018	0.9598	156	11	152	10	92	48
MK_399m_4	0.1472	0.0095	0.0210	0.0013	0.9428	134	8	139	8	234	49
MK_399m_6	0.1739	0.0105	0.0258	0.0009	0.5729	164	6	163	9	146	117
MK_399m_7	0.1582	0.0108	0.0234	0.0015	0.9779	149	10	149	9	149	34
MK_399m_8	0.1567	0.0109	0.0233	0.0015	0.9451	149	9	148	10	133	54
MK_399m_9	0.1702	0.0142	0.0243	0.0009	0.5306	155	6	160	12	227	164
MK_399m_10	0.1652	0.0105	0.0241	0.0015	0.9722	154	10	155	9	179	35
MK_399m_11	0.1652	0.0109	0.0241	0.0015	0.9838	154	10	155	9	181	28
MK_399m_12	0.1567	0.0115	0.0229	0.0015	0.8727	146	9	148	10	178	84
MK_399m_13	0.1605	0.0166	0.0231	0.0017	0.7137	147	10	151	15	209	168
MK_399m_14	0.1597	0.0105	0.0233	0.0014	0.9480	148	9	150	9	181	49
MK_399m_15	0.1438	0.0109	0.0227	0.0014	0.8521	144	9	136	10	-1	0
MK_399m_16	0.1674	0.0111	0.0230	0.0014	0.9513	147	9	157	10	318	47
MK_399m_18	0.1718	0.0101	0.0255	0.0015	0.9897	162	9	161	9	142	20
MK_399m_19	0.1756	0.0124	0.0246	0.0010	0.6604	157	6	164	11	275	123
MK_399m_20	0.1507	0.0103	0.0221	0.0014	0.9498	141	9	143	9	170	50
MK_399m_21	0.1351	0.0160	0.0222	0.0014	0.5766	141	9	129	14	-1	0
MK_399m_22	0.1683	0.0098	0.0249	0.0014	0.9809	158	9	158	9	150	27
MK_399m_23	0.1674	0.0096	0.0248	0.0014	0.9818	158	9	157	8	143	25

MK_399m_25	0.1460	0.0106	0.0220	0.0013	0.8751	140	8	138	9	105	83
MK_399m_26	0.1520	0.0117	0.0236	0.0017	0.7981	150	11	144	10	37	113
Sample: Manicouagan	**$^{207}Pb/^{235}U$ Value**	**1 s.e.**	**$^{206}Pb/^{238}U$ Value**	**1 s.e.**	**Correlation of Concordia Ellipses**	**$^{206}Pb/^{238}U$ Age (Ma)**	**1 s.e. (Ma)**	**$^{207}Pb/^{235}U$ Age (Ma)**	**1 s.e. (Ma)**	**$^{207}Pb/^{206}Pb$ Age (Ma)**	**1 s.e. (Ma)**
MC_MM_1	0.2219	0.0104	0.0342	0.0010	0.6352	217	7	204	9	51	87
MC_MM_2	0.2300	0.0119	0.0343	0.0011	0.6246	218	7	210	10	128	95
MC_MM_3	0.2206	0.0085	0.0321	0.0010	0.8457	203	6	202	7	190	48
MC_MM_4	0.2392	0.0091	0.0348	0.0011	0.8589	220	7	218	7	191	45
MC_MM_5	0.2197	0.0169	0.0321	0.0010	0.4864	204	6	202	14	180	157
MC_MM_6	0.2397	0.0084	0.0352	0.0011	0.8486	223	7	218	7	167	43
MC_MM_8	0.2434	0.0133	0.0349	0.0011	0.5956	221	7	221	11	221	102
MC_MM_9	0.2451	0.0090	0.0342	0.0010	0.7978	217	6	223	7	285	51
MC_MM_10	0.2150	0.0129	0.0334	0.0011	0.5954	212	7	198	11	30	116
MC_MM_11	0.2157	0.0117	0.0326	0.0010	0.6176	207	6	198	10	96	101
MC_MM_12	0.2352	0.0081	0.0337	0.0010	0.8986	214	6	214	7	221	35
MC_MM_13	0.2378	0.0153	0.0339	0.0012	0.5449	215	7	217	13	234	124
MC_MM_14	0.2231	0.0115	0.0333	0.0011	0.6294	211	7	205	10	129	94
MC_MM_16	0.2317	0.0095	0.0338	0.0011	0.7941	214	7	212	8	180	58
MC_MM_18	0.2372	0.0084	0.0339	0.0010	0.8543	215	6	216	7	228	42
MC_MM_20	0.2153	0.0169	0.0336	0.0010	0.3945	213	6	198	14	21	174
MC_MM_21	0.2659	0.0216	0.0354	0.0012	0.5474	224	8	239	17	389	154
MC_MM_22	0.2231	0.0239	0.0339	0.0011	0.4688	215	7	205	20	85	228
MC_MM_23	0.2371	0.0151	0.0338	0.0011	0.5377	214	7	216	12	236	124
MC_MM_24	0.2428	0.0107	0.0340	0.0011	0.7086	216	7	221	9	276	71
MC_MM_26	0.2425	0.0126	0.0340	0.0011	0.6543	216	7	220	10	274	90
MC_MM_27	0.2356	0.0167	0.0337	0.0011	0.5806	214	7	215	14	226	136
MC_MM_28	0.2309	0.0100	0.0335	0.0010	0.7219	212	6	211	8	194	70
MC_MM_29	0.2318	0.0120	0.0333	0.0011	0.6316	211	7	212	10	221	93
MC_MM_30	0.2518	0.0147	0.0355	0.0011	0.5909	225	7	228	12	259	108
MC_MM_31	0.2258	0.0124	0.0339	0.0011	0.5308	215	7	207	10	118	110
MC_MM_32	0.2306	0.0125	0.0333	0.0010	0.6304	211	6	211	10	206	98
MC_MM_33	0.2025	0.0153	0.0317	0.0011	0.4788	202	7	187	13	12	159
MC_MM_34	0.2387	0.0156	0.0339	0.0011	0.6073	215	7	217	13	242	120
MC_MM_35	0.2250	0.0161	0.0340	0.0011	0.5034	216	7	206	13	99	146
MC_MM_36	0.2462	0.0112	0.0349	0.0011	0.6210	221	7	224	9	251	82
MC_MM_37	0.2262	0.0131	0.0336	0.0011	0.6283	213	7	207	11	144	106

Sample: Popigai	$^{207}Pb/^{235}U$ Value	1 s.e.	$^{206}Pb/^{238}U$ Value	1 s.e.	Correlation of Concordia Ellipses	$^{206}Pb/^{238}U$ Age (Ma)	1 s.e. (Ma)	$^{207}Pb/^{235}U$ Age (Ma)	1 s.e. (Ma)	$^{207}Pb/^{206}Pb$ Age (Ma)	1 s.e. (Ma)
PG_RR_1	0.1811	0.0082	1.8970	0.0897	0.9879	1073	45	1080	31	1095	15
PG_RR_2	0.3422	0.0147	5.7330	0.2440	0.9769	1897	71	1936	37	1979	16
PG_RR_3	0.3700	0.0192	6.0590	0.3120	0.9954	2029	91	1984	45	1938	9
PG_RR_4	0.2798	0.0147	4.5550	0.2410	0.9939	1591	74	1741	44	1927	11
PG_RR_5	0.2917	0.0123	4.7620	0.1970	0.9945	1650	61	1778	35	1932	8
PG_RR_6	0.2812	0.0128	4.8080	0.2210	0.9971	1598	64	1786	39	2014	6
PG_RR_7	0.3541	0.0137	5.7810	0.2200	0.9926	1954	65	1944	33	1933	8
PG_RR_8	0.2043	0.0101	3.4440	0.1940	0.9209	1199	54	1515	44	1989	39
PG_RR_9	0.3858	0.0177	6.5760	0.2990	0.9980	2103	82	2056	40	2009	5
PG_RR_10	0.3515	0.0196	5.8130	0.3180	0.9955	1942	93	1948	48	1955	9
PG_RR_11	0.3458	0.0142	5.7230	0.2370	0.9912	1914	68	1935	36	1957	10
PG_RR_12	0.3394	0.0134	5.7080	0.2270	0.9957	1884	64	1933	34	1985	7
PG_RR_13	0.3651	0.0213	6.2190	0.3710	0.9974	2006	101	2007	52	2008	8
PG_RR_14	0.3613	0.0170	6.1350	0.2850	0.9891	1988	81	1995	41	2003	12
PG_RR_15	0.3511	0.0160	5.9440	0.2770	0.9907	1940	77	1968	40	1997	11
PG_RR_16	0.1809	0.0071	2.9670	0.1190	0.9941	1072	39	1399	31	1940	8
PG_RR_17	0.3729	0.0194	6.1340	0.3180	0.9955	2043	91	1995	45	1946	9
PG_RR_18	0.3717	0.0256	6.1360	0.4280	0.9928	2037	120	1995	61	1952	15
PG_RR_19	0.1139	0.0014	1.7670	0.0220	0.9590	696	8	1033	8	1840	6
PG_RR_20	0.0144	0.0002	0.1145	0.0036	0.5085	92	1	110	3	524	60
PG_RR_21	0.3497	0.0207	6.0190	0.3620	0.9861	1933	99	1979	52	2026	18
PG_RR_22	0.0675	0.0039	0.5146	0.0341	0.9331	421	24	422	23	423	54
PG_RR_23	0.3753	0.0219	6.2200	0.3630	0.9969	2054	103	2007	51	1959	8
PG_RR_24	0.4025	0.0214	6.7570	0.3630	0.9981	2180	99	2080	48	1982	6
PG_RR_25	0.3631	0.0159	6.0670	0.2660	0.9966	1997	75	1986	38	1974	6
PG_RR_26	0.3542	0.0177	5.8090	0.2920	0.9960	1954	84	1948	44	1941	8
PG_RR_27	0.4989	0.0281	11.5000	0.6440	0.9958	2609	121	2564	52	2529	9
PG_RR_28	0.3131	0.0150	5.1460	0.2500	0.9935	1756	73	1844	41	1945	10
PG_RR_29	0.3731	0.0176	6.2190	0.2950	0.9974	2044	83	2007	42	1969	6
PG_RR_30	0.3558	0.0161	6.0260	0.3120	0.9143	1962	76	1980	45	1998	38
PG_RR_31	0.3627	0.0137	6.0330	0.2290	0.9978	1995	65	1981	33	1966	5
PG_RR_32	0.3669	0.0159	6.1480	0.2590	0.9972	2015	75	1997	37	1979	6
PG_RR_33	0.0297	0.0015	0.1936	0.0235	0.4316	188	9	180	20	67	260
PG_RR_35	0.0536	0.0082	0.3055	0.1040	0.4586	336	50	271	81	-1	0

PG_RR_36	0.2949	0.0169	4.9260	0.2880	0.9949	1666	84	1807	49	1973	11
PG_RR_37	0.3430	0.0186	5.8310	0.3060	0.9912	1901	90	1951	46	2005	13
PG_RR_38	0.2221	0.0101	3.6610	0.1720	0.9731	1293	53	1563	38	1950	19
PG_RR_39	0.3563	0.0185	5.9510	0.3100	0.9970	1965	88	1969	45	1973	7
PG_RR_40	0.3489	0.0151	5.7410	0.2510	0.9962	1929	72	1938	38	1947	7
PG_SG_2	5.6320	0.2350	0.3475	0.0147	0.9946	1923	70	1921	36	1919	8
PG_SG_3	5.8210	0.2380	0.3551	0.0144	0.9976	1959	69	1949	35	1939	5
PG_SG_4	5.4560	0.2240	0.3391	0.0139	0.9950	1882	67	1894	35	1906	7
PG_SG_5	5.8480	0.2520	0.3597	0.0154	0.9987	1981	73	1954	37	1925	4
PG_SG_6	5.6200	0.1990	0.3350	0.0118	0.9924	1863	57	1919	31	1981	8
PG_SG_7	4.7380	0.2100	0.2879	0.0124	0.9853	1631	62	1774	37	1947	14
PG_SG_8	6.7940	0.2970	0.3805	0.0158	0.9503	2079	74	2085	39	2091	24
PG_SG_9	4.9120	0.1840	0.2809	0.0105	0.9962	1596	53	1804	32	2055	6
PG_SG_10	6.3580	0.3400	0.3705	0.0174	0.8956	2032	82	2026	47	2021	42
PG_SG_12	6.0460	0.2400	0.3549	0.0141	0.9932	1958	67	1982	35	2008	8
PG_SG_13	6.6270	0.2740	0.3729	0.0153	0.9944	2043	72	2063	36	2083	8
PG_SG_14	5.6750	0.2300	0.3485	0.0140	0.9957	1927	67	1928	35	1928	7
PG_SG_15	4.4230	0.1770	0.2715	0.0108	0.9927	1548	55	1717	33	1928	9
PG_SG_16	6.3160	0.2530	0.3662	0.0146	0.9981	2011	69	2021	35	2030	4
PG_SG_17	6.1210	0.2530	0.3668	0.0152	0.9920	2014	72	1993	36	1971	9
PG_SG_18	5.0360	0.2000	0.2919	0.0117	0.9928	1651	58	1825	34	2031	8
PG_SG_19	3.9210	0.1620	0.2337	0.0096	0.9964	1354	50	1618	33	1981	6
PG_SG_20	5.4220	0.2210	0.3303	0.0133	0.9942	1840	65	1888	35	1942	8
PG_SG_21	2.9890	0.1310	0.1819	0.0074	0.9274	1077	41	1405	33	1944	29
PG_SG_22	6.4240	0.2610	0.3523	0.0140	0.9941	1946	67	2036	36	2128	8
PG_SG_24	5.6380	0.2230	0.3460	0.0137	0.9933	1916	66	1922	34	1929	8
PG_SG_25	5.8720	0.2250	0.3546	0.0134	0.9924	1957	64	1957	33	1958	8
PG_SG_26	5.1800	0.2230	0.3081	0.0120	0.9474	1731	59	1849	37	1985	25
PG_SG_27	6.2090	0.2510	0.3649	0.0144	0.9914	2005	68	2006	35	2006	9
PG_SG_28	6.1210	0.4210	0.3686	0.0204	0.8743	2023	96	1993	60	1963	60
PG_SG_29	5.5610	0.2180	0.3173	0.0124	0.9968	1776	61	1910	34	2059	6
PG_SG_30	6.7720	0.2680	0.3856	0.0152	0.9962	2102	71	2082	35	2062	6
PG_SG_31	5.4380	0.2110	0.3262	0.0126	0.9934	1820	61	1891	33	1970	8
PG_SG_32	3.0630	0.0678	0.2005	0.0036	0.8447	1178	19	1423	17	1812	22
PG_SG_33	5.6660	0.2260	0.3245	0.0124	0.9480	1812	60	1926	34	2052	22
PG_SG_34	4.3880	0.1440	0.2539	0.0081	0.9722	1459	42	1710	27	2033	14
PG_SG_35	5.7440	0.2290	0.3469	0.0135	0.9947	1920	65	1938	35	1958	7

PG_SG_36	4.6790	0.1930	0.2894	0.0118	0.9913	1638	59	1764	35	1915	10
PG_SG_37	5.2400	0.2250	0.2980	0.0123	0.9920	1681	61	1859	37	2064	10
PG_SG_38	5.7630	0.2820	0.3569	0.0160	0.9097	1967	76	1941	42	1913	37
PG_SG_39	5.4670	0.2550	0.3424	0.0130	0.8706	1898	63	1895	40	1892	42
PG_SG_40	4.3690	0.1470	0.2565	0.0087	0.9687	1472	45	1707	28	2008	15
PG_SG_41	5.6760	0.2000	0.3434	0.0117	0.9680	1903	56	1928	30	1954	16
PG_SG_42	6.9610	0.2310	0.3759	0.0124	0.9977	2057	58	2106	29	2155	4
PG_SG_43	5.5040	0.2100	0.3359	0.0128	0.9945	1867	62	1901	33	1939	7
PG_SG_44	5.8090	0.2310	0.3402	0.0135	0.9977	1888	65	1948	34	2012	5
PG_SG_45	5.0650	0.1710	0.3027	0.0101	0.9840	1705	50	1830	29	1976	11
PG_SG_46	5.6460	0.2160	0.3458	0.0132	0.9965	1914	63	1923	33	1933	6
PG_SG_47	3.9650	0.1510	0.2419	0.0091	0.9870	1397	47	1627	31	1939	11
PG_SG_48	6.1090	0.2370	0.3436	0.0127	0.9529	1904	61	1992	34	2084	21
PG_SG_49	6.8920	0.2780	0.3838	0.0146	0.9756	2094	68	2098	36	2101	16
PG_SG_50	5.3940	0.2040	0.3316	0.0125	0.9967	1846	60	1884	32	1925	6
PG_SG_51	5.3230	0.2010	0.3256	0.0119	0.9800	1817	58	1872	32	1935	14
PG_SG_52	5.7640	0.2160	0.3400	0.0127	0.9991	1887	61	1941	32	1999	3
PG_SG_53	5.5890	0.2350	0.3502	0.0132	0.9076	1935	63	1914	36	1892	32
PG_SG_54	5.8810	0.2230	0.3491	0.0152	0.8680	1930	73	1958	33	1989	39
PG_SG_56	6.3810	0.2590	0.3820	0.0152	0.9960	2085	71	2030	36	1973	7
PG_SG_57	7.1190	0.2840	0.3670	0.0142	0.9891	2015	67	2126	36	2236	10
PG_SG_61	5.4610	0.2130	0.3342	0.0131	0.9925	1859	63	1894	34	1934	9
PG_SG_62	5.6580	0.2220	0.3479	0.0132	0.9903	1925	63	1925	34	1925	10
PG_SG_63	5.5780	0.2010	0.3146	0.0114	0.9957	1763	56	1913	31	2079	6
PG_SG_64	5.5640	0.1990	0.3244	0.0115	0.9978	1811	56	1910	31	2020	4
PG_SG_65	5.2450	0.1940	0.3105	0.0116	0.9941	1743	57	1860	32	1993	7
PG_SG_66	6.9210	0.8930	0.3867	0.0431	0.9916	2108	200	2101	114	2095	41
PG_SG_67	0.8075	0.0376	0.0469	0.0021	0.9303	295	13	601	21	2028	30
PG_SG_68	5.3690	0.1950	0.3123	0.0112	0.9878	1752	55	1880	31	2025	10
PG_SG_70	9.3090	0.3740	0.4461	0.0178	0.9963	2378	79	2369	37	2361	6
PG_SG_71	6.3030	0.3290	0.3846	0.0203	0.9963	2098	95	2019	46	1939	8

VD - Vredefort impact: 1A & 1B are in-situ analysis from thin sections of pseudotachylite breccia, INL are grains from drill core of Kamo et al. (1996), PB are grains from pseudotachylite breccia, G are grains from granophyre.

Sud - Sudbury impact: F are grains from the felsic portion of the norite, M are grains from the mafic portion of the norite.

MK - Morokweng impact: 157 & 399 m denotes from which part of drill core M3 the grains were extracted.

MC - Manicouagan impact: MM are from the main melt sheet.

PG - Popigai impact: RR are grains from the Rassokha River, SG are grains from shocked gneiss samples.

7.2 Appendix 2

Table 7.2.1 - SIMS REE abundance data table for all zircon extracted from terrestrial impactites.

Sample: Vredefort	**^{139}La** ppm	**1σ**	**^{140}Ce** ppm	**1σ**	**^{141}Pr** ppm	**1σ**	**^{143}Nd** ppm	**1σ**	**^{149}Sm** ppm	**1σ**	**^{151}Eu** ppm	**1σ**	**^{156}Gd** ppm	**1σ**
VD_INL_3	0	0	54	1	2	0	5	0	17	1	4	1	68	4
VD_INL_16	15	2	77	2	19	2	22	1	39	2	8	1	108	5
Sample: Vredefort	**^{159}Tb** ppm	**1σ**	**^{161}Dy** ppm	**1σ**	**^{165}Ho** ppm	**1σ**	**^{168}Er** ppm	**1σ**	**^{169}Tm** ppm	**1σ**	**^{172}Yb** ppm	**1σ**	**^{175}Lu** ppm	**1σ**
VD_INL_3	129	14	205	7	348	35	514	18	723	120	922	75	1320	35
VD_INL_16	174	13	292	9	537	44	953	30	1437	186	2104	149	3499	116
Sample: Sudbury	**^{139}La** ppm	**1σ**	**^{140}Ce** ppm	**1σ**	**^{141}Pr** ppm	**1σ**	**^{143}Nd** ppm	**1σ**	**^{149}Sm** ppm	**1σ**	**^{151}Eu** ppm	**1σ**	**^{156}Gd** ppm	**1σ**
Sud_F_2	53	8	385	7	48	8	59	7	132	4	35	3	506	30
Sud_F_3	4	0	216	3	14	2	37	2	184	6	14	1	569	22
Sud_F_8	58	8	487	8	59	9	107	7	437	11	40	2	1471	50
Sud_F_12	1	0	473	5	26	3	83	2	431	11	33	2	1390	31
Sud_F_16	0	0	297	3	7	1	23	1	127	4	9	1	479	14
Sud_F_26	0	0	194	2	13	1	40	1	189	5	18	1	728	19
Sud_M_5	1	0	80	1	5	1	10	1	54	3	11	1	191	11
Sud_M_7	12	2	262	4	31	4	57	2	186	12	52	2	647	19
Sud_M_9	4	0	265	4	30	3	64	2	241	6	58	3	849	23
Sud_M_18	12	1	295	5	30	4	47	2	145	7	67	5	432	16
Sud_M_19	1	0	290	3	21	2	60	2	244	6	36	2	876	22
Sud_M_22	1	0	265	24	17	3	48	5	200	15	39	4	712	74
Sample: Sudbury	**^{159}Tb** ppm	**1σ**	**^{161}Dy** ppm	**1σ**	**^{165}Ho** ppm	**1σ**	**^{168}Er** ppm	**1σ**	**^{169}Tm** ppm	**1σ**	**^{172}Yb** ppm	**1σ**	**^{175}Lu** ppm	**1σ**

Sud_F_2	908	112	1447	37	2416	94	3339	86	4341	348	5273	322	6558	122
Sud_F_3	1054	78	1536	37	2446	93	3203	67	4036	370	4731	202	5803	101
Sud_F_8	2731	179	4116	95	6487	214	8457	162	10360	585	12105	453	14152	179
Sud_F_12	2479	89	3659	80	5559	170	7260	138	8724	593	10111	259	11624	108
Sud_F_16	896	50	1402	32	2278	89	3132	61	4040	484	4947	175	5865	108
Sud_F_26	1413	62	2196	48	3565	117	4838	114	6042	454	7285	209	8660	111
Sud_M_5	365	45	562	22	905	50	1215	27	1512	140	1880	114	2336	49
Sud_M_7	1150	67	1745	74	2800	208	3664	128	4240	233	4844	210	5901	159
Sud_M_9	1538	77	2195	57	3415	108	4342	95	4934	235	5633	178	6799	104
Sud_M_18	744	34	1107	37	1761	99	2306	49	2724	207	3172	128	3907	80
Sud_M_19	1592	64	2347	56	3623	115	4459	99	5046	314	5578	159	6684	134
Sud_M_22	1253	180	1849	171	2866	332	3598	321	4217	505	4713	623	5749	457
Sample:	**^{139}La**	**1σ**	**^{140}Ce**	**1σ**	**^{141}Pr**	**1σ**	**^{143}Nd**	**1σ**	**^{149}Sm**	**1σ**	**^{151}Eu**	**1σ**	**^{156}Gd**	**1σ**
Morokweng	ppm		ppm		ppm		ppm		ppm		ppm		ppm	
MK_157m_1	30	1	173	6	30	3	51	3	222	9	9	1	727	31
MK_157m_2	6	0	324	11	45	3	122	4	550	18	24	2	1486	62
MK_157m_3	6	0	439	15	92	7	232	8	944	27	29	2	2071	85
MK_157m_4	1	0	133	5	14	1	34	2	188	7	5	1	762	33
MK_157m_5	41	1	429	15	71	5	150	6	602	17	30	3	1629	67
MK_157m_6	47	2	493	21	41	3	55	2	257	9	8	1	965	46
MK_157m_7	14	1	152	5	18	1	37	2	197	7	3	1	763	32
MK_157m_8	2	0	99	4	12	1	26	3	137	5	9	1	494	21
MK_157m_9	27	1	454	16	37	3	61	3	290	10	30	2	926	38
MK_157m_11	223	57	450	45	147	36	141	27	285	17	26	4	798	82
MK_157m_13	4	0	200	7	18	2	51	2	301	10	5	1	1090	45
MK_157m_15	22	2	140	9	25	3	28	1	72	4	10	3	216	18
MK_157m_16	13	1	120	4	15	1	40	3	205	7	48	2	620	26
MK_157m_17	49	3	411	15	74	6	122	7	499	16	37	3	1354	57
MK_157m_18	79	21	235	23	75	19	89	12	265	9	33	2	984	97
MK_157m_19	50	3	406	36	67	8	97	4	365	12	37	2	1212	112
MK_157m_20	17	1	295	10	9	1	68	2	68	2	2	0	238	10
MK_157m_21	303	12	703	27	333	26	516	17	1352	41	48	2	2365	107
MK_157m_22	16	2	114	5	21	2	33	4	127	7	10	1	441	22
MK_157m_23	72	7	140	9	61	9	60	5	122	5	15	1	374	28
MK_157m_24	37	2	156	5	56	4	94	4	303	13	16	1	611	27
MK_157m_25	31	6	89	7	26	6	25	3	66	5	7	1	219	21
MK_157m_26	22	1	110	5	18	2	23	1	83	4	4	1	339	18

MK_157m_27	20	1	545	19	118	9	296	9	1183	33	23	2	2750	112
MK_157m_28	15	1	72	3	12	1	11	1	34	2	20	1	132	6
MK_157m_29	40	3	143	6	39	3	47	2	124	5	12	1	380	18
MK_157m_30	1	0	212	7	21	2	60	2	362	11	6	1	1140	47
MK_157m_31	1	0	109	4	12	1	33	2	198	8	4	1	769	32
MK_157m_32	40	15	341	67	41	13	65	9	292	32	21	2	954	211
MK_157m_33	1	0	554	19	14	1	35	2	204	8	9	1	703	29
MK_157m_34	11	1	228	8	18	1	36	2	178	7	9	1	583	24
MK_399m_7	0	0	132	1	4	0	9	0	46	3	5	1	185	7
MK_399m_8	1	0	427	21	14	1	33	1	154	7	25	3	656	20
MK_399m_10	0	0	489	5	15	1	41	2	205	7	11	1	769	26
MK_399m_11	2	0	111	1	5	1	12	1	63	3	9	1	287	14
MK_399m_12	1	0	100	2	4	0	11	1	58	2	7	1	221	14
MK_399m_14	1	0	398	4	12	1	37	1	204	6	12	1	738	23
MK_399m_18	1	0	158	2	4	0	11	1	43	2	7	1	181	8
MK_399m_20	2	0	24	1	6	1	22	1	185	8	5	1	821	34
MK_399m_22	4	0	76	1	8	1	17	1	82	4	12	1	304	15
MK_399m_23	3	1	130	22	163	43	427	82	749	131	5	1	628	97
Sample: Morokweng	**^{159}Tb** ppm	**1σ**	**^{161}Dy** ppm	**1σ**	**^{165}Ho** ppm	**1σ**	**^{168}Er** ppm	**1σ**	**^{169}Tm** ppm	**1σ**	**^{172}Yb** ppm	**1σ**	**^{175}Lu** ppm	**1σ**
MK_157m_1	1458	99	2070	56	2877	134	3536	96	4295	468	4805	206	5324	149
MK_157m_2	2751	121	3680	99	4713	194	5330	144	6151	429	6370	268	6813	202
MK_157m_3	3498	139	4115	111	4645	178	4817	130	5327	348	5544	226	5549	179
MK_157m_4	1814	112	3017	83	4816	223	6437	173	8157	1540	8981	404	9893	294
MK_157m_5	2900	137	3827	103	4940	186	5761	155	6847	730	7582	308	8171	222
MK_157m_6	1934	91	2607	81	3250	138	3574	139	4062	557	4368	210	4488	203
MK_157m_7	1763	89	2872	78	4572	200	6121	170	7465	1445	8264	364	9180	256
MK_157m_8	1079	117	1750	53	2900	132	4077	110	5275	539	6587	280	7975	217
MK_157m_9	1701	81	2335	64	3109	132	3594	98	3980	280	4277	179	4323	137
MK_157m_11	1563	299	2203	67	3001	191	3415	93	3904	567	4159	429	4437	123
MK_157m_13	2499	118	3944	106	6019	244	7688	206	9258	1805	10172	418	10981	298
MK_157m_15	471	33	772	26	1203	90	1555	69	1980	656	2330	212	2598	138
MK_157m_16	1139	80	1551	42	1990	82	2265	62	2493	119	2631	122	2635	73
MK_157m_17	2812	183	3975	129	5303	219	6396	253	7682	570	8887	414	9028	289
MK_157m_18	1986	278	2935	79	4294	180	5292	143	6255	384	6747	666	7539	206
MK_157m_19	2497	109	3763	101	5664	236	7335	197	8996	526	10820	996	11992	349
MK_157m_20	79	3	751	21	227	9	772	22	138	7	979	42	164	4

MK_157m_21	3604	147	3980	115	4422	179	4651	125	5118	273	5391	244	5687	156
MK_157m_22	1009	124	1749	48	3029	181	4342	117	5767	583	6993	350	8274	229
MK_157m_23	821	80	1378	53	2270	147	3199	164	4124	354	4848	380	5808	299
MK_157m_24	998	47	1272	48	1575	88	1754	49	1942	161	2133	116	2279	73
MK_157m_25	500	67	913	36	1564	125	2367	95	3102	383	3890	377	4802	142
MK_157m_26	840	50	1554	67	2735	151	4210	178	5780	1162	7049	377	8399	235
MK_157m_27	4549	181	5410	146	6214	228	6771	182	7650	550	8115	348	8911	243
MK_157m_28	349	33	704	20	1310	89	2072	57	2953	217	3720	176	4436	153
MK_157m_29	858	43	1470	47	2557	123	3676	136	4891	483	5789	300	7039	241
MK_157m_30	2167	101	2840	77	3623	152	4104	116	4560	709	4809	198	5007	166
MK_157m_31	1737	90	2770	79	4326	208	5560	150	6809	1195	7499	321	8363	228
MK_157m_32	2049	335	3147	263	4541	618	5662	368	6737	652	7607	1725	7971	405
MK_157m_33	1461	103	2153	58	2963	132	3498	95	4125	574	4350	180	4583	127
MK_157m_34	1170	60	1729	48	2471	110	3003	83	3603	390	3940	172	4289	119
MK_399m_7	368	28	610	12	1036	79	1497	14	1986	391	2533	171	3174	49
MK_399m_8	1249	77	2008	37	3343	226	4739	127	6072	804	7488	483	9203	230
MK_399m_10	1302	87	1776	24	2407	130	2809	30	3027	287	3288	215	3600	41
MK_399m_11	677	66	1203	30	2197	145	3285	58	4275	426	5304	394	6455	121
MK_399m_12	453	40	742	36	1269	87	1836	49	2475	260	3187	270	3988	60
MK_399m_14	1302	78	1809	25	2493	133	2931	24	3333	290	3662	229	4033	59
MK_399m_18	336	25	558	8	969	65	1423	16	1919	289	2526	175	3208	74
MK_399m_20	2004	162	3340	45	5267	327	6709	55	7746	946	8627	598	9250	116
MK_399m_22	648	55	1042	38	1706	114	2337	76	2855	272	3460	255	4068	70
MK_399m_23	893	195	943	50	955	174	1021	11	1061	250	1080	177	1122	36
Sample:	**^{139}La**	**1σ**	**^{140}Ce**	**1σ**	**^{141}Pr**	**1σ**	**^{143}Nd**	**1σ**	**^{149}Sm**	**1σ**	**^{151}Eu**	**1σ**	**^{156}Gd**	**1σ**
Manicouagan	ppm		ppm		ppm		ppm		ppm		ppm		ppm	
MC_MM_1	5	0	220	8	31	2	69	3	323	10	16	2	999	41
MC_MM_2	5	0	1026	45	82	7	230	8	1009	28	48	2	2856	141
MC_MM_3	1	0	293	10	10	1	27	1	159	6	12	1	601	25
MC_MM_4	3	0	604	21	25	2	63	2	354	11	19	2	1178	48
MC_MM_5	2	0	73	3	6	1	15	2	80	4	5	1	311	13
MC_MM_6	2	0	736	26	53	4	160	5	724	24	43	5	2138	88
MC_MM_8	1	2	89	3	12	1	33	2	172	5	8	11	581	24
MC_MM_9	3	3	292	10	29	2	72	3	322	8	22	15	1053	43
MC_MM_10	1	3	207	7	11	1	30	2	183	5	11	12	661	28
MC_MM_11	1	5	609	21	29	2	95	4	572	15	35	22	2053	86
MC_MM_12	0	4	542	19	15	2	44	3	274	7	14	15	1025	42

MC_MM_13	1	1	73	3	6	1	18	1	87	2	6	8	285	13
MC_MM_14	1	2	98	3	13	2	40	2	173	5	10	10	535	22
MC_MM_16	4	2	180	6	30	2	71	4	298	8	11	13	846	35
MC_MM_18	10	4	446	15	28	2	58	3	295	8	16	28	993	41
MC_MM_20	1	7	111	4	8	1	22	2	113	3	7	9	387	16
MC_MM_21	6	2	96	3	10	2	24	2	111	3	7	9	434	18
MC_MM_22	2	2	94	3	10	1	23	2	127	3	8	9	410	18
MC_MM_23	6	7	315	11	22	2	64	3	367	10	21	20	1191	49
MC_MM_24	0	2	82	3	5	1	14	3	97	3	6	9	381	17
MC_MM_26	3	4	187	6	23	2	62	3	323	9	14	14	1015	49
MC_MM_27	1	5	175	6	10	1	25	2	131	4	7	19	500	21
MC_MM_28	4	16	292	10	30	2	85	4	466	12	22	23	1474	62
MC_MM_30	6	13	460	16	27	2	57	4	319	8	26	23	1160	48
MC_MM_31	2	36	296	10	19	2	32	3	168	5	12	37	693	30
MC_MM_32	8	28	449	15	26	2	51	3	232	7	23	14	841	36
MC_MM_34	0	2	127	4	8	1	27	2	158	4	7	11	555	23
MC_MM_35	1	2	93	3	10	1	35	3	177	5	9	11	590	27
MC_MM_36	1	2	101	3	15	1	44	5	230	6	9	24	731	33
MC_MM_37	1	2	207	7	9	1	28	2	181	5	9	12	688	28
Sample:	**^{159}Tb**	**1σ**	**^{161}Dy**	**1σ**	**^{165}Ho**	**1σ**	**^{168}Er**	**1σ**	**^{169}Tm**	**1σ**	**^{172}Yb**	**1σ**	**^{175}Lu**	**1σ**
Manicouagan	ppm		ppm		ppm		ppm		ppm		ppm		ppm	
MC_MM_1	1991	90	3119	84	5020	206	6893	204	8866	1028	10863	446	12829	348
MC_MM_2	5108	210	7355	197	11202	416	14704	393	18437	961	22356	1098	26684	718
MC_MM_3	1298	71	2147	59	3751	169	5538	151	7685	908	9788	444	12386	335
MC_MM_4	2510	113	4055	114	6630	266	9240	263	11823	1068	13966	573	16022	433
MC_MM_5	714	94	1222	42	2159	113	3215	89	4406	1070	5624	242	7198	210
MC_MM_6	4177	171	6304	169	9634	398	12182	326	14589	1695	15934	652	17306	468
MC_MM_8	1172	93	1861	52	3072	110	4243	114	5596	7248	6863	284	8699	649
MC_MM_9	2099	107	3282	102	5191	192	6910	191	8836	6109	10414	438	12398	1081
MC_MM_10	1455	105	2447	76	4241	152	6214	166	8331	8803	10303	442	12830	558
MC_MM_11	4225	219	6410	175	9494	345	11511	308	13031	7919	14024	586	15256	537
MC_MM_12	2067	132	3235	89	5166	184	6897	184	8669	9053	10105	412	11839	807
MC_MM_13	592	48	971	29	1675	64	2415	66	3279	4221	4060	180	5080	350
MC_MM_14	1052	61	1611	51	2540	116	3320	89	4081	4358	4734	196	5494	351
MC_MM_16	1662	114	2525	70	3819	136	4932	132	6165	7445	7285	299	8531	408
MC_MM_18	2005	111	3231	89	5453	194	8002	223	11100	19408	14165	578	18359	1071
MC_MM_20	819	66	1303	38	2264	88	3347	90	4737	6434	6211	268	8112	395

MC_MM_21	1020	73	1678	66	2689	104	3498	96	4143	5543	4855	213	5346	393
MC_MM_22	868	75	1443	41	2487	91	3716	100	5235	6186	6864	294	9013	412
MC_MM_23	2488	137	3681	101	5348	199	6333	177	7008	6658	7434	303	8203	399
MC_MM_24	845	167	1501	45	2682	106	3980	117	5471	8367	6832	305	8638	997
MC_MM_26	2031	123	3170	87	4993	179	6641	178	8399	8318	10130	488	12186	661
MC_MM_27	1028	103	1629	46	2813	103	4019	117	5483	14936	6982	293	8948	873
MC_MM_28	2951	152	4419	120	6651	239	8306	223	9868	10254	11084	460	12713	489
MC_MM_30	2547	202	4301	119	7367	280	10176	274	12840	11670	15472	634	17555	615
MC_MM_31	1493	152	2499	70	4323	171	6243	167	8301	26234	10277	450	12785	1167
MC_MM_32	1764	115	2909	81	4908	193	6830	183	9103	5439	11069	466	13537	488
MC_MM_34	1216	96	2023	70	3496	130	5137	142	7180	11322	8898	369	11468	527
MC_MM_35	1223	107	1947	55	3269	119	4492	121	5751	7407	6820	320	8419	419
MC_MM_36	1459	167	2236	63	3446	123	4433	119	5479	14053	6367	292	7468	682
MC_MM_37	1530	115	2552	71	4371	156	6343	170	8330	10662	10324	437	12437	471

VD - Vredefort impact: INL are grains from drill core of Kamo et al. (1996).

Sud - Sudbury impact: F are grains from the felsic portion of the norite, M are grains from the mafic portion of the norite.

MK - Morokweng impact: 157 & 399 m denotes from which part of drill core M3 the grains were extracted.

MC - Manicouagan impact: MM are from the main melt sheet.

7.3 Appendix 3

Table 7.3.1 - SIMS Ti concentration and Ti-in-zircon thermometry data table for all zircon extracted from terrestrial impactites.

Sample: Vredefort	**$^{49}Ti_{mc}$ ppm**	**1σ**	**$^{49}Ti_{sc}$ ppm**	**1σ**	**Temp (mc) (°C)**	**1σ**	**Temp (sc) (°C)**	**1σ**
VD_INL_3			20.3	1.1			807.1	45.2
VD_INL_16			11.5	0.7			753.1	46.7
Sample: Sudbury	**$^{49}Ti_{mc}$ ppm**	**1σ**	**$^{49}Ti_{sc}$ ppm**		**Temp (mc) (°C)**	**1σ**	**Temp (sc) (°C)**	**1σ**

Sud_F_2			16.1	0.8			784.2	40.2
Sud_F_3			6.1	0.5			698.8	57.5
Sud_F_8			8.3	0.6			724.6	51.7
Sud_F_12			6.9	0.5			709.1	51.9
Sud_F_16			8.5	0.6			726.9	48.3
Sud_F_26			4.3	0.4			671.3	60.9
Sud_M_5			10.8	0.6			747.7	41.7
Sud_M_7			8.0	0.6			721.8	51.3
Sud_M_9			14.0	0.8			771.6	41.9
Sud_M_18			16.1	0.8			784.4	39.1
Sud_M_19			10.8	0.6			748.0	44.5
Sud_M_22			9.0	0.6			731.3	46.8
Sud_F_1	7.8	0.2			719.7	21.8		
Sud_F_4	29.8	0.9			846.7	25.6		
Sud_F_7	20.1	0.6			806.1	24.4		
Sud_F_9	13.8	0.4			769.9	23.3		
Sud_F_10	9.7	0.3			737.9	22.3		
Sud_F_14	5.6	0.2			692.2	20.9		
Sud_F_25	15.5	0.5			781.0	23.6		
Sud_M_1	79.9	2.4			963.6	29.1		
Sud_M_4	14.0	0.4			771.1	23.3		
Sud_M_10	4.2	0.1			669.6	20.2		
Sud_M_11	12.5	0.4			760.5	23.0		
Sud_M_15	7.3	0.2			714.3	21.6		
Sud_M_16	5.6	0.2			692.0	20.9		
Sud_M_21	7.4	0.2			715.1	21.6		
Sample: Morokweng	**$^{49}Ti_{mc}$ ppm**	**1σ**	**$^{49}Ti_{sc}$ ppm**		**Temp (mc) (°C)**	**1σ**	**Temp (sc) (°C)**	**1σ**
MK_157m_1			19.4	1.0			802.8	40.4

MK_157m_2			12.6	0.9			761.2	52.4
MK_157m_3			15.2	0.8			778.8	42.8
MK_157m_4			10.7	0.7			747.0	47.1
MK_157m_5			54.0	2.6			914.5	44.2
MK_157m_6			22.4	1.1			817.2	38.5
MK_157m_7			13.7	0.8			769.3	43.4
MK_157m_8			11.9	0.7			756.1	43.2
MK_157m_9			97.4	40.5			993.8	63.4
MK_157m_11			38.8	5.4			875.9	122.9
MK_157m_13			12.5	0.7			760.5	44.5
MK_157m_15			18.2	1.0			796.1	44.3
MK_157m_16			51.5	1.8			908.8	30.9
MK_157m_17			19.1	2.5			801.0	103.6
MK_157m_18			21.7	3.9			813.8	147.6
MK_157m_19			26.6	1.3			834.7	39.7
MK_157m_20			23.5	1.1			821.7	36.9
MK_157m_21			58.7	2.1			924.7	32.7
MK_157m_22			15.6	0.8			781.3	41.0
MK_157m_23			20.7	1.3			809.3	49.6
MK_157m_24			46.4	2.0			896.5	39.3
MK_157m_25			12.8	1.1			763.3	66.9
MK_157m_26			12.5	0.7			760.7	44.9
MK_157m_27			41.4	1.6			883.2	34.6
MK_157m_28			9.3	0.6			734.9	46.5
MK_157m_29			16.7	0.9			787.7	41.3
MK_157m_30			15.7	0.8			782.1	42.3
MK_157m_31			12.2	0.7			758.4	45.6
MK_157m_32			7.9	1.1			720.6	98.1
MK_157m_33			23.1	1.1			820.0	38.8
MK_157m_34			15.1	0.8			778.6	43.0

MK_399m_1	14.3	1.5			773.0	82.9		
MK_399m_3	4.1	0.4			668.0	71.6		
MK_399m_4	9.1	1.0			732.5	78.5		
MK_399m_5	16.0	1.7			783.9	84.1		
MK_399m_7			16.9	0.6			789.1	28.9
MK_399m_8			28.4	0.8			841.7	25.0
MK_399m_10			26.2	0.8			833.3	25.4
MK_399m_11			6.8	0.4			708.4	39.9
MK_399m_12			10.9	0.5			748.2	33.8
MK_399m_13	12.1	1.3			758.1	81.3		
MK_399m_14			26.2	0.8			833.3	24.5
MK_399m_16	5.3	0.6			687.2	73.7		
MK_399m_18			15.5	0.6			780.8	30.1
MK_399m_19	9.0	1.0			731.8	78.5		
MK_399m_20			12.7	0.5			762.6	32.0
MK_399m_22			11.3	0.7			751.3	44.6
MK_399m_23			41.3	1.5			883.1	32.6
MK_399m_25	9.2	1.0			733.7	78.7		
MK_399m_26	8.2	0.9			723.7	77.6		
Sample: Manicouagan	**$^{49}Ti_{mc}$ ppm**	**1σ**	**$^{49}Ti_{sc}$ ppm**		**Temp (mc) (°C)**	**1σ**	**Temp (sc) (°C)**	**1σ**
MC_MM_1	11.6	0.3	13.4	1.5	753.8	18.7	767.2	86.5
MC_MM_2	37.3	0.9	36.3	1.4	871.4	21.6	868.3	34.7
MC_MM_3	10.8	0.3	11.0	0.7	747.8	18.6	748.9	46.4
MC_MM_4	12.8	0.3	18.1	0.9	763.0	18.9	795.8	39.7
MC_MM_5	10.3	0.3	10.6	0.7	743.8	18.5	745.7	46.1
MC_MM_6	8.3	0.2	12.8	0.9	725.1	18.0	762.9	52.8
MC_MM_8	6.3	0.2	9.1	1.4	701.9	17.4	732.7	113.3
MC_MM_9	14.5	0.4	19.2	7.3	774.7	19.2	801.3	306.2

MC_MM_10	5.5	0.1	7.7	0.9	691.4	17.2	718.9	84.7
MC_MM_11	12.0	0.3	13.0	1.1	757.5	18.8	764.2	63.5
MC_MM_12	13.4	0.3	12.7	1.5	767.1	19.0	761.9	87.4
MC_MM_13	7.8	0.2	8.9	1.2	719.1	17.8	730.8	100.7
MC_MM_14	9.9	0.2	21.2	3.0	739.6	18.4	811.6	113.7
MC_MM_16	15.7	0.4	11.8	6.0	782.4	19.4	755.3	384.5
MC_MM_18	15.8	0.4	18.1	2.8	782.9	19.4	795.9	124.0
MC_MM_20	8.2	0.2	10.7	2.7	723.3	18.0	746.7	186.7
MC_MM_21	14.9	0.4	12.6	7.2	777.1	19.3	761.8	435.7
MC_MM_22	10.3	0.3	11.7	5.3	743.8	18.5	755.0	342.2
MC_MM_23	14.8	0.4	39.4	6.6	776.5	19.3	877.7	148.0
MC_MM_24	7.9	0.2	6.5	0.6	720.2	17.9	704.3	69.9
MC_MM_26	7.3	0.2	10.7	6.1	713.9	17.7	746.9	422.7
MC_MM_27	14.0	0.3	13.3	4.6	771.6	19.1	766.3	264.8
MC_MM_28	9.2	0.2	22.4	1.5	733.2	18.2	817.1	56.3
MC_MM_29	8.0	0.2			721.9	17.9		
MC_MM_30	7.9	0.2	8.1	4.8	720.2	17.9	722.6	429.5
MC_MM_31	6.7	0.2	8.6	3.1	706.3	17.5	728.0	264.3
MC_MM_32	19.5	0.5	34.9	6.8	803.3	19.9	863.9	169.1
MC_MM_33	13.9	0.3			770.3	19.1		
MC_MM_34	8.8	0.2	6.4	2.5	729.7	18.1	703.4	269.4
MC_MM_35	10.0	0.2	9.7	2.4	740.5	18.4	738.1	181.7
MC_MM_36	10.2	0.3	9.3	2.6	742.1	18.4	734.1	203.1
MC_MM_37	7.1	0.2	6.4	1.1	712.1	17.7	702.9	116.7

VD - Vredefort impact: INL are grains from drill core of Kamo et al. (1996).

Sud - Sudbury impact: F are grains from the felsic portion of the norite, M are grains from the mafic portion of the norite.

MK - Morokweng impact: 157 & 399 m denotes from which part of drill core M3 the grains were extracted.

MC - Manicouagan impact: MM are from the main melt sheet.

Note: MC - multi-collection, SC - single-collection.

Ti-in-zircon crystallization temperature calculated according to Watson & Harrison (2005).

7.4 Appendix 4

Table 7.4.1 - SIMS $\delta^{18}O$ data table for all zircon extracted from terrestrial impactites.

Standard name	^{16}O cps	^{18}O cps	$^{18}O/^{16}O$	$^{18}O/^{16}O$ 1 s.e.	$\delta^{18}O$	$\delta^{18}O$ 1 s.e.	$\delta^{18}O$ correction		#
Sud_AS3@2.ais	2.24E+09	4.48E+06	2.0037E-03	1.67E-07	1.87E+00	8.33E-02	-3.47		2
Sud_AS3@3.ais	2.21E+09	4.43E+06	2.0036E-03	1.67E-07	1.80E+00	8.35E-02	-3.54		3
Sud_AS3@4.ais	2.22E+09	4.45E+06	2.0032E-03	1.35E-07	1.59E+00	6.73E-02	-3.75		4
Sud_AS3@6.ais	2.28E+09	4.56E+06	2.0043E-03	2.00E-07	2.13E+00	1.00E-01	-3.21		6
Sud_AS3@7.ais	2.29E+09	4.58E+06	2.0041E-03	2.69E-07	2.07E+00	1.34E-01	-3.27		7
Sud_AS3@8.ais	2.27E+09	4.56E+06	2.0046E-03	9.62E-08	2.32E+00	4.81E-02	-3.02		13
Sud_AS3@9.ais	2.28E+09	4.57E+06	2.0043E-03	1.73E-07	2.16E+00	8.64E-02	-3.18		14
Sud_AS3@10.ais	2.28E+09	4.57E+06	2.0053E-03	1.31E-07	2.66E+00	6.57E-02	-2.68		20
Sud_AS3@11.ais	2.25E+09	4.52E+06	2.0051E-03	1.68E-07	2.57E+00	8.38E-02	-2.77		21
Sud_AS3@12.ais	2.26E+09	4.54E+06	2.0037E-03	2.31E-07	1.87E+00	1.15E-01	-3.47		28
Sud_AS3@13.ais	2.27E+09	4.56E+06	2.0050E-03	1.17E-07	2.48E+00	5.83E-02	-2.86		29
Sud_AS3@14.ais	2.28E+09	4.57E+06	2.0040E-03	1.85E-07	1.99E+00	9.25E-02	-3.35		35
Sud_AS3@15.ais	2.26E+09	4.52E+06	2.0046E-03	1.51E-07	2.28E+00	7.53E-02	-3.06		36
Sud_AS3@16.ais	2.26E+09	4.54E+06	2.0045E-03	1.31E-07	2.25E+00	6.56E-02	-3.09		42

Sud_AS3@17.ais	2.26E+09	4.53E+06	2.0051E-03	9.80E-08	2.57E+00	4.90E-02	-2.77		43
Sud_AS3@18.ais	2.29E+09	4.59E+06	2.0050E-03	1.71E-07	2.52E+00	8.54E-02	-2.82		48
Sud_AS3@19.ais	2.29E+09	4.58E+06	2.0053E-03	1.58E-07	2.63E+00	7.91E-02	-2.71		49
Sud_AS3@20.ais	2.30E+09	4.61E+06	2.0059E-03	1.84E-07	2.96E+00	9.20E-02	-2.38		50
Sud_AS3@21.ais	2.20E+09	4.42E+06	2.0043E-03	2.54E-07	2.15E+00	1.27E-01	-3.19		51
Sud_AS3@22.ais	2.25E+09	4.50E+06	2.0046E-03	1.47E-07	2.30E+00	7.34E-02	-3.04		52
MC_AS3@1.ais	2.22E+09	4.45E+06	2.0059E-03	2.90E-07	2.94E+00	1.45E-01	-2.40		53
MC_AS3@2.ais	2.23E+09	4.48E+06	2.0057E-03	1.50E-07	2.84E+00	7.52E-02	-2.50		54
MC_AS3@3.ais	2.23E+09	4.47E+06	2.0064E-03	1.37E-07	3.20E+00	6.84E-02	-2.14		55
MC_AS3@4.ais	2.19E+09	4.38E+06	2.0056E-03	2.75E-07	2.79E+00	1.38E-01	-2.55		56
MC_AS3@5.ais	2.18E+09	4.37E+06	2.0053E-03	2.01E-07	2.63E+00	1.00E-01	-2.71		62
MC_AS3@6.ais	2.19E+09	4.40E+06	2.0063E-03	1.71E-07	3.17E+00	8.57E-02	-2.17		63
MC_AS3@7.ais	2.21E+09	4.43E+06	2.0064E-03	1.59E-07	3.22E+00	7.97E-02	-2.12		69
MC_AS3@8.ais	2.19E+09	4.40E+06	2.0060E-03	1.36E-07	3.01E+00	6.78E-02	-2.33		70
MC_AS3@9.ais	2.19E+09	4.40E+06	2.0066E-03	1.89E-07	3.31E+00	9.43E-02	-2.03		77
MC_AS3@10.ais	2.20E+09	4.41E+06	2.0070E-03	2.16E-07	3.49E+00	1.08E-01	-1.85		78
MC_AS3@11.ais	2.19E+09	4.40E+06	2.0063E-03	1.76E-07	3.17E+00	8.80E-02	-2.17		84
MC_AS3@12.ais	2.19E+09	4.39E+06	2.0073E-03	2.04E-07	3.67E+00	1.02E-01	-1.67		85
MC_AS3@13.ais	2.19E+09	4.40E+06	2.0073E-03	9.22E-08	3.67E+00	4.61E-02	-1.67		91
MC_AS3@14.ais	2.20E+09	4.42E+06	2.0069E-03	2.40E-07	3.44E+00	1.20E-01	-1.90		92

MC_AS3@15.ais	2.20E+09	4.41E+06	2.0071E-03	3.35E-07	3.57E+00	1.68E-01	-1.77		98
MC_AS3@16.ais	2.18E+09	4.38E+06	2.0066E-03	1.27E-07	3.29E+00	6.35E-02	-2.05		99
MC_AS3@17.ais	2.21E+09	4.43E+06	2.0062E-03	1.96E-07	3.10E+00	9.78E-02	-2.24		107
MC_AS3@18.ais	2.19E+09	4.40E+06	2.0067E-03	1.62E-07	3.37E+00	8.10E-02	-1.97		108
MC_AS3@19.ais	2.20E+09	4.41E+06	2.0065E-03	1.39E-07	3.26E+00	6.94E-02	-2.08		109
MC_AS3@20.ais	2.20E+09	4.41E+06	2.0063E-03	1.40E-07	3.15E+00	6.99E-02	-2.19		110
MC_AS3@21.ais	2.19E+09	4.40E+06	2.0065E-03	1.76E-07	3.23E+00	8.79E-02	-2.11		111
MK_157_AS3@1.ais	2.25E+09	4.52E+06	2.0045E-03	1.85E-07	2.25E+00	9.26E-02	-3.09		112
MK_157_AS3@2.ais	2.22E+09	4.45E+06	2.0044E-03	1.20E-07	2.20E+00	5.99E-02	-3.14		113
MK_157_AS3@3.ais	2.27E+09	4.54E+06	2.0042E-03	1.68E-07	2.08E+00	8.41E-02	-3.26		114
MK_157_AS3@4.ais	2.25E+09	4.51E+06	2.0048E-03	1.02E-07	2.39E+00	5.11E-02	-2.95		115
MK_157_AS3@5.ais	2.25E+09	4.51E+06	2.0040E-03	1.61E-07	2.02E+00	8.07E-02	-3.32		121
MK_157_AS3@6.ais	2.23E+09	4.48E+06	2.0045E-03	1.15E-07	2.25E+00	5.74E-02	-3.09		122
MK_157_AS3@7.ais	2.23E+09	4.47E+06	2.0049E-03	2.29E-07	2.46E+00	1.15E-01	-2.88		128
MK_157_AS3@8.ais	2.23E+09	4.47E+06	2.0046E-03	1.15E-07	2.30E+00	5.76E-02	-3.04		129
MK_157_AS3@9.ais	2.23E+09	4.47E+06	2.0043E-03	1.53E-07	2.17E+00	7.66E-02	-3.17		135
MK_157_AS3@10.ais	2.23E+09	4.47E+06	2.0050E-03	1.33E-07	2.49E+00	6.64E-02	-2.85		136
MK_157_AS3@11.ais	2.23E+09	4.48E+06	2.0040E-03	1.14E-07	2.02E+00	5.70E-02	-3.32		142
MK_157_AS3@12.ais	2.22E+09	4.45E+06	2.0051E-03	2.34E-07	2.54E+00	1.17E-01	-2.80		143
MK_157_AS3@13.ais	2.25E+09	4.52E+06	2.0058E-03	1.37E-07	2.91E+00	6.84E-02	-2.43		149

MK_157_AS3@14.ais	2.23E+09	4.48E+06	2.0056E-03	1.72E-07	2.78E+00	8.62E-02	-2.56		150
MK_157_AS3@15.ais	2.22E+09	4.45E+06	2.0035E-03	1.50E-07	1.77E+00	7.48E-02	-3.57		156
MK_157_AS3@16.ais	2.20E+09	4.42E+06	2.0048E-03	1.70E-07	2.42E+00	8.52E-02	-2.92		157
MK_157_AS3@17.ais	2.23E+09	4.48E+06	2.0052E-03	1.02E-07	2.59E+00	5.10E-02	-2.75		162
MK_157_AS3@18.ais	2.23E+09	4.47E+06	2.0045E-03	1.24E-07	2.25E+00	6.20E-02	-3.09		163
MK_157_AS3@19.ais	2.24E+09	4.50E+06	2.0045E-03	1.42E-07	2.25E+00	7.10E-02	-3.09		164
MK_157_AS3@20.ais	2.22E+09	4.44E+06	2.0038E-03	2.57E-07	1.92E+00	1.29E-01	-3.42		165
MK_399_AS3@1.ais	2.20E+09	4.41E+06	2.0059E-03	1.63E-07	2.95E+00	8.16E-02	-2.39		166
MK_399_AS3@2.ais	2.21E+09	4.43E+06	2.0058E-03	1.25E-07	2.92E+00	6.23E-02	-2.42		167
MK_399_AS3@3.ais	2.22E+09	4.44E+06	2.0058E-03	2.53E-07	2.91E+00	1.26E-01	-2.43		168
MK_399_AS3@4.ais	2.19E+09	4.39E+06	2.0060E-03	1.63E-07	2.98E+00	8.13E-02	-2.36		169
MK_399_AS3@5.ais	2.21E+09	4.43E+06	2.0058E-03	1.57E-07	2.92E+00	7.83E-02	-2.42		175
MK_399_AS3@6.ais	2.20E+09	4.41E+06	2.0065E-03	2.06E-07	3.26E+00	1.03E-01	-2.08		176
MK_399_AS3@7.ais	2.16E+09	4.34E+06	2.0063E-03	1.41E-07	3.14E+00	7.04E-02	-2.20		182
MK_399_AS3@8.ais	2.15E+09	4.31E+06	2.0054E-03	1.25E-07	2.69E+00	6.23E-02	-2.65		183
MK_399_AS3@9.ais	2.18E+09	4.37E+06	2.0062E-03	1.34E-07	3.12E+00	6.69E-02	-2.22		189
MK_399_AS3@10.ais	2.19E+09	4.39E+06	2.0052E-03	1.71E-07	2.61E+00	8.56E-02	-2.73		190
MK_399_AS3@11.ais	2.15E+09	4.31E+06	2.0062E-03	1.69E-07	3.11E+00	8.43E-02	-2.23		196
MK_399_AS3@12.ais	2.15E+09	4.31E+06	2.0067E-03	1.77E-07	3.36E+00	8.84E-02	-1.98		197
MK_399_AS3@13.ais	2.14E+09	4.29E+06	2.0052E-03	1.62E-07	2.60E+00	8.11E-02	-2.74		204

MK_399_AS3@14.ais	2.13E+09	4.28E+06	2.0061E-03	1.80E-07	3.07E+00	8.99E-02	-2.27		205
MK_399_AS3@15.ais	2.15E+09	4.30E+06	2.0053E-03	1.75E-07	2.67E+00	8.73E-02	-2.67		206
MK_399_AS3@16.ais	2.15E+09	4.32E+06	2.0056E-03	1.60E-07	2.78E+00	8.01E-02	-2.56		207
VD_INL_AS3@1.ais	2.11E+09	4.23E+06	2.0047E-03	2.01E-07	2.33E+00	1.01E-01	-3.01		208
VD_INL_AS3@1.ais	2.11E+09	4.23E+06	2.0047E-03	2.01E-07	2.33E+00	1.01E-01	-3.01		209
VD_INL_AS3@2.ais	2.12E+09	4.25E+06	2.0044E-03	2.45E-07	2.20E+00	1.22E-01	-3.14		210
VD_INL_AS3@3.ais	2.11E+09	4.22E+06	2.0041E-03	2.12E-07	2.07E+00	1.06E-01	-3.27		211
VD_INL_AS3@4.ais	2.15E+09	4.32E+06	2.0056E-03	1.97E-07	2.79E+00	9.83E-02	-2.55		217
VD_INL_AS3@5.ais	2.16E+09	4.32E+06	2.0043E-03	1.88E-07	2.15E+00	9.40E-02	-3.19		218
VD_INL_AS3@6.ais	2.13E+09	4.28E+06	2.0038E-03	1.43E-07	1.92E+00	7.13E-02	-3.42		219

Unknown name	**^{16}O cps**	**^{18}O cps**	**$^{18}O/^{16}O$**	**$^{18}O/^{16}O$ 1 s.e.**	**$\delta^{18}O$**	**$\delta^{18}O$ 1 s.e.**	**$\delta^{18}O$ corrected**	**1 s.e.**	**Analysis #**
Sud_1@1.ais	2.27E+09	4.56E+06	2.0052E-03	1.11E-07	2.59E+00	5.57E-02	5.29	0.208	8
Sud_1@2.ais	2.30E+09	4.60E+06	2.0054E-03	1.26E-07	2.68E+00	6.29E-02	5.38	0.210	9
Sud_1@3.ais	2.29E+09	4.60E+06	2.0055E-03	9.92E-08	2.76E+00	4.96E-02	5.46	0.206	10
Sud_1@4.ais	2.32E+09	4.66E+06	2.0040E-03	1.13E-07	2.00E+00	5.63E-02	4.70	0.208	11
Sud_1@5.ais	2.29E+09	4.59E+06	2.0060E-03	1.63E-07	3.00E+00	8.13E-02	5.70	0.216	12
Sud_1@6.ais	2.27E+09	4.55E+06	2.0062E-03	1.36E-07	3.11E+00	6.81E-02	5.81	0.211	15
Sud_1@7.ais	2.30E+09	4.62E+06	2.0062E-03	2.31E-07	3.12E+00	1.16E-01	5.82	0.231	16
Sud_1@8.ais	2.28E+09	4.58E+06	2.0055E-03	2.14E-07	2.77E+00	1.07E-01	5.47	0.227	17
Sud_1@9.ais	2.30E+09	4.62E+06	2.0064E-03	1.73E-07	3.21E+00	8.65E-02	5.91	0.218	18

Sud_1@10.ais	2.40E+09	4.81E+06	2.0057E-03	1.39E-07	2.83E+00	6.94E-02	5.53	0.212	19
Sud_1@11.ais	2.28E+09	4.58E+06	2.0054E-03	1.97E-07	2.70E+00	9.86E-02	5.40	0.223	22
Sud_1@15.ais	2.28E+09	4.57E+06	2.0060E-03	1.54E-07	3.02E+00	7.70E-02	5.73	0.214	23
Sud_1@16.ais	2.28E+09	4.58E+06	2.0060E-03	2.36E-07	3.02E+00	1.18E-01	5.72	0.232	24
Sud_1(crater)@18.ais	2.25E+09	4.51E+06	2.0069E-03	1.82E-07	3.45E+00	9.10E-02	6.15	0.220	25
Sud_1@19.ais	2.25E+09	4.50E+06	2.0050E-03	1.82E-07	2.48E+00	9.10E-02	5.18	0.220	26
Sud_1@21.ais	2.24E+09	4.50E+06	2.0056E-03	1.36E-07	2.82E+00	6.81E-02	5.52	0.211	27
Sud_1@22.ais	2.28E+09	4.57E+06	2.0057E-03	1.56E-07	2.83E+00	7.80E-02	5.53	0.215	30
Sud_2@1.ais	2.27E+09	4.55E+06	2.0057E-03	1.63E-07	2.87E+00	8.15E-02	5.57	0.216	31
Sud_2@2.ais	2.26E+09	4.53E+06	2.0059E-03	1.29E-07	2.96E+00	6.44E-02	5.66	0.210	32
Sud_2@3.ais	2.27E+09	4.55E+06	2.0028E-03	4.06E-07	1.41E+00	2.03E-01	4.11	0.285	33
Sud_2@4.ais	2.25E+09	4.52E+06	2.0082E-03	1.92E-07	4.11E+00	9.58E-02	6.81	0.222	34
Sud_2@7.ais	2.32E+09	4.67E+06	2.0094E-03	1.17E-07	4.69E+00	5.87E-02	7.39	0.208	37
Sud_2@8.ais	2.29E+09	4.60E+06	2.0050E-03	1.34E-07	2.49E+00	6.68E-02	5.19	0.211	38
Sud_2@9.ais	2.33E+09	4.67E+06	2.0070E-03	1.19E-07	3.49E+00	5.97E-02	6.20	0.209	39
Sud_2@10.ais	2.32E+09	4.66E+06	2.0051E-03	2.05E-07	2.57E+00	1.02E-01	5.27	0.225	40
Sud_2@12.ais	2.24E+09	4.50E+06	2.0059E-03	1.59E-07	2.96E+00	7.93E-02	5.66	0.215	41
Sud_2@14.ais	2.20E+09	4.42E+06	2.0046E-03	1.55E-07	2.29E+00	7.73E-02	4.99	0.214	44
Sud_2@16.ais	2.24E+09	4.49E+06	2.0052E-03	3.02E-07	2.61E+00	1.51E-01	5.32	0.251	45
Sud_2@18.ais	2.29E+09	4.60E+06	2.0062E-03	2.01E-07	3.09E+00	1.01E-01	5.79	0.224	46

Sud_2@25.ais	2.25E+09	4.51E+06	2.0044E-03	1.69E-07	2.19E+00	8.43E-02	4.89	0.217	47
Sud_2@26.ais	2.29E+09	4.59E+06	2.0032E-03	3.35E-07	1.59E+00	1.68E-01	4.30	0.261	57
MC@1.ais	2.19E+09	4.40E+06	2.0043E-03	1.38E-07	2.14E+00	6.90E-02	4.84	0.212	58
MC@2.ais	2.19E+09	4.38E+06	2.0054E-03	1.47E-07	2.69E+00	7.33E-02	5.39	0.213	59
MC@3.ais	2.20E+09	4.42E+06	2.0044E-03	1.66E-07	2.22E+00	8.31E-02	4.93	0.217	60
MC@4.ais	2.12E+09	4.25E+06	1.9996E-03	2.58E-07	-2.02E-01	1.29E-01	2.50	0.238	61
MC@5.ais	2.16E+09	4.33E+06	2.0032E-03	1.61E-07	1.58E+00	8.04E-02	4.28	0.216	64
MC@6.ais	2.16E+09	4.32E+06	1.9998E-03	1.48E-07	-1.20E-01	7.40E-02	2.58	0.213	65
MC@7.ais	2.26E+09	4.53E+06	2.0026E-03	1.69E-07	1.31E+00	8.47E-02	4.01	0.217	66
MC@8.ais	2.21E+09	4.43E+06	2.0043E-03	1.39E-07	2.15E+00	6.94E-02	4.85	0.212	67
MC@9.ais	2.20E+09	4.41E+06	2.0045E-03	2.01E-07	2.25E+00	1.01E-01	4.95	0.224	68
MC@10.ais	2.20E+09	4.40E+06	2.0041E-03	1.72E-07	2.04E+00	8.62E-02	4.74	0.218	71
MC@11.ais	2.20E+09	4.40E+06	2.0043E-03	1.35E-07	2.14E+00	6.75E-02	4.84	0.211	72
MC@12.ais	2.22E+09	4.44E+06	2.0048E-03	1.40E-07	2.41E+00	7.01E-02	5.11	0.212	73
MC@13.ais	2.19E+09	4.40E+06	2.0048E-03	2.33E-07	2.42E+00	1.17E-01	5.12	0.231	74
MC@14.ais	2.21E+09	4.44E+06	2.0041E-03	1.80E-07	2.03E+00	9.01E-02	4.73	0.219	75
MC@15.ais	2.21E+09	4.43E+06	2.0022E-03	1.97E-07	1.11E+00	9.84E-02	3.81	0.223	76
MC@16.ais	2.20E+09	4.42E+06	2.0052E-03	1.38E-07	2.58E+00	6.92E-02	5.28	0.212	79
MC@17.ais	2.21E+09	4.44E+06	2.0054E-03	9.05E-08	2.70E+00	4.53E-02	5.40	0.205	80
MC@18.ais	2.13E+09	4.26E+06	2.0030E-03	1.83E-07	1.48E+00	9.16E-02	4.18	0.220	81

MC@19.ais	2.18E+09	4.36E+06	2.0044E-03	1.41E-07	2.21E+00	7.03E-02	4.91	0.212	82
MC@20.ais	2.21E+09	4.43E+06	2.0052E-03	1.99E-07	2.62E+00	9.96E-02	5.32	0.223	83
MC@21.ais	2.21E+09	4.42E+06	2.0047E-03	1.40E-07	2.33E+00	6.98E-02	5.03	0.212	86
MC@22.ais	2.23E+09	4.46E+06	2.0045E-03	2.27E-07	2.25E+00	1.13E-01	4.95	0.230	87
MC@23.ais	2.21E+09	4.44E+06	2.0054E-03	1.66E-07	2.71E+00	8.28E-02	5.41	0.216	88
MC@24.ais	2.23E+09	4.46E+06	2.0059E-03	1.85E-07	2.94E+00	9.24E-02	5.64	0.220	89
MC@25.ais	2.21E+09	4.45E+06	2.0086E-03	1.19E-07	4.30E+00	5.95E-02	7.00	0.209	90
MC@26.ais	2.21E+09	4.44E+06	2.0052E-03	1.38E-07	2.61E+00	6.92E-02	5.31	0.212	93
MC@27.ais	2.23E+09	4.47E+06	2.0036E-03	1.85E-07	1.81E+00	9.24E-02	4.51	0.220	94
MC@28.ais	2.05E+09	4.11E+06	2.0028E-03	1.97E-07	1.42E+00	9.86E-02	4.12	0.223	95
MC@29.ais	2.15E+09	4.31E+06	2.0041E-03	1.81E-07	2.03E+00	9.04E-02	4.74	0.219	96
MC@30.ais	2.18E+09	4.36E+06	2.0032E-03	2.12E-07	1.60E+00	1.06E-01	4.30	0.226	97
MC@31.ais	2.19E+09	4.40E+06	2.0052E-03	2.19E-07	2.58E+00	1.10E-01	5.28	0.228	100
MC@32.ais	2.20E+09	4.40E+06	2.0036E-03	1.32E-07	1.78E+00	6.60E-02	4.48	0.211	101
MC@33.ais	2.20E+09	4.41E+06	2.0042E-03	2.36E-07	2.09E+00	1.18E-01	4.79	0.232	102
MC@34.ais	2.19E+09	4.38E+06	2.0046E-03	2.43E-07	2.31E+00	1.22E-01	5.01	0.234	103
MC@35.ais	2.14E+09	4.29E+06	2.0051E-03	2.38E-07	2.54E+00	1.19E-01	5.24	0.233	104
MC@36.ais	2.23E+09	4.46E+06	2.0045E-03	1.07E-07	2.23E+00	5.35E-02	4.93	0.207	105
MC@37.ais	2.20E+09	4.42E+06	2.0061E-03	2.33E-07	3.06E+00	1.16E-01	5.76	0.231	106
MK_157@17.ais	2.24E+09	4.47E+06	1.9951E-03	1.16E-07	-2.43E+00	5.78E-02	0.27	0.208	138

MK_157@21.ais	2.18E+09	4.35E+06	1.9961E-03	1.53E-07	-1.96E+00	7.63E-02	0.74	0.214	144
MK_157@10.ais	2.22E+09	4.43E+06	1.9971E-03	2.04E-07	-1.47E+00	1.02E-01	1.23	0.225	127
MK_157@13.ais	2.23E+09	4.45E+06	1.9974E-03	1.62E-07	-1.31E+00	8.11E-02	1.39	0.216	132
MK_157@16.ais	2.22E+09	4.43E+06	1.9982E-03	1.43E-07	-8.83E-01	7.13E-02	1.82	0.212	137
MK_157@30.ais	2.22E+09	4.43E+06	1.9989E-03	2.06E-07	-5.69E-01	1.03E-01	2.13	0.225	155
MK_157@24.ais	2.20E+09	4.39E+06	1.9990E-03	1.49E-07	-5.14E-01	7.45E-02	2.19	0.213	147
MK_157@1.ais	2.25E+09	4.51E+06	2.0004E-03	1.95E-07	1.92E-01	9.74E-02	2.89	0.222	116
MK_157@4.ais	2.26E+09	4.53E+06	2.0011E-03	2.00E-07	5.42E-01	9.98E-02	3.24	0.224	119
MK_157@27.ais	2.08E+09	4.16E+06	2.0013E-03	2.52E-07	6.41E-01	1.26E-01	3.34	0.237	152
MK_157@34.ais	2.05E+09	4.10E+06	2.0018E-03	2.02E-07	9.14E-01	1.01E-01	3.62	0.224	161
MK_157@5.ais	2.21E+09	4.43E+06	2.0028E-03	1.54E-07	1.40E+00	7.71E-02	4.11	0.214	120
MK_157@31.ais	2.22E+09	4.45E+06	2.0035E-03	1.49E-07	1.74E+00	7.44E-02	4.44	0.213	158
MK_157@11.ais	2.24E+09	4.48E+06	2.0037E-03	1.55E-07	1.85E+00	7.75E-02	4.55	0.214	130
MK_157@2.ais	2.25E+09	4.52E+06	2.0037E-03	1.32E-07	1.86E+00	6.60E-02	4.56	0.211	117
MK_157@15.ais	2.22E+09	4.44E+06	2.0038E-03	1.88E-07	1.90E+00	9.42E-02	4.60	0.221	134
MK_157@8.ais	2.24E+09	4.48E+06	2.0040E-03	1.30E-07	2.00E+00	6.51E-02	4.70	0.210	125
MK_157@6.ais	2.22E+09	4.45E+06	2.0042E-03	1.55E-07	2.08E+00	7.75E-02	4.78	0.215	123
MK_157@33.ais	2.22E+09	4.45E+06	2.0045E-03	1.57E-07	2.27E+00	7.83E-02	4.97	0.215	160
MK_157@7.ais	2.24E+09	4.49E+06	2.0046E-03	1.21E-07	2.32E+00	6.05E-02	5.02	0.209	124
MK_157@32.ais	2.21E+09	4.43E+06	2.0047E-03	1.40E-07	2.34E+00	7.01E-02	5.04	0.212	159

MK_157@9.ais	2.22E+09	4.46E+06	2.0049E-03	1.67E-07	2.45E+00	8.35E-02	5.15	0.217	126
MK_157@22.ais	2.21E+09	4.42E+06	2.0049E-03	1.90E-07	2.45E+00	9.49E-02	5.16	0.221	145
MK_157@29.ais	2.22E+09	4.46E+06	2.0049E-03	1.34E-07	2.47E+00	6.70E-02	5.17	0.211	154
MK_157@19.ais	2.21E+09	4.42E+06	2.0051E-03	1.50E-07	2.55E+00	7.49E-02	5.25	0.214	140
MK_157@23.ais	2.12E+09	4.25E+06	2.0055E-03	1.84E-07	2.75E+00	9.21E-02	5.45	0.220	146
MK_157@28.ais	2.22E+09	4.46E+06	2.0060E-03	1.38E-07	3.01E+00	6.92E-02	5.71	0.212	153
MK_157@25.ais	2.23E+09	4.48E+06	2.0061E-03	1.93E-07	3.04E+00	9.64E-02	5.74	0.222	148
MK_157@14.ais	2.20E+09	4.41E+06	2.0067E-03	1.93E-07	3.33E+00	9.63E-02	6.03	0.222	133
MK_157@20.ais	2.20E+09	4.41E+06	2.0068E-03	1.89E-07	3.38E+00	9.47E-02	6.08	0.221	141
MK_157@18.ais	2.22E+09	4.46E+06	2.0069E-03	9.85E-08	3.44E+00	4.92E-02	6.14	0.206	139
MK_157@26.ais	2.09E+09	4.19E+06	2.0069E-03	1.68E-07	3.46E+00	8.39E-02	6.16	0.217	151
MK_157@3.ais	2.25E+09	4.53E+06	2.0071E-03	2.17E-07	3.56E+00	1.09E-01	6.26	0.228	118
MK_157@12.ais	2.23E+09	4.48E+06	2.0079E-03	9.53E-08	3.95E+00	4.77E-02	6.65	0.206	131
MK_399@2.ais	2.21E+09	4.44E+06	2.0056E-03	8.66E-08	2.82E+00	4.33E-02	5.53	0.205	171
MK_399@3.ais	2.22E+09	4.46E+06	2.0061E-03	2.02E-07	3.06E+00	1.01E-01	5.76	0.224	172
MK_399@4.ais	2.21E+09	4.44E+06	2.0062E-03	2.08E-07	3.11E+00	1.04E-01	5.82	0.225	173
MK_399@5.ais	2.21E+09	4.43E+06	2.0061E-03	2.09E-07	3.06E+00	1.05E-01	5.76	0.226	174
MK_399@7.ais	2.21E+09	4.44E+06	2.0052E-03	2.03E-07	2.62E+00	1.01E-01	5.32	0.224	178
MK_399@8.ais	2.22E+09	4.44E+06	2.0055E-03	9.00E-08	2.76E+00	4.50E-02	5.46	0.205	179
MK_399@10.ais	2.18E+09	4.38E+06	2.0055E-03	1.95E-07	2.73E+00	9.74E-02	5.43	0.222	181

MK_399@11.ais	2.15E+09	4.32E+06	2.0062E-03	1.01E-07	3.12E+00	5.07E-02	5.83	0.206	184
MK_399@12.ais	2.16E+09	4.33E+06	2.0061E-03	2.17E-07	3.07E+00	1.08E-01	5.78	0.227	185
MK_399@13.ais	2.17E+09	4.36E+06	2.0066E-03	1.63E-07	3.32E+00	8.16E-02	6.02	0.216	186
MK_399@14.ais	2.18E+09	4.38E+06	2.0057E-03	2.21E-07	2.83E+00	1.11E-01	5.53	0.229	187
MK_399@15.ais	2.18E+09	4.38E+06	2.0066E-03	1.05E-07	3.32E+00	5.25E-02	6.02	0.207	188
MK_399@16.ais	2.16E+09	4.32E+06	2.0060E-03	2.06E-07	2.98E+00	1.03E-01	5.68	0.225	191
MK_399@17.ais	2.14E+09	4.30E+06	2.0066E-03	1.64E-07	3.31E+00	8.18E-02	6.01	0.216	192
MK_399@18.ais	2.15E+09	4.30E+06	2.0052E-03	2.25E-07	2.59E+00	1.12E-01	5.29	0.229	193
MK_399@20.ais	2.16E+09	4.33E+06	2.0061E-03	1.62E-07	3.04E+00	8.08E-02	5.74	0.216	195
MK_399@26.ais	2.12E+09	4.26E+06	2.0060E-03	1.59E-07	2.98E+00	7.97E-02	5.68	0.215	198
MK_399@21.ais	2.19E+09	4.40E+06	2.0046E-03	2.03E-07	2.28E+00	1.02E-01	4.98	0.224	199
MK_399@22.ais	2.15E+09	4.31E+06	2.0033E-03	1.65E-07	1.63E+00	8.23E-02	4.33	0.216	200
MK_399@23.ais	2.14E+09	4.28E+06	2.0049E-03	1.68E-07	2.45E+00	8.38E-02	5.15	0.217	201
MK_399@24.ais	2.20E+09	4.40E+06	2.0017E-03	1.86E-07	8.46E-01	9.29E-02	3.55	0.221	202
MK_399@25.ais	2.15E+09	4.31E+06	2.0063E-03	2.09E-07	3.14E+00	1.05E-01	5.84	0.226	203
VD_INL@3.ais	2.07E+09	4.16E+06	2.0055E-03	1.56E-07	2.76E+00	7.80E-02	5.47	0.215	214
VD_INL@16.ais	2.10E+09	4.22E+06	2.0051E-03	4.00E-07	2.54E+00	2.00E-01	5.24	0.283	215

VD - Vredefort impact: INL are grains from drill core of Kamo et al. (1996).

Sud - Sudbury impact: F are grains from the felsic portion of the norite, M are grains from the mafic portion of the norite.

MK - Morokweng impact: 157 & 399 m denotes from which part of drill core M3 the grains were extracted.

MC - Manicouagan impact: MM are from the main melt sheet.

Note: AS3=5.34 (Trail et al., 2007)

$\delta^{18}O = ((^{18}O/^{16}O)/2e\text{-}3\text{-}1)*1000$

Instrumental mass fractionation = -2.701

7.5 Appendix 5

Table 7.5.1 - Model results for zircon saturation in simulated LHB impact event on Archean terrestrial surface

SiO_2	TiO_2	Al_2O_3	CaO	K_2O	NA_2O	Zr	Rock Temp.	Impact ΔT	Final Temp.	'M'	Total Mol.	Solidus	Solidus @ 15% melt	Liquidus	% Melt	'M' adjusted	Final Zircon Temp
77.9	0.13	10.1	1.95	3.27	0.02	110	19	200	219	0.89	1.64	610	639	803		0.89	0
52.5	0.93	16.8	8.88	0.60	3.94	52	273	20	293	2.77	1.75	640	703	1061		2.77	0
50.7	0.66	13.1	3.67	0.38	1.36	46	196	100	296	1.30	1.54	617	653	858		1.30	0
42.1	0.70	15.9	7.17	0.16	1.23	30	55	50	105	2.23	1.63	631	685	987		2.23	0
53.5	0.77	14.1	8.37	0.40	3.05	66	565	50	615	2.85	1.74	641	705	1071		2.85	0
47.7	0.59	14.7	11.50	0.54	2.41	22	236	300	536	3.75	1.72	655	736	1194		3.75	0
51.6	0.46	5.9	10.89	1.39	0.70	41	507	20	527	7.95	1.81	720	878	1770		7.95	0
49.3	1.24	15.2	8.70	0.04	3.78	76	797	100	897	3.12	1.76	645	714	1108	45	1.44	851
46.9	0.50	11.6	9.97	0.06	3.86	20	79	100	179	4.62	1.70	668	765	1313		4.62	0
50.6	1.48	15.3	9.40	0.34	2.44	31	633	50	683	2.86	1.72	641	706	1073		2.86	0
50.1	1.08	14.6	1.02	0.63	1.78	110	660	20	680	0.69	1.54	607	633	775	43	0.31	680
76.1	0.38	14.6	1.01	2.14	3.60	289	307	50	357	0.96	1.77	612	642	812		0.96	0
50.5	0.39	4.7	13.54	0.26	0.41	26	489	400	889	11.46	1.76	774	996	2250		11.46	0
53.8	0.95	13.2	11.14	0.63	0.51	37	98	50	148	3.12	1.69	645	714	1108		3.12	0
49.7	1.19	7.6	13.28	0.18	1.90	66	533	100	633	7.56	1.74	714	864	1716		7.56	0
49.8	0.50	7.1	9.50	0.01	0.11	39	183	20	203	5.44	1.82	681	793	1426		5.44	0
53.2	0.58	15.2	7.05	0.11	5.34	37	771	1000	1771	2.88	1.79	641	706	1076	39	1.21	813
53.0	0.75	14.8	11.20	0.01	1.77	50	509	50	559	3.14	1.77	645	715	1111		3.14	0
57.6	1.02	12.0	7.34	1.49	3.29	127	265	20	285	3.12	1.76	645	714	1108		3.12	0

47.8	0.49	8.9	7.42	0.00	0.20	27	220	200	420	3.56	1.83	652	729	1169		3.56	0
83.4	0.19	8.4	0.50	0.66	3.55	301	249	50	299	1.10	1.72	614	646	831		1.10	0
50.7	2.26	12.7	7.29	0.46	3.16	197	454	20	474	2.97	1.69	643	710	1088		2.97	0
51.0	0.68	13.2	10.10	0.69	1.37	33	498	20	518	3.37	1.76	649	723	1142		3.37	0
48.4	1.49	14.7	10.71	0.09	2.11	89	615	50	665	3.33	1.71	648	722	1137		3.33	0
58.9	0.70	16.4	7.68	1.28	2.42	96	458	20	478	2.12	1.76	630	681	972		2.12	0
50.2	0.68	10.5	8.22	0.23	2.06	37	542	50	592	3.69	1.73	654	734	1185		3.69	0
50.6	0.62	11.4	10.10	0.08	2.30	38	261	50	311	4.15	1.79	661	749	1250		4.15	0
49.0	0.63	7.4	9.89	0.05	0.09	52	745	200	945	5.35	1.78	680	790	1413	25	1.57	861
52.1	1.94	14.0	6.97	0.38	3.70	131	212	20	232	2.76	1.75	639	702	1058		2.76	0
83.7	0.14	8.9	0.52	5.95	0.28	183	611	200	811	1.09	1.72	614	646	831	91	0.95	811
64.7	0.42	15.2	2.82	1.52	5.73	260	60	20	80	1.72	1.74	623	667	916		1.72	0
53.4	0.35	19.0	9.57	0.14	2.71	20	54	50	104	2.28	1.75	632	686	994		2.28	0
49.7	1.43	12.9	6.21	1.22	2.97	152	693	50	743	2.74	1.67	639	702	1056	25	0.81	743
47.7	1.57	15.2	8.52	0.34	1.80	99	547	100	647	2.61	1.67	637	697	1038		2.61	0
63.2	0.71	17.3	2.83	2.86	3.10	150	121	50	171	1.29	1.75	617	653	857		1.29	0
51.0	0.90	15.0	10.00	0.10	2.70	48	390	20	410	3.07	1.72	644	713	1101		3.07	0
46.8	0.33	3.4	5.67	0.08	0.12	27	748	50	798	7.51	1.89	713	862	1709		7.51	0
48.7	0.97	14.9	11.30	0.20	1.50	61	59	50	109	3.37	1.75	649	723	1142		3.37	0
45.4	0.99	16.9	8.37	0.16	2.10	52	787	700	1487	2.51	1.69	635	694	1024	49	1.25	824
49.2	1.01	14.0	11.30	0.48	1.28	90	427	50	477	3.46	1.71	650	726	1155		3.46	0
47.4	0.54	12.6	9.10	0.17	0.87	22	733	20	753	2.90	1.59	642	707	1078	26	0.87	753
56.0	1.03	16.9	6.47	1.90	2.60	134	707	20	727	1.96	1.71	627	675	949	31	1.15	727
55.2	0.90	14.4	7.08	2.64	2.40	147	561	50	611	2.57	1.73	636	696	1032		2.57	0
80.4	0.31	8.3	0.18	1.48	0.82	101	119	50	169	0.49	1.66	604	626	747		0.49	0
49.0	1.13	14.7	8.71	3.80	0.54	60	47	50	97	3.01	1.73	643	711	1094		3.01	0
52.9	0.93	13.4	8.24	0.06	5.39	82	402	50	452	3.54	1.75	652	729	1166		3.54	0
43.3	1.22	16.0	8.80	0.62	2.12	83	540	50	590	2.59	1.48	637	697	1035		2.59	0
54.5	0.59	13.2	5.84	1.53	2.11	75	599	50	649	2.27	1.73	632	686	991		2.27	0
63.8	0.41	17.9	8.60	1.80	0.60	135	699	100	799	1.71	1.75	623	667	915	60	1.23	799
54.0	0.31	17.5	11.30	0.17	1.36	21	175	50	225	2.55	1.74	636	695	1030		2.55	0
49.5	0.93	14.7	10.46	0.15	2.75	50	713	50	763	3.38	1.73	649	723	1144	23	0.94	763
77.5	0.27	12.6	0.06	3.87	0.09	390	722	50	772	0.47	1.72	604	625	745	100	0.43	745
48.5	1.15	17.3	7.04	0.26	1.93	65	657	50	707	1.93	1.66	627	674	945	25	0.57	707
50.3	0.27	6.4	10.23	0.02	0.30	13	620	100	720	6.65	1.85	700	833	1591		6.65	0
64.8	0.61	16.0	2.92	2.48	3.54	158	400	50	450	1.42	1.77	619	657	875		1.42	0
46.8	1.63	18.4	1.15	7.98	0.37	101	538	50	588	1.31	1.65	617	653	860		1.31	0

55.0	0.91	13.6	5.67	0.56	3.25	175	590	100	690	2.11	1.61	629	680	969	18	1.11	690
48.3	0.65	6.0	10.40	0.07	1.55	45	609	50	659	7.88	1.76	719	875	1760		7.88	0
48.5	0.11	6.5	0.56	0.09	0.03	9	7	20	27	0.44	1.95	603	624	740		0.44	0
51.1	1.42	15.2	6.91	0.51	3.91	88	245	700	945	2.68	1.77	638	700	1048	52	1.42	852
55.5	0.62	14.7	10.26	0.19	3.38	192	126	100	226	3.11	1.73	645	714	1106		3.11	0
67.4	0.28	15.8	3.43	1.42	4.08	77	485	300	785	1.39	1.71	618	656	872	66	1.04	785
56.2	1.67	13.9	6.29	0.08	2.12	148	456	100	556	1.98	1.71	627	676	951		1.98	0
46.9	0.48	19.7	10.70	0.53	2.57	7	128	50	178	2.81	1.78	640	704	1065		2.81	0
51.7	0.80	13.8	8.58	0.14	4.39	37	605	20	625	3.37	1.74	649	723	1143		3.37	0
56.7	1.40	17.9	8.50	0.60	3.70	129	284	20	304	2.31	1.75	632	687	996		2.31	0
81.9	0.43	11.3	0.19	3.32	0.52	307	458	50	508	0.53	1.70	605	627	753		0.53	0
49.5	0.89	13.7	6.46	1.86	0.42	52	736	20	756	2.19	1.71	631	683	981	36	0.85	756
60.4	0.69	17.6	3.03	1.71	5.35	164	81	50	131	1.63	1.78	622	664	904		1.63	0
66.0	0.70	15.2	3.19	1.60	5.33	154	757	100	857	1.71	1.75	623	667	914	80	1.39	857
50.7	1.13	13.2	5.70	3.30	2.90	382	104	50	154	2.74	1.63	639	702	1056		2.74	0
50.9	0.90	14.5	10.43	0.10	2.64	47	139	200	339	3.27	1.72	647	720	1129		3.27	0
47.3	0.60	10.7	5.68	3.67	2.50	84	195	50	245	3.63	1.66	653	732	1177		3.63	0
74.9	0.47	9.6	2.36	2.13	0.44	173	248	50	298	1.05	1.72	613	645	825		1.05	0
68.5	0.39	16.1	3.13	3.52	0.54	244	244	50	294	0.95	1.68	611	641	811		0.95	0
50.1	0.81	12.1	11.10	0.11	2.45	22	598	100	698	4.16	1.73	661	750	1251		4.16	0
38.4	1.55	12.8	14.23	0.08	0.42	70	389	50	439	5.39	1.65	680	791	1418		5.39	0
49.5	0.34	18.9	9.87	0.26	1.47	23	229	20	249	2.32	1.75	633	688	999		2.32	0
47.4	0.26	5.5	5.74	0.02	0.12	14	398	100	498	4.64	1.90	669	766	1316		4.64	0
65.9	0.37	14.3	2.86	2.79	0.63	150	151	100	251	0.96	1.63	612	642	813		0.96	0
49.4	0.83	8.8	12.70	0.13	0.99	49	236	20	256	6.08	1.77	691	814	1514		6.08	0
72.7	0.22	15.1	1.88	3.51	4.33	115	705	50	755	1.40	1.79	618	657	873	54	0.97	755
41.1	2.21	11.0	7.71	0.05	3.47	42	271	50	321	3.96	1.51	658	743	1223		3.96	0
46.1	0.85	13.7	11.70	0.08	2.29	30	207	20	227	4.01	1.68	659	744	1230		4.01	0
53.5	1.08	14.1	6.91	0.66	3.68	164	550	100	650	2.64	1.71	638	698	1043		2.64	0
71.0	0.75	16.2	1.37	2.19	5.65	210	610	50	660	1.33	1.79	617	654	862	17	0.70	660
53.1	0.67	16.1	7.75	0.06	2.70	46	296	100	396	2.28	1.74	632	686	993		2.28	0
49.4	0.70	20.4	2.97	4.51	4.42	185	180	100	280	1.89	1.81	626	673	940		1.89	0
76.9	0.29	13.2	1.49	2.33	2.66	221	375	20	395	1.00	1.75	612	643	817		1.00	0
53.1	0.99	14.1	3.70	0.15	0.86	117	235	400	635	1.08	1.62	613	646	828		1.08	0
46.9	0.24	9.4	8.20	0.00	0.26	13	501	100	601	3.86	1.84	657	740	1210		3.86	0
47.8	2.20	8.2	11.40	0.10	2.70	120	747	200	947	6.61	1.71	699	832	1586	25	1.93	917
41.3	0.90	2.8	3.30	0.01	0.11	71	513	100	613	5.87	1.82	688	807	1485		5.87	0

60.7	0.37	20.0	1.40	3.43	1.79	110	591	50	641	0.78	1.70	609	635	787	18	0.41	641
48.4	0.65	16.3	10.26	0.42	1.59	57	229	1000	1229	2.90	1.75	642	707	1078	44	1.33	834
73.8	0.22	9.4	2.01	3.15	0.11	210	115	50	165	1.01	1.62	612	643	820		1.01	0
61.6	0.65	20.0	1.09	3.85	1.03	114	64	50	114	0.66	1.72	607	631	771		0.66	0
63.1	0.42	18.2	4.12	2.77	5.50	77	440	20	460	1.85	1.81	625	671	933		1.85	0
51.1	0.51	9.1	6.57	0.09	0.62	31	246	200	446	3.09	1.84	645	714	1105		3.09	0
68.5	0.50	15.6	2.59	1.52	4.90	125	479	400	879	1.44	1.78	619	658	878	89	1.23	850
50.3	0.64	18.4	10.81	0.55	2.80	68	484	200	684	2.85	1.76	641	705	1072		2.85	0
48.7	1.07	13.9	8.47	0.27	2.57	95	704	700	1404	3.10	1.76	645	714	1106	47	1.51	862
49.6	0.51	5.3	8.57	0.01	0.21	5	734	300	1034	6.34	1.75	695	823	1549	15	1.33	0
43.4	1.25	19.4	11.27	0.44	1.42	99	697	50	747	2.92	1.76	642	708	1081	24	0.84	747
46.7	11.87	1.4	10.71	0.09	3.13	97	323	50	373	37.69	1.64	1181	1881	5844		37.69	0
70.5	0.33	16.2	3.20	1.63	4.87	140	759	50	809	1.47	1.79	619	659	882	72	1.14	809
63.7	0.43	15.9	4.03	3.70	3.57	120	36	200	236	1.79	1.75	624	670	926		1.79	0
49.3	0.77	8.1	12.20	0.15	0.53	46	522	50	572	6.19	1.77	693	818	1528		6.19	0
49.9	0.60	13.3	9.12	0.03	2.97	41	567	20	587	3.35	1.72	649	722	1140		3.35	0
49.5	1.45	14.4	10.50	0.29	1.79	100	666	50	716	3.27	1.73	647	720	1129		3.27	0
49.9	0.69	12.4	9.99	0.33	1.88	15	582	50	632	3.67	1.75	653	733	1183		3.67	0
50.0	0.73	15.5	9.00	0.13	2.30	54	10	50	60	2.72	1.73	639	701	1054		2.72	0
45.2	0.54	12.7	10.50	0.38	1.64	30	765	500	1265	3.55	1.53	652	729	1167	31	1.24	813
64.5	0.53	14.8	3.19	2.53	4.19	141	727	1100	1827	1.70	1.75	623	666	913	81	1.39	858
49.2	0.96	13.9	8.97	0.27	2.82	57	357	50	407	3.23	1.73	647	718	1123		3.23	0
54.0	0.48	12.6	8.17	1.07	2.20	88	386	200	586	2.98	1.72	643	710	1090		2.98	0
52.6	0.49	9.6	8.06	0.00	2.22	30	723	700	1423	3.92	1.81	657	741	1218	29	1.28	818
56.0	1.03	16.9	6.47	1.90	2.60	134	650	1100	1750	1.96	1.71	627	675	949	71	1.51	855
63.6	0.45	16.9	4.44	2.36	4.20	139	359	20	379	1.73	1.77	623	668	918		1.73	0
49.4	1.71	13.8	9.06	1.09	2.69	153	573	100	673	3.39	1.74	649	723	1145		3.39	0
47.4	0.04	30.1	15.21	0.16	2.42	5	199	20	219	2.43	1.81	634	691	1013		2.43	0
55.4	0.85	14.7	3.04	0.13	1.42	106	144	1000	1144	0.98	1.66	612	642	814	100	0.89	814
65.8	0.45	13.6	2.66	2.82	3.24	95	557	50	607	1.48	1.67	620	659	884		1.48	0
50.4	0.57	13.5	8.93	0.05	2.66	50	653	20	673	3.12	1.72	645	715	1108		3.12	0
55.7	0.79	16.3	7.30	3.50	1.10	124	625	50	675	2.18	1.75	630	683	980		2.18	0
42.4	0.50	11.5	11.60	0.25	1.44	22	371	200	571	4.37	1.49	664	757	1279		4.37	0
41.3	0.64	3.8	4.51	0.02	0.10	39	99	50	149	5.49	1.72	682	794	1432		5.49	0
53.0	0.58	16.1	8.45	1.75	2.55	82	465	50	515	2.59	1.71	637	697	1036		2.59	0
47.1	0.43	8.8	8.75	0.09	0.78	27	120	50	170	4.60	1.82	668	764	1311		4.60	0
56.5	0.58	14.7	8.59	1.25	2.83	93	159	1100	1259	2.73	1.75	639	701	1054	47	1.80	835

52.7	0.76	8.0	10.54	0.08	1.90	60	518	100	618	5.64	1.77	684	799	1453		5.64	0
52.8	0.79	14.2	9.89	0.04	2.18	48	141	200	341	3.04	1.76	644	712	1097		3.04	0
49.1	1.00	9.4	11.05	0.57	1.97	66	510	100	610	5.41	1.73	680	792	1422		5.41	0
48.2	0.86	9.3	9.13	0.05	1.84	56	618	100	718	4.56	1.73	667	763	1305		4.56	0
49.1	0.34	10.5	11.70	0.36	0.90	41	664	100	764	4.72	1.75	670	768	1327		4.72	0
69.9	0.39	15.2	2.33	2.61	4.78	258	642	20	662	1.49	1.77	620	659	885	16	0.77	662
40.1	0.63	7.6	8.13	1.94	0.93	40	98	200	298	5.18	1.43	677	784	1390		5.18	0
49.9	1.15	13.9	12.00	0.30	3.72	67	788	50	838	4.26	1.74	663	753	1265	29	1.41	838
67.5	0.35	15.5	2.48	4.79	1.44	130	40	20	60	1.18	1.70	615	649	842		1.18	0
72.3	0.29	12.1	2.82	0.87	5.63	230	114	50	164	1.83	1.74	625	671	931		1.83	0
49.7	0.50	14.1	8.71	0.16	2.27	29	588	50	638	2.92	1.72	642	708	1080		2.92	0
47.6	0.48	7.6	4.79	2.63	0.30	63	306	20	326	3.62	1.81	653	731	1176		3.62	0
49.3	0.17	18.4	15.60	0.10	1.00	4	388	50	438	3.59	1.80	652	730	1173		3.59	0
54.7	1.43	15.8	5.77	0.02	4.49	89	535	1100	1635	2.22	1.78	631	684	985	61	1.34	846
42.0	0.45	9.9	6.49	0.01	0.16	23	323	20	343	2.98	1.70	643	710	1089		2.98	0
49.8	0.80	13.6	8.70	0.09	2.27	22	298	20	318	2.97	1.71	643	709	1088		2.97	0
54.5	0.22	4.7	3.48	0.29	0.05	47	521	20	541	2.48	1.56	635	693	1020		2.48	0
47.1	0.84	15.7	11.50	0.15	2.25	49	410	200	610	3.49	1.73	651	727	1159		3.49	0
48.3	1.26	15.3	10.50	0.10	3.00	74	294	100	394	3.42	1.74	650	725	1149		3.42	0
50.4	0.69	14.2	8.03	0.14	2.40	44	220	50	270	2.66	1.69	638	699	1045		2.66	0
48.6	0.71	15.5	11.80	0.11	1.96	45	774	700	1474	3.42	1.73	650	725	1149	36	1.34	830
56.3	1.03	15.8	6.46	0.47	3.99	230	754	20	774	2.23	1.75	631	684	985	40	1.40	774
50.0	1.64	17.3	9.57	1.19	3.23	132	794	100	894	2.92	1.75	642	708	1081	54	1.58	877
50.5	0.37	17.7	6.47	1.37	1.66	27	528	50	578	1.93	1.80	627	674	945		1.93	0
73.1	0.32	9.8	0.14	0.70	0.11	188	332	50	382	0.16	1.64	599	615	703		0.16	0
50.8	0.72	11.3	7.77	3.17	3.32	97	168	20	188	4.06	1.69	660	746	1237		4.06	0
40.3	0.07	1.6	0.12	0.02	0.15	4	711	50	761	0.78	1.74	609	635	787	43	0.35	685
46.5	0.92	14.3	11.11	0.94	3.12	54	418	20	438	4.15	1.74	661	749	1249		4.15	0
84.9	0.65	9.7	0.05	2.51	0.20	210	66	50	116	0.39	1.69	603	622	734		0.39	0
45.8	0.86	28.3	0.55	0.01	0.12	55	447	50	497	0.09	1.58	598	612	693		0.09	0
54.1	88.00	15.0	7.60	2.70	0.40	112	406	20	426	3.61	2.80	653	731	1175		3.61	0
45.7	0.78	16.7	8.32	0.13	2.55	44	608	100	708	2.66	1.73	638	699	1044	17	0.61	708
53.5	0.63	14.6	11.20	0.11	1.47	22	326	20	346	3.03	1.72	644	711	1095		3.03	0
64.9	0.44	14.4	4.20	2.15	2.94	148	222	50	272	1.58	1.66	621	662	897		1.58	0
66.6	0.31	15.2	3.17	2.18	5.58	68	556	20	576	1.81	1.76	625	670	928		1.81	0
50.7	1.83	13.2	9.68	0.01	1.62	166	709	50	759	3.07	1.68	644	713	1102	25	0.91	759
70.1	0.30	16.0	2.70	2.00	5.10	160	93	50	143	1.49	1.80	620	659	885		1.49	0

48.1	0.12	26.9	15.00	0.30	2.20	7	96	20	116	2.63	1.81	637	698	1041		2.63	0
48.4	3.10	11.2	8.32	0.76	2.02	178	160	200	360	3.51	1.64	651	727	1161		3.51	0
45.9	0.99	11.0	8.84	2.93	3.95	210	272	700	972	5.02	1.64	674	779	1369	37	1.99	930
58.7	0.95	15.5	4.01	0.64	4.38	120	121	50	171	1.71	1.71	623	667	915		1.71	0
49.6	0.61	12.9	7.80	0.09	4.10	22	328	200	528	3.45	1.75	650	725	1153		3.45	0
41.4	0.64	10.4	7.78	0.01	0.16	39	504	50	554	3.47	1.72	650	726	1156		3.47	0
73.9	0.35	12.5	2.64	1.24	4.00	183	464	20	484	1.44	1.74	619	658	878		1.44	0
57.6	0.48	15.2	14.50	0.10	0.73	28	160	200	360	3.31	1.74	648	721	1134		3.31	0
42.7	0.43	11.3	3.54	2.34	1.47	81	648	50	698	2.47	1.73	635	692	1018	16	0.55	698
51.5	0.73	12.7	9.03	0.26	3.17	30	455	100	555	3.52	1.75	651	728	1163		3.52	0
59.6	1.22	16.6	4.66	1.31	3.04	166	246	600	846	1.55	1.71	621	661	893	83	1.28	846
42.0	0.76	3.4	6.67	0.03	0.07	33	422	20	442	8.75	1.68	732	904	1879		8.75	0
50.1	0.27	19.8	6.55	0.28	1.51	17	555	200	755	1.60	1.80	621	663	900	48	0.79	755
47.3	0.72	13.1	12.10	0.10	1.51	100	98	50	148	4.11	1.72	660	748	1243		4.11	0
49.8	0.88	8.5	10.30	0.52	1.65	46	605	100	705	5.49	1.75	682	794	1432		5.49	0
49.7	0.29	7.9	8.65	0.03	0.27	17	19	100	119	4.56	1.84	667	763	1306		4.56	0
67.4	0.52	15.5	2.96	0.91	5.94	112	371	100	471	1.68	1.81	623	666	911		1.68	0
47.0	0.53	17.4	12.10	0.30	2.40	29	344	500	844	3.48	1.80	651	727	1157	32	1.23	811
49.6	0.72	9.6	12.32	0.48	0.81	7	332	400	732	5.39	1.75	680	791	1419		5.39	0
53.9	0.57	16.1	9.10	0.90	1.80	71	65	50	115	2.47	1.74	635	693	1019		2.47	0
55.5	1.25	14.4	7.97	1.44	3.84	158	757	100	857	2.97	1.77	643	710	1088	48	1.98	857
47.6	0.46	16.9	4.27	2.77	2.31	28	503	100	603	1.83	1.67	625	671	931		1.83	0
40.8	0.87	9.9	10.20	2.18	3.58	281	350	200	550	6.09	1.52	691	814	1514		6.09	0
56.1	0.90	17.2	2.06	2.15	2.12	120	637	100	737	1.01	1.69	612	643	819	60	0.73	737
48.7	0.85	14.4	9.37	0.25	2.86	30	569	50	619	3.23	1.71	647	718	1124		3.23	0
50.3	0.62	15.9	11.46	0.09	1.38	39	12	50	62	3.10	1.78	645	714	1106		3.10	0
76.4	0.42	12.2	0.63	3.87	3.32	347	659	20	679	1.23	1.77	616	651	850	27	0.70	679
51.4	0.86	14.7	10.10	0.18	2.30	66	258	20	278	3.13	1.76	645	715	1109		3.13	0
45.6	0.12	3.9	3.02	0.12	0.19	3	329	200	529	3.90	1.95	657	741	1215		3.90	0
56.0	0.69	17.4	6.77	0.00	4.63	99	312	20	332	2.22	1.80	631	684	985		2.22	0
51.3	0.46	15.6	9.31	0.83	3.51	42	76	50	126	3.19	1.80	646	717	1117		3.19	0
49.5	1.20	15.3	10.70	0.15	2.10	68	87	50	137	3.19	1.74	646	717	1117		3.19	0

Table 8.5.2 - Model results for zircon saturation in simulated LHB impact event on lunar surface.

SiO_2	TiO_2	Al_2O_3	CaO	K_2O	NA_2O	Zr	Rock Temp.	Impact ΔT	Final Temp.	M'	Total Mol.	Solidus	Solidus @ 15% melt	Liquidus	% Melt	M' adjusted	Final Zircon Temp
45.3	3.33	10.2	11.10	0.39	0.08	200	408	50	458	4.43	1.64	898	950	1249		4.43	0
48.1	1.70	17.4	10.79	0.58	0.70	150	13	50	63	2.70	1.76	877	931	1235		2.70	0
44.1	0.36	28.6	16.50	0.04	0.41	27	614	50	664	2.61	1.78	907	959	1255		2.61	0
44.0	2.79	9.0	9.02	0.05	0.27	150	-52	500	448	4.35	1.69	908	960	1255		4.35	0
44.7	0.23	29.5	17.35	0.03	0.30	30	399	50	449	2.61	1.78	902	955	1251		2.61	0
49.6	1.43	17.6	10.79	0.47	0.74	150	588	20	608	2.58	1.76	866	921	1227		2.58	0
44.7	0.15	31.2	17.63	0.02	0.10	280	192	200	392	2.48	1.78	902	955	1251		2.48	0
44.0	3.53	15.5	12.07	0.10	0.36	150	479	50	529	3.46	1.74	908	960	1255		3.46	0
44.6	3.79	11.8	10.46	0.13	0.34	150	110	400	510	3.79	1.68	903	956	1252		3.79	0
62.5	1.18	15.7	6.86	3.20	0.98	150	494	50	544	1.86	1.73	771	830	1162		1.86	0
44.9	0.23	28.5	16.79	0.04	0.30	49	256	500	756	2.59	1.77	901	953	1250		2.59	0
44.4	0.19	30.7	18.20	0.02	0.39	220	623	400	1023	2.66	1.79	904	957	1253	30	0.89	1008
45.0	0.34	25.3	14.80	0.04	0.37	65	170	50	220	2.58	1.78	900	953	1250		2.58	0
43.4	0.14	28.2	16.10	0.36	0.02	17	487	400	887	2.60	1.78	912	964	1258		2.60	0
44.5	0.27	28.1	16.50	0.09	0.41	995	349	100	449	2.63	1.78	904	956	1253		2.63	0
44.9	0.22	29.3	16.65	0.04	0.31	50	673	50	723	2.51	1.78	901	953	1250		2.51	0
43.7	0.17	27.6	16.80	0.34	0.01	38	-83	20	-63	2.69	1.75	910	962	1257		2.69	0
73.1	0.50	12.4	1.27	5.97	0.64	150	500	200	700	1.10	1.68	694	756	1109		1.10	0
53.4	2.08	15.6	9.57	1.11	1.01	150	294	50	344	2.52	1.72	839	894	1208		2.52	0
43.6	0.12	29.2	16.60	0.01	0.36	85	281	20	301	2.60	1.79	910	962	1257		2.60	0
37.6	12.04	8.5	8.81	0.13	0.54	150	-10	100	90	5.25	1.63	954	1004	1287		5.25	0
44.9	0.20	28.9	16.93	0.03	0.31	39	261	800	1061	2.59	1.79	901	953	1250	15	0.55	0
44.0	0.15	27.2	15.50	0.04	0.33	24	61	50	111	2.59	1.80	907	959	1255		2.59	0
44.9	0.22	28.9	16.79	0.04	0.32	46	-6	100	94	2.57	1.78	901	953	1250		2.57	0
44.0	3.53	15.5	12.07	0.10	0.36	150	410	200	610	3.46	1.74	908	960	1255		3.46	0
44.9	0.17	29.3	16.79	0.03	0.22	33	68	100	168	2.52	1.78	901	953	1250		2.52	0
37.6	12.04	8.5	8.81	0.13	0.54	150	409	50	459	5.25	1.63	954	1004	1287		5.25	0
43.7	0.17	27.6	16.80	0.34	0.01	38	-40	100	60	2.69	1.75	910	962	1257		2.69	0
43.4	0.14	28.2	16.10	0.36	0.02	17	244	900	1144	2.60	1.78	912	964	1258	15	0.55	0
44.3	0.25	28.0	16.37	0.07	0.35	35	567	50	617	2.64	1.79	905	958	1254		2.64	0
44.9	0.22	28.9	16.79	0.04	0.32	46	292	100	392	2.57	1.78	901	953	1250		2.57	0
43.0	0.14	27.0	19.87	0.08	0.32	25	95	50	145	3.39	1.78	915	966	1260		3.39	0
43.2	2.76	8.4	8.74	0.19	0.53	530	461	50	511	4.81	1.70	913	965	1259		4.81	0

46.2	3.07	13.7	10.55	0.27	0.48	150	413	50	463	3.32	1.73	891	944	1244		3.32	0
44.0	1.55	16.6	12.96	0.32	0.06	103	533	900	1433	3.32	1.68	907	959	1255	19	0.81	974
62.5	1.18	15.7	6.86	3.20	0.98	150	-36	50	14	1.86	1.73	771	830	1162		1.86	0
43.2	2.76	8.4	8.74	0.19	0.53	530	264	800	1064	4.81	1.70	913	965	1259	30	1.62	1016
42.5	7.67	13.8	12.12	0.15	0.44	150	689	50	739	4.02	1.71	919	970	1263		4.02	0
73.1	0.50	12.4	1.27	5.97	0.64	150	515	100	615	1.10	1.68	694	756	1109		1.10	0
44.9	0.20	29.1	16.79	0.03	0.32	33	61	50	111	2.55	1.79	901	953	1250		2.55	0
44.3	0.22	29.6	18.00	0.08	0.24	43	251	100	351	2.74	1.80	905	957	1254		2.74	0
45.3	3.33	10.2	11.10	0.39	0.08	200	417	200	617	4.43	1.64	898	950	1249		4.43	0
44.3	0.09	30.8	17.30	0.01	0.36	30	443	200	643	2.54	1.80	905	957	1254		2.54	0
46.5	0.75	13.0	11.20	0.36	0.05	112	496	50	546	3.46	1.67	889	942	1243		3.46	0
42.5	7.67	13.8	12.12	0.15	0.44	150	483	50	533	4.02	1.71	919	970	1263		4.02	0
44.9	0.23	28.5	16.79	0.04	0.30	49	-93	50	-43	2.59	1.77	901	953	1250		2.59	0
46.6	1.25	18.8	11.60	0.12	0.37	150	599	50	649	2.66	1.78	889	942	1242		2.66	0
45.1	0.56	27.2	15.79	0.11	0.47	150	464	50	514	2.62	1.80	899	952	1250		2.62	0
46.5	0.23	25.3	14.80	0.03	0.30	30	447	50	497	2.54	1.81	889	942	1243		2.54	0
44.0	1.55	16.6	12.96	0.32	0.06	103	715	20	735	3.32	1.68	907	959	1255	19	3.32	0
44.7	0.23	29.5	17.35	0.03	0.30	30	637	50	687	2.61	1.78	902	955	1251		2.61	0
39.9	9.42	11.0	10.62	0.08	0.35	150	-82	800	718	4.55	1.66	938	988	1276		4.55	0
45.2	0.24	28.3	16.90	0.34	0.03	170	-74	20	-54	2.60	1.78	899	951	1249		2.60	0
44.9	0.17	28.3	16.93	0.04	0.33	34	237	50	287	2.64	1.78	901	953	1250		2.64	0
44.0	1.55	16.6	12.96	0.32	0.06	103	746	100	846	3.32	1.68	907	959	1255	19	3.32	0
44.5	0.27	28.1	16.50	0.09	0.41	995	48	500	548	2.63	1.78	904	956	1253		2.63	0
53.4	2.08	15.6	9.57	1.11	1.01	150	616	200	816	2.52	1.72	839	894	1208		2.52	0
44.3	0.25	28.0	16.37	0.07	0.35	35	277	300	577	2.64	1.79	905	958	1254		2.64	0
44.3	0.09	30.8	17.30	0.01	0.36	30	-29	50	21	2.54	1.80	905	957	1254		2.54	0
47.9	0.97	13.2	11.60	0.42	0.06	141	68	100	168	3.48	1.69	879	932	1236		3.48	0
44.9	0.18	28.1	16.65	0.38	0.04	21	129	1100	1229	2.58	1.76	901	953	1250	15	0.55	0
44.0	0.15	29.7	16.90	0.01	0.34	25	9	50	59	2.58	1.79	907	959	1255		2.58	0
44.9	0.22	28.9	16.79	0.04	0.32	46	25	50	75	2.57	1.78	901	953	1250		2.57	0
44.7	0.23	29.5	17.35	0.03	0.30	30	650	20	670	2.61	1.78	902	955	1251		2.61	0
48.1	1.70	17.4	10.79	0.58	0.70	150	258	20	278	2.70	1.76	877	931	1235		2.70	0
46.2	0.68	20.6	13.50	0.51	0.19	132	-94	50	-44	2.83	1.76	891	944	1244		2.83	0
44.1	0.36	28.6	16.50	0.04	0.41	27	175	50	225	2.61	1.78	907	959	1255		2.61	0
44.9	0.22	28.9	16.79	0.04	0.32	46	720	50	770	2.57	1.78	901	953	1250		2.57	0
53.4	2.08	15.6	9.57	1.11	1.01	150	666	100	766	2.52	1.72	839	894	1208		2.52	0
45.2	0.24	28.3	16.90	0.34	0.03	170	282	100	382	2.60	1.78	899	951	1249		2.60	0

45.3	3.33	10.2	11.10	0.39	0.08	200	-47	50	3	4.43	1.64	898	950	1249		4.43	0
49.6	1.43	17.6	10.79	0.47	0.74	150	529	200	729	2.58	1.76	866	921	1227		2.58	0
44.7	0.23	29.5	17.35	0.03	0.30	30	432	50	482	2.61	1.78	902	955	1251		2.61	0
45.7	1.60	13.3	10.41	0.10	0.30	150	546	200	746	3.35	1.73	895	948	1247		3.35	0
44.5	0.27	28.1	16.50	0.09	0.41	995	235	50	285	2.63	1.78	904	956	1253		2.63	0
45.1	0.22	29.3	16.65	0.04	0.31	16	432	50	482	2.50	1.78	899	952	1249		2.50	0
43.2	2.76	8.4	8.74	0.19	0.53	530	190	50	240	4.81	1.70	913	965	1259	30	4.81	0
45.7	1.60	13.3	10.41	0.10	0.30	150	-15	50	35	3.35	1.73	895	948	1247		3.35	0
44.7	0.23	29.5	17.35	0.03	0.30	30	97	1100	1197	2.61	1.78	902	955	1251	15	0.55	0
44.7	0.15	31.2	17.63	0.02	0.10	280	-87	600	513	2.48	1.78	902	955	1251		2.48	0
44.9	0.17	29.3	16.79	0.03	0.22	33	-81	50	-31	2.52	1.78	901	953	1250		2.52	0
44.7	0.20	29.3	17.07	0.04	0.32	33	53	300	353	2.59	1.79	902	955	1251		2.59	0
44.1	0.36	28.6	16.50	0.04	0.41	27	298	50	348	2.61	1.78	907	959	1255		2.61	0
48.4	0.90	8.9	12.13	0.21	0.01	36	501	50	551	5.21	1.67	875	929	1233		5.21	0
44.9	0.20	28.9	16.93	0.03	0.31	39	157	200	357	2.59	1.79	901	953	1250	15	2.59	0
44.3	0.22	29.6	18.00	0.08	0.24	43	-14	900	886	2.74	1.80	905	957	1254		2.74	0
45.5	0.60	24.0	15.90	0.00	0.60	150	686	50	736	2.96	1.80	896	949	1248		2.96	0
39.9	9.42	11.0	10.62	0.08	0.35	150	109	50	159	4.55	1.66	938	988	1276		4.55	0
44.3	0.09	30.8	17.30	0.01	0.36	30	-68	50	-18	2.54	1.80	905	957	1254		2.54	0
44.7	0.20	29.3	17.07	0.04	0.32	33	581	400	981	2.59	1.79	902	955	1251	15	0.55	0
44.3	0.25	28.0	16.37	0.07	0.35	35	125	100	225	2.64	1.79	905	958	1254		2.64	0
44.7	0.15	31.2	17.63	0.02	0.10	280	498	50	548	2.48	1.78	902	955	1251		2.48	0
46.2	3.07	13.7	10.55	0.27	0.48	150	471	50	521	3.32	1.73	891	944	1244		3.32	0
43.6	0.12	29.2	16.60	0.01	0.36	85	621	50	671	2.60	1.79	910	962	1257		2.60	0
47.9	0.97	13.2	11.60	0.42	0.06	141	172	20	192	3.48	1.69	879	932	1236		3.48	0
44.9	0.22	29.3	16.65	0.04	0.31	50	424	20	444	2.51	1.78	901	953	1250		2.51	0
44.3	0.09	30.8	17.30	0.01	0.36	30	497	500	997	2.54	1.80	905	957	1254	15	0.54	0
44.7	0.15	31.2	17.63	0.02	0.10	280	157	50	207	2.48	1.78	902	955	1251		2.48	0
44.3	0.22	29.6	18.00	0.08	0.24	43	48	100	148	2.74	1.80	905	957	1254		2.74	0
46.2	0.68	20.6	13.50	0.51	0.19	132	279	200	479	2.83	1.76	891	944	1244		2.83	0
45.1	0.22	29.3	16.65	0.04	0.31	16	564	20	584	2.50	1.78	899	952	1249		2.50	0
44.6	3.79	11.8	10.46	0.13	0.34	150	256	50	306	3.79	1.68	903	956	1252		3.79	0
44.0	3.53	15.5	12.07	0.10	0.36	150	161	20	181	3.46	1.74	908	960	1255		3.46	0
44.4	0.43	28.0	15.64	0.01	0.19	150	-58	300	242	2.53	1.81	905	957	1253		2.53	0
44.3	0.09	30.8	17.30	0.01	0.36	30	559	1200	1759	2.54	1.80	905	957	1254	15	0.53	0
46.2	2.16	10.3	9.74	0.10	0.31	150	-30	50	20	3.96	1.71	891	944	1244		3.96	0
45.1	0.22	29.3	16.65	0.04	0.31	16	208	200	408	2.50	1.78	899	952	1249		2.50	0

44.9	0.17	29.3	16.79	0.03	0.22	33	50	50	100	2.52	1.78	901	953	1250		2.52	0
45.0	0.49	23.1	14.07	0.08	0.35	150	255	100	355	2.73	1.80	900	953	1250		2.73	0
49.6	1.43	17.6	10.79	0.47	0.74	150	252	50	302	2.58	1.76	866	921	1227		2.58	0
44.0	2.79	9.0	9.02	0.05	0.27	150	654	500	1154	4.35	1.69	908	960	1255	20	1.09	977
44.9	0.22	28.9	16.79	0.04	0.32	46	303	100	403	2.57	1.78	901	953	1250		2.57	0
44.7	0.15	31.2	17.63	0.02	0.10	280	530	50	580	2.48	1.78	902	955	1251		2.48	0
44.3	0.25	28.0	16.37	0.07	0.35	35	91	50	141	2.64	1.79	905	958	1254		2.64	0
44.1	0.13	29.9	16.80	0.01	0.34	43	251	50	301	2.55	1.80	907	959	1255		2.55	0
44.9	0.20	28.9	16.93	0.03	0.31	39	17	50	67	2.59	1.79	901	953	1250	15	2.59	0
44.3	0.09	30.8	17.30	0.01	0.36	30	364	20	384	2.54	1.80	905	957	1254	15	2.54	0
47.9	0.97	13.2	11.60	0.42	0.06	141	643	900	1543	3.48	1.69	879	932	1236	23	0.98	963
44.1	0.36	28.6	16.50	0.04	0.41	27	639	50	689	2.61	1.78	907	959	1255		2.61	0
44.3	0.25	28.0	16.37	0.07	0.35	35	599	100	699	2.64	1.79	905	958	1254		2.64	0
44.4	0.19	30.7	18.20	0.02	0.39	220	209	50	259	2.66	1.79	904	957	1253	30	2.66	0
43.7	0.17	27.6	16.80	0.34	0.01	38	488	600	1088	2.69	1.75	910	962	1257	15	0.57	0
46.5	0.23	25.3	14.80	0.03	0.30	30	426	100	526	2.54	1.81	889	942	1243		2.54	0
44.4	0.19	30.7	18.20	0.02	0.39	220	346	300	646	2.66	1.79	904	957	1253	30	2.66	0
44.0	1.55	16.6	12.96	0.32	0.06	103	471	300	771	3.32	1.68	907	959	1255	19	3.32	0
45.0	0.49	23.1	14.07	0.08	0.35	150	37	100	137	2.73	1.80	900	953	1250		2.73	0
45.1	0.22	29.3	16.65	0.04	0.31	16	331	50	381	2.50	1.78	899	952	1249		2.50	0
43.9	0.16	28.5	15.90	0.02	0.36	44	740	100	840	2.53	1.79	908	960	1256		2.53	0
62.5	1.18	15.7	6.86	3.20	0.98	150	523	50	573	1.86	1.73	771	830	1162		1.86	0
73.1	0.50	12.4	1.27	5.97	0.64	150	634	20	654	1.10	1.68	694	756	1109		1.10	0
43.9	0.16	28.5	15.90	0.02	0.36	44	520	20	540	2.53	1.79	908	960	1256		2.53	0
45.4	0.71	22.6	14.90	0.36	0.06	61	499	50	549	2.83	1.75	897	950	1248		2.83	0
39.9	9.42	11.0	10.62	0.08	0.35	150	672	20	692	4.55	1.66	938	988	1276		4.55	0
46.2	2.16	10.3	9.74	0.10	0.31	150	31	50	81	3.96	1.71	891	944	1244		3.96	0
45.4	1.66	11.5	11.99	0.04	0.50	120	437	50	487	4.35	1.66	897	950	1248		4.35	0
44.3	0.25	28.0	16.37	0.07	0.35	35	207	50	257	2.64	1.79	905	958	1254		2.64	0
46.6	1.25	18.8	11.60	0.12	0.37	150	-22	500	478	2.66	1.78	889	942	1242		2.66	0
48.1	1.70	17.4	10.79	0.58	0.70	150	145	50	195	2.70	1.76	877	931	1235		2.70	0
44.3	0.25	28.0	16.37	0.07	0.35	35	196	50	246	2.64	1.79	905	958	1254		2.64	0
46.2	0.68	20.6	13.50	0.51	0.19	132	-88	20	-68	2.83	1.76	891	944	1244		2.83	0
62.5	1.18	15.7	6.86	3.20	0.98	150	532	50	582	1.86	1.73	771	830	1162		1.86	0
43.6	0.12	29.2	16.60	0.01	0.36	85	369	50	419	2.60	1.79	910	962	1257		2.60	0
46.2	0.68	20.6	13.50	0.51	0.19	132	716	100	816	2.83	1.76	891	944	1244		2.83	0
44.9	0.20	29.1	16.79	0.03	0.32	33	696	50	746	2.55	1.79	901	953	1250		2.55	0

46.2	2.16	10.3	9.74	0.10	0.31	150	498	50	548	3.96	1.71	891	944	1244		3.96	0
44.7	0.18	28.5	16.93	0.04	0.30	36	214	900	1114	2.63	1.78	902	955	1251	15	0.55	0
44.5	0.27	28.1	16.50	0.09	0.41	995	459	50	509	2.63	1.78	904	956	1253		2.63	0
44.7	0.30	26.6	15.67	0.05	0.34	50	240	100	340	2.62	1.78	902	955	1251		2.62	0
37.6	12.04	8.5	8.81	0.13	0.54	150	-35	300	265	5.25	1.63	954	1004	1287		5.25	0
44.5	0.27	28.1	16.50	0.09	0.41	995	312	1000	1312	2.63	1.78	904	956	1253	51	1.37	1083
43.4	0.14	28.2	16.10	0.36	0.02	17	613	50	663	2.60	1.78	912	964	1258	15	2.60	0
46.5	0.23	25.3	14.80	0.03	0.30	30	-51	800	749	2.54	1.81	889	942	1243		2.54	0
44.9	0.18	28.1	16.65	0.38	0.04	21	-27	50	23	2.58	1.76	901	953	1250	15	2.58	0
44.0	2.79	9.0	9.02	0.05	0.27	150	28	20	48	4.35	1.69	908	960	1255	20	4.35	0
43.6	0.12	29.2	16.60	0.01	0.36	85	150	50	200	2.60	1.79	910	962	1257		2.60	0
73.1	0.50	12.4	1.27	5.97	0.64	150	487	20	507	1.10	1.68	694	756	1109		1.10	0
44.0	0.15	29.7	16.90	0.01	0.34	25	521	50	571	2.58	1.79	907	959	1255		2.58	0
44.4	0.19	30.7	18.20	0.02	0.39	220	10	20	30	2.66	1.79	904	957	1253	30	2.66	0
44.7	0.15	31.2	17.63	0.02	0.10	280	-54	20	-34	2.48	1.78	902	955	1251		2.48	0
45.5	0.60	24.0	15.90	0.00	0.60	150	-27	100	73	2.96	1.80	896	949	1248		2.96	0
44.4	0.43	28.0	15.64	0.01	0.19	150	-39	50	11	2.53	1.81	905	957	1253		2.53	0
44.1	0.36	28.6	16.50	0.04	0.41	27	407	50	457	2.61	1.78	907	959	1255		2.61	0
44.9	0.20	29.1	16.79	0.03	0.32	33	561	50	611	2.55	1.79	901	953	1250		2.55	0
46.2	3.07	13.7	10.55	0.27	0.48	150	35	100	135	3.32	1.73	891	944	1244		3.32	0
46.2	3.07	13.7	10.55	0.27	0.48	150	230	200	430	3.32	1.73	891	944	1244		3.32	0
46.2	3.07	13.7	10.55	0.27	0.48	150	100	100	200	3.32	1.73	891	944	1244		3.32	0
44.9	0.20	29.1	16.79	0.03	0.32	33	141	100	241	2.55	1.79	901	953	1250		2.55	0
44.0	3.53	15.5	12.07	0.10	0.36	150	679	50	729	3.46	1.74	908	960	1255		3.46	0
49.6	1.43	17.6	10.79	0.47	0.74	150	290	300	590	2.58	1.76	866	921	1227		2.58	0
44.3	0.25	28.0	16.37	0.07	0.35	35	749	20	769	2.64	1.79	905	958	1254		2.64	0
37.6	12.04	8.5	8.81	0.13	0.54	150	290	1200	1490	5.25	1.63	954	1004	1287	16	1.13	1006
73.1	0.50	12.4	1.27	5.97	0.64	150	-45	200	155	1.10	1.68	694	756	1109		1.10	0
48.1	1.70	17.4	10.79	0.58	0.70	150	234	50	284	2.70	1.76	877	931	1235		2.70	0
44.7	0.20	29.3	17.07	0.04	0.32	33	129	100	229	2.59	1.79	902	955	1251	15	2.59	0
43.2	2.76	8.4	8.74	0.19	0.53	530	526	200	726	4.81	1.70	913	965	1259	30	4.81	0
53.4	2.08	15.6	9.57	1.11	1.01	150	511	100	611	2.52	1.72	839	894	1208		2.52	0
44.7	0.18	28.5	16.93	0.04	0.30	36	303	50	353	2.63	1.78	902	955	1251	15	2.63	0
44.1	0.13	29.9	16.80	0.01	0.34	43	489	50	539	2.55	1.80	907	959	1255		2.55	0
43.7	0.17	27.6	16.80	0.34	0.01	38	405	50	455	2.69	1.75	910	962	1257	15	2.69	0
45.2	0.24	28.3	16.90	0.34	0.03	170	281	50	331	2.60	1.78	899	951	1249		2.60	0
43.2	2.76	8.4	8.74	0.19	0.53	530	115	1200	1315	4.81	1.70	913	965	1259	30	1.62	1016

44.0	2.79	9.0	9.02	0.05	0.27	150	715	50	765	4.35	1.69	908	960	1255	20	4.35	0
44.1	0.36	28.6	16.50	0.04	0.41	27	513	50	563	2.61	1.78	907	959	1255		2.61	0
44.0	0.15	27.2	15.50	0.04	0.33	24	514	20	534	2.59	1.80	907	959	1255		2.59	0
44.3	0.22	29.6	18.00	0.08	0.24	43	632	500	1132	2.74	1.80	905	957	1254	15	0.58	0
44.7	0.23	29.5	17.35	0.03	0.30	30	83	20	103	2.61	1.78	902	955	1251	15	2.61	0
44.3	0.09	30.8	17.30	0.01	0.36	30	263	50	313	2.54	1.80	905	957	1254	15	2.54	0
44.3	0.22	29.6	18.00	0.08	0.24	43	398	200	598	2.74	1.80	905	957	1254	15	2.74	0
44.0	0.15	27.2	15.50	0.04	0.33	24	20	50	70	2.59	1.80	907	959	1255		2.59	0
44.0	0.15	29.7	16.90	0.01	0.34	25	335	20	355	2.58	1.79	907	959	1255		2.58	0
49.6	1.43	17.6	10.79	0.47	0.74	150	62	20	82	2.58	1.76	866	921	1227		2.58	0
48.4	0.90	8.9	12.13	0.21	0.01	36	627	50	677	5.21	1.67	875	929	1233		5.21	0
44.5	0.27	28.1	16.50	0.09	0.41	995	184	50	234	2.63	1.78	904	956	1253	51	2.63	0
44.3	0.25	28.0	16.37	0.07	0.35	35	200	50	250	2.64	1.79	905	958	1254		2.64	0
45.4	0.71	22.6	14.90	0.36	0.06	61	332	50	382	2.83	1.75	897	950	1248		2.83	0
48.1	1.70	17.4	10.79	0.58	0.70	150	128	100	228	2.70	1.76	877	931	1235		2.70	0
46.2	0.68	20.6	13.50	0.51	0.19	132	408	50	458	2.83	1.76	891	944	1244		2.83	0
45.4	3.90	14.9	11.80	0.00	0.60	150	68	50	118	3.46	1.73	897	950	1248		3.46	0
42.5	7.67	13.8	12.12	0.15	0.44	150	705	50	755	4.02	1.71	919	970	1263		4.02	0

Table 8.5.3 - Model results for zircon saturation in simulated LHB impact event on Martian surface.

SiO_2	TiO_2	Al_2O_3	CaO	K_2O	NA_2O	Zr	Rock Temp.	Impact ΔT	Final Temp.	M'	Total Mol.	Solidus	Solidus @ 15% melt	Liquidus	% Melt	M' adjusted	Final Zircon Temp
47.7	0.35	4.2	7.83	0.03	0.55	8	588	50	638	7.90	1.73	880	934	1236		7.90	0
51.2	0.61	3.2	13.07	0.32	0.94	30	87	50	137	15.86	1.70	855	910	1219		15.86	0
37.0	0.13	0.9	0.84	0.05	0.17	8	195	50	245	6.53	1.86	959	1008	1290		6.53	0
47.7	0.35	4.2	7.83	0.03	0.55	8	297	100	397	7.90	1.73	880	934	1236		7.90	0
45.4	0.35	2.3	4.06	0.03	0.36	63	1048	20	1068	8.18	1.79	897	950	1248	15	1.72	0
52.9	0.81	6.8	10.24	0.13	1.28	69	953	50	1003	5.94	1.71	842	897	1211	20	1.52	917
49.2	0.07	3.6	15.00	0.29	1.01	23	973	50	1023	16.64	1.67	869	923	1229	15	3.52	0
51.7	1.16	6.5	9.32	0.10	1.26	59	33	1200	1233	5.87	1.71	851	906	1217	18	1.41	919
51.7	1.16	6.5	9.32	0.10	1.26	59	1126	200	1326	5.87	1.71	851	906	1217	18	1.41	919
47.6	0.43	3.3	5.66	0.08	0.59	23	294	20	314	7.70	1.78	881	934	1237		7.70	0
47.6	0.43	3.3	5.66	0.08	0.59	23	254	100	354	7.70	1.78	881	934	1237		7.70	0

46.8	0.77	5.8	7.91	0.16	1.14	62	-26	50	24	6.43	1.75	887	940	1241		6.43	0
51.2	0.61	3.2	13.07	0.32	0.94	30	318	20	338	15.86	1.70	855	910	1219		15.86	0
47.6	0.43	3.3	5.66	0.08	0.59	23	224	20	244	7.70	1.78	881	934	1237		7.70	0
37.0	0.13	0.9	0.84	0.05	0.17	8	187	20	207	6.53	1.86	959	1008	1290		6.53	0
47.7	0.35	4.2	7.83	0.03	0.55	8	383	1100	1483	7.90	1.73	880	934	1236	15	1.67	0
47.6	0.43	3.3	5.66	0.08	0.59	23	1024	50	1074	7.70	1.78	881	934	1237	15	1.62	0
47.6	0.43	3.3	5.66	0.08	0.59	23	849	50	899	7.70	1.78	881	934	1237	15	7.70	0
37.0	0.13	0.9	0.84	0.05	0.17	8	1175	500	1675	6.53	1.86	959	1008	1290	15	1.38	0
47.7	0.35	4.2	7.83	0.03	0.55	8	618	20	638	7.90	1.73	880	934	1236	15	7.90	0
48.4	0.63	7.0	7.08	0.05	0.72	17	618	50	668	4.32	1.73	875	929	1233		4.32	0
37.0	0.13	0.9	0.84	0.05	0.17	8	77	100	177	6.53	1.86	959	1008	1290	15	6.53	0
47.7	0.35	4.2	7.83	0.03	0.55	8	662	50	712	7.90	1.73	880	934	1236	15	7.90	0
48.4	0.63	7.0	7.08	0.05	0.72	17	75	50	125	4.32	1.73	875	929	1233		4.32	0
48.4	0.63	7.0	7.08	0.05	0.72	17	910	100	1010	4.32	1.73	875	929	1233	15	0.91	0
46.8	0.77	5.8	7.91	0.16	1.14	62	869	200	1069	6.43	1.75	887	940	1241	16	1.40	943
49.2	0.07	3.6	15.00	0.29	1.01	23	253	20	273	16.64	1.67	869	923	1229	15	16.64	0
49.2	0.07	3.6	15.00	0.29	1.01	23	832	100	932	16.64	1.67	869	923	1229	15	3.52	0
48.4	0.63	7.0	7.08	0.05	0.72	17	324	50	374	4.32	1.73	875	929	1233	15	4.32	0
49.2	0.07	3.6	15.00	0.29	1.01	23	572	100	672	16.64	1.67	869	923	1229	15	16.64	0
45.4	0.35	2.3	4.06	0.03	0.36	63	-54	100	46	8.18	1.79	897	950	1248	15	8.18	0
51.2	0.61	3.2	13.07	0.32	0.94	30	268	50	318	15.86	1.70	855	910	1219		15.86	0
48.4	0.63	7.0	7.08	0.05	0.72	17	182	50	232	4.32	1.73	875	929	1233	15	4.32	0
46.8	0.77	5.8	7.91	0.16	1.14	62	1136	20	1156	6.43	1.75	887	940	1241	16	1.40	943
47.7	0.35	4.2	7.83	0.03	0.55	8	139	20	159	7.90	1.73	880	934	1236	15	7.90	0
45.4	0.35	2.3	4.06	0.03	0.36	63	946	20	966	8.18	1.79	897	950	1248	15	1.72	0
51.2	0.61	3.2	13.07	0.32	0.94	30	171	50	221	15.86	1.70	855	910	1219		15.86	0
46.8	0.77	5.8	7.91	0.16	1.14	62	1064	50	1114	6.43	1.75	887	940	1241	16	1.40	943
52.9	0.81	6.8	10.24	0.13	1.28	69	1103	50	1153	5.94	1.71	842	897	1211	20	1.52	917
46.8	0.77	5.8	7.91	0.16	1.14	62	743	50	793	6.43	1.75	887	940	1241	16	6.43	0
46.8	0.77	5.8	7.91	0.16	1.14	62	576	200	776	6.43	1.75	887	940	1241	16	6.43	0
46.8	0.77	5.8	7.91	0.16	1.14	62	990	20	1010	6.43	1.75	887	940	1241	16	1.40	943
47.6	0.43	3.3	5.66	0.08	0.59	23	402	50	452	7.70	1.78	881	934	1237	15	7.70	0
51.7	1.16	6.5	9.32	0.10	1.26	59	460	50	510	5.87	1.71	851	906	1217	18	5.87	0
49.2	0.07	3.6	15.00	0.29	1.01	23	-83	100	17	16.64	1.67	869	923	1229	15	16.64	0
47.6	0.43	3.3	5.66	0.08	0.59	23	86	100	186	7.70	1.78	881	934	1237	15	7.70	0
37.0	0.13	0.9	0.84	0.05	0.17	8	1183	20	1203	6.53	1.86	959	1008	1290	15	1.38	0
37.0	0.13	0.9	0.84	0.05	0.17	8	-23	100	77	6.53	1.86	959	1008	1290	15	6.53	0

46.8	0.77	5.8	7.91	0.16	1.14	62	206	50	256	6.43	1.75	887	940	1241	16	6.43	0
47.7	0.35	4.2	7.83	0.03	0.55	8	89	50	139	7.90	1.73	880	934	1236	15	7.90	0
46.8	0.77	5.8	7.91	0.16	1.14	62	265	200	465	6.43	1.75	887	940	1241	16	6.43	0
51.7	1.16	6.5	9.32	0.10	1.26	59	-35	50	15	5.87	1.71	851	906	1217	18	5.87	0
47.6	0.43	3.3	5.66	0.08	0.59	23	809	50	859	7.70	1.78	881	934	1237	15	7.70	0
51.7	1.16	6.5	9.32	0.10	1.26	59	372	20	392	5.87	1.71	851	906	1217	18	5.87	0
52.9	0.81	6.8	10.24	0.13	1.28	69	716	50	766	5.94	1.71	842	897	1211	20	5.94	0
47.7	0.35	4.2	7.83	0.03	0.55	8	1039	50	1089	7.90	1.73	880	934	1236	15	1.66	0
48.4	0.63	7.0	7.08	0.05	0.72	17	3	300	303	4.32	1.73	875	929	1233	15	4.32	0
52.9	0.81	6.8	10.24	0.13	1.28	69	278	100	378	5.94	1.71	842	897	1211	20	5.94	0
47.6	0.43	3.3	5.66	0.08	0.59	23	-89	20	-69	7.70	1.78	881	934	1237	15	7.70	0
49.2	0.07	3.6	15.00	0.29	1.01	23	228	50	278	16.64	1.67	869	923	1229	15	16.64	0
51.7	1.16	6.5	9.32	0.10	1.26	59	-8	20	12	5.87	1.71	851	906	1217	18	5.87	0
49.2	0.07	3.6	15.00	0.29	1.01	23	63	20	83	16.64	1.67	869	923	1229	15	16.64	0
51.2	0.61	3.2	13.07	0.32	0.94	30	1039	50	1089	15.86	1.70	855	910	1219	15	3.34	0
48.4	0.63	7.0	7.08	0.05	0.72	17	736	200	936	4.32	1.73	875	929	1233	15	0.91	0
52.9	0.81	6.8	10.24	0.13	1.28	69	26	50	76	5.94	1.71	842	897	1211	20	5.94	0
48.4	0.63	7.0	7.08	0.05	0.72	17	1180	50	1230	4.32	1.73	875	929	1233	15	0.91	0
46.8	0.77	5.8	7.91	0.16	1.14	62	172	50	222	6.43	1.75	887	940	1241	16	6.43	0
47.7	0.35	4.2	7.83	0.03	0.55	8	483	50	533	7.90	1.73	880	934	1236	15	7.90	0
51.2	0.61	3.2	13.07	0.32	0.94	30	831	20	851	15.86	1.70	855	910	1219	15	15.86	0
37.0	0.13	0.9	0.84	0.05	0.17	8	247	20	267	6.53	1.86	959	1008	1290	15	6.53	0
47.6	0.43	3.3	5.66	0.08	0.59	23	556	50	606	7.70	1.78	881	934	1237	15	7.70	0
45.4	0.35	2.3	4.06	0.03	0.36	63	674	50	724	8.18	1.79	897	950	1248	15	8.18	0
48.4	0.63	7.0	7.08	0.05	0.72	17	765	20	785	4.32	1.73	875	929	1233	15	4.32	0
37.0	0.13	0.9	0.84	0.05	0.17	8	565	50	615	6.53	1.86	959	1008	1290	15	6.53	0
49.2	0.07	3.6	15.00	0.29	1.01	23	261	50	311	16.64	1.67	869	923	1229	15	16.64	0
47.6	0.43	3.3	5.66	0.08	0.59	23	1096	50	1146	7.70	1.78	881	934	1237	15	1.62	0
47.6	0.43	3.3	5.66	0.08	0.59	23	478	100	578	7.70	1.78	881	934	1237	15	7.70	0
47.7	0.35	4.2	7.83	0.03	0.55	8	284	100	384	7.90	1.73	880	934	1236	15	7.90	0
47.7	0.35	4.2	7.83	0.03	0.55	8	717	50	767	7.90	1.73	880	934	1236	15	7.90	0
48.4	0.63	7.0	7.08	0.05	0.72	17	1005	100	1105	4.32	1.73	875	929	1233	15	0.91	0
45.4	0.35	2.3	4.06	0.03	0.36	63	953	20	973	8.18	1.79	897	950	1248	15	1.72	0
37.0	0.13	0.9	0.84	0.05	0.17	8	121	50	171	6.53	1.86	959	1008	1290	15	6.53	0
51.7	1.16	6.5	9.32	0.10	1.26	59	1004	50	1054	5.87	1.71	851	906	1217	19	1.41	919
51.2	0.61	3.2	13.07	0.32	0.94	30	1027	1200	2227	15.86	1.70	855	910	1219	15	3.35	0
49.2	0.07	3.6	15.00	0.29	1.01	23	194	20	214	16.64	1.67	869	923	1229	15	16.64	0

47.7	0.35	4.2	7.83	0.03	0.55	8	359	50	409	7.90	1.73	880	934	1236	15	7.90	0
47.6	0.43	3.3	5.66	0.08	0.59	23	18	200	218	7.70	1.78	881	934	1237	15	7.70	0
52.9	0.81	6.8	10.24	0.13	1.28	69	431	200	631	5.94	1.71	842	897	1211	20	5.94	0
37.0	0.13	0.9	0.84	0.05	0.17	8	1058	20	1078	6.53	1.86	959	1008	1290	15	1.38	0
49.2	0.07	3.6	15.00	0.29	1.01	23	305	50	355	16.64	1.67	869	923	1229	15	16.64	0
51.2	0.61	3.2	13.07	0.32	0.94	30	708	50	758	15.86	1.70	855	910	1219	15	15.86	0
47.6	0.43	3.3	5.66	0.08	0.59	23	682	20	702	7.70	1.78	881	934	1237	15	7.70	0
51.7	1.16	6.5	9.32	0.10	1.26	59	330	20	350	5.87	1.71	851	906	1217	19	5.87	0
47.6	0.43	3.3	5.66	0.08	0.59	23	574	100	674	7.70	1.78	881	934	1237	15	7.70	0
51.7	1.16	6.5	9.32	0.10	1.26	59	730	200	930	5.87	1.71	851	906	1217	19	1.41	919
37.0	0.13	0.9	0.84	0.05	0.17	8	551	100	651	6.53	1.86	959	1008	1290	15	6.53	0
51.2	0.61	3.2	13.07	0.32	0.94	30	138	50	188	15.86	1.70	855	910	1219	15	15.86	0
37.0	0.13	0.9	0.84	0.05	0.17	8	539	50	589	6.53	1.86	959	1008	1290	15	6.53	0
48.4	0.63	7.0	7.08	0.05	0.72	17	216	50	266	4.32	1.73	875	929	1233	15	4.32	0
37.0	0.13	0.9	0.84	0.05	0.17	8	672	50	722	6.53	1.86	959	1008	1290	15	6.53	0
47.6	0.43	3.3	5.66	0.08	0.59	23	459	200	659	7.70	1.78	881	934	1237	15	7.70	0
46.8	0.77	5.8	7.91	0.16	1.14	62	1007	20	1027	6.43	1.75	887	940	1241	16	1.40	943
51.7	1.16	6.5	9.32	0.10	1.26	59	340	20	360	5.87	1.71	851	906	1217	19	5.87	0
49.2	0.07	3.6	15.00	0.29	1.01	23	39	50	89	16.64	1.67	869	923	1229	15	16.64	0
47.7	0.35	4.2	7.83	0.03	0.55	8	563	50	613	7.90	1.73	880	934	1236	15	7.90	0
52.9	0.81	6.8	10.24	0.13	1.28	69	174	50	224	5.94	1.71	842	897	1211	20	5.94	0
45.4	0.35	2.3	4.06	0.03	0.36	63	1106	50	1156	8.18	1.79	897	950	1248	15	1.72	0
47.6	0.43	3.3	5.66	0.08	0.59	23	416	50	466	7.70	1.78	881	934	1237	15	7.70	0
52.9	0.81	6.8	10.24	0.13	1.28	69	1137	20	1157	5.94	1.71	842	897	1211	20	1.52	917
45.4	0.35	2.3	4.06	0.03	0.36	63	202	50	252	8.18	1.79	897	950	1248	15	8.18	0
52.9	0.81	6.8	10.24	0.13	1.28	69	1064	200	1264	5.94	1.71	842	897	1211	20	1.51	917
51.7	1.16	6.5	9.32	0.10	1.26	59	432	300	732	5.87	1.71	851	906	1217	19	5.87	0
37.0	0.13	0.9	0.84	0.05	0.17	8	621	200	821	6.53	1.86	959	1008	1290	15	6.53	0
51.7	1.16	6.5	9.32	0.10	1.26	59	960	100	1060	5.87	1.71	851	906	1217	19	1.41	919
49.2	0.07	3.6	15.00	0.29	1.01	23	512	1000	1512	16.64	1.67	869	923	1229	15	3.52	0
52.9	0.81	6.8	10.24	0.13	1.28	69	816	50	866	5.94	1.71	842	897	1211	20	5.94	0
47.6	0.43	3.3	5.66	0.08	0.59	23	133	20	153	7.70	1.78	881	934	1237	15	7.70	0
49.2	0.07	3.6	15.00	0.29	1.01	23	428	100	528	16.64	1.67	869	923	1229	15	16.64	0
46.8	0.77	5.8	7.91	0.16	1.14	62	633	20	653	6.43	1.75	887	940	1241	16	6.43	0
47.6	0.43	3.3	5.66	0.08	0.59	23	587	900	1487	7.70	1.78	881	934	1237	15	1.62	0
37.0	0.13	0.9	0.84	0.05	0.17	8	804	50	854	6.53	1.86	959	1008	1290	15	6.53	0
46.8	0.77	5.8	7.91	0.16	1.14	62	451	100	551	6.43	1.75	887	940	1241	16	6.43	0

46.8	0.77	5.8	7.91	0.16	1.14	62	190	20	210	6.43	1.75	887	940	1241	16	6.43	0
51.2	0.61	3.2	13.07	0.32	0.94	30	-77	100	23	15.86	1.70	855	910	1219	15	15.86	0
51.2	0.61	3.2	13.07	0.32	0.94	30	187	300	487	15.86	1.70	855	910	1219	15	15.86	0
51.2	0.61	3.2	13.07	0.32	0.94	30	389	20	409	15.86	1.70	855	910	1219	15	15.86	0
46.8	0.77	5.8	7.91	0.16	1.14	62	-12	200	188	6.43	1.75	887	940	1241	16	6.43	0
47.7	0.35	4.2	7.83	0.03	0.55	8	214	50	264	7.90	1.73	880	934	1236	15	7.90	0
49.2	0.07	3.6	15.00	0.29	1.01	23	641	20	661	16.64	1.67	869	923	1229	15	16.64	0
46.8	0.77	5.8	7.91	0.16	1.14	62	127	1100	1227	6.43	1.75	887	940	1241	16	1.40	943
47.6	0.43	3.3	5.66	0.08	0.59	23	820	50	870	7.70	1.78	881	934	1237	15	7.70	0
47.6	0.43	3.3	5.66	0.08	0.59	23	962	200	1162	7.70	1.78	881	934	1237	15	1.62	0
51.7	1.16	6.5	9.32	0.10	1.26	59	509	20	529	5.87	1.71	851	906	1217	19	5.87	0
47.6	0.43	3.3	5.66	0.08	0.59	23	590	100	690	7.70	1.78	881	934	1237	15	7.70	0
45.4	0.35	2.3	4.06	0.03	0.36	63	742	50	792	8.18	1.79	897	950	1248	15	8.18	0
47.7	0.35	4.2	7.83	0.03	0.55	8	137	800	937	7.90	1.73	880	934	1236	15	1.66	0
51.2	0.61	3.2	13.07	0.32	0.94	30	907	1200	2107	15.86	1.70	855	910	1219	15	3.35	0
51.7	1.16	6.5	9.32	0.10	1.26	59	282	200	482	5.87	1.71	851	906	1217	19	5.87	0
45.4	0.35	2.3	4.06	0.03	0.36	63	470	20	490	8.18	1.79	897	950	1248	15	8.18	0
37.0	0.13	0.9	0.84	0.05	0.17	8	140	50	190	6.53	1.86	959	1008	1290	15	6.53	0
45.4	0.35	2.3	4.06	0.03	0.36	63	360	50	410	8.18	1.79	897	950	1248	15	8.18	0
46.8	0.77	5.8	7.91	0.16	1.14	62	907	20	927	6.43	1.75	887	940	1241	16	6.43	0
47.7	0.35	4.2	7.83	0.03	0.55	8	1104	50	1154	7.90	1.73	880	934	1236	15	1.66	0
48.4	0.63	7.0	7.08	0.05	0.72	17	680	50	730	4.32	1.73	875	929	1233	15	4.32	0
49.2	0.07	3.6	15.00	0.29	1.01	23	823	200	1023	16.64	1.67	869	923	1229	15	3.52	0
51.7	1.16	6.5	9.32	0.10	1.26	59	-12	20	8	5.87	1.71	851	906	1217	19	5.87	0
49.2	0.07	3.6	15.00	0.29	1.01	23	559	50	609	16.64	1.67	869	923	1229	15	16.64	0
45.4	0.35	2.3	4.06	0.03	0.36	63	553	50	603	8.18	1.79	897	950	1248	15	8.18	0
37.0	0.13	0.9	0.84	0.05	0.17	8	308	100	408	6.53	1.86	959	1008	1290	15	6.53	0
47.7	0.35	4.2	7.83	0.03	0.55	8	-46	20	-26	7.90	1.73	880	934	1236	15	7.90	0
46.8	0.77	5.8	7.91	0.16	1.14	62	66	300	366	6.43	1.75	887	940	1241	16	6.43	0
51.2	0.61	3.2	13.07	0.32	0.94	30	1119	20	1139	15.86	1.70	855	910	1219	15	3.34	0
46.8	0.77	5.8	7.91	0.16	1.14	62	732	200	932	6.43	1.75	887	940	1241	16	6.43	0
52.9	0.81	6.8	10.24	0.13	1.28	69	194	50	244	5.94	1.71	842	897	1211	20	5.94	0
45.4	0.35	2.3	4.06	0.03	0.36	63	79	300	379	8.18	1.79	897	950	1248	15	8.18	0
47.7	0.35	4.2	7.83	0.03	0.55	8	808	20	828	7.90	1.73	880	934	1236	15	7.90	0
48.4	0.63	7.0	7.08	0.05	0.72	17	1106	600	1706	4.32	1.73	875	929	1233	15	0.91	0
47.7	0.35	4.2	7.83	0.03	0.55	8	248	50	298	7.90	1.73	880	934	1236	15	7.90	0
47.7	0.35	4.2	7.83	0.03	0.55	8	-100	20	-80	7.90	1.73	880	934	1236	15	7.90	0

51.7	1.16	6.5	9.32	0.10	1.26	59	366	50	416	5.87	1.71	851	906	1217	19	5.87	0
48.4	0.63	7.0	7.08	0.05	0.72	17	904	50	954	4.32	1.73	875	929	1233	15	0.91	0
46.8	0.77	5.8	7.91	0.16	1.14	62	576	20	596	6.43	1.75	887	940	1241	16	6.43	0
47.6	0.43	3.3	5.66	0.08	0.59	23	236	20	256	7.70	1.78	881	934	1237	15	7.70	0
51.7	1.16	6.5	9.32	0.10	1.26	59	444	50	494	5.87	1.71	851	906	1217	19	5.87	0
37.0	0.13	0.9	0.84	0.05	0.17	8	859	200	1059	6.53	1.86	959	1008	1290	15	1.38	0
47.6	0.43	3.3	5.66	0.08	0.59	23	411	50	461	7.70	1.78	881	934	1237	15	7.70	0
51.2	0.61	3.2	13.07	0.32	0.94	30	986	100	1086	15.86	1.70	855	910	1219	15	3.34	0
47.7	0.35	4.2	7.83	0.03	0.55	8	307	200	507	7.90	1.73	880	934	1236	15	7.90	0
46.8	0.77	5.8	7.91	0.16	1.14	62	113	50	163	6.43	1.75	887	940	1241	16	6.43	0
51.7	1.16	6.5	9.32	0.10	1.26	59	-92	20	-72	5.87	1.71	851	906	1217	19	5.87	0
52.9	0.81	6.8	10.24	0.13	1.28	69	-48	800	752	5.94	1.71	842	897	1211	20	5.94	0
37.0	0.13	0.9	0.84	0.05	0.17	8	677	200	877	6.53	1.86	959	1008	1290	15	6.53	0
46.8	0.77	5.8	7.91	0.16	1.14	62	271	200	471	6.43	1.75	887	940	1241	16	6.43	0
48.4	0.63	7.0	7.08	0.05	0.72	17	545	200	745	4.32	1.73	875	929	1233	15	4.32	0
49.2	0.07	3.6	15.00	0.29	1.01	23	860	50	910	16.64	1.67	869	923	1229	15	16.64	0
52.9	0.81	6.8	10.24	0.13	1.28	69	478	100	578	5.94	1.71	842	897	1211	20	5.94	0
45.4	0.35	2.3	4.06	0.03	0.36	63	1166	50	1216	8.18	1.79	897	950	1248	15	1.72	0
47.6	0.43	3.3	5.66	0.08	0.59	23	-21	50	29	7.70	1.78	881	934	1237	15	7.70	0
48.4	0.63	7.0	7.08	0.05	0.72	17	273	500	773	4.32	1.73	875	929	1233	15	4.32	0
51.7	1.16	6.5	9.32	0.10	1.26	59	-94	800	706	5.87	1.71	851	906	1217	19	5.87	0
51.2	0.61	3.2	13.07	0.32	0.94	30	920	50	970	15.86	1.70	855	910	1219	15	3.34	0
51.2	0.61	3.2	13.07	0.32	0.94	30	388	50	438	15.86	1.70	855	910	1219	15	15.86	0
49.2	0.07	3.6	15.00	0.29	1.01	23	610	100	710	16.64	1.67	869	923	1229	15	16.64	0
47.7	0.35	4.2	7.83	0.03	0.55	8	336	50	386	7.90	1.73	880	934	1236	15	7.90	0
51.2	0.61	3.2	13.07	0.32	0.94	30	375	50	425	15.86	1.70	855	910	1219	15	15.86	0
37.0	0.13	0.9	0.84	0.05	0.17	8	-83	50	-33	6.53	1.86	959	1008	1290	15	6.53	0
47.6	0.43	3.3	5.66	0.08	0.59	23	125	100	225	7.70	1.78	881	934	1237	15	7.70	0
52.9	0.81	6.8	10.24	0.13	1.28	69	491	300	791	5.94	1.71	842	897	1211	20	5.94	0
45.4	0.35	2.3	4.06	0.03	0.36	63	978	900	1878	8.18	1.79	897	950	1248	15	1.72	0
49.2	0.07	3.6	15.00	0.29	1.01	23	106	400	506	16.64	1.67	869	923	1229	15	16.64	0
45.4	0.35	2.3	4.06	0.03	0.36	63	847	50	897	8.18	1.79	897	950	1248	15	8.18	0
46.8	0.77	5.8	7.91	0.16	1.14	62	628	50	678	6.43	1.75	887	940	1241	16	6.43	0
51.2	0.61	3.2	13.07	0.32	0.94	30	822	50	872	15.86	1.70	855	910	1219	15	15.86	0
48.4	0.63	7.0	7.08	0.05	0.72	17	1099	20	1119	4.32	1.73	875	929	1233	15	0.91	0
49.2	0.07	3.6	15.00	0.29	1.01	23	1131	50	1181	16.64	1.67	869	923	1229	15	3.52	0
47.7	0.35	4.2	7.83	0.03	0.55	8	512	20	532	7.90	1.73	880	934	1236	15	7.90	0

37.0	0.13	0.9	0.84	0.05	0.17	8	342	50	392	6.53	1.86	959	1008	1290	15	6.53	0
51.7	1.16	6.5	9.32	0.10	1.26	59	1174	1100	2274	5.87	1.71	851	906	1217	18	1.41	919
51.7	1.16	6.5	9.32	0.10	1.26	59	1091	20	1111	5.87	1.71	851	906	1217	19	1.41	919

First seven columns: whole rock geochemistry of target surface

Rock temp: ambient rock temperature based on Archean geotherm of Condie (1984), Selenotherm of Dyal et al. (1973) and Martian-therm of Squyres and Kasting (1994).

Impact ΔT: increase in rock temp associated with LHB style bombardment from Abramov & Mojzsis (2009).

Final temp: ambient temperature and impact generated temperature

'M': cation ratio = (Na+K+2Ca)/(Al*Si)

Total mol: normalizing factor for 'M' = $(SiO_2/60)+(TiO_2/80)+(Al_2O_3/51)+(FeO_{Tot}/80)+(MgO/40)+(CaO/56)+(Na_2O/31)+(K_2O/47)$

Solidus, solidus @ 15% melt and liquidus: translated from composition and classic melting experiments of Wyllie (1977).

% melt: estimated melt percent from final temperature

'M' adjusted: parameterized cation ratio 'M' from MELTS (Ghiorso and Sack, 1995).

Final zircon temp: modeled crystallization temperature of zircon within impact melts.

8.6 Appendix 6

Table 8.6.1 - SIMS U-Pb data for Pb-loss investigation including depth profiles and multi-spot analyses.

Sample: Morokweng	**$^{207}Pb/^{235}U$ Value**	**1s.e.**	**$^{206}Pb/^{238}U$ Value**	**1s.e.**	**Correlation of Concordia Ellipses**	**$^{206}Pb/^{238}U$ Age(Ma)**	**1s.e. (Ma)**	**$^{207}Pb/^{235}U$ Age(Ma)**	**1s.e. (Ma)**	**$^{207}Pb/^{206}Pb$ Age(Ma)**	**1s.e. (Ma)**
MK_1069m_1_core	23.0800	1.4600	0.2687	0.0018	0.6230	3122	152	3230	62	3298	10
MK_1069m_1_rim	24.9900	0.9300	0.2689	0.0006	0.6741	3322	98	3308	36	3299	3
MK_1069m_2_core	13.2600	0.4250	0.4683	0.0162	0.9629	2476	71	2699	30	2870	15

MK_1069m_2_rim	12.4300	0.3320	0.4367	0.0120	0.9965	2336	54	2637	25	2878	4
MK_1069m_3_core	27.9100	1.1700	0.2837	0.0011	0.7135	3471	109	3416	41	3384	6
MK_1069m_3_rim	23.7300	0.7210	0.2748	0.0008	0.6264	3135	74	3258	30	3334	4
MK_1069m_4_core	19.7700	0.5880	0.2820	0.0005	0.5085	2650	65	3080	29	3374	3
MK_1069m_4_rim	15.8000	0.4340	0.2437	0.0011	0.4703	2485	57	2865	26	3144	7
MK_1069m_5_core	17.2400	0.7460	0.5801	0.0253	0.9912	2949	103	2948	42	2947	9
MK_1069m_5_rim	19.6500	0.9090	0.5750	0.0264	0.9970	2928	108	3074	45	3171	6
MK_1069m_6_core	26.6600	0.7690	0.2868	0.0009	0.6743	3322	77	3371	28	3400	5
MK_1069m_6_rim	21.7700	0.7770	0.2197	0.0008	0.7185	3490	94	3173	35	2979	6
MK_1069m_7_core	22.1400	1.0300	0.2401	0.0018	0.6689	3302	108	3190	45	3121	12
MK_1069m_7_rim	15.8300	0.5110	0.2655	0.0007	0.4325	2317	62	2867	31	3279	4
MK_1069m_8_core	21.1500	0.5800	0.2531	0.0005	0.6061	3054	66	3146	27	3204	3
MK_1069m_8_rim	18.3000	0.6460	0.2205	0.0009	0.6018	3037	90	3006	34	2984	6
MK_1069m_1_depth_profile	21.0000	1.2300	0.5370	0.0318	0.9890	2771	133	3139	57	3383	14
5 cycles	21.3000	1.3300	0.5330	0.0341	0.9880	2754	143	3151	60	3415	16
10 cycles	20.5000	1.2100	0.5250	0.0310	0.9900	2722	131	3115	57	3379	13
15 cycles	20.6000	1.1800	0.5280	0.0296	0.9800	2732	125	3118	55	3378	18
20 cycles	19.8000	1.0700	0.4990	0.0264	0.9870	2611	113	3081	52	3403	14
25 cycles	21.6000	1.4200	0.5450	0.0367	0.9470	2806	153	3168	64	3406	34
30 cycles	21.1000	1.2800	0.5330	0.0327	0.9630	2752	137	3143	59	3403	26
35 cycles	21.4000	1.2700	0.5510	0.0332	0.9810	2831	138	3156	58	3369	18
40 cycles	20.4000	1.3200	0.5240	0.0336	0.9840	2718	142	3109	63	3373	18
45 cycles	19.5000	1.1100	0.5070	0.0280	0.9640	2645	120	3067	55	3357	24
50 cycles	20.7000	1.3500	0.5320	0.0327	0.9790	2751	137	3126	63	3376	21
55 cycles	20.8000	1.3600	0.5290	0.0350	0.9630	2736	148	3131	63	3395	28
60 cycles	20.6000	1.2000	0.5230	0.0304	0.9890	2711	129	3121	57	3397	13
65 cycles	20.8000	1.3200	0.5370	0.0325	0.9540	2770	136	3127	62	3365	30
70 cycles	21.0000	1.2400	0.5340	0.0317	0.9850	2760	133	3139	57	3392	16
75 cycles	19.8000	1.1200	0.5060	0.0294	0.9690	2641	126	3084	55	3387	22
80 cycles	20.0000	1.1900	0.5130	0.0291	0.9850	2671	124	3092	58	3378	16
85 cycles	20.1000	1.1700	0.5080	0.0288	0.9980	2647	123	3096	56	3401	6
90 cycles	19.3000	1.1200	0.4990	0.0286	0.9840	2608	123	3058	56	3368	16
95 cycles	18.9000	1.1600	0.4940	0.0293	0.9730	2589	126	3039	59	3351	22
MK_1069m_2_depth_profile	8.2800	0.7600	0.4030	0.0270	0.7740	2181	124	2262	83	2336	100
5 cycles	10.0000	0.8370	0.4420	0.0225	0.2510	2357	101	2436	77	2502	145
10 cycles	9.0400	0.6440	0.3980	0.0178	0.8730	2159	82	2342	65	2506	65
15 cycles	9.0400	0.7100	0.4310	0.0206	0.9060	2310	93	2342	72	2369	69

20 cycles	10.3000	0.7150	0.4430	0.0262	0.8300	2366	117	2464	64	2547	65
25 cycles	11.3000	0.5460	0.4810	0.0347	0.7880	2534	151	2549	45	2561	76
30 cycles	10.2000	0.6670	0.4440	0.0216	0.7600	2369	97	2451	61	2520	72
35 cycles	10.3000	0.5880	0.4530	0.0209	0.9340	2408	93	2461	53	2506	36
40 cycles	10.3000	0.6520	0.4560	0.0234	0.5310	2423	103	2462	59	2495	95
45 cycles	11.4000	0.5100	0.4820	0.0330	0.8590	2538	144	2554	42	2566	63
50 cycles	12.1000	0.7930	0.4890	0.0267	0.8720	2564	116	2612	62	2648	54
55 cycles	12.0000	0.6730	0.4810	0.0271	0.9890	2532	118	2606	53	2664	14
60 cycles	13.4000	0.6110	0.5110	0.0263	0.8830	2662	112	2710	43	2746	40
65 cycles	13.3000	0.5790	0.5200	0.0253	0.9510	2700	107	2700	41	2700	25
70 cycles	12.2000	0.7930	0.4730	0.0314	0.8440	2498	137	2620	61	2717	61
75 cycles	13.0000	0.7690	0.5010	0.0275	0.8610	2618	118	2679	56	2726	50
80 cycles	12.5000	0.5230	0.5040	0.0308	0.6210	2632	132	2640	39	2646	80
85 cycles	13.8000	0.7330	0.5420	0.0346	0.9650	2793	145	2737	50	2696	31
90 cycles	12.9000	0.6890	0.4890	0.0236	0.7590	2568	102	2674	50	2754	59
95 cycles	13.3000	1.0200	0.5070	0.0360	0.7550	2645	154	2703	73	2747	86
MK_1069m_3_depth_profile	18.5000	1.4700	0.5300	0.0470	0.9630	2741	198	3016	76	3205	39
5 cycles	18.8000	1.7500	0.5560	0.0537	0.9630	2848	223	3032	90	3157	41
10 cycles	17.9000	1.6000	0.5530	0.0475	0.8840	2836	197	2984	86	3086	68
15 cycles	16.9000	1.0300	0.5020	0.0196	0.8550	2622	84	2928	59	3145	55
20 cycles	18.5000	0.9890	0.5320	0.0387	0.8110	2748	163	3015	52	3199	68
25 cycles	20.9000	2.6700	0.6410	0.0736	0.9770	3191	289	3134	124	3097	46
30 cycles	18.6000	1.0800	0.5770	0.0366	0.5600	2935	150	3021	56	3079	91
35 cycles	19.5000	0.8100	0.5750	0.0225	0.8770	2927	92	3066	40	3159	32
40 cycles	20.1000	1.5900	0.6140	0.0511	0.9700	3084	204	3097	76	3104	33
45 cycles	19.4000	1.1400	0.5830	0.0226	0.7480	2963	92	3062	57	3128	63
50 cycles	22.0000	2.2200	0.6560	0.0802	0.9460	3250	312	3184	98	3142	67
55 cycles	20.8000	1.3800	0.6010	0.0387	0.8830	3033	156	3130	64	3193	50
60 cycles	20.5000	0.7470	0.5990	0.0219	0.9510	3026	88	3114	35	3171	18
65 cycles	21.4000	1.5700	0.6540	0.0526	0.9490	3242	205	3159	71	3106	41
70 cycles	21.3000	1.6800	0.6040	0.0415	0.8700	3045	167	3152	77	3221	61
75 cycles	19.8000	0.9540	0.5770	0.0251	0.9520	2936	102	3082	47	3179	24
80 cycles	20.8000	2.0800	0.5810	0.0431	0.7740	2954	176	3130	97	3245	100
85 cycles	20.2000	1.3000	0.5900	0.0264	0.8780	2988	107	3102	62	3177	52
90 cycles	21.5000	1.2300	0.6250	0.0426	0.9470	3131	169	3163	55	3183	37
95 cycles	20.2000	0.8330	0.5830	0.0181	0.9190	2960	74	3102	40	3195	28
MK_1069m_4_depth_profile	23.6000	1.5600	0.6080	0.0374	0.9350	3060	150	3253	64	3374	36

5 cycles	23.5000	1.4300	0.5850	0.0352	0.9460	2970	143	3247	59	3423	31
10 cycles	24.2000	1.5800	0.6150	0.0348	0.9470	3090	139	3276	64	3392	34
15 cycles	22.4000	1.2500	0.5800	0.0340	0.9510	2948	139	3201	54	3363	28
20 cycles	23.2000	1.1200	0.5830	0.0278	0.9770	2961	113	3234	47	3408	16
25 cycles	25.9000	1.6700	0.6470	0.0415	0.9830	3217	162	3342	63	3418	19
30 cycles	25.0000	1.5700	0.6160	0.0363	0.9470	3095	145	3307	61	3438	32
35 cycles	25.0000	1.6600	0.6260	0.0386	0.9770	3135	153	3307	65	3412	23
40 cycles	24.1000	1.3300	0.6050	0.0362	0.9710	3050	146	3271	54	3409	23
45 cycles	25.1000	1.5900	0.6310	0.0413	0.9820	3153	163	3311	62	3409	19
50 cycles	24.5000	1.4100	0.6200	0.0341	0.9560	3110	136	3288	56	3398	26
55 cycles	24.8000	1.6000	0.6150	0.0397	0.9140	3090	158	3299	63	3428	42
60 cycles	24.4000	1.4400	0.6130	0.0367	0.9810	3081	147	3284	58	3411	18
65 cycles	23.8000	1.3900	0.6030	0.0372	0.9680	3043	149	3260	57	3397	24
70 cycles	24.1000	1.4300	0.5910	0.0372	0.9340	2993	151	3272	58	3448	35
75 cycles	25.3000	1.8800	0.6380	0.0420	0.9860	3181	165	3320	73	3405	23
80 cycles	24.5000	1.5000	0.6120	0.0359	0.9660	3080	143	3290	60	3421	25
85 cycles	25.1000	1.5500	0.6260	0.0382	0.9840	3133	152	3313	60	3423	17
90 cycles	24.9000	1.7400	0.6320	0.0417	0.9510	3159	165	3305	68	3395	34
95 cycles	24.1000	1.4400	0.6000	0.0371	0.9820	3030	149	3274	58	3426	18
100 cycles	24.3000	1.7700	0.6210	0.0443	0.9980	3114	176	3280	71	3383	7
105 cycles	24.8000	1.5400	0.6240	0.0388	0.9820	3126	154	3300	61	3408	18
110 cycles	24.8000	1.6300	0.6120	0.0370	0.9680	3080	148	3302	64	3439	26
115 cycles	24.7000	1.3500	0.6210	0.0353	0.9610	3113	140	3296	54	3409	24
120 cycles	23.9000	1.3700	0.6080	0.0334	0.9500	3061	134	3263	56	3389	28
125 cycles	24.9000	1.7000	0.6250	0.0404	0.9790	3129	160	3304	67	3411	22
130 cycles	23.6000	1.4100	0.5890	0.0360	0.9180	2986	146	3250	58	3418	38
135 cycles	23.9000	1.6700	0.6010	0.0417	0.9760	3035	168	3266	68	3410	24
140 cycles	23.3000	1.2700	0.5900	0.0312	0.9730	2991	126	3238	53	3395	19
145 cycles	24.0000	1.5000	0.6180	0.0426	0.9510	3103	170	3267	61	3370	34
150 cycles	24.7000	1.4500	0.6230	0.0355	0.9620	3120	141	3295	57	3403	25
155 cycles	22.6000	1.1900	0.5710	0.0318	0.9720	2912	131	3211	51	3404	20
160 cycles	23.9000	1.3200	0.5970	0.0335	0.9840	3016	135	3263	54	3419	16
165 cycles	24.2000	1.3900	0.6070	0.0358	0.8860	3057	144	3275	56	3412	43
170 cycles	22.4000	1.4200	0.5600	0.0363	0.9960	2866	150	3200	62	3417	9
175 cycles	23.8000	1.7000	0.6030	0.0414	0.9790	3042	166	3261	70	3398	23
180 cycles	23.3000	1.4000	0.5950	0.0376	0.9360	3008	152	3239	59	3385	35
185 cycles	22.5000	1.2300	0.5640	0.0300	0.9670	2884	124	3207	53	3416	22

190 cycles	23.3000	1.5200	0.5880	0.0391	0.9880	2980	159	3241	64	3406	16
195 cycles	23.5000	1.3900	0.5910	0.0362	0.9930	2995	147	3246	58	3405	11
200 cycles	22.3000	1.1700	0.5640	0.0337	0.9470	2884	139	3195	51	3397	31
205 cycles	21.8000	1.3100	0.5530	0.0356	0.9690	2837	148	3173	59	3393	25
210 cycles	23.1000	1.3600	0.5800	0.0328	0.9900	2948	134	3232	57	3413	13
215 cycles	22.6000	1.2700	0.5670	0.0317	0.9810	2896	130	3209	55	3411	17
220 cycles	22.7000	1.4600	0.5690	0.0368	0.9850	2904	151	3214	63	3414	17
225 cycles	22.3000	1.2200	0.5490	0.0300	0.9530	2821	125	3196	53	3440	26
230 cycles	22.4000	1.4200	0.5610	0.0373	0.9910	2870	154	3199	62	3412	14
235 cycles	21.6000	1.2000	0.5540	0.0317	0.9500	2840	132	3166	54	3379	28
240 cycles	21.4000	1.1600	0.5430	0.0303	0.9560	2795	127	3155	53	3393	26
245 cycles	21.0000	1.0900	0.5280	0.0258	0.9440	2733	109	3137	51	3406	27
250 cycles	21.0000	1.1000	0.5380	0.0300	0.9170	2776	126	3140	51	3382	35
255 cycles	21.4000	1.1800	0.5420	0.0284	0.9880	2790	119	3157	54	3400	14
260 cycles	21.7000	1.1200	0.5490	0.0282	0.9870	2823	117	3170	50	3398	13
265 cycles	21.4000	1.1300	0.5410	0.0271	0.9520	2786	113	3158	51	3403	25
270 cycles	20.9000	1.1400	0.5340	0.0296	0.9760	2758	124	3135	53	3385	19
275 cycles	21.9000	1.2500	0.5510	0.0304	0.9900	2828	127	3178	55	3407	13
280 cycles	21.9000	1.5200	0.5550	0.0361	0.9630	2846	150	3177	67	3394	29
285 cycles	20.7000	1.1700	0.5340	0.0303	0.9260	2758	127	3124	55	3368	34
290 cycles	22.0000	1.1700	0.5570	0.0295	0.9780	2854	122	3184	52	3398	17
295 cycles	22.0000	1.3300	0.5520	0.0317	0.9680	2835	132	3183	59	3410	24
MK_1069m_5_depth_profile	19.8000	1.1200	0.5010	0.0278	0.9890	2617	119	3080	55	3397	13
5 cycles	20.3000	1.1500	0.5170	0.0294	0.9910	2687	125	3104	55	3386	12
10 cycles	20.3000	1.2500	0.5110	0.0297	0.9910	2659	127	3106	60	3410	13
15 cycles	20.5000	1.1100	0.5230	0.0280	0.9940	2711	119	3113	52	3384	10
20 cycles	20.7000	1.3800	0.5180	0.0326	0.9770	2689	139	3125	65	3419	22
25 cycles	20.3000	1.1600	0.5110	0.0293	0.9860	2662	125	3105	55	3405	15
30 cycles	21.4000	1.2000	0.5360	0.0322	0.9770	2765	135	3156	54	3415	20
35 cycles	20.2000	1.1000	0.5170	0.0279	0.9670	2686	119	3100	53	3380	22
40 cycles	21.2000	1.2300	0.5290	0.0307	0.9660	2736	130	3146	57	3419	24
45 cycles	20.4000	1.0900	0.5200	0.0265	0.9750	2701	112	3112	51	3389	18
50 cycles	20.5000	1.0700	0.5180	0.0263	0.9740	2689	112	3114	51	3401	19
55 cycles	20.6000	1.0700	0.5190	0.0277	0.9030	2697	118	3119	51	3404	36
60 cycles	21.5000	1.2000	0.5420	0.0295	0.9460	2790	123	3160	54	3404	28
65 cycles	20.6000	1.0000	0.5250	0.0262	0.9680	2721	111	3118	47	3386	20
70 cycles	20.9000	1.0800	0.5310	0.0271	0.9750	2745	114	3134	50	3394	18

75 cycles	20.8000	1.1200	0.5260	0.0281	0.9970	2725	119	3130	52	3401	7
80 cycles	21.5000	1.1500	0.5450	0.0287	0.9930	2805	120	3160	52	3394	10
85 cycles	21.5000	1.0700	0.5370	0.0266	0.9920	2769	112	3161	48	3420	10
90 cycles	21.3000	1.0800	0.5470	0.0273	0.9760	2811	114	3152	49	3377	17
95 cycles	21.8000	1.1300	0.5520	0.0273	0.9810	2832	113	3176	50	3402	16
100 cycles	21.8000	1.2800	0.5490	0.0310	0.9810	2819	129	3174	57	3407	18
105 cycles	22.4000	1.1400	0.5650	0.0283	0.9540	2889	116	3200	50	3401	24
110 cycles	21.3000	1.1100	0.5400	0.0277	0.9510	2781	116	3152	51	3398	25
115 cycles	22.5000	1.2000	0.5680	0.0308	0.9540	2899	127	3207	52	3406	26
120 cycles	21.7000	1.2700	0.5510	0.0289	0.9720	2830	120	3170	57	3392	23
125 cycles	21.6000	1.1000	0.5450	0.0289	0.9900	2803	120	3168	50	3407	12
130 cycles	21.8000	1.0700	0.5500	0.0272	0.9680	2823	113	3173	48	3403	19
135 cycles	21.4000	0.9810	0.5390	0.0261	0.9560	2779	109	3158	44	3408	22
140 cycles	22.0000	1.3000	0.5520	0.0284	0.9690	2832	118	3182	58	3410	25
145 cycles	21.4000	1.2600	0.5500	0.0324	0.9160	2826	135	3158	57	3376	38
150 cycles	21.0000	1.0900	0.5300	0.0250	0.9680	2743	105	3138	51	3401	21
155 cycles	20.8000	1.2300	0.5250	0.0333	0.9920	2721	141	3127	57	3400	14
160 cycles	21.0000	1.0800	0.5270	0.0274	0.9910	2727	116	3138	50	3413	11
165 cycles	21.8000	1.1800	0.5470	0.0298	0.9820	2812	124	3173	53	3410	16
170 cycles	21.0000	1.0900	0.5300	0.0269	0.9680	2742	113	3136	50	3399	20
175 cycles	21.7000	1.2900	0.5530	0.0309	0.9740	2839	128	3171	58	3389	21
180 cycles	21.1000	1.1400	0.5360	0.0277	0.9430	2767	116	3141	52	3390	28
185 cycles	21.7000	1.1000	0.5460	0.0292	0.9780	2809	122	3169	50	3405	18
190 cycles	22.2000	1.5600	0.5660	0.0387	0.9730	2890	159	3191	68	3386	25
195 cycles	21.9000	1.4600	0.5480	0.0336	0.9760	2818	140	3179	65	3415	24
200 cycles	22.6000	1.3900	0.5640	0.0323	0.9670	2884	133	3211	60	3421	25
VD_INL_10@2.ais	4.4160	0.7970	0.2974	0.0331	0.5648	1679	164	1715	149	1761	273
block 2	4.2960	0.7480	0.2591	0.0281	0.5679	1485	144	1693	143	1960	256
block 3	5.2730	0.7510	0.3150	0.0347	0.6336	1765	170	1864	122	1977	200
block 4	4.4900	0.6190	0.2621	0.0273	0.5918	1501	139	1729	114	2018	201
block 5	5.7540	0.6320	0.2680	0.0275	0.6556	1531	140	1940	95	2409	150
block 6	5.2380	0.7320	0.2866	0.0299	0.6088	1624	150	1859	119	2132	197
block 7	5.4970	0.6610	0.2938	0.0304	0.6539	1660	152	1900	103	2173	164
block 8	5.0990	0.6520	0.2815	0.0286	0.6221	1599	144	1836	109	2116	180
block 9	5.0370	0.5440	0.2595	0.0259	0.6535	1487	133	1826	91	2237	150
block 10	6.4550	0.7480	0.3095	0.0319	0.6814	1738	157	2040	102	2360	151
block 11	5.3870	0.6630	0.2833	0.0284	0.6256	1608	143	1883	105	2201	172

block 12	4.3850	0.5430	0.2581	0.0249	0.5952	1480	128	1710	102	2004	181
block 13	5.9700	0.8600	0.3041	0.0324	0.6076	1712	160	1971	125	2256	200
block 14	5.8990	0.6400	0.2868	0.0291	0.6571	1625	146	1961	94	2337	149
block 15	6.2430	0.7090	0.3314	0.0352	0.6881	1845	170	2010	99	2185	151
block 16	5.5670	0.6120	0.2957	0.0302	0.6844	1670	150	1911	95	2184	147
block 17	5.2810	0.7110	0.2849	0.0294	0.5868	1616	147	1866	115	2157	195
block 18	5.3980	0.5800	0.2829	0.0282	0.6502	1606	142	1885	92	2207	151
block 19	5.9690	0.6540	0.3157	0.0323	0.6659	1769	158	1971	95	2191	151
block 20	5.8370	0.6270	0.2995	0.0300	0.6800	1689	149	1952	93	2244	144
block 21	6.0740	0.6920	0.3031	0.0305	0.6425	1707	151	1987	99	2292	157
block 22	6.4390	0.6850	0.3134	0.0314	0.6686	1757	154	2038	94	2335	144
block 23	6.5600	0.6690	0.3054	0.0293	0.6803	1718	145	2054	90	2410	135
block 24	7.4820	0.8460	0.3702	0.0381	0.7437	2030	179	2171	101	2306	134
block 25	6.9820	0.7090	0.3353	0.0321	0.7074	1864	155	2109	90	2358	129
block 26	6.8430	0.7010	0.3275	0.0317	0.7322	1826	154	2091	91	2364	125
block 27	7.9290	0.8540	0.3915	0.0402	0.7774	2130	186	2223	97	2310	121
block 28	6.4310	0.6350	0.2944	0.0264	0.6878	1664	131	2036	87	2439	127
block 29	7.2050	0.7320	0.3383	0.0315	0.7122	1879	152	2137	91	2396	126
block 30	8.8270	0.9330	0.3718	0.0368	0.7859	2038	173	2320	96	2579	112
block 31	8.1350	0.7790	0.3225	0.0288	0.7161	1802	140	2246	87	2680	116
block 32	7.4530	0.6850	0.3237	0.0283	0.7107	1808	138	2167	82	2528	115
block 33	7.3300	0.7870	0.3396	0.0303	0.6952	1885	146	2152	96	2418	133
block 34	8.4780	0.8070	0.3628	0.0323	0.7468	1995	153	2284	87	2553	110
block 35	8.8150	0.8010	0.3575	0.0312	0.7467	1970	148	2319	83	2642	105
block 36	7.4520	0.6800	0.3566	0.0302	0.7189	1966	143	2167	82	2363	113
block 37	8.4190	0.7620	0.3479	0.0296	0.7323	1925	141	2277	82	2611	107
block 38	8.4830	0.7590	0.3563	0.0306	0.7630	1965	145	2284	81	2584	101
block 39	8.1180	0.6860	0.3297	0.0267	0.7138	1837	129	2244	76	2640	104
block 40	9.1960	0.8600	0.3836	0.0335	0.7745	2093	156	2358	86	2595	102
block 41	8.3730	0.7390	0.3651	0.0303	0.7305	2006	143	2272	80	2521	106
block 42	7.6300	0.6720	0.3495	0.0282	0.7287	1932	135	2188	79	2438	106
block 43	9.0800	0.7650	0.3633	0.0295	0.7518	1998	139	2346	77	2665	97
block 44	8.7840	0.7210	0.3375	0.0263	0.7364	1874	127	2316	75	2732	96
block 45	10.2300	0.8860	0.3866	0.0324	0.7930	2107	151	2456	80	2759	90
block 46	8.8560	0.7000	0.3520	0.0268	0.7295	1944	128	2323	72	2675	95
block 47	9.3280	0.7570	0.3557	0.0275	0.7470	1962	131	2371	74	2744	93
block 48	9.4030	0.7710	0.3700	0.0290	0.7743	2029	136	2378	75	2692	89

block 49	9.3090	0.7390	0.3612	0.0274	0.7567	1988	130	2369	73	2715	89
block 50	9.1540	0.7270	0.3762	0.0285	0.7529	2058	133	2353	73	2620	91
block 51	9.2370	0.7170	0.3702	0.0277	0.7580	2030	130	2362	71	2662	88
block 52	9.9260	0.8140	0.4037	0.0318	0.7922	2186	146	2428	76	2637	86
block 53	9.6760	0.7530	0.3789	0.0285	0.7691	2071	133	2404	72	2700	86
block 54	8.8180	0.6660	0.3737	0.0272	0.7520	2047	128	2319	69	2569	87
block 55	10.2800	0.8360	0.3992	0.0309	0.7947	2165	143	2460	75	2714	84
block 56	9.8230	0.7520	0.3806	0.0282	0.7704	2079	132	2418	71	2718	84
block 57	9.5370	0.7360	0.3875	0.0287	0.7777	2111	133	2391	71	2639	84
block 58	10.0100	0.7520	0.3733	0.0270	0.7678	2045	127	2436	69	2781	82
block 59	9.6780	0.7120	0.3650	0.0260	0.7617	2006	123	2405	68	2762	82
block 60	9.4500	0.7090	0.3836	0.0278	0.7633	2093	130	2383	69	2641	84
block 61	9.7280	0.7540	0.4101	0.0305	0.7844	2215	139	2409	71	2578	84
block 62	10.1300	0.7570	0.3757	0.0272	0.7737	2056	128	2447	69	2790	81
block 63	9.2190	0.6850	0.3776	0.0271	0.7764	2065	127	2360	68	2626	81
block 64	9.4040	0.6800	0.3755	0.0260	0.7449	2055	122	2378	66	2668	84
block 65	10.3900	0.7640	0.3851	0.0273	0.7628	2100	127	2470	68	2791	82
block 66	8.9090	0.6960	0.3931	0.0289	0.7872	2137	134	2329	71	2501	84
block 67	9.4330	0.6620	0.3638	0.0247	0.7397	2000	117	2381	64	2725	82
block 68	9.3820	0.6720	0.3737	0.0259	0.7606	2047	122	2376	66	2672	81
block 69	9.1800	0.6950	0.3825	0.0273	0.7725	2088	127	2356	69	2597	83
block 70	10.1400	0.7300	0.3835	0.0266	0.7601	2092	124	2448	67	2758	80
block 71	9.7520	0.7310	0.4053	0.0290	0.7868	2194	133	2412	69	2601	80
block 72	9.8710	0.6960	0.3838	0.0262	0.7632	2094	122	2423	65	2712	79
block 73	10.1700	0.7420	0.4054	0.0287	0.7933	2194	132	2451	67	2671	77
block 74	10.3400	0.7740	0.3978	0.0286	0.8004	2159	132	2466	69	2729	76
block 75	11.2700	0.8760	0.4391	0.0331	0.8272	2347	148	2546	72	2709	74
block 76	11.1400	0.8060	0.4131	0.0291	0.7944	2229	133	2535	68	2790	75
block 77	11.1300	0.8580	0.4365	0.0328	0.8299	2335	147	2534	72	2697	73
block 78	10.3900	0.7500	0.4030	0.0283	0.7952	2183	130	2470	67	2715	75
block 79	10.2900	0.7270	0.3996	0.0272	0.7722	2167	125	2462	65	2714	77
block 80	10.9300	0.7900	0.4127	0.0291	0.8022	2227	133	2517	67	2760	74
block 81	11.2300	0.8340	0.4421	0.0320	0.8124	2360	143	2542	69	2691	74
block 82	11.3500	0.8490	0.4434	0.0323	0.8106	2366	144	2552	70	2704	75
block 83	10.8100	0.7910	0.4228	0.0299	0.8075	2273	136	2507	68	2702	74
block 84	11.4900	0.8400	0.4286	0.0302	0.7987	2300	136	2564	68	2780	75
block 85	11.4100	0.8450	0.4395	0.0316	0.8172	2348	141	2557	69	2727	73

block 86	10.1600	0.6950	0.3972	0.0264	0.7677	2156	122	2450	63	2703	76
block 87	10.9700	0.7820	0.4215	0.0291	0.7904	2267	132	2520	66	2731	75
block 88	10.4400	0.7090	0.3923	0.0259	0.7580	2133	120	2475	63	2768	76
block 89	12.5100	0.9900	0.4877	0.0376	0.8496	2561	163	2644	74	2708	71
block 90	10.3000	0.7160	0.4093	0.0273	0.7680	2212	125	2462	64	2676	77
block 91	10.8200	0.7850	0.4362	0.0306	0.7972	2333	137	2508	67	2653	75
block 92	11.2200	0.7850	0.4261	0.0290	0.7864	2288	131	2541	65	2750	74
block 93	11.9900	0.8910	0.4506	0.0327	0.8241	2398	145	2604	70	2768	72
block 94	10.3700	0.7140	0.3972	0.0264	0.7795	2156	122	2468	64	2736	74
block 95	10.9300	0.7570	0.4268	0.0287	0.7787	2291	130	2517	64	2705	75
block 96	10.5300	0.7280	0.4108	0.0276	0.7831	2219	126	2482	64	2706	74
VD_INL_11@1.ais	10.4300	0.4410	0.3895	0.0147	0.9663	2121	68	2474	39	2778	19
VD_INL_11@2.ais	14.9800	0.4350	0.5034	0.0140	0.9846	2628	60	2814	28	2950	8
VD_INL_11@3.ais	16.0500	0.6070	0.5296	0.0193	0.9890	2740	81	2880	36	2979	9
VD_INL_11@4.ais	16.2800	0.7740	0.5360	0.0243	0.9833	2767	102	2894	46	2983	14
VD_INL_11@5.ais	13.9100	0.4010	0.4732	0.0136	0.9796	2498	59	2743	27	2930	9
VD_INL_11@6.ais	15.2100	0.5290	0.5165	0.0178	0.9895	2684	76	2828	33	2933	8
VD_INL_11@7.ais	12.2900	0.4730	0.4443	0.0176	0.9810	2370	79	2627	36	2831	13

VD - Vredefort impact: INL are grains from drill core of Kamo et al. (1996). G are grains from granophyre.

MK - Morokweng impact: 1069 m denotes from which part of drill core M3 the grains were extracted.

7.7 Appendix 7

Table 7.7.1 - Raw (U-Th)/He data for Morokweng, Vredefort and Popigai impact structures.

Sample	mineral	Age, Ma	err., Ma	U (ppm)	Th (ppm)	147Sm (ppm)	[U]e	Th/U	He (nmol/g)	mass (ug)	Ft	ESR
zMKB-1	zircon	163.4	13.07	998.3	31.2	0.3	1005.5	0.03	620.8	3.35	0.70	36.15
zMKB-11	zircon	266.3	21.31	976.8	42.8	0.4	986.6	0.04	926.2	1.96	0.65	30.47
zMKB-14	zircon	151.1	12.09	1090.5	91.7	0.5	1111.7	0.08	651.8	3.08	0.71	39.07
zMKB-15	zircon	132.1	10.57	1422.1	71.2	0.5	1438.5	0.05	787.0	5.97	0.76	47.77
zMKB-16	zircon	132.6	10.61	1277.9	338.9	0.6	1355.9	0.27	786.7	11.73	0.80	60.04

zMKB-2	zircon	142.3	11.39	137.7	8.7	0.5	139.7	0.06	63.4	0.83	0.59	25.62
zMKB-4	zircon	543.5	43.48	173.3	29.3	0.7	180.0	0.17	353.0	1.31	0.65	31.31
zMKB-5	zircon	151.5	12.12	2020.9	89.6	0.8	2041.5	0.04	1076.6	1.24	0.64	30.06
zMKB-7	zircon	144.6	11.56	1561.1	231.4	1.1	1614.3	0.15	958.8	5.60	0.76	46.76
zMKB-9	zircon	137.6	11.01	356.6	93.2	0.4	378.1	0.26	199.2	2.67	0.70	38.27
zPG39-1	zircon	37.3	2.98	169.2	68.8	1.7	185.0	0.41	28.6	4.90	0.77	49.78
zPG39-2	zircon	32.7	2.62	285.9	55.6	0.7	298.7	0.19	40.2	4.52	0.76	48.22
zPG39-3	zircon	35.4	2.83	200.2	63.2	1.1	214.8	0.32	33.0	7.84	0.80	59.49
zPG39-5	zircon	31.8	2.55	147.9	28.2	0.3	154.4	0.19	19.5	2.94	0.73	42.77
zPG39-7	zircon	30.9	2.47	126.4	197.3	2.9	171.9	1.56	23.3	9.81	0.81	64.06
zPG39-8	zircon	35.6	2.85	165.5	33.9	0.7	173.3	0.20	27.1	9.46	0.81	63.13
zPG7407K-1	zircon	34.6	2.77	147.8	15.2	0.7	151.3	0.10	22.9	9.28	0.81	61.36
zPG7407K-2	zircon	35.1	2.81	151.6	9.5	0.8	153.8	0.06	23.8	9.34	0.82	62.86
zPG7407K-3	zircon	67.0	5.36	66.8	3.9	0.4	67.7	0.06	18.6	3.74	0.76	46.48
zPG7407W-1	zircon	33.1	2.65	238.7	91.0	0.5	259.7	0.38	37.1	7.64	0.80	58.27
zPG7407W-2	zircon	36.1	2.89	899.7	70.9	0.8	916.0	0.08	137.9	4.74	0.77	50.16
zPG7407W-4	zircon	35.0	2.80	197.7	27.1	0.5	203.9	0.14	32.9	20.70	0.85	81.28
zPG7407W-5	zircon	35.7	2.85	85.9	51.8	1.0	97.9	0.60	16.1	21.50	0.85	82.77
zPG7407W-6	zircon	30.9	2.47	422.0	142.6	1.0	454.8	0.34	61.2	8.79	0.80	60.50
zVDPB-1	zircon	117.2	9.37	381.9	224.3	4.9	433.6	0.59	181.0	1.60	0.66	32.80
zVDPB-12	zircon	300.8	24.06	318.4	68.8	10.0	334.3	0.22	397.3	3.23	0.72	40.50
zVDPB-13	zircon	364.4	29.15	414.1	68.2	8.5	429.9	0.16	644.5	4.32	0.75	44.93
zVDPB-14	zircon	391.3	31.31	209.7	51.5	3.8	221.6	0.25	355.6	4.00	0.74	44.52
zVDPB-16	zircon	254.9	20.39	308.9	156.4	5.1	345.0	0.51	327.4	2.54	0.68	35.58
zVDPB-19	zircon	188.0	15.04	362.7	149.6	18.5	397.3	0.41	302.7	4.78	0.74	45.00
zVDPB-3	zircon	156.6	12.53	264.1	116.5	2.1	290.9	0.44	158.5	1.20	0.64	30.91
zVDPB-5	zircon	156.6	12.53	407.7	155.5	31.3	443.7	0.38	271.0	3.25	0.72	40.34
zVDPB-6	zircon	300.4	24.04	199.3	72.9	4.4	216.1	0.37	258.0	3.12	0.72	41.54
zVDPB-7	zircon	567.8	45.42	43.6	9.1	3.7	45.8	0.21	101.0	2.25	0.70	37.08
zVDPB-8	zircon	253.0	20.24	309.0	138.2	3.3	340.9	0.45	317.4	2.01	0.67	34.52
zVDPB-9	zircon	225.6	18.05	207.9	66.7	8.0	223.3	0.32	181.3	1.57	0.66	32.69
zUTFCT2-15	zircon	25.8	2.06	160.9	81.3	0.7	179.6	0.51	20.5	12.10	0.82	65.77
zUTFCT2-16	zircon	30.9	2.47	166.6	77.1	0.4	184.3	0.46	24.3	7.43	0.79	55.31

MK - Morokweng impact: B denotes the brecciated basement of drill core M3.

PG - Popigai impact: 39 denotes sample from Rassokha river, 7407K & W are samples of shocked gneiss.

VD - Vredefort impact: PB denotes pseudotachylite breccia.

Uncertainty (2σ) is 8% (as deduced from measurement of FCT zircon).

[U]e: is the effective uranium concentration (effectively U and Th turned into U).

Ft: is the ejection correction (for ejected alphas - geometric correction).

ESR: is the equivalent spherical radius of the zircon grains.

8. References

Abbott, S.S., Harrison, T.M., Schmitt, A.K., and Mojzsis, S.J., 2012, A search for thermal excursions from ancient extraterrestrial impacts using Hadean zircon Ti-U-Th-Pb depth profiles: Proceedings of the National Academy of Sciences of the United States of America, v. 109, p. 13486–92.

Abramov, O., 2004, Numerical modeling of an impact-induced hydrothermal system at the Sudbury crater: Journal of Geophysical Research, v. 109, p. E10007.

Abramov, O., and Kring, D.A., 2005, Impact-induced hydrothermal activity on early Mars: Journal of Geophysical Research, v. 110, p. E12S09.

Abramov, O., Kring, D.A., and Mojzsis, S.J., 2013, The impact environment of the Hadean Earth: Chemie der Erde - Geochemistry, v. 73, p. 227–248.

Abramov, O., and Mojzsis, S.J., 2009, Microbial habitability of the Hadean Earth during the late heavy bombardment.: Nature, v. 459, p. 419–22.

Ahrens, T.J., 1993, Impact erosion of terrestrial planteray atmospheres: Annual Review of Astronomy and Astrophysics, v. 21, p. 525–555.

Aikman, A.B., 2007, Tectonics of the eastern Tethyan Himalaya: Australian National University.

Alexander, C.M.O., Bowden, R., Fogel, M.L., Howard, K.T., Herd, C.D.K., and Nittler, L.R., 2012, The provenances of asteroids, and their contributions to the volatile inventories of the terrestrial planets.: Science, v. 337, no. 6095, p. 721–3.

Andreoli, M.A.G., Ashwal, L.D., Hart, R.J., and Huizenga, J.M., 1999, Petrology and geochemistry of nickel and iridium-rich quartz norite from the late Jurassic Morokweng impact structure, South Africa (eds), 339 (1999: Geological Society of America Special Paper, v. 339, p. 91–108.

Andreoli, M.A.G., Hart, R.J., Cooper, G.R., and Webb, S.J., 2008, The Morokweng Impact Crater, South Africa: A Complex, Multiring Structure with a ~130 km Radius External Ring and Asymmetric Radial Sectors (R. L. Gibson & W. U. Reimold, Eds.): Special Papers - Geological Society of America,.

Barnes, S., and Fiorentini, M., 2008, Iridium, ruthenium and rhodium in komatiites: Evidence for iridium alloy saturation: Chemical Geology, v. 257, p. 44–58.

Barnosky, A.D., Matzke, N., Tomiya, S., Wogan, G.O.U., Swartz, B., Quental, T.B., Marshall, C., McGuire, J.L., Lindsey, E.L., Maquire, K.C., Mersey, B., and Ferrer, E.A., 2011, Has the Earth's sixth mass extinction already arrived?: Nature, v. 471, p. 51–57.

Bell, E.A., and Harrison, T.M., 2013, Post-Hadean transitions in Jack Hills zircon provenance: A signal of the Late Heavy Bombardment?: Earth and Planetary Science Letters, v. 364, p. 1–11.

Bjorkman, M., and Holsapple, K., 1987, Velocity scaling impact melt volume: International Journal of Impact Engineering, v. 5, p. 155–163.

Boehnke, P., Watson, E.B., Trail, D., Harrison, T.M., and Schmitt, A.K., 2013, Zircon saturation re-revisited: Chemical Geology, v. 351, p. 324–334.

Bottke, W.F., Vokrouhlický, D., Minton, D., Nesvorný, D., Morbidelli, A., Brasser, R., Simonson, B., and Levison, H.F., 2012, An Archaean heavy bombardment from a destabilized extension of the asteroid belt: Nature,, p. 5–8.

Bottomley, R., Grieve, R.A.F., York, D., and Masaitis, V., 1997, The age of the Popigai impact event and its relation to events at the Eocene/Oligocene boundary: Nature, v. 388, p. 365–368.

Brown, P.G., Assink, J.D., Astiz, L., Blaauw, R., Boslough, M.B., Borovička, J., Brachet, N., Brown, D., Campbell-Brown, M., Ceranna, L., Cooke, W., de Groot-Hedlin, C., Drob, D.P., Edwards, W., et al., 2013, A 500-kiloton airburst over Chelyabinsk and an enhanced hazard from small impactors.: Nature, v. 503, no. 7475, p. 238–41.

Burnham, A.D., and Berry, A.J., 2012, An experimental study of trace element partitioning between zircon and melt as a function of oxygen fugacity: Geochimica et Cosmochimica Acta, v. 95, p. 196–212.

Canup, R.M., and Asphaug, E., 2001, Origin of the Moon in a giant impact near the end of the Earth's formation.: Nature, v. 412, p. 708–12.

Cherniak, D.J., Hanchar, J.M., and Watson, E.B., 1997, Rare-earth diffusion in zircon: Chemical Geology, v. 134, p. 289–301.

Cherniak, D.J., Lanford, W.A., and Ryerson, F.J., 1991, Lead diffusion in apatite and zircon using ion implantation and Rutherford Backscattering techniques: Geochimica et Cosmochimica Acta, v. 55, p. 1663–1673.

Cherniak, D.J., and Watson, E.B., 2003, Diffusion in Zircon: Reviews in Mineralogy and Geochemistry, v. 53, p. 113–143.

Cherniak, D.J., and Watson, E.B., 2000, Pb diffusion in zircon: Chemical Geology, v. 172, p. 5–24.

Chyba, C., Thomas, P., and Zahnle, K., 1993, The 1908 Tunguska explosion: atmospheric disruption of a stony asteroid: Nature, v. 361, p. 40–44.

Clymer, A.K., Bice, D.M., and Montanari, A., 1996, Shocked quartz from the late Eocene : Impact evidence from Massignano , Italy Shocked quartz from the late Eocene : Impact evidence from Massignano , Italy: Geology, v. 24, p. 483–486.

Cohen, B.A., Swindle, T.D., and Kring, D.A., 2000, Support for the Lunar Cataclysm Hypothesis from Lunar Meteorite Impact Melt Ages: Science, v. 290, p. 1754–1756.

Collins, G., 2002, Hydrocode Simulations of Chicxulub Crater Collapse and Peak-Ring Formation: Icarus, v. 157, p. 24–33.

Collins, G.S., Melosh, H.J., and Osinski, G.R., 2012, The Impact-Cratering Process: Elements, v. 8, no. 1, p. 25–30.

Condie, K.C., 1984, Archean geotherms and supracrustal assemblages: Tectonophysics, v. 105, p. 29–41.

Corfu, F., Hanchar, J.M., and Hoskin, P.W.O., 2003, Atlas of Zircon Textures: Reviews in Mineralogy and Geochemistry, v. 53, p. 469–500.

Cox, R.A., Dunning, G.R., and Indares, A., 1998, Petrology and U – Pb geochronology of mafic , high-pressure , metamorphic coronites from the Tshenukutish domain , eastern Grenville Province: Precambrian Research, v. 90, p. 59–83.

Cronin, J.R., and Pizzarello, S., 1983, Amino acids in meteorites.: Advances in space research, v. 3, p. 5–18.

D'Hondt, S.L., Keller, G., and Stallard, R.F., 1987, Major element compositional variation within and between different late Eocene microtektite strewnfields: Meteoritics, v. 22, p. 61–79.

Dalrymple, G.B., and Ryder, G., 1993, Age Spectra of Apollo 15 Impact Melt Rocks by Laser Heating and Their Bearing on the History of Lunar Basin Formation: Journal of Geophysical Research, v. 98, p. 13,085–13,095.

Darling, J., Storey, C., and Hawkesworth, C., 2009, Impact melt sheet zircons and their implications for the Hadean crust: Geology, v. 37, no. 10, p. 927–930.

Davis, D.W., 2008, Sub-million-year age resolution of Precambrian igneous events by thermal extraction–thermal ionization mass spectrometer Pb dating of zircon: Application to crystallization of the Sudbury impact melt sheet: Geology, v. 36, p. 383–386.

Deconto, R.M., Pollard, D., Wilson, P.A., Pälike, H., Lear, C.H., and Pagani, M., 2008, Thresholds for Cenozoic bipolar glaciation.: Nature, v. 455, p. 652–656.

Dence, M.R., 1964, The Extraterrestrial Origin Of Canadian Craters: Annals of the New York Academy of Sciences, v. 123, p. 941–969.

Dyal, P., Parkin, C.W., and Daily, W.D., 1973a, Surface magnetometer experiments: Internal lunar Properties: Geochimica et Cosmochimica Acta, v. 3, p. 2925–2945.

Dyal, P., Parkin, C.W., and Daily, W.D., 1973b, Surface magnetometer experiments: Internal lunar Properties: Geochimica et Cosmochimica Acta, v. 3, p. 2925–2945.

Earth Impact Database, 2014, Planetary and Space Science Centre,.

Efron, B., 1979, Bootstrap method: another look at the jackknife:.

Erickson, T.M., Cavosie, A.J., Moser, D.E., Barker, I.R., and Radovan, H.A., 2013, Correlating planar microstructures in shocked zircon from the Vredefort Dome at multiple scales : Crystallographic modeling , external and internal imaging , and EBSD structural analysis: American Mineralogist, v. 98, p. 53–65.

Erwin, D.H., 2000, The permo-triassic extinction, *in* Shaking the Tree: Readings from Nature in the History of Life, p. 189.

Farley, K.A., Montanari, A., Shoemaker, E.M., and Shoemaker, C.S., 2005, Geochemical Evidence for a Comet Shower in the Late Eocene: Science, v. 280, p. 1250–1253.

Fassett, C.I., and Minton, D. a., 2013, Impact bombardment of the terrestrial planets and the early history of the Solar System: Nature Geoscience, v. 6, p. 520–524.

Ferry, J.M., and Watson, E.B., 2007, New thermodynamic models and revised calibrations for the Ti-in-zircon and Zr-in-rutile thermometers: Contributions to Mineralogy and Petrology, v. 154, no. 4, p. 429–437.

Finch, R.J., and Hanchar, J.M., 2003, Structure and Chemistry of Zircon and Zircon-Group Minerals: Reviews in Mineralogy and Geochemistry, v. 53, p. 1–25.

Floran, R.J., Grieve, R.A.F., Phinney, W.C., Warner, J.L., Simonds, C.H., Blanchard, D.P., and Dence, M.R., 1978, Manicouagan impact melt, Quebec, 1, Stratigraphy, petrology, and chemistry: Journal of Geophysical Research: Solid Earth, v. 83, p. 2737–2759.

French, B.M., 1966, Shock Metamorphism of Natural Materials: Science, v. 153, p. 903–906.

Gao, S., Luo, T.C., Zhang, B.R., Zhang, H.F., Han, Y.W., Zhao, Z.D., and Hu, Y.K., 1998, Chemical composition of the continental crust as revealed by studies in East China: Geochimica et Cosmochimica Acta, v. 62, p. 1959–1975.

Ghiorso, M.S., and Sack, R.O., 1995, Chemical mass transfer in magmatic processes IV . A revised and internally consistent thermodynamic model for the interpolation and extrapolation of liquid-solid equilibria in magmatic systems at elevated temperatures and pressures: Contributions to Mineralogy and Petrology, v. 119, p. 197–212.

Gibson, R.L., Armstrong, R.A., and Reimold, W.U., 1997, The age and thermal evolution of the Vredefort impact structure : A single-grain U-Pb zircon study F-q: Geochimica et Cosmochimica Acta, v. 61, p. 1531–1540.

Gibson, R.L., and Reimold, W.U., 2005, Shock pressure distribution in the Vredefort impact structure, South Africa: Large Meteorite Impacts, v. 3, p. 329–349.

Glass, B.P., 2002, Upper Eocene Impact Ejecta/Spherule Layers in Marine Sediments: Chemie der Erde - Geochemistry, v. 62, p. 173–196.

Glass, B.P., and Burns, C.A., 1987, Late Eocene crytal-bearing spherules: Two layers or one?: Meteoritics, v. 22, p. 265–279.

Glass, B.P., and Koeberl, C., 1999, Ocean Drilling Project Hole 689B spherules and upper Eocene microtektite and clinopyroxene-bearing spherule strewn fields: Meteoritics & Planetary Science, v. 34, p. 197–208.

Glass, B.P., Liu, S., and Montanari, A., 2004, Impact ejecta in upper Eocene deposits at Massignano, Italy: Meteoritics & Planetary Science, v. 39, p. 589–597.

Glass, B.P., and Simonson, B.M., 2012, Distal Impact Ejecta Layers: Spherules and More: Elements, v. 8, no. 1, p. 43–48.

Glass, B.. P., and Zwart, M.J., 1973, North American microtektites in Deep Sea Drilling Project cores from the Caribbean Sea and Gulf of Mexico: Geological Society of America Bulletin, v. 90, p. 595–602.

Gnos, E., Hofmann, B. a, Al-Kathiri, A., Lorenzetti, S., Eugster, O., Whitehouse, M.J., Villa, I.M., Jull, a J.T., Eikenberg, J., Spettel, B., Krähenbühl, U., Franchi, I. a, and Greenwood, R.C., 2004a, Pinpointing the source of a lunar meteorite: implications for the evolution of the Moon.: Science, v. 305, no. 5684, p. 657–9, doi: 10.1126/science.1099397.

Gnos, E., Hofmann, B. a, Al-Kathiri, A., Lorenzetti, S., Eugster, O., Whitehouse, M.J., Villa, I.M., Jull, a J.T., Eikenberg, J., Spettel, B., Krähenbühl, U., Franchi, I. a, and Greenwood, R.C., 2004b, Support for the Lunar Cataclysm Hypothesis from Lunar Meteorite Impact Melt Ages: Science, v. 305, p. 657–659.

Gomes, R., Levison, H.F., Tsiganis, K., and Morbidelli, a, 2005, Origin of the cataclysmic Late Heavy Bombardment period of the terrestrial planets.: Nature, v. 435, no. 7041, p. 466–9, doi: 10.1038/nature03676.

Grange, M.L., Pidgeon, R.T., Nemchin, A.A., Timms, N.E., and Meyer, C., 2013, Interpreting U–Pb data from primary and secondary features in lunar zircon: Geochimica et Cosmochimica Acta, v. 101, p. 112–132.

Grieve, A.F., 1991, The Sudbury Structure: Controversial or Misunderstood: Geophysical Research Letters, v. 96, p. 22,753–22,764.

Grieve, R. a. F., Ames, D.E., Morgan, J. V., and Artemieva, N., 2010, The evolution of the Onaping Formation at the Sudbury impact structure: Meteoritics & Planetary Science, v. 45, no. 5, p. 759–782.

Grieve, R.A.F., Cintala, M., and Therriault, A.M., 2006, Large-scale impacts and the evolution of the Earth's crust: The early years., *in* Processes of the Early Earth: Geological Society of America Special Paper 405:, p. 22–31.

Grimes, C.B., John, B.E., Kelemen, P.B., Mazdab, F.K., Wooden, J.L., Cheadle, M.J., Hanghøj, K., and Schwartz, J.J., 2007, Trace element chemistry of zircons from oceanic crust: A method for distinguishing detrital zircon provenance: Geology, v. 35, no. 7, p. 643, doi: 10.1130/G23603A.1.

Hansen, T.A., 1987, Extinction of Late Eocene to Oligocene Molluscs : Relationship to Shelf Area, Temperature Changes, and Impact Events: Palaios, v. 2, p. 69–75.

Harrison, T.M., 2009, The Hadean Crust : Evidence from > 4 Ga Zircons: Annual Review of Earth and Planetary Sciences, v. 37, p. 479–505.

Harrison, T.M., and Lovera, O.M., 2013a, The Multi-diffusion Domain Model : Past , Present and Future: Geological Society, London, Special Publications, v. 378, p. 1–36.

Harrison, T.M., and Lovera, O.M., 2013b, The Multi-diffusion Domain Model : Past, Present and Future: Geological Society, London, Special Publications, v. 378, p. 1–36.

Harrison, T.M., and Schmitt, A.K., 2007, High sensitivity mapping of Ti distributions in Hadean zircons: Earth and Planetary Science Letters, v. 261, no. 1-2, p. 9–19.

Harrison, T.M., and Watson, E.B., 1983, Kinetics of zircon dissolution and zirconium diffusion in granitic melts of variable water content: Contributions to Mineralogy and Petrology, v. 84, no. 1, p. 66–72.

Harrison, T.M., Watson, E.B., and Aikman, A.B., 2007, Temperature spectra of zircon crystallization in plutonic rocks: Geology, v. 35, no. 7, p. 635.

Hart, R.J., Andreoli, M.A.G., Tredoux, M., Moser, D., Ashwal, L.D., Eide, E.A., Webb, S.J., and Brandt, D., 1997, Late Jurassic age for the Morokweng impact structure , southern Africa: Earth and Planetary Science Letters, v. 147, p. 25–35.

Hart, R.J., Cloete, M., McDonald, I., Carlson, R.W., and Andreoli, M.A.G., 2002, Siderophile-rich inclusions from the Morokweng impact melt sheet, South Africa: possible fragments of a chondritic meteorite: Earth and Planetary Science Letters, v. 198, no. 1-2, p. 49–62.

Hazel, J.E., 2014, Chronostratigraphy of Upper Eocene Microspherules: Palaios, v. 4, p. 318–329.

Head, J.W., Murchie, S., Mustard, J.F., Pieters, C.M., Neukum, G., McEwen, A., Greeley, R., Nagel, E., and Belton, M.J.S., 1993, Lunar impact basins: New data for the western limb and far side (Orientale and South Pole-Aitken Basins) from the first Galileo flyby: Journal of Geophysical Research, v. 98, p. 17,149–17,181.

Hildebrand, A.R., Penfield, G.T., Kring, D.A., Pilkington, M.Z., Camargo, A., Jacobsen, S.B., and Boynton, W. V, 1991, Chicxulub Crater : A possible Cretaceous/Tertiary boundary impact crater on the Yucatán Peninsula, Mexico: Geologische Rundschau, v. 19, p. 867–871.

Hodych, J.P., and Dunning, G.R., 1992, Did the Manicouagan impact trigger end-of-Triassic mass extinction ?: Geology, v. 20, p. 51–54.

Holzheid, A., Sylvester, P., O'Neill, H., Rubie, D.C., and Palme, H., 2000, Evidence for a late chondritic veneer in the Earth's mantle from high-pressure partitioning of palladium and platinum: Nature, v. 406, p. 396–9.

Hopkins, M.D., Harrison, T.M., and Manning, C.E., 2010, Constraints on Hadean geodynamics from mineral inclusions in >4Ga zircons: Earth and Planetary Science Letters, v. 298, no. 3-4, p. 367–376.

Hoskin, P.W.O., and Schaltegger, U., 2003, The Composition of Zircon and Igneous and Metamorphic Petrogenesis Metamorphic Petrogenesis: Reviews in Mineralogy and Geochemistry, v. 53, p. 27–62.

Hoskins, P.W.O., and Black, L.P., 2000, Metamorphic zircon formation by solid-state recrystallization of protolith igneous zircon: Journal of Metamorphic Geology, v. 18, p. 423–439.

Hren, M.T., Sheldon, N.D., Grimes, S.T., Collinson, M.E., Hooker, J.J., Bugler, M., and Lohmann, K.C., 2013, Terrestrial cooling in Northern Europe during the eocene-oligocene transition.: Proceedings of the National Academy of Sciences of the United States of America, v. 110, p. 7562–7.

Ivanov, B.A., 1991, Impact crater processes: Advances in Space Research, v. 11, p. 67–75.

Ivany, L.C., Patterson, W.P., and Lohmann, K.C., 2000, Cooler winters as a possible cause of mass extinctions at the Eocene/Oligocene boundary.: Nature, v. 407, p. 887–90.

Jourdan, F., Andreoli, M.A.G., McDonald, I., and Maier, W.D., 2010, 40Ar/39Ar thermochronology of the fossil LL6-chondrite from the Morokweng crater, South Africa: Geochimica et Cosmochimica Acta, v. 74, p. 1734–1747.

Jourdan, F., Reimold, W.U., and Deutsch, A., 2012, Dating Terrestrial Impact Structures: Elements, v. 8, p. 49–53.

Kamo, S.L., Czamanske, G.K., Amelin, Y., Fedorenko, V.A., Davis, D.., and Trofimov, V.., 2003, Rapid eruption of Siberian flood-volcanic rocks and evidence for coincidence with the Permian–Triassic boundary and mass extinction at 251 Ma: Earth and Planetary Science Letters, v. 214, p. 75–91.

Kamo, S.L., Reimold, W.U., Krogh, T.E., and Colliston, W.P., 1996, A 2.023 Ga age for the Vredefort impact event and a first report of shock metamorphosed zircons in pseudotachylitic breccias and Granophyre: Earth and Planetary Science Letters, v. 144, p. 369–387.

Kettrup, B.K., Deutsch, A.D., and Masaitis, V.L.M., 2003, Homogeneous impact melts produced by a heterogeneous target? Sr-Nd isotopic evidence from the Popigai crater, Russia: Geochimica et Cosmochimica Acta, v. 67, p. 733–750.

Kiefer, W.S., 2003, Impact Craters in the Solar System: Space Science Reference Guide, v. 2.

Koeberl, C., Armstrong, R.A., and Reimold, W.U., 1997, Morokweng , South Africa : A large impact structure of Jurassic-Cretaceous boundary age: Geology, v. 25, p. 731–734.

Koeberl, C., and Reimold, W.U., 2003, Geochemistry and petrography of impact breccias and target rocks from the 145 Ma Morokweng impact structure , South Africa: Geochimica et Cosmochimica Acta, v. 67, p. 1837–1862.

Kring, D.A., 2003, Environmental consequences of impact cratering events as a function of ambient conditions on Earth.: Astrobiology, v. 3, p. 133–52.

Krogh, T.E., Davis, D.., and Corfu, F., 1984, Precise U-Pb zircon and baddeleyite ages for the Sudbury area: The geology and ore deposits of the Sudbury structure, v. 1, p. 431–446.

Krogh, T.E., and Kamo, S.L., 1993, U-Pb ages of single schocked zircons linking distal K/T ejecta to the Chicxulub crater: Earth and Planetary Science Letters, v. 119, p. 425–429.

Krogh, T.E., Kamo, S.L., and Bohor, B.F., 1996a, Shock metamorphosed zircons with correlated U-Pb discordance and melt rocks with concordant protolith ages indicate an impact origin for the Sudbury Structure: Geophysical Monograph Series, v. 95, p. 343–353.

Krogh, T.E., Kamo, S.L., and Bohor, B.F., 1996b, Shock Metamorphosed Zircons with Correlated U-Pb Discordance and Melt Rocks with Concordant Protolith Ages Indicate an Impact Origin for the Sudbury Structure: Geophysical Monograph Series, v. 95, p. 343–353.

Krogh, T.E., Kamo, S.L., Sharpton, V.L., Marin, L.E., and Hildebrand, A.R., 1993, U-Pb ages of single schocked zircons linking distal K/T ejecta to the Chicxulub crater: Nature, v. 366, p. 731–734.

Langenhorst, F., and Clymer, A.K., 1996, Characteristics of shocked quartz in late Eocene impact ejecta from Massignano (Ancona, Italy): Clues to shock conditions and source crater: Geology, v. 24, p. 487–490.

Lightfoot, P.C., and Zotov, I.A., 2005, Geology and geochemistry of the Sudbury Igneous Complex, Ontario, Canada: Origin of nickel sulfide mineralization associated with an impact-generated melt sheet.: Geology of Ore Deposits, v. 47, p. 349–381.

Liu, D., Jolliff, B.L., Zeigler, R.A., Korotev, R.L., Wan, Y., Xie, H., Zhang, Y., Dong, C., and Wang, W., 2012, Comparative zircon U–Pb geochronology of impact melt breccias from Apollo 12 and lunar meteorite SaU 169, and implications for the age of the Imbrium impact: Earth and Planetary Science Letters, v. 319-320, p. 277–286.

Liu, Z., Pagani, M., Zinniker, D., Deconto, R., Huber, M., Brinkhuis, H., Shah, S.R., Leckie, R.M., and Pearson, A., 2009, Eocene-Oligocene Climate Transition: Science, v. 323, p. 1187–1190.

Lunar "Cataclysm": A Misconception ?, 1975, Earth, v. 187.

Maas, R., and Mcculloch, M.T., 1991, The provenance of Archean elastic metasediments in the Narryer Gneiss Complex , Western Australia : Trace element geochemistry , Nd isotopes , and U-Pb ages for detrital zircons: Geochimica, v. 55, p. 1915–1932.

Mahon, K.I., 1996, The New "York" regression: Application of an improved statistical method to geochemistry: International Geology Review, v. 38, p. 293–303.

Mak, E.K., York, D., Grieve, R.A.F., and Dence, M.R., 1976, The age of the Mistastin Lake Crater, Labrador, Canada: Earth and Planetary Science Letters, v. 31, p. 345–357.

Mann, U., Frost, D.J., Rubie, D.C., Becker, H., and Audétat, A., 2012, Partitioning of Ru, Rh, Pd, Re, Ir and Pt between liquid metal and silicate at high pressures and high temperatures - Implications for the origin of highly siderophile element concentrations in the Earth's mantle: Geochimica et Cosmochimica Acta, v. 84, p. 593–613.

Masaitis, V.L., 1994, Impactites from Poigai crater: Special Papers - Geological Society of America, v. 293, p. 153–162.

Masaitis, V.L., Naumov, M.V., and Mashchak, M.S., 1999, Anatomy of the Popigai impact crater, Russia: Special Papers - Geological Society of America,, p. 1–18.

Meisel, T., Walker, R.J., and Morgan, J.W., 1996, The osmium isotopic composition of the Earth's primitive upper mantle: Nature, v. 383, p. 517–520.

Melosh, H.J., 1989, Impact cratering - A geologic process: Oxford University Press, New York, NY.

Melosh, H.J., and Ivanov, B. a., 1999, Impact Crater Collapse: Annual Review of Earth and Planetary Sciences, v. 27, p. 385–415.

Morbidelli, a., Marchi, S., Bottke, W.F., and Kring, D. a., 2012, A sawtooth-like timeline for the first billion years of lunar bombardment: Earth and Planetary Science Letters, v. 355-356, p. 144–151.

Moser, D.E., 1997, Dating the shock wave and thermal imprint of the giant Vredefort impact , South Africa: Geology, v. 25, p. 7–10.

Moser, D.E., Cupelli, C.L., Barker, I.R., Flowers, R.M., Bowman, J.R., Wooden, J., and Hart, J.R., 2011, New zircon shock phenomena and their use for dating and reconstruction of large impact structures revealed by electron nanobeam (EBSD, CL, EDS) and isotopic U–Pb and (U–Th)/He analysis of the Vredefort dome: Canadian Journal of Earth Sciences, v. 48, p. 117–139.

Moser, D.E., Davis, W.J., Reddy, S.M., Flemming, R.L., and Hart, R.J., 2009, Zircon U–Pb strain chronometry reveals deep impact-triggered flow: Earth and Planetary Science Letters, v. 277, p. 73–79.

Nasdala, L., Wenzel, M., Vavra, G., Irmer, G., Wenzel, T., and Kober, B., 2004, Metamictisation of natural zircon: accumulation versus thermal annealing of radioactivity-induced damage: Contributions to Mineralogy and Petrology, v. 141, p. 125–144.

Nelson, S.T., and Montana, A., 1992, Sieve-textured plagioclase in volcanic rocks produced by rapid decompression: American Mineralogist, v. 77, p. 1242–1249.

Nemchin, A.A., Pidgeon, R.T., Whitehouse, M.J., Vaughan, J.P., and Meyer, C., 2008, SIMS U–Pb study of zircon from Apollo 14 and 17 breccias: Implications for the evolution of lunar KREEP: Geochimica et Cosmochimica Acta, v. 72, p. 668–689.

Neukum, G., Ivanov, B.A., and Hartmann, W.K., 2001, Cratering records in the inner Solar System in relation to the lunar reference system: Chronology and Evolution of Mars, v. 96, p. 55–86.

Norman, M.D., and Nemchin, A. a., 2014, A 4.2 billion year old impact basin on the Moon: U–Pb dating of zirconolite and apatite in lunar melt rock 67955: Earth and Planetary Science Letters, v. 388, p. 387–398.

O'Connell-Cooper, C.D., and Spray, J.G., 2011, Geochemistry of the impact-generated melt sheet at Manicouagan: Evidence for fractional crystallization: Journal of Geophysical Research, v. 116, no. B6, p. 1–22.

Ohno, S., Kadono, T., Kurosawa, K., Hamura, T., Sakaiya, T., Shigemori, K., Hironaka, Y., Sano, T., Watari, T., Otani, K., Matsui, T., and Sugita, S., 2014, Production of sulphate-rich

vapour during the Chicxulub impact and implications for ocean acidification: Nature Geoscience, v. 7, p. 279–282.

Omar, G., Johnson, K.R., Hickey, L.E.O.J., Robertson, P.B., Dawson, M.R., and Barnosky, C.W., 2014, Fission-Track Dating of Haughton Astrobleme and: v. 237, p. 1603–1605.

Osinski, G.R., Lee, P., Parnell, J., Spray, J.G., and Baron, M., 2005, A case study of impact-induced hydrothermal activity: The Haughton impact structure, Devon Island, Canadian High Arctic: Meteoritics & Planetary Science, v. 40, no. 12, p. 1859–1877.

Pace, N.R., 1997, A Molecular View of Microbial Diversity and the Biosphere: Science, v. 276, p. 333–336.

Paces, J., and Miller, J.D., 1993, Precise U-Pb Ages of Duluth Complex and Related Mafic Intrusions, Northeastern Minnesota' Geochronological Insights to Physical, Petrogenetic, Paleomagnetic, and Tectonomagmatic Processes Associated With the 1.1 Ga Midcontinent Rift System: Journal of Geophysical Research, v. 98, p. 13,997–14,013.

Paulikas, G., Pieters, C.M., WB, B., Burch, J., Chaikin, A., Cohen, B.A., Duke, M., England, A., Hiesinger, H., Hinners, N., Howard, A., Lawernece, D., Lester, D., Lucey, P., et al., 2007, The Scientific Context for the Exploration of the Moon, *in* Final Report: Washington D.C., The Nartional Acadamies Press, p. 1–108.

Pearce, N.J.G., Perkins, W.T., Westgate, J. a., Gorton, M.P., Jackson, S.E., Neal, C.R., and Chenery, S.P., 1997, A Compilation of New and Published Major and Trace Element Data for NIST SRM 610 and NIST SRM 612 Glass Reference Materials: Geostandards, v. 21, p. 115–144.

Peck, W.H., Valley, J.W., Wilde, S.A., and Graham, C.M., 2001, Oxygen isotope ratios and rare earth elements in 3 . 3 to 4 . 4 Ga zircons : Ion microprobe evidence for high □ 18 O continental crust and oceans in the Early Archean: Science, v. 65, no. 22, p. 4215–4229.

Pidgeon, R.T., Nemchin, A.A., and Meyer, C., 2010, The contribution of the sensitive high-resolution ion microprobe (SHRIMP) to lunar geochronology: Precambrian Research, v. 183, p. 44–49.

Pidgeon, R., Nemchin, A., Vanbronswijk, W., Geisler, T., Meyer, C., Compston, W., and Williams, I., 2007, Complex history of a zircon aggregate from lunar breccia 73235: Geochimica et Cosmochimica Acta, v. 71, no. 5, p. 1370–1381.

Pierazzo, E., and Melosh, H.J., 2000, Melt Production in Oblique Impacts: Icarus, v. 145, p. 252–261.

Pierazzo, E., Vickery, A.M., and Melosh, H.J., 1997, A Reevaluation of Impact Melt Production: Icarus, v. 127, p. 408–423.

Pope, K.O., Baines, K.H., Ocampo, A.C., and Ivanov, B.A., 1994, Impact winter and the Cretaceous/Tertiary extinctions: results of a Chicxulub asteroid impact model: Earth and planetary science letters, v. 128, p. 719–725.

Poujol, M., Anhaeusser, C.., and Armstrong, R.., 2002, Episodic granitoid emplacement in the Archaean Amalia–Kraaipan terrane, South Africa: confirmation from single zircon U–Pb geochronology: Journal of African Earth Sciences, v. 35, p. 147–161.

Prothero, D.R., 1994, The Eocene-Oligocene transition: paradise lost: Columbia University Press.

R Core Team, 2013, R: A language and environment for statistical computing:.

Raup, D.M., and Sepkoski, J.J., 1986, Periodic Extinction of Families and Genera: Science, v. 231, p. 833–836.

Reimold, W.U., 1991, The geochemistry of pseudotachylites from the Vredefort Dome, South Africa: NEUES JAHRBUCH FUR MINERALOGIE-ABHANDLUNGEN, , no. 162.2, p. 151–184.

Reimold, W.U., and Gibson, R.L., 1996, Geology and evolution of the Vredefort impact structure, South Africa: Journal of African Earth Sciences, v. 23, p. 125–162.

Reimold, W.U., and Gibson, R.L., 2006, The melt rocks of the Vredefort impact structure – Vredefort Granophyre and pseudotachylitic breccias: Implications for impact cratering and the evolution of the Witwatersrand Basin: Chemie der Erde - Geochemistry, v. 66, p. 1–35.

Reimold, W.U., Koeberl, C., Brandstatter, F., Kruger, F.J., and Armstrong, R.A., 1999, Morokweng impact structure, South Africa: Geologic, petrographic, and isotopic results, and implications for the size of the structure: Special Papers - Geological Society of America,, p. 61–90.

Reimold, W.U., Pybus, G.Q.J., Kruger, F.J., Layer, P.W., and Koeberl, C., 2000, The Anna ' s Rust Sheet and related gabbroic intrusions in the Vredefort Dome-Kibaran magmatic event on the Kaapvaal Craton and beyond ?: Journal of African Earth Sciences, v. 31, p. 499–521.

Reiners, P.W., 2005, Zircon (U-Th)/He thermochronometry: Reviews in Mineralogy and Geochemistry, v. 58, p. 151–179.

Reiners, P.W., Spell, T.L., Nicolescu, S., and Zanetti, K. a., 2004, Zircon (U-Th)/He thermochronometry: He diffusion and comparisons with 40Ar/39Ar dating: Geochimica et Cosmochimica Acta, v. 68, p. 1857–1887.

Rousell, D.H., Fedorowich, J.S., and Dressler, B.O., 2003, Sudbury Breccia (Canada): a product of the 1850 Ma Sudbury Event and host to footwall Cu–Ni–PGE deposits: Earth-Science Reviews, v. 60, no. 3-4, p. 147–174.

Rudnick, R.L., and Fountain, D.M., 1995, Nature and composition of the crust: a lower crustal perspective: Reviews of Geophysics, , no. 95, p. 267–309.

Rudnick, R.L., and Gao, S., 2003, Composition of the continental crust: Treatise of Geochemistry, v. 3, p. 1–64.

Ryder, G., 2002, Mass flux in the ancient Earth-Moon system and benign implications for the origin of life on Earth: Journal of Geophysical Research, v. 107, p. 5022.

Sato, M., Hickling, N.L., and McLane, J.E., 1973, Oxygen fugacity values of Apollo 12, 14, and 15 lunar samples and reduced state of lunar magmas, *in* Lunar and Planetary Science Conference Proceedings V4,.

Schmitz, M.D., Bowring, S. a, de Wit, M.J., and Gartz, V., 2004, Subduction and terrane collision stabilize the western Kaapvaal craton tectosphere 2.9 billion years ago: Earth and Planetary Science Letters, v. 222, p. 363–376.

Schultz, P.H., and Gault, D.E., 1985, Clustered Impacts' Experiments and Implications: Journal of Geophysical Research, v. 90, p. 3701–3732.

Schwarzer, G., 2013, meta: Meta-Analysis with R:.

Scoates, J.S., and Chamberlain, K.R., 1995, Baddeleyite (ZrO2) and zircon (ZrSiO4) from anorthositic rocks of the Laramie anorthosite complex, Wyoming: Petrologic consequences and U-Pb ages: American Mineralogist, v. 80, p. 1317–1327.

Shoemaker, E.M., 1963, Impact mechanics at Meteor crater, Arizona: The Moon Meteorites and Comets, v. 1, p. 301.

Van Soest, M.C., Hodges, K. V., Wartho, J.-A., Biren, M.B., Monteleone, B.D., Ramezani, J., Spray, J.G., and Thompson, L.M., 2011, (U-Th)/He dating of terrestrial impact structures: The Manicouagan example: Geochemistry Geophysics Geosystems, v. 12, no. 5, p. 1–8.

Spray, J.G., and Thompson, L.M., 2008, Constraints on central uplift structure from the Manicouagan impact crater: Meteoritics & Planetary Science, v. 43, p. 2049–2057.

Squyres, S.W., and Kasting, J.F., 1994, Early Mars : How Warm and How Wet ?: Science, v. 265, p. 744–749.

Stoffler, D., Klaus, K., and Scott, E.R.D., 1991, Shock metamorphism of ordinary chondrites: Geochimica et Cosmochimica Acta, v. 55, p. 3845–3867.

Swinski, M.B., and Glass, B.P., 1979, North American tektites from the Pacific and Indian Oceans: EOS, Trans. Am. Geophys. Union, v. 60, p. 308.

Taylor, D.J., McKeegan, K.D., and Harrison, T.M., 2009, Lu–Hf zircon evidence for rapid lunar differentiation: Earth and Planetary Science Letters, v. 279, p. 157–164.

Tera, F., Papanastassiou, D.A., and Wasserburg, G.J., 1974, Isotopic evidence for a terminal lunar cataclysm: Apollo The International Magazine Of Art And Antiques, v. 22, p. 1–21.

Therriault, A.M., Fowler, A.D., and Grieve, R.A.F., 2002, The Sudbury Igneous Complex: A differentiated impact melt sheet.: Economic Geology, v. 97, p. 1521–1540.

Therriault, A.M., Grieve, R.A.F., and Reimold, W.U., 1997, Original size of the Vredefort Structure: Implications for the geological evolution of the Witwatersrand Basin: Meteoritics & Planetary Science, v. 32, p. 71–77.

Trail, D., Mojzsis, S.J., and Harrison, T.M., 2007a, Thermal events documented in Hadean zircons by ion microprobe depth profiles: Geochimica et Cosmochimica Acta, v. 71, p. 4044–4065.

Trail, D., Mojzsis, S.J., Harrison, T.M., Schmitt, A.K., Watson, E.B., and Young, E.D., 2007b, Constraints on Hadean zircon protoliths from oxygen isotopes, Ti-thermometry, and rare earth elements: Geochemistry Geophysics Geosystems, v. 8, p. 2–3.

Turner, G., Cadogan, P.H., and Yonge, C.J., 1973, Argon selenochronology: Lunar and Planetary Science Conference Proceedings, v. 4, p. 1889–1914.

Valley, J.W., Kinny, P.D., Schulze, D.J., and Spicuzza, M.J., 1998, Zircon megacrysts from kimberlite: oxygen isotope variability among mantle melts: Contributions to Mineralogy and Petrology, v. 133, p. 1–11.

Vonhof, H.B., Smit, J., Brinkhuis, H., Montanari, A., and Nederbragt, A.J., 2000, Global cooling accelerated by early late Eocene impacts?: Geologische Rundschau, v. 28, p. 687–690.

Walker, R.J., Horan, M.F., Shearer, C.K., and Papike, J.J., 2004, Low abundances of highly siderophile elements in the lunar mantle: evidence for prolonged late accretion: Earth and Planetary Science Letters, v. 224, p. 399–413.

Watson, E.B., 2011, Dissolution, growth and survival of zircons during crustal fusion: kinetic principals, geological models and implications for isotopic inheritance: Transactions of the Royal Society of Edinburgh: Earth Sciences, v. 87, p. 43–56.

Watson, E.B., 1996, Surface enrichment and trace-element uptake during crystal growth: Geochimica et Cosmochimica Acta, v. 60, p. 5013–5020.

Watson, E.B., and Cherniak, D.J., 2013, Simple equations for diffusion in response to heating: Chemical Geology, v. 335, p. 93–104.

Watson, E.B., and Harrison, T.M., 1983, Zircon saturation revisited ' temperature and composition effects in a variety of crustal magma types: Earth and Planetary Science Letters, v. 64, p. 295–304.

Watson, E.B., and Harrison, T.M., 2005a, Zircon thermometer reveals minimum melting conditions on earliest Earth.: Science, v. 308, p. 841–4.

Watson, E.B., and Harrison, T.M., 2005b, Zircon thermometer reveals minimum melting conditions on earliest Earth.: Science, v. 308, no. 5723, p. 841–4, doi: 10.1126/science.1110873.

Web of Science, 2014,.

Whitehead, J.Y., Papanastassiou, D.A.Y., Spray, J.G., Grieve, R.A.F., and Wasserburg, G.J., 2000, Late Eocene impact ejecta: geochemical and isotopic connections with the Popigai impact structure: Earth and Planetary Science Letters, v. 181, p. 473–487.

Wiedenbeck, M., Hanchar, J.M., Peck, W.H., Sylvester, P., Valley, J., Whitehouse, M., Kronz, A., Morishita, Y., and Nasdala, L. Further Characterisation of the 91500 Zircon Crystal: Geostandards and Geoanalytical Research, v. 28, p. 9–39.

Wielicki, M.M., Harrison, T.M., Boehnke, P., and Schmitt, A.K., 2012a, Modeling Zircon Saturation within Simulated Impact events: Implications on impact histories of planetary bodies, *in* 43rd Lunar and Planetary Conference, p. #2912.

Wielicki, M.M., Harrison, T.M., and Schmitt, A.K., 2012b, Geochemical signatures and magmatic stability of terrestrial impact produced zircon: Earth and Planetary Science Letters, v. 321-322, p. 20–31.

Wittmann, A., Kenkmann, T., Schmitt, R.T., and Stoffler, D., 2006, Shock-metamorphosed zircon in terrestrial impact craters: Meteoritics & Planetary Science, v. 454, p. 433–454.

Wolfe, M.R., and Stockli, D.F., 2010, Zircon (U–Th)/He thermochronometry in the KTB drill hole, Germany, and its implications for bulk He diffusion kinetics in zircon: Earth and Planetary Science Letters, v. 295, p. 69–82.

Wünnemann, K., Collins, G.S., and Osinski, G.R., 2008, Numerical modelling of impact melt production in porous rocks: Earth and Planetary Science Letters, v. 269, p. 530–539.

Wyllie, P.J., 1977, Crustal anatexis: An experimental review: Tectonophysics, v. 43, p. 41–71.

Young, K.E., van Soest, M.C., Hodges, K. V., Watson, E.B., Adams, B. a., and Lee, P., 2013, Impact thermochronology and the age of Haughton impact structure, Canada: Geophysical Research Letters, v. 40, p. 3836–3840.

Zachos, J., Pagani, M., Sloan, L., Thomas, E., and Billups, K., 2001, Trends, rhythms, and aberrations in global climate 65 Ma to present: Science, v. 292, p. 686–693.

Zahnle, K., Arndt, N., Cockell, C., Halliday, A., Nisbet, E., Selsis, F., and Sleep, N.H., 2007, Emergence of a Habitable Planet: Space Science Reviews, v. 129, no. 1-3, p. 35–78.

Zanazzi, A., Kohn, M.J., MacFadden, B.J., and Terry, D.O., 2007, Large temperature drop across the Eocene-Oligocene transition in central North America: Nature, v. 445, p. 639–42.

Zieg, M.J., and Marsh, B.D., 2005, The Sudbury Igneous Complex : Viscous emulsion differentiation of a superheated impact melt sheet: Geological Society Of America Bulletin, v. 117, p. 1427–1450.